Mechanical Performance of a PLA-based Biodegradable Plastic for Liquid Packaging Application

Indah Widiastuti

A thesis submitted in partial fulfillment of the requirement for the degree of
Doctor of Philosophy

Industrial Research Institute Swinburne (IRIS)
Faculty of Engineering and Industrial Science
Swinburne University of Technology
Melbourne, Australia
February 2014

Abstract

Polylactide (PLA) is a polyester derived from renewable resources, which has been receiving attention to be used as a commodity thermoplastic in packaging applications as an alternative solution to address the ecological problem of petrochemical-based plastic waste accumulation. Despite possessing good mechanical and optical properties, deterioration of the material properties in PLA-based materials could occur after prolonged exposure to the environment during their service time. PLA-based packaging could show material degradation due to interaction involving the packaging, product constituent and environment, which can initiate changes in thermal, chemical and physical properties of the material.

The objective of this research is to assess the mechanical performance of PLA-based materials for chemical liquid packaging applications by taking into account the undergoing dimensional and material property changes influenced by the absorbed substances into the package.

In evaluating new opportunities of PLA-based material for chemical product or other aggressive liquid packaging, it is important to understand not only the chemical resistance of the material but also the potential route for degradation, which affect the mechanical behaviour of the package during its service time. Degradation of PLA material with amount of sorption should be carefully controlled in order to maintain its mechanical performance in response to various loading conditions ranging from production and storage to distribution and service of the product. Furthermore, the phenomenon of swelling induced by liquid diffusion can also contribute to the development of internal stress which may lead to failure in the package.

Distribution of the absorbed liquid within the package is firstly evaluated by identifying the characteristics of the mass transport. Gravimetric analysis is employed to investigate the liquid sorption mechanism and the induced expansion over a particular period. The profile of absorbed liquid content is numerically obtained and verified with the analytic solution. A finite element model is developed to simulate the diffusion and permeation of the packaged product substances in a PLA-based package.

The changes in mechanical performances were investigated by measuring the properties of specimens containing saturated liquid content. Different levels of liquid content are obtained from different levels of immersion temperature. The dependence of mechanical properties with time and position can be acquired from the relation between material properties and liquid content. The time dependent properties of material are also investigated through a series of creep experiments. A material constitutive equation is developed to represent the coupling of

two time-dependent variables in viscoelastic material which also include the variable of environment temperature.

Using prescribed material response characteristics, the evolution of stress and deformation fields in the package is analysed. The finite element analysis stress model is developed based on the convergence analysis of simplified problem to study the coupled diffusion and stress in packaging application. The simulation was performed to investigate the significance of the stresses induced due to the diffusion effect in relation to the top loading and the internal vacuum pressure in the package. Effect of liquid diffusion is incorporated on the stress profile through the swelling coefficient and liquid-dependent material parameters for both the elastic and transient (time-dependent) properties by simulating varying parameters of degradation rate, swelling coefficient and environment temperature.

In this study, a methodology to evaluate the mechanical behaviour of a PLA-based package, which is significantly affected by mass transport of packaged substances, is presented. It is found that the stress is concentrated in the package wall at a time when significant variation of liquid content is observed within the package. The stress concentration, which is mainly caused by high swelling coefficient, may lead to a failure in the package. The results of this study also emphasize the importance of considering the deterioration of mechanical properties in the design of packaging for chemical or other organic liquid using the PLA-based material.

Acknowledgments

I thank God (the most gracious and most merciful) for giving me strength and patience to complete this thesis.

This research project would not have been possible without support and assistance of many individuals. First and foremost, I am very grateful to my primary supervisor, Assoc. Prof. Igor Sbarski for his guidance, instructions and encouragement at all stages of my candidature. I would also thank Prof. Syed H. Masood for his feedback and support throughout this research. I thank both of them in pushing me to complete this project, and instilling confidence in my research capabilities.

I would like to express my special thanks to Indonesian Directorate General of Higher Education (DIKTI) for the fellowship awarded. I also thank to all my colleagues in Sebelas Maret University (UNS) Solo for giving me chance to take a leave in pursuing knowledge.

I also have to thank and appreciate the senior technical officers Brian Dempster and Andrew Moore for always being a problem solver during many experimental works. I acknowledge Mr Kelvin Davies for providing valuable information on mechanical testing and polymer processing.

Last but not least, I am especially thankful to my husband and my girls for always keep supporting me and also for their prayers to complete this research work. To my mother and all the families at home, we will be back soon. This work is dedicated to my father who has passed away when I just started this research project and whom I respected most and will always love.

Declaration

I declare that this thesis contains no material which has been accepted for the award of any other degree or diploma, except where due reference is made in the text. To the best of my knowledge, this thesis contains no material previously published or written by another person, except where due reference is made in the text.

Indah Widiastuti

Table of Contents

List of Tables

List of Figures

List of Symbols

β	Coefficient of swelling,
α	Coefficient of thermal expansion
η	Polymer viscosity
δ	Thickness of the plate
$\sigma(t)$	Time dependent stress
$\varepsilon(t)$	Time dependent strain
ε_0	Time-independent strain
ε_f	Coefficients of time-dependent terms of Findley Power model
ΔH_c	Crystallization enthalpy
ΔH_m	Melting enthalpy
ΔL	Dimensional change
ΔM	Weight gain
ΔT	Temperature changes
A_n	Material reduction factor
a_T	Shift factor
C(t)	Concentration of diffusing substances
C_0	Reference liquid content
D	Diffusion coefficient (cm^2/s)
D_0	A constant of Arrhenius equation
E	Elastic modulus
E(t)	Time dependent modulus
E’	Storage modulus
E”	Loss modulus
E_a	Activation energy of Arrhenius equation

E_K	Stiffness of the Kelvin unit in the viscoelastic Burger model
E_M	Instantaneous modulus of the Maxwell spring in the viscoelastic Burger model
F	Rate of transfer of diffusing substances
F_0	Dimensionless Fourier number
G(t)	Relaxation modulus
J(t)	Creep compliance
k	Constant independent of stress of Findley Power model
LS	Length swelling
M_m	Mass of saturated absorption
M_t	Mass of diffusant after absorption time of t
P	Permeability coefficient
ν	Poisson's ratio
r	Radius of curvature
R	Universal gas constant of Arrhenius equation
R^2	Correlation coefficient
τ	Retardation time
S	Solubility coefficient of the permeant
S_f	Safety factor
t	Time
t'	Reduced time in time-temperature superposition concept
T	Absolute temperature
T_0	Reference temperature
T_c	Crystallization temperature
T_g	Glass transition temperature
δ	Thickness of the plate
Tm	Melting temperature
u	Displacement component in x direction of Cartesian coordinate system
v	Displacement component in y direction of Cartesian coordinate system

w	Displacement component in z direction of Cartesian coordinate system
x	Position in x direction of Cartesian coordinate system
X_c	Relative crystallinity
y	Position in y direction of Cartesian coordinate system
z	Position in z direction of Cartesian coordinate system

List of Abbreviations

DMA	Dynamic Mechanical Analyser
DOF	Degree of Freedom
DSC	Differential Scanning Calorimeter
ESCR	Environment stress cracking resistance
FEM	Finite Element Method
HDPE	High density polyethylene
ITS	Integration time step
MFI	Melt flow index
PC	Polycarbonate
PE	Polyethylene
PET	Polyethylene terephthalate
PHA	Poly(hidroxyalkanoate)
PLA	Polylactides
PP	Polypropylene
PS	Polystyrene
SLS	Standard linear solid
SSE	Sum of squared error
TGA	Thermogravimetric
WLF	William-Landel-Ferry
WVTR	Water vapour transmission rate

CHAPTER 1 INTRODUCTION

1.1 Background

Recently, worldwide production of petroleum-based plastic material has experienced a spectacular growth with approximately 140 million tons per year (Madhavan Nampoothiri et al., 2010). Having outstanding material properties, flexibility in design and relatively low cost, this material is extensively used for packaging applications (PCIA, 2007). Plastics can be found in diverse forms, from single films to rigid solid, and applied to great variety of products, from food and beverages to electrics and electronics.

The environmental awareness of the society has risen to the point that plastic waste must be reduced for protection of natural resources and reduction of CO_2 emission. Plastics, which degrade very slowly and are resistant to natural process, make up significant proportion of the volume of domestic and industrial waste (10 - 30%) (Kolybaba et al., 2003). They contain chemical substances that could present a hazard for the environment and they also need more energy to produce (Marsh, 2003). Accumulation of plastic residue makes it difficult for water and oxygen to circulate and causes damage to the environment and all living creatures.

Conventional method used to get rid of plastic waste was disposal in land fill sites. Nowadays, the focus is on the reuse and recycling of waste materials because of ecological concern and limited space of land filling. Even though the reuse of plastic products could be made environment-friendly, there should be further checks to make sure that the material meets the required quality. Several problems are also faced in recycling, such as difficulty to recycle due to complex polymer structure, loss of some advantageous properties and requirement of sophisticated technology or greater energy (Allred, 2000, Ashori, 2008, Bellmann, 1999). Recycling conventional plastic composites releases dust and hazardous gasses (CO2, NO_x and SO_x) into the atmosphere. To overcome these problems, the packaging industry need to seek more environmental friendly material to minimize the creation of plastic waste. An innovative solution to growing need of plastic packaging can be the use of biodegradable plastic.

After disposal, biodegradable plastics can be degraded naturally into harmless substances in an industrial composting environment. The emergence of biodegradable plastics was driven by the

increasing use of plastic materials in packaging applications. In relatively short-lived application of packaging, it is widely accepted that the use of long-lasting polymers is not entirely adequate. Biodegradable packaging takes advantage of the relatively fast degradation in an industrial composting environment. Biodegradable plastics can be based on either synthetic or natural resin (Environment_Australia, 2002). Synthetic biodegradable plastics are derived from petroleum-based products, a non-renewable resource. Meanwhile, the natural biodegradable plastics can be primarily based on renewable resources or synthesized from renewable substances. Renewable-based biodegradable plastics have been attracting more attention since they are made from plant material, which would create a sustainable industry. In addition, bio-based polymers have the potential to reduce the reliance on petroleum supply and cut the carbon emission into the atmosphere.

Numerous types of biodegradable biopolymers have been introduced for various packaging applications. According to their source of origin, there are three groups of natural biodegradable polymers: (1) biomass product such as starches and ligno-celullosic products, (2) polymers obtained by extraction of microorganisms such as poly(hidroxyalkanoate) (PHA), and (3) polymers synthesized from renewable materials such as polylactides (PLA) (Leblanc et al., 2008). Figure 1-1 shows global production capacity of the natural biodegradable polymers and the share for each type as in 2011. Currently, the biggest production share is held by PLA accounting for about 38% of the biopolymer production, followed by thermoplastic starch (and blends made thereof).

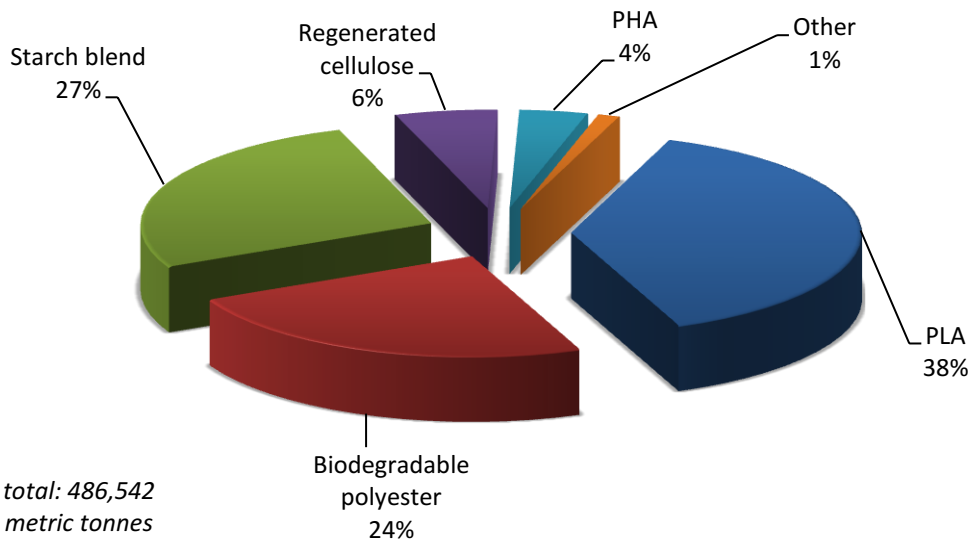

Figure 1-1: Global production capacity of biopolymer production (Source: European Bioplastics/Institute for Bioplastic and Biocomposites)

The good mechanical properties, such as high stiffness and high tensile strength, combined with good optical properties (transparency) makes PLA an attractive commodity thermoplastic in packaging applications. PLA material has comparable mechanical and physical properties to those of some commercial thermoplastics (Almeida, 2011, Auras et al., 2003) and it can be easily processed in most polymer processing equipment (Henton et al., 2005). High value film and rigid thermoform are the most common form of PLA used for short shelf life products (Auras et al., 2004b). Market specialty niches such as fresh fruit container, drinking cup, blister package and wrapping film are examples of popular application of PLA material. Recent developments have widened its processing capability in the production of not only flexible packaging but also of rigid container for longer service life products such as beverages (plain water, soft drink and fruit juices), edible oil, and health/beauty products (NatureWorks).

To be an ideal candidate for packaging, the PLA material should accomplish basic requirements of some critical properties, which includes mechanical, thermal and barrier properties. PLA-based materials, however, have some limitations as packaging material. These limitations are associated with: (1) rigidity and brittleness of material (Obuchi and Ogawa, 2011, Ahmed and Varshney, 2011) with low ability to plastic deformation below glass transition temperature, (2) low heat deflection temperature (Obuchi and Ogawa, 2011), (3) hydrolytic degradation in aqueous solution (Van Aardt et al., 2007) and the conditions of high humidity at high temperature (Sharp et al., 2001, Holm et al., 2006), and (4) barrier properties to permeation of low molecular components, such as water vapour, O_2 and CO_2 (Cairncross et al., 2006, Auras et al., 2006a)

Currently, several efforts have intensified to improve the critical properties of PLA material according to required packaging applications. The barrier and mechanical properties of this material have been enhanced through some attempts including the use of impact modifier (Taib et al., 2012) to reduce the brittleness of the material, blending with other flexible/biodegradable material (Cabedo et al., 2006) and addition of filler material into PLA matrix (Harris and Lee, 2008). Surface polymer modification with coating material is also reported in improving the gas barrier properties of the virgin PLA (Siracusa et al., 2012). In recent years, polymer nanocomposites made by dispersing nanoparticles into polymeric material have gained considerable interests in improving material properties. Significant enhancement in thermomechanical and barrier properties has been reported on PLA based nanocomposites (Pinto et al., 2013, Wu and Liao, 2007, Park et al., 2012, Sinha Ray et al., 2003). The improvements in production technologies of PLA promise the expanding applications in more severe circumstances for broader array of products. Evaluation on mechanical performance during the service lifetime is on-going research in response to the demand for extending applications range of PLA-based material.

1.2 Motivation of Research

Under typical use conditions, PLA is very stable and will retain its molecular weight and physical properties for years. This is typified by its growing use for clothing and durable applications. However, deterioration of the material properties might be observed after prolonged exposure to the environment as may occur during their service time. Interaction involving the packaging, product constituent and environment may impact on material degradability and can initiate changes in thermal, chemical and physical properties of the material.

Numerous researches have observed the effect of environment condition on PLA materials (Ho et al., 1999, Copinet et al., 2004, Holm et al., 2006, Harris and Lee, 2010, Niaounakis et al., 2011). The decreasing of mechanical performance has been reported after absorbing moisture under particular humidity condition. On the other hand, the study on the sorption of product constituent by the PLA package has attracted only few studies to date. As the majority of existing commercial applications are for food packaging, the studies mainly focused on the barrier properties of food solutions related to the quality of the packaged product (Auras et al., 2006b, Colomines et al., 2010, Haugaard et al., 2002, Dmytrów et al., 2011). Recent reports on interaction between PLA package and its product constituent revealed changes of thermomechanical properties after sorption of a hydrophilic chemical compound into the package (Salazar et al., 2012, Courgneau et al., 2012, Colomines et al., 2010). This finding signified sorption-induced plasticization in PLA package during its interaction with a particular substance of a packaged product.

In packaging application, a stable material is required to maintain its mechanical performance in response for various loading conditions subjected during production and storage to distribution and service of the product. The material properties depend on the composition (coating, blending, filler), but the behaviour of material in contact with the product constituent may affect durability of the material during its service lifetime. Degradation of PLA material with amount of sorption should be carefully controlled in order to avoid the structure deteriorating before the end of its useful lifetime.

Growing awareness in eco-friendly packaging has led to rising demand for PLA packaging in broader array of products. More semi-durable and rigid packaging has been brought to and widely accepted into market, not only for food related products but also for consumer products. Finding new applications of PLA package for non-food commodities and other products is a logical consequence of an increasing environmental awareness. Consequently the increasing use of the material in packaging application has renewed interest in mechanical behaviour analysis of material, which continuously degrades with exposure to the environment. Resistance testing

may provide a relative indication of material suitability in short-time period, but there is usually a lack of information about the behaviour of material in contact with the product substance over time.

In evaluating new opportunities of PLA-based material for chemical product or other aggressive liquid packaging, it is important to understand not only the chemical resistance of the material but also the potential route for degradation (Duncan et al., 2005). The diffusion of chemicals within plastic materials may affect the mechanical performance of material similar to the effect of moisture and product substances as discussed above. Information regarding the chemical mass transport through a plastic package is essential for understanding the accumulation of chemical inside the package and providing prediction of performance degradation. The standard protocol proposed by Abbes et al (2010) might be adopted to investigate the performance of a package in contact with a particular chemical compound. They systematically studied the deterioration of mechanical properties in a saturated polypropylene package and evaluated the corresponding strength to withstand load under columnar crush conditions. Although this approach can provide better understanding about the changes of mechanical behaviour due to the sorption effect, it is of limited value to predict the actual end-use performance of a relatively thick package since dependence of mechanical properties on substance uptake was not taken into account. If the substance of packaged product is spatially distributed in a non-uniform manner and varied with time, this will cause variations of property to develop within the package. Moreover, full coupling of two time-dependent variables may occur in viscoelastic packaging material where mechanical properties are time-dependent (Chiang and McKenna, 1996). One variable accounts for the time-dependent response toward load, which characterizes the viscoelastic nature of a material while the time-dependent behaviour is strongly influenced by the substance content within material. In mechanical behaviour analysis of a package, it is also important to take into account the contribution of diffusion-induced swelling in predicting more realistic stress state under loads. Different parts of the body tend to expand in different amounts due to the non-uniform distribution of the substance content. The variation of swelling acts as an internal constraint, as it may induce stresses that are developed during sorption of packaged product. In addition, there is little consistent or reliable information available on degradation of PLA packaging under combined sustained load and elevated temperature.

With the expectation to use PLA-based material as an alternative material for application in chemical liquid packaging, a critical evaluation of the stress and deformation is needed to predict the reliability and failure behaviour of such applications. These are important areas in the development of models for predicting the mechanical behaviour of a bio-based packaging in which the performances decrease with degradation.

1.3 Research Objectives

This thesis aims to evaluate the performance of PLA-based material in applications of chemical liquid packaging by proposing a methodology which correlates the degradation of mechanical properties and diffusion-induced swelling with the accumulation of absorbed substances into the package. The study is designed to model reasonable "worst" case extraction when the polymer is used in commercial fluid container application for intermediate time periods at various temperatures using the considerably aggressive fluid simulant.

The objectives of this research are as follow:

1) To characterize the transport process of the model fluid into PLA specimens including the rate of transport and the effect of environment temperature. In this investigation, hydrocarbon liquid is used as a model fluid even though the method can also be applied to other liquid.
2) To analytically and numerically model the distribution of absorbed substance within various PLA shapes for further mechanical behaviour analysis.
3) To assess the changes of mechanical properties in PLA specimens with the sorption of model fluid and then to evaluate the relation between those two variables to identify the function of mechanical properties with the content of packaged product within the material.
4) To investigate effect of fluid sorption on viscoelastic behaviour of the PLA specimen at different temperature conditions and then to characterize the material response with time-temperature-and fluid content dependence.
5) To evaluate the evolution of mechanical behaviour during sorption of the model fluid using a stress model that accounts for the time-dependent material response and swelling of material.
6) To numerically analyse the stress and deformation on a design of PLA liquid container by taking into account the swelling and degradation of material properties due to sorption of packaged product.
7) To investigate the significance of swelling coefficient, fluid-dependent properties and time-dependent properties on the state of stress and deformation in the package.
8) To evaluate the performance of PLA-based packaged for application of chemical or aggressive liquid packaging by taking into account the characteristics of the liquid diffusion into the material.

1.4 Significance of Research and Major Contribution

This research is expected to make important contribution in bulk of studies investigating PLA-based material for packaging application. The proposed methodology in this thesis is applicable not only for chemical liquid but also for other products which interact with the package. In the issues related to the packaged product and the package interaction, most of the studies focus on the quality of the product in relation with the barrier properties. Considering the fact that performance of PLA-based plastic may decrease with degradation of material in contact with its environment, it is necessary to monitor its degradation rate during its useful service life.

The major contributions of this research are as follow:

1) The study proposed a methodology in evaluating new application for PLA packaging whereas material properties degrade during diffusion process to predict the deterioration before its useful lifetime ends.

2) By understanding the characteristics of substance diffusion inside the material, the material properties can be modelled more accurately for precise prediction of mechanical performance under various loading condition over the service time.

3) The study takes into account the importance of mass transport characteristics in packaging application related to mechanical behaviour and failure of the package from the aspect of swelling and deterioration of material properties due to sorption of product substances.

4) It encourages more application of biodegradable plastic derived from sustainable material as an alternative solution for the disposal of petroleum-based polymeric materials.

1.5 An Introduction to PLA for Packaging Material

Recently, the development of bio-sourced plastics has increased due to increasing environmental concern of plastics materials. One of the most promising biopolymer, Polylactide (PLA), is aliphatic polyester produced by polymerisation of the renewable fermentation product of lactic acid. Initially, this material gained significant research interest for use in medical applications such as drug delivery system, sutures and surgical implants due its biocompatibility to human body (Brannon-Peppas, 1995). Recent breakthrough in PLA production has led to significant reduction of the material cost and opened up possibility for wider application range. It is now being applied in automotive interior components (Kim et al., 2011), durable consumer goods (NEC, 2006, Kimura and Horikoshi, 2005), and also for the flexible to rigid packaging

required for a broad array of products (Auras et al., 2004b, Obuchi and Ogawa, 2011, Madhavan Nampoothiri et al., 2010). Increasing environment concern and higher carbon-fuel price has led to more development in current technologies and new applications for PLA material.

In PLA production, plant materials containing starch-based constituents from renewable materials such as corn, beet-sugar and cane-sugar are fermented to produce the lactic acid. This lactic acid is then converted into lactide, which serves as a monomer for PLA production (Vaidya et al., 2005). Lactic acid is chemically synthesised mainly based on the hydrolysis of lactonitrile using strong acid. High molecular weight polylactide can be made by ring opening polymerisation (ROP) from lactide monomer which is produced by oligomerized lactic acid (Ahmed and Varshney, 2011).

PLA material is easily processed on standard processing equipment such as injection moulding, blow moulding, sheet extrusion and thermoforming (Garlotta, 2001, Auras et al., 2004b) and can be formed into transparent films or blow mouldable preform for bottle. Some PLA manufacturers such as NatureWorks LLC (NatureWorks, 2103) and Mitsubishi Plastics (Mitsubishi, 2012) commercialized their product in different grades according to application and processing method. Due to thermal degradation that may occur in PLA material at temperature above 200°C, it is required to control its stability during processing.

Degradation of PLA material might be observed after prolonged exposure to the environment as may occur during their service time (Singh and Sharma, 2008). Degradation reflects changes in material properties, which affect the thermal stability, mechanical properties and the degree of crystallinity. These changes may be undesirable sometimes while in use, or desirable, as in biodegradation in landfill environment. The hydrolytic degradation in aqueous media finds advantage for use in medical and pharmaceutical application (Tsuji, 2010, Grizzi et al., 1995). For commodity and industrial application, where PLA materials are used as alternative to petroleum-based polymeric material, degradation during service life is unfavourable since the material performance will decrease during its degradation. Belonging to the family of aliphatic polyesters, hydrolysis is the primary mode of degradation in PLA (Auras et al., 2004b, Harris and Lee, 2010). The absorbed water molecules, which attack the ester linkage, are self-catalysed by protons on the carboxyl (COOH), causing breakdown of the long molecular chains. Absorbed fluid can also behave as a plasticizer that facilitates molecular chain movement in the material and results in faster nucleation and crystallization of the PLA molecules (Niaounakis et al., 2011).

1.6 Structure of Thesis

In the beginning of this chapter, the background and objectives of the research project have been outlined. As an introduction to PLA for packaging application, a brief explanation of the material is presented.

Chapter 2 is the literature review, which reported the main characteristics of polylactide material for packaging application. The deterioration of PLA material in contact with its environment with respect to the research objective is reviewed. Basic theory related to mass transfer in packaging, time-dependent properties and the finite element method addressing the research objectives will be presented. This chapter will also discuss the basic approach in solving the problem of diffusion induced stress for the specified research objectives.

The third chapter of the thesis describes the research method including the experimental work on characterizing the diffusion of a model fluid in PLA material and measurement of mechanical properties. Procedures performed on several mechanical tests such as tensile, flexural, impact and dynamic mechanical analysis are presented. The way to evaluate time and temperature dependent properties using creep test and development of creep compliance function are also shown.

In the fourth chapter, diffusion characteristics of organic liquid as the model fluid into the PLA is obtained from the experimental work including the diffusion coefficient and saturated liquid content. The influence of environment temperature on the characteristics of diffusion is also investigated. Distribution of liquid content within the thickness of a simple geometry is analytically presented. Numerical simulation of moisture and liquid diffusion on a particular package design with different scenarios of diffusion parameters is shown. This includes the anomalous diffusion behaviour which might occur in the real application.

The fifth chapter discusses the effect of absorbed liquid on the mechanical performance of material represented by its material properties and critical in-service parameters. Mechanical data from different levels of liquid content are obtained from measurements on saturated specimens of different conditioned temperatures. Results from a series of creep experiment exhibit the influence of liquid content and temperature on evolution of material properties with time. According to these results, the relations, which describe the dependence of material properties to the liquid content, are established. The outcomes of this chapter are material response characteristics which represented from the constitutive functions with temperature and liquid content dependence derived from the experiment data. Therefore, the material properties at any given location and time are dependent on the liquid content.

The next chapter, Chapter 6, examines the mechanical behaviour of a liquid package made from PLA-based material in contact with the model fluid. The material model implemented in the

analysis is derived from previous chapter, which characterizes the material response due to liquid diffusion effect. A series of convergence study on simple geometries is performed to examine some factors that may affect the accuracy of the results obtained. The converged model, which accounts for the effect of time, liquid content, temperature and swelling-induced strain, is then simulated to analyse the mechanical behaviour evaluation. Effect of different parameters including the time-dependent properties and the liquid-dependent properties are investigated in this chapter.

The overall project conclusions are given in Chapter 7. Suggestions for further study are also included in this chapter.

CHAPTER 2
LITERATURE REVIEW

2.1 Introduction

The application of PLA for commodity and industrial products requires that the material retain sufficient stiffness and strength during the service life. Therefore, understanding of the mechanism of deterioration in material properties is primary requisite in evaluating the overall performance of an application.

This chapter reviews related literatures with respect to the research objective, including brief review of the material properties of PLA package material. Diffusion in polymer is presented to understand the mass transfer phenomena on PLA package along with the common effect related to changes of properties and dimensions. The time-dependent properties represented by the viscoelastic nature are discussed in order to carry out a comprehensive analysis on mechanical response of fluid-exposed material. The last section concerns the application of Finite Element Method (FEA) related to the research objectives.

2.2 Critical Properties of PLA as Packaging Material

For use in packaging application, plastic materials need to possess some critical properties such as: morphology, thermophysical, mechanical, barrier and optical properties (Harper, 2002). This section presents a brief discussion on some important properties of PLA-based material such as the mechanical and barrier properties.

2.2.1 Mechanical and thermal properties

Thermal properties of PLA which cover some parameters such as glass transition temperature, melting temperature and crystallization behaviour, were reported to be dependent on the polymer microstructure and molecular weight (Ahmed et al., 2009). It is necessary to understand the crystallisation behaviour of PLA material since it significantly influences the thermal resistance as well as the barrier and mechanical properties (Saeidlou et al., 2012). Several ways including addition of nucleating agent and plasticizers (Saeidlou et al., 2012), post-annealing of specimens and optimization of material processing parameters (Harris and Lee, 2008) can be used to increase the material crystallinity.

Table 2-1: Thermal properties of poly(L-lactide) and poly(D-lactide) adapted from Ahmed et al. (2009)

Property	L-PLA		D-PLA	
	M_n* = 4.7x10^3	M_n = 17.5x10^3	M_n = 13.8x10^3	M_n =16.5x10^3
Glass transition temperature, T_g (°C)	45.6	62.54	65.69	69.1
Melting temperature, T_m (°C)	157.82	173.98	170.26	173.49
Melting enthalpy, ΔH_m (J/g)	55	69.54	67.01	64.55
Crystallization temperature, T_c (°C)	98.25	105.71	107.57	109
Crystallization enthalpy, ΔH_c (J/g)	47.82	44.82	52.38	51.6

*M_n = number average molecular mass

The glass transition temperature, T_g and the melting temperature, T_m increase rapidly with increasing of molecular weight until a particular value and then reach constant after that point (Ahmed et al., 2009, Saeidlou et al., 2012). Table 2-1 shows effect of isomer type and molecular weight on thermal properties of PLA.

One of the advantages present in PLA material is the fact that its mechanical properties can be easily manipulated to satisfy different applications. It is possible to have varying mechanical properties of PLA by modifying its parameters such as crystallinity, polymer structure and molecular weight, material formulation (plasticizer, blend, composites) and processing (Sin et al., 2012). Table 2-2 gives example on variation of mechanical properties with different condition.

Table 2-2: Mechanical properties of poly(L-lactide), adapted from Perego et al. (1996)

Property	L-PLA			Annealed L-PLA		
	Mv* = 5.8 x10^4			Mv = 4.7 x10^4		
	T = 23°C	T = 36°C	T = 56°C	T = 23°C	T = 36°C	T = 56°C
Tensile strength (MPa)	58			59		
Elongation at break (%)	5			3.5		
Modulus of elasticity (GPa)	3.60	3.40	0.05	4.15	3.6	0.95
Flexural strength (MPa)	100	77	0.4	113	83	28
Impact strength (J/m)	25			70		
Vicat penetrating	59			163		

*M_v = molecular weight

Data in Table 2-2 derived from Perego et al. (1996) are used to give an overview effect of molecular weight, degree of crystallinity and temperature condition on the mechanical properties of PLA material. Annealing treatment on PLLA, poly(L-lactide) was implemented to improve the crystallinity. The mechanical parameters presented in the table indicate that PLA is a brittle material with high elastic modulus and low percentage elongation of break. The table shows significant decrease of mechanical properties with increasing temperature. Much more substantial decline was observed at temperature very near to glass transition temperature (T_g). Annealed PLA is shown to have better behaviour at high temperature which still reaches useful mechanical properties even with only 25% of modulus at room temperature. Increasing of modulus and impact strength was observed for material with higher degree of crystallinity (after annealing). The impact strength and flexural strength were also influenced by molecular weight.

To further extend the range of mechanical and thermal properties achievable and thus to optimize the material for specific end use applications, many attempts have been made in modifying the PLA material. Some approaches used to manipulate this biodegradable polyester include blending with other polymer, using plasticizing material (Martin and Avérous, 2001), impact modifying and development of PLA nanocomposites.

Compatibility of PLA blending with other polymer such as polyethylene (Kim et al., 2004, Anderson and Hillmyer, 2004), poly(methyl metacrylate) (Zhang et al., 2002) and polycarbonate (Wang et al., 2012) for packaging material has been investigated. The toughness of PLA has been significantly improved by blending the material with a commercial grade of low density polyethylene (LDPE). However, toughening was only achieved upon addition of block copolymer, which acts as compatibilizer. Increasing of impact resistance as well as the heat resistance was also reported in polycarbonate (PC) and PLA blends.

A number of researchers have applied nanocompostites technology, a relatively new area of polymeric composites using Nano metric scale reinforcing material in PLA material (Sangwan et al., 2009, Ray et al., 2002, Pluta et al., 2002). Various PLA-based nanocomposites, mostly developed using layered silicate clay mineral as the reinforcing phase showed dramatic improvement in term of mechanical and physical properties.

2.2.2 Barrier properties

The resistance of PLA package material toward permeation of small molecules and sorption of production component measured on its barrier properties is indicated by the value of permeability coefficient. It has been reported that PLA has medium resistance to oxygen and carbon dioxide with slightly higher permeability coefficient compared to that of polyethylene terephthalate (PET) and lower than that of polystyrene (PS) (Auras et al., 2003, Auras et al.,

2005). However, PLA shows lower performance in water barrier compared to other commercial polymer material such as PET, PS (Auras et al., 2005), polyethylene (PE) and polypropylene (PP) (Petersen et al., 2001). Concerning the resistance to chemical compounds, it was indicated that PLA has a good barrier properties to a hydrophobic aroma compound, D-limonene and more hydrophilic compound, ethyl acetate (Auras et al., 2006a). However, even that PLA has proven to maintain the flavour loss of a hydrophilic compound, other research showed a significant decrease of glass transition temperature (T_g) (Colomines et al., 2010) after sorption to the compound. The change of thermomechanical properties needs to be carefully examined in assuring the stability of packaged material during its service life. This important finding shows the need to take into account the mass transfer that may occur in a package material.

Application of PLA packaging for products with longer shelf life requires appropriate barrier properties not only to guarantee the quality of packaged product but also to maintain its functionality in ensuring safety of packed product during its shelf life. The study on the relation between crystallinity and barrier properties by Colomines et al. (2010) showed that crystallinity seems to contribute to the improvement of the barrier properties of PLA package against sorption of a hydrophilic aroma compound. Enhancement of barrier properties can be achieved by surface polymer modification, for example by coating PLA material with particular surface treatment (Siracusa et al., 2012).

2.3 Mass Transfer in PLA Packaging

As with many other plastic materials, molecular exchange between the product and the PLA package is inevitable. This section highlights various attributes of the mass transport process in polymer and undesirable effects related to mass transfer in PLA package.

2.3.1 Mass transfer effect on mechanical performance of PLA package

Interaction of the PLA package material with the packaged product and the environment as shown in Figure 2-1 allows transfer of low-molecular-weight compounds, which causes: (1) permeation of small molecules (water vapour, O_2 and CO_2) both from product-content water and from surrounding atmosphere, (2) sorption of larger volatiles molecules from the packaged product such as aroma or flavour compounds, and (3) migration of substances like lactic acid, lactide and oligomers from PLA packaging material into the product constituent.

Loss of the product substance through the package material, permeation of undesirable compound from the environment and migration of package substance into the product will affect the quality of packaged product. The shelf life of product packaged in PLA material,

mostly food product, has been evaluated through the calculation of its permeability coefficient (Auras et al., 2006a, Colomines et al., 2010) as well as the organoleptic attributes and physicochemical properties of the packaged product (Dmytrów et al., 2011, Haugaard et al., 2002). Migration of lactic acid may also affect the quality of packaged product as well as the safety to be consumed. The migration levels of PLA substances can be correlated with the decomposition of the material under hydrolytic degradation (Conn, 1995, Mutsuga et al., 2008). Later, stability of the package material can be affected by either sorption of product substance and the environment conditions, which in turn, influences its ability to maintain the protection of packaged product.

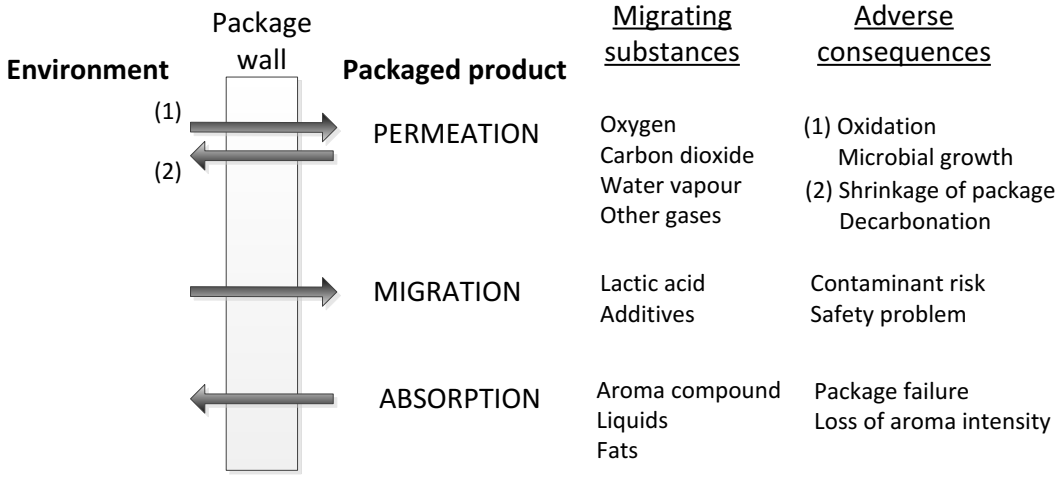

Figure 2-1: Interaction of environment-PLA package material-packaged product and the adverse consequences, modified from Sajilata et al. (2007)

The integrity of PLA material in relation with its surrounding environment has been widely studied (Cairncross et al., 2006, Holm et al., 2006, Sharp et al., 2001, Ho et al., 1999, Copinet et al., 2004, Harris and Lee, 2010, Niaounakis et al., 2011). Those researches investigate the role of humidity and temperature on mechanical performance of the material. The studies have shown that PLA is a sensitive material which easily absorbs water with increasing humidity. Interaction of water sorption with a polymeric material can involve both hydrolysis of ester linkage and modifications in the degree of plasticization (Kajorncheappunngam, 1999). The hydrolysis process breaks down long molecular chain and results in decreasing of T_g. In addition, reduction of T_g is caused by increasing of polymer chain mobility due to plasticization effect.

With presence of water, hydrolysis in plasticised amorphous region causes a decrease in the molecular weight of PLA. Decrease of molecular weight weakens the structure of material,

which is strongly related to the mechanical properties. Decreasing of mechanical performance represented by the mechanical strength, rigidity and brittleness of material was observed with the water uptake. Holm et al. (2006) reported a declining of 45% in tensile strength of a PLA film with 80% moisture uptake after being exposed to 98% relative humidity at room temperature. The studies also confirmed significant role of temperature in increasing the degradation rate. Decrement of 20% for the elastic modulus was observed after 130 days exposure at 20°C, which was sufficiently lower as compared to 51.4% decrement after 100 days and 50°C exposure (Niaounakis et al., 2011).

However, to date, interaction of PLA material with product containing higher molecules has been the subject of only a few studies, which may be related to relatively short shelf-life and low requirements of current products packaged in PLA material. As previously discussed in section 2.1.2, changes of T_g was observed after 3 days when exposed to a hydrophilic aroma compound. Recent report on this issue also confirmed morphological changes induced by sorption of the substance into PLA package (Salazar et al., 2012, Courgneau et al., 2012) which evidenced plasticizing and induced crystallisation. A chemical resistance study of PLA film performed by Auras et al. (2005) revealed minimal strength degradation toward weak and strong acid solution but showed a decrease of tensile strength and elongation at break towards vegetable oil. In comparison, this subject has attracted more attention in other commercial packaging material such as polypropylene (Abbès et al., 2010), low density poly ethylene, and PET (Harte et al., 1991). There is much information available on the investigation of hydrocarbon liquid effects on polymers (Mouzakis and Karger-Kocsis, 1998, McCourt, 2004, Giannis et al., 2008), however most works concern on non-biodegradable composite. With broader extending application of biodegradable material, it is necessary to obtain more information about the PLA material behaviour when it is in contact with other packaged products containing various chemical compounds, including hydrocarbon liquid.

In evaluating new applications for PLA package, it should be noted that presence of liquid which usually penetrates into the amorphous phase (Paterson and White, 1992) can have one or more detrimental effects, such as plasticization, solubilization, environmental stress cracking and macromolecular chains breaking. Plasticizing materials actually cause no chemical degradation of the polymer, but the absorbed chemicals may cause dimensional changes (swelling/contraction), weight gain/loss, softening and losing of yield strength.

It is for this reason that this research presents an examination of mechanical performance of a package made from material which sensitively interacts with its environment. The characteristics of the mass transport involved are related to the state of stress and deformation in evaluating the applicability during the service life of the package.

2.3.2 Fundamentals of mass transport process

In packaging material, the molecules transport through a polymer occurs due to random molecular motion of individual molecules and driven by the concentration difference between the two phases (George and Thomas, 2001). The multistep process of mass transport described in Figure 2-2 provides the rationale for packaging design and modelling the quality and shelf life of packaged products. First, the molecules collide with the package wall and then adsorb into the polymer mass. The molecules diffuse randomly in the package to the side with a low concentration of permeant which is then desorbed from the surface.

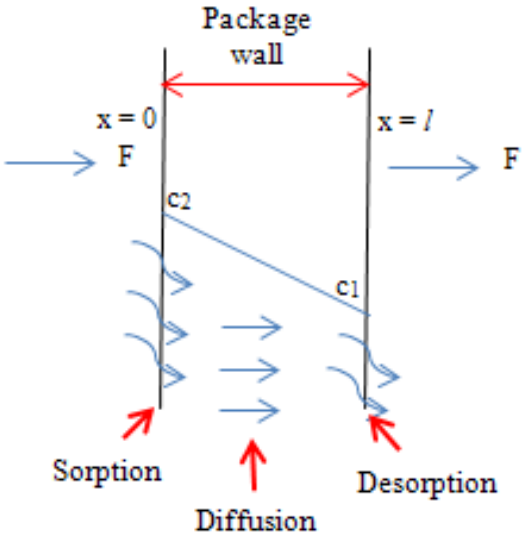

Figure 2-2: Mass transport of molecules through a polymer packaging (Hernandez, 2002)

The mass transport in packaging system including permeation, migration and sorption process can be described on a quantitative basis by a mathematical equation known as the Fick's law of diffusion (Hernandez, 2002). In isotropic substances, it is indicated that the rate of transfer of a diffusing substance through unit area, F, is proportional to the concentration gradient of the section (Neogi, 1996) and is known as Fick's law of diffusion, given by

$$F_x = -D\frac{\partial C}{\partial x} \tag{2.1}$$

where F_x is the rate of transfer per unit area of section in the x-direction, C the concentration of diffusing substances (g/cm^3), x is the space coordinate measured normal to the section (cm) and D is called the diffusion coefficient (cm^2/s). This law is applicable only when concentration is independent of time and it is said to be in steady state diffusion. While the fundamental equation for unsteady-state is derived by differentiation equation of Equation (2.1) as the Fick's second law of diffusion (Neogi, 1996), so that:

$$\frac{\partial C}{\partial t} = D\frac{\partial^2 C}{\partial x^2} \tag{2.2}$$

where diffusion is only limited on x-direction and t indicates time.

When the permeation involves high diffusant concentration and highly interactive organic penetrants such as aroma or solvent molecules, the diffusion coefficient may vary as a function of penetrant concentration and time (Willige, 2002). In this case, non-Fickian diffusion may apply to model behaviour of mass transport in the packaging.

2.4 Mechanical Behaviour Analysis

A package is subjected to various types of stress and force during its useful life. High load occur in stacking at filling lines, warehouse and transit. Appropriate package design requires sufficient information about the way the material behaves under stress in preventing damage to the product. The package is often subjected to stress for prolonged period of times, thereby detailed knowledge of the viscoelastic properties is required to know how a package will respond to a particular load during the period of loading. Mostly applied in load-bearing biomedical application, it has been reported that PLA-based material shows stress relaxation (and creep) and undergoes large deformation when subjected to mechanical loads (Muliana and Rajagopal, 2012). In a case when time-dependent effects cannot be neglected, viscoelastic material model can represent the change of stress-strain behaviour with time.

2.4.1 Governing equation for stress and deformation in elastic material

The stress associated with a diffused liquid can be analysed using the general technique of thermal stress analogy since liquid diffusion is mathematically equivalent to the heat transfer process (Huang et al., 2008). The constitutive relation of a linearly elastic plate with hygroscopic swelling can be obtained from any book on the elementary strength of materials (Noda et al., 2003, Ugural, 2009, Barron and Barron, 2011), where liquid content, C(z, t) and coefficient of swelling, β is analogous to temperature changes, ΔT and coefficient of thermal expansion, α, respectively. In the case of linearized isotropic material, the parameters used are elastic modulus, E and Poisson's ratio, ν. In simplifying, it is assumed that Poisson's ratio remains constant while the effective Young's Modulus is liquid content dependent.

The total strain is the sum of the mechanical strain that is directly related to stress and swelling strain, an expansion due to liquid diffusion. In the case of a rectangular plate, the strain

components in the Cartesian coordinate with temperature changes across the thickness δ of the plate may be written as follows:

$$\varepsilon(\mathrm{z,t}) = \begin{bmatrix} \varepsilon_{\mathrm{x}}(z,t) \\ \\ \varepsilon_{\mathrm{y}}(z,t) \end{bmatrix} = \begin{bmatrix} \frac{1}{E\delta} & -\frac{v}{E\delta} \\ -\frac{v}{E\delta} & \frac{1}{E\delta} \end{bmatrix} \begin{bmatrix} \mathrm{N_x} \\ \\ N_y \end{bmatrix} + \mathrm{C(z,t)} \begin{bmatrix} \beta \\ \\ \beta \end{bmatrix} \tag{2.3}$$

The coefficient of swelling was determined using an approach similar to the method presented by Lin (2006) by correlating the results from weight gain (ΔM) and dimensional change (ΔL) measurements. It is assumed here that the swelling coefficient is time independent.

The in-plane force and moment components that represent stress distribution over the thickness of plate are given by

$$\begin{bmatrix} \mathrm{N_x} \\ \\ \mathrm{N_y} \end{bmatrix} = \int_{-\delta/2}^{\delta/2} \begin{bmatrix} \sigma_{\mathrm{x}} \\ \\ \sigma_{\mathrm{y}} \end{bmatrix} \mathrm{dz}$$

$$\begin{bmatrix} \mathrm{M_x} \\ \\ \mathrm{M_y} \end{bmatrix} = \int_{-\delta/2}^{\delta/2} \begin{bmatrix} \sigma_{\mathrm{x}} \\ \\ \sigma_{\mathrm{y}} \end{bmatrix} z\,\mathrm{dz} \tag{2.4}$$

The on-axis expansions, ε_x and ε_y, can be expressed in terms of displacements as

$$\begin{bmatrix} \varepsilon_{\mathrm{x}} \\ \\ \varepsilon_{\mathrm{y}} \end{bmatrix} = \begin{bmatrix} \frac{\partial \mathrm{u}}{\partial \mathrm{x}} - z\frac{\partial^2 w}{\partial x^2} \\ \\ \frac{\partial \mathrm{v}}{\partial \mathrm{y}} - z\frac{\partial^2 w}{\partial y^2} \end{bmatrix} \tag{2.5}$$

In the case for opened-end cylinder, the stress components are derived from one-dimensional equilibrium equation in the radial direction as follow

$$\frac{d\sigma_{rr}}{dr} + \frac{\sigma_{rr} - \sigma_{\theta\theta}}{r} = 0 \tag{2.6}$$

The generalized Hooke's law for plane stress and strain problems in a cylindrical coordinate system is given by

$$\varepsilon_{rr} = \frac{1}{E^*}\left(\sigma_{rr} - v^*\sigma_{\theta\theta}\right) + \beta^* C(r,t) - c^*$$

$$\varepsilon_{\theta\theta} = \frac{1}{E^*}\left(\sigma_{\theta\theta} - v^*\sigma_{rr}\right) + \beta^* C(r,t) - c^* \qquad (2.7)$$

where

$$E^* = \begin{cases} \dfrac{E}{1-v^2} & for\ plane\quad strain \\ E & for\ plane\quad stress \end{cases}$$

$$v^* = \begin{cases} \dfrac{v}{1-v} & for\ plane\quad strain \\ v & for\ plane\quad stress \end{cases}$$

$$\beta^* = \begin{cases} (1+v)\beta & for\ plane\quad strain \\ \beta & for\ plane\quad stress \end{cases}$$

$$c^* = \begin{cases} v\varepsilon_0 & for\ plane\quad strain \\ 0 & for\ plane\quad stress \end{cases}$$

in which the axial stress ($\sigma_{zz} = 0$). When all strains and stresses are functions of r, the strain-displacement relations are

$$\varepsilon_{rr} = \frac{du}{dr}, \quad \varepsilon_{\theta\theta} = \frac{u}{r}, \quad \varepsilon_{r\theta} = 0 \qquad (2.8)$$

where u is the radial displacement.

The components of stress can be obtained by using Equations (2.7) and (2.8) as

$$\sigma_{rr} = \frac{E^*}{1-v^{*2}}\left[\frac{du}{dr} + v^*\frac{u}{r} - (1+v^*)\beta^* C(r,t) + (1+v^*)c^*\right]$$

$$\sigma_{\theta\theta} = \frac{E^*}{1-v^{*2}}\left[v^*\frac{du}{dr} + \frac{u}{r} - (1+v^*)\beta^* C(r,t) + (1+v^*)c^*\right] \qquad (2.9)$$

2.4.2 Mechanical response of viscoelastic material

A viscoelastic material is the one which exhibits both viscous and elastic characteristics when undergoing deformation. If a constant displacement is applied in a viscoelastic material, the stresses gradually relax over time. Meanwhile, as more elastic strain continues to accumulate, the more it is deformed under a constant load (Imaoka, 2008). Viscoelasticity means that quantities such as modulus, strength, ductility and coefficient of fiction are sensitive to straining rate, elapsed time, loading history and temperature.

In the analysis of stress and deformation, three kinds of equation are needed: equilibrium equations, kinematic equations and constitutive equations of the material, plus the boundary conditions. The first two kinds of equations are the same for elastic as well as for viscoelastic stress analysis problems, but in the constitutive equation, the variables are dependent explicitly on time (Findley et al., 1976). The constitutive equations that relate the stress, strain and time in term of the material properties are used to predict material response under different loading conditions.

Viscoelastic constitutive laws can be expressed using either a relaxation or creep-based formulation. Creep experiment is most commonly applied to investigate the viscoelastic behaviour of a polymer (Beijer and Spoormaker, 2002), which consists of an applied constant load to a specimen (Figure 2-3). The progressive deformation, $\varepsilon(t)$ due to applied stress, σ_0, is recorded for a period of time.

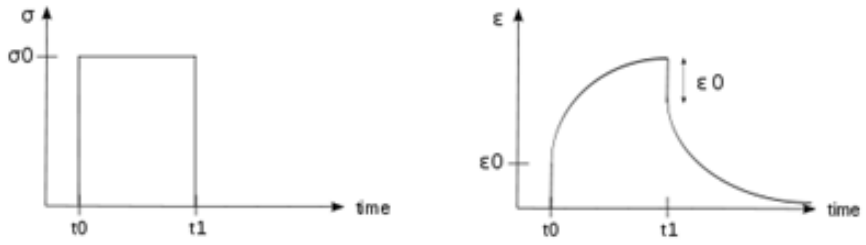

Figure 2-3: Creep test for viscoelastic material characterization (Beijer and Spoormaker, 2002)

Functional relation which describes the viscoelastic behaviour can be expressed either in integral or differential forms. Integral forms are very general and suitable for theoretical analysis while differential forms are related to rheological models that provide direct physical interpretation of viscoelastic behaviour (Marques and Creus, 2012).

2.4.2.1 General integral relations

Linear viscoelasticity has been successfully used in representing time-dependent mechanical behaviour under small deformation and low stress (Roberts-Tompkins, 2009). In linear viscoelastic materials, the constitutive equation which relates some physical phenomenon such as time dependent stress, σ(t), time dependent strain, ε(t), time and temperature with each other relating and can be evaluated with the Boltzmann integral as follow (Oza et al., 2003, Beijer and Spoormaker, 2002)

$$\sigma(t) = \int_0^t E(t-\tau)\frac{d\varepsilon(\tau)}{d\tau}d\tau \tag{2.10}$$

and the inverse relation

$$\varepsilon(t) = \int_0^t J(t-\tau)\frac{d\sigma(\tau)}{d\tau}d\tau \tag{2.11}$$

where J(t) is the creep compliance and E(t) is the relaxation modulus.

2.4.2.2 Rheological models

A classic description and a way to derive a viscoelastic constitutive model is through the use of mechanical analogue based on the series and parallel association of elastic and viscous elements. Simple mechanical analogies used to represent the linear viscoelastic constitutive material consist of linear elastic spring and linear viscous dashpot (Chen, 2000). The constitutive equation for linear elastic component is

$$\sigma = E.\varepsilon \tag{2.12}$$

The constitutive equation for the viscous component is

$$\sigma = \eta.\frac{d\varepsilon}{dt} \tag{2.13}$$

Superimposing components with constitutive equations given by Equations (2.12) and (2.13) construct the linear viscoelastic models. Numerous constitutive models have been implemented to explain the viscoelastic behaviour of polymeric materials (Beijer and Spoormaker, 2002, Park and Balatinecz, 1998, Young and Lovell, 2011, Nunez et al., 2004, Pérez et al., 2008, Marais and Villoutreix, 1998). The simplest models are combination of a spring and a dashpot which are put in series and parallel, known as the Maxwell and Kelvin-Voigt models, respectively (Figure 2-4).

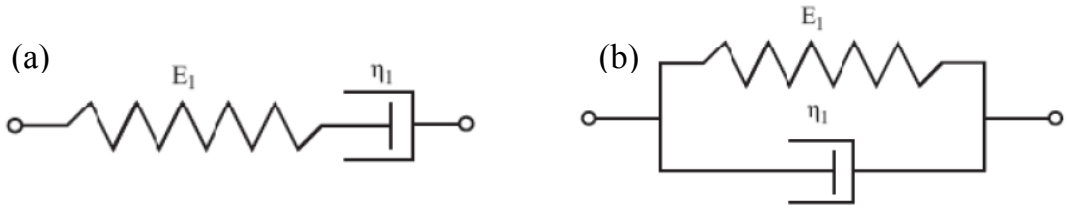

Figure 2-4: The basic mechanical viscoelastic models: (a) Maxwell model which put the spring in series with the dashpot and (b) Kelvin-Voigt model with spring and dashpot in parallel (Wineman and Rajagopal, 2000)

Although both of the models do not provide inadequate representation of viscoelastic behaviour (Roberts-Tompkins, 2009) of real materials, they can illustrate some important aspects of a viscoelastic material including the stress relaxation function G(t) and the creep function J(t). A more elaborate model is required to be able to incorporate comprehensive viscoelastic behaviour such as instantaneous elastic strain, deformation with decreasing strain rate and steady relaxation of strain with time

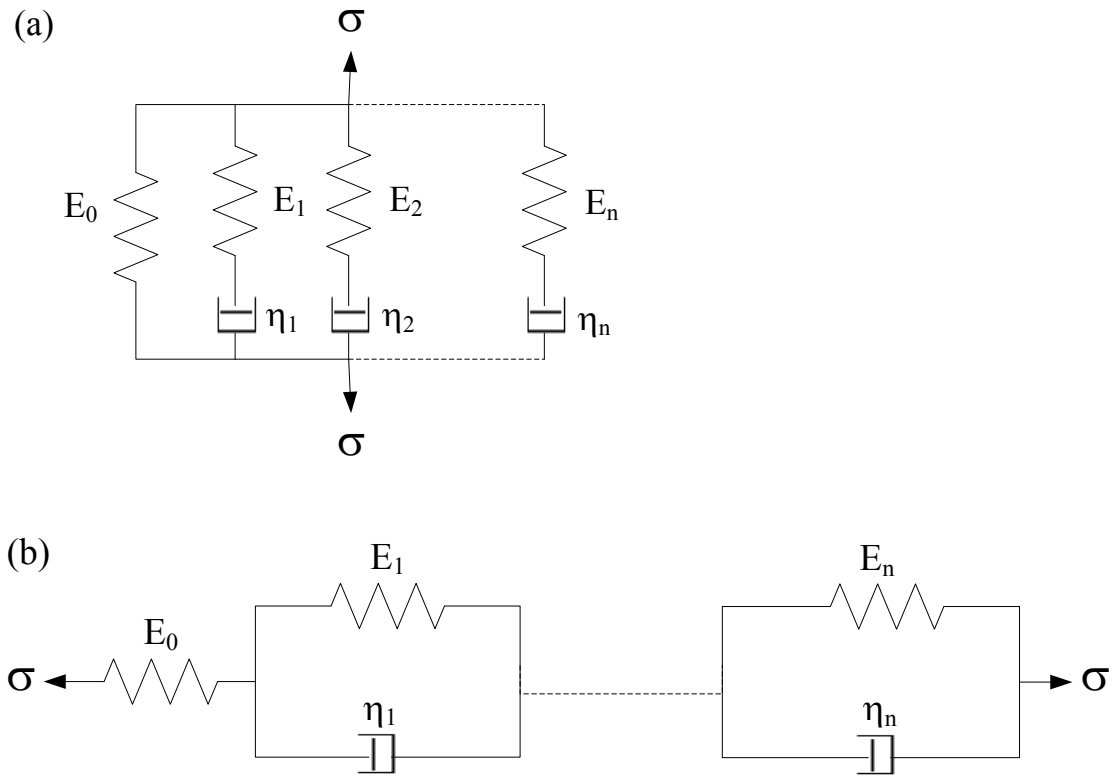

Figure 2-5: The generalized (a) Maxwell and (b) Kelvin models with instantaneous elasticity

The representation of viscoelastic model can be improved by increasing the number of parameters (Marques and Creus, 2012) through combination of some spring and dashpot elements, consisting of at least three elements (Tschoegl, 1989). A systematic way to do that is to develop generalized Maxwell and Kelvin model (Marques and Creus, 2012), which is shown in Figure 2.5. The generalized Maxwell model contains a linear spring in parallel with n number of Maxwell elements. In other hand, the generalized Kelvin model is composed of n + 1 constituent element in series, which consist of n Kelvin elements and a linear spring. Generalized Kelvin model is used to represent viscoelastic behaviour investigated from creep tests (Brazel and Rosen, 2012).

For the cases of one Maxwell unit and a Hookean spring in parallel, or one Kelvin unit and a spring in series, is known as the three-parameter viscoelastic model (Tomopoluos and Genin, 2013) or the standard linear solid (SLS). The SLS gives a relatively good description of the polymer behavior (Zhang and Wang, 2012) which is used to predict the viscoelastic behaviour of a solid-like material capable to predict both creep and relaxation. In this model, the modulus will gradually approach an equilibrium "elastic-like" value after a specified time. Figure 2-6 shows the schematic of the standard linear solid viscoelastic model, where E_0, E_1 and η_1 are the viscoelastic parameters to be determined.

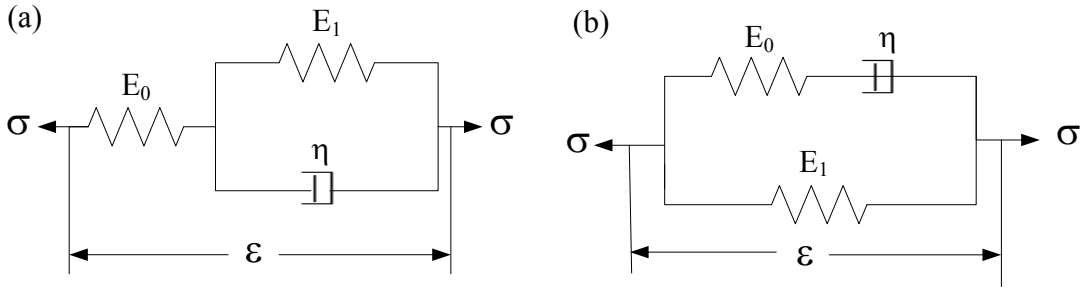

Figure 2-6: The standard linear solid model with: (a) Kelvin and spring in series and (b) Maxwell and spring in parallel

According to the SLS model where a spring and a Kelvin unit are in series, the creep strain is given by:

$$\varepsilon(t) = \frac{\sigma}{E_0} + \frac{\sigma}{E_1}\left[1 - \exp\left(-t\frac{E_1}{\eta_1}\right)\right] \tag{2.14}$$

where σ is the applied stress, t is time, E_0 is the elasticity component of instantaneous strain at t = 0 (moment of loading), E_1 is the elastic modulus of the spring, and η_1 is the polymer viscosity

of the dashpot element. The first term of the equation represents an elastic term, and the last term expresses the viscoelastic effect. The retardation time $\tau = \frac{\eta_1}{E_1}$ is a measure of the time required for the extension of the spring to its equilibrium length while being retarded by the dashpot. The parameters of Equation 2.14 can be obtained by fitting the equation to the experimental data.

There have been several attempts in building more complex models that can give a better representation of the viscoelastic behaviour of polymers. However, it is worth noting that as the number of elements increases, the models become physically less meaningful and mathematics becomes more difficult to calculate (Young and Lovell, 2011, Bandhyopadhya and Bose, 2013). The Burgers model has been extensively used and applied satisfactorily to model linear viscoelastic behaviour of several polymeric materials (Nunez et al., 2004, Xu et al., 2010, Tang et al., 2012, Ludueña et al., 2012, Pérez et al., 2008). This model is a series combination of the Maxwell and Kelvin models as illustrated in Figure 2.7. It divides the creep strain of a polymer into three parts: (1) the instantaneous deformation (Maxwell spring), (2) viscoelastic deformation (Kelvin element), and (3) the viscous deformation (Maxwell dashpot) which can be represented by

$$\varepsilon(t) = \varepsilon_1 + \varepsilon_2 + \varepsilon_3$$

$$\varepsilon(t) = \sigma\left\{\frac{1}{E_M} + \frac{1}{E_K}\left[1 - \exp\left(-t\frac{E_K}{\eta_K}\right)\right] + \frac{t}{\eta_M}\right\} \tag{2.15}$$

where ε(t) is the creep strain, σ is the stress, t is time, E_M and E_K are the elastic moduli of the Maxwell and the Kelvin springs, and η_M and η_K are viscosities of the Maxwell and Kelvin dashpots. This model has one retardation time, $\tau = E_K/\eta_K$.

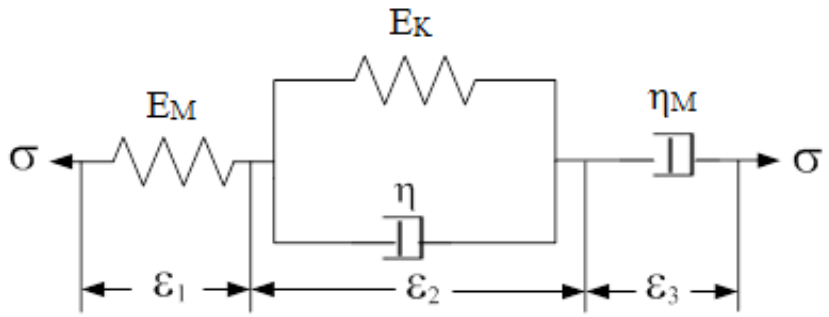

Figure 2-7: Schematic diagram of Burger's model in representing viscoelastic behaviour of material

2.4.2.3 Empirical model

Besides the mechanical analogue models previously discussed, molecular models such as Kohlrausch-Williams-Watts (KWW) model and power law model have also been used to describe the viscoelastic response of polymers (Ranade et al., 2005). The Findley power law model is an empirical mathematical model, which has been used to represent the creep data of polymer materials (Xu et al., 2010, Pérez et al., 2008, Tang et al., 2012).

$$\varepsilon(t) = \varepsilon_0 + \varepsilon_f t^k \tag{2.16}$$

where ε_0 is the time-independent strain, ε_f is the coefficients of time-dependent terms and k is a constant independent of stress.

This empirical model offers a relatively simple mathematical model, however it has a lack of providing qualitative descriptions of creep phenomenon.

2.4.3 Effect of fluid diffusion on viscoelastic constitutive model

The time dependent behaviour of polymeric materials depends not only on material properties but also on external conditions such as applied stress, temperature, humidity and absorbed liquid (Jia et al., 2009, Hatzigrigoriou et al., 2012). It is expected that viscoelastic properties may also change with the presence of liquid. These properties vary with time and result in the full coupling of two time-dependent variables (Chiang and McKenna, 1996). One variable accounts for the time-dependent response toward load, which characterizes the viscoelastic nature of a material while the other one is strongly influenced by the liquid content. Therefore, mechanical response assessment of a viscoelastic body requires to consider the variables as it accounts for the rate of stress relaxation (or creep) in the viscoelastic body, and also as it incorporates the changes in material properties during the diffusion process (Muliana and Rajagopal, 2011). For a thick material, the fluid diffusion process will attain equilibrium within a particular long period of time and may take slower than that of polymer relaxation (Weitsman, 2012).

The action of mechanical loads coupled with environmental factors such as humidity, temperature, and the presence of diffusant give rise to complex phenomena on material properties (Miranda Guedes et al., 2000). In analysing the mechanical response of a material, the constitutive equations should not only describe the time dependency of the material but also the environmental dependence.

Stouffer and Wineman (1971) developed a general constitutive relation for an environmentally-dependent linear viscoelastic material as an extension of the model by Morland and Lee (1960). The relaxation function is dependent on the transient environmental history, whereas the

parameters become a function of position and time. Drozdov (1997) has presented an in-depth review concerning the effect of temperature on viscoelastic behaviour. Studies on the effect of liquid content are later than those on temperature, but it is now receiving more attention from researchers.

2.4.3.1 Time-liquid content superposition

It has been reported that absorbed fluid has an analogous effect on temperature, where the effect of increasing liquid content on the decreasing storage modulus may be equivalent to that of the rising temperature. Thus, the effect of liquid content on viscoelastic behaviour can be described using a similar mathematical function of time-temperature superposition (Chaléat et al., 2008) and a time-liquid content superposition may hold. The applicability of the time-liquid content superposition principle for creep or stress relaxation data has been shown to various kinds of polymer (Zhou and Tashiro, 2001, Ishisaka and Kawagoe, 2004, Onogi et al., 1962). In developing a constitutive model based on the superposition, it is suggested that the effect of temperature and fluid content be taken into account not only with the relaxation parameter, but also on the elastic modulus (Drozdov, 1997).

The concept of time-temperature superposition suggests describing temperature effects by simply shifting the timescale of the viscoelastic response through a shift factor (Pramanick and Sain, 2006, Wineman and Rajagopal, 2000). The time shift factor is a parameter used to express the compliance function at any temperature, J (T), which can be expressed in terms of the reference compliance function J (T_0) as shown in the relations

$$J(t,T) = J(t', T_0) \tag{2.17}$$

where t is the actual time of observation measured from the first application of load and t' is the "reduced time", "intrinsic time" or "pseudo time". The shift factor $a_T = a(T,T_0)$ relates the real time t and the reduced time t' where T_0 is the reference temperature.

$$a(T,T_0) = \frac{t}{t'} \tag{2.18}$$

If creep compliance is measured at different temperatures and then plotted against log t, the horizontal distance between the curve at a reference temperature for which $a_T = 1$ and another curve at temperature T, is equal to log a_T. Thus, substituting Equation (2.17) to Equation (2.18) yields

$$J(t,T) = J\left(\frac{t}{a(T,T_0)},T_0\right) \tag{2.19}$$

Therefore, the analogy of time-temperature superposition can be applied as time-liquid content superposition in the following equation

$$J(t,C) = J\left(\frac{t}{a(C,C_0)},C_0\right) \tag{2.20}$$

Where $J(t,C)$ is the compliance function at liquid content C and log a_C is the horizontal distance between the curve at a reference liquid content, C_0 and another curve at liquid concentration C.

2.5 Finite Element Analysis (FEA) in Packaging Applications

The finite element (FE) is a numerical method of finding solutions to complex engineering problems, which are usually represented in the form of differential and integral equations. The basic principle of FEA is to divide the continuum problem of real structure into discrete problem having smaller elements in order to reduce the numerical complexity and error. The small elements are interconnected at points common to two or more elements (nodal points or nodes) and each of them are singly solved by a relatively simple mathematical equation. The solution of the whole body is obtained by combining the formulation of each finite element. Figure 2-8 illustrates the basic approach of the FEM to determine temperature distribution in a plate. The solution for this non-structural problem is to determine the temperature at each node by specifying a heat balance equation for each point in the plate which is then combined in a sum.

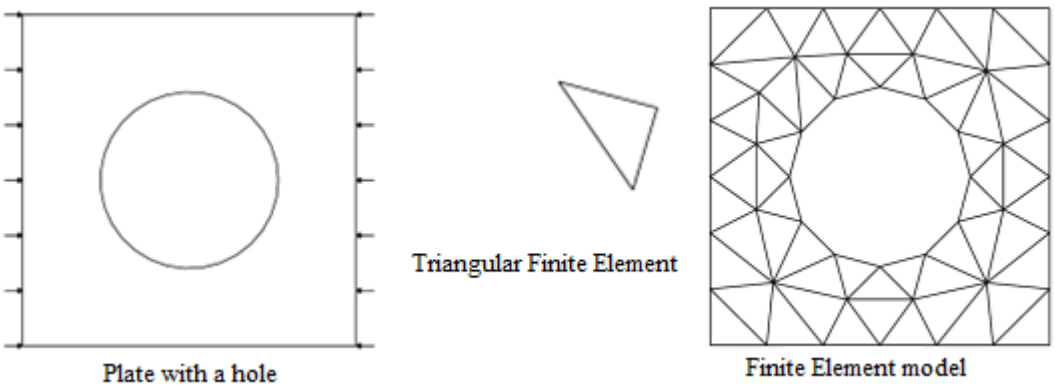

Figure 2-8: Finite element structure for thermal analysis, adapted from Fish and Belytschko (2007)

2.5.1 Structural analysis of packaging application

Finite Element Method (FEM) has been widely applied for evaluating the deformation behaviour of plastic packaging during development process (Abbès et al., 2010, Masood et al., 2006, Karalekas et al., 2001, Demirel and Daver, 2009, Vaidya, 2012). It is required that a plastic package is capable to maintain its desired configuration under various loading and environmental conditions. Some of those studies were performed by experimental investigation in validating the FE numerical studies and they reported a good agreement between them.

In structural analysis using FEA, initially, the packaged design is generated either using built-in design module in FEA software or other commercial parametric CAD (Computer Aided Design) software. Appropriate linear or non-linear method should be selected to represent the mechanical behaviour of material in response to applied load as discussed in Section 2.3. Complete analysis requires application of restraints and loads in the body representing the boundary conditions. Common loads applied in the package are pressure from the packaged product used to simulate carbonation pressure of packaged beverage (Demirel and Daver, 2009), bending which usually occurs in transportation of light–weight packaging (Vaidya, 2012) and top load crushing that assesses the axial load capacity of the package (Abbès et al., 2010, Karalekas et al., 2001, Masood et al., 2006). In achieving accurate result, it is crucial to specify suitable mesh geometry and dimensions. Once the model is defined, the processor performs the solution and results are presented as calculated stress and deformation.

2.5.2 Modelling of diffusion

Finite element analysis (FEA) is used to simulate and calculate the distribution of liquid diffusion. Most commercial FE software is not equipped with liquid diffusion modelling factor. But, analysis of liquid diffusion can be modelled using thermal mechanics function of commercial software (Jiang et al., 2008, Zhou et al., 2005) with an appropriate thermal-fluid analogy. An analogous technique to conduct liquid diffusion analysis should be used to enable modelling with commercial FEA package. The FEA implementation scheme is presented in Table 2-3.

Table 2-3: FEA thermal analogy for liquid diffusion modelling

Properties	Thermal	Liquid Diffusion
Field variable	Temperature, T	Concentration, C
Density	P (kg/cm^3)	1
Conductivity	K ($W/m.^0C$)	D (m^2/s)
Specific capacity	C ($J/kg.^0C$)	1
Coefficient of thermal expansion	α	β

Galloway and Miles (1997) simulated moisture weight gain or loss in plastic ball as a function of time, considering effects of package geometry and material selection. Moisture transport is modelled using standard equation for diffusion as described earlier in Equation (2.2) that was solved using standard separation variable techniques. The total weight gain was expressed analytically as a function of time that is obtained by integrating the local concentration over the volume of the rectangular block sample. Moisture diffusivity data were gathered by periodically weighing samples soaked in a humidity chamber. They were then used in the Finite Element Method (FEM) to model moisture absorption using a 3-D eight-noded transient diffusion element. FEM was also utilized by Cai et al. (2002) to simulate moisture-diffusion behaviour inside plastic packaging.

2.5.3 FE model development

Basically, the development of the FEA model consists of three main stages: (1) pre-processing, (2) analysis, and (3) post processing (Demirel, 2008). A commercial FEA software, ANSYS Workbench 14.0 will be used to numerically analyse the stress and deformation resulting from coupled thermal and mechanical load.

2.5.3.1 Pre-processing stage

In this stage, geometry of the component to be studied is defined as well as its finite element model. The models analysed in this thesis are created directly in 3D solid using ANSYS Design Modeller. This type of body is meshed with higher-order tetrahedral or hexahedral solid elements with quadratic shape functions. The material properties are then defined and assigned to the parts through an Engineering Data. A default mesh is automatically generated during initiation of solution, but it will be evaluated to check whether it produces more precise solution with a finer mesh. According to the defined boundary conditions, loads and supports in terms of degree of freedom (DOF) are applied on geometric entities.

2.5.3.2 Analysis stage

The ANSYS Solver solves the mathematical equations relating the forces to the displacement within a particular time frame. Since transient analysis is applied in the model, a time integration procedure is used to obtain solutions to the system equation at discrete points in time. The integration time step (ITS) which represents the change in time between solutions is determined using the following equation

$$\Delta t = \frac{\Delta x^2}{4D} \tag{2.21}$$

where Δt is the time step size, Δx is the average element length and D is diffusion coefficient.

2.5.3.3 Post-processing stage

The numerical results achieved from the analysis are shown in this stage, including directional and total deformation, components of stresses and strains. In analysing the diffusion process, temperature variable represents the diffusant/liquid content. Those results are presented in contour and vector plot on the deformed geometry.

2.6 Proposed Methodology

In evaluating a package performance by taking into account the mass transport (diffusion) of product substances, this research will utilize the procedure proposed by (Springer, 1988) which calculates the hygrothermal stress of composites. The modified methodology in analysing the mechanical response of a package under liquid diffusion is presented in Figure 2-9.

The procedure for assessing the effect of liquid diffusion on mechanical behaviour of a liquid-sensitive material is as follows:

1) Identify the characteristics of diffused liquid into a specified geometry, including the rate of diffusion, saturated liquid content (if applicable) and the diffusion behaviour (Fick's or non-Fick's diffusion)
2) Calculate the distribution of liquid content inside the material as a function of time and position
3) Determine swelling and changes in mechanical properties due to liquid diffusion to develop the appropriate material constitutive equation
4) Calculate the diffusion-induced stress and deformation based on the distribution of liquid content combining with applied external load

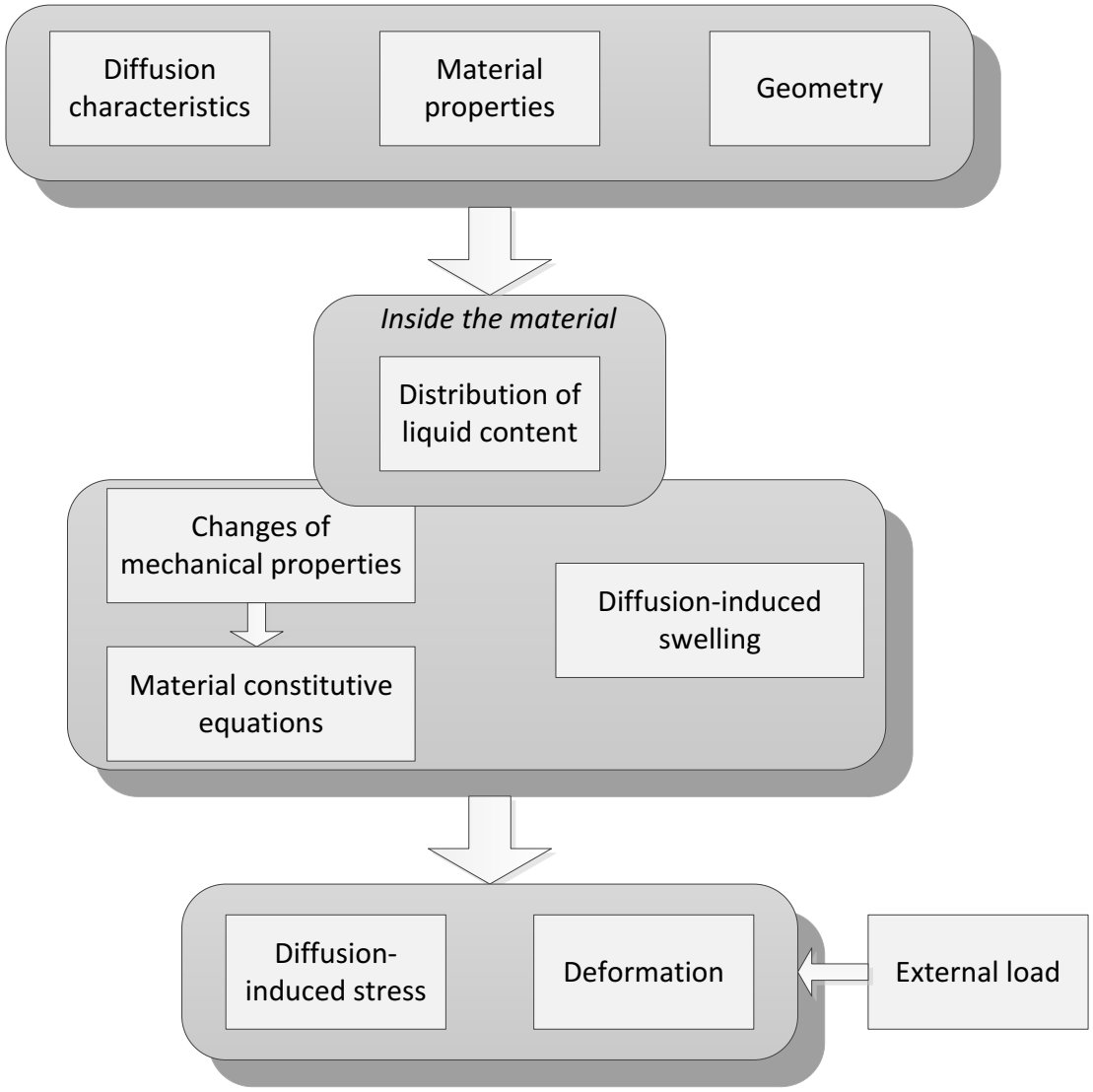

Figure 2-9: Proposed methodology in evaluating mechanical performance of a package considering the mass transport of packaged substances

2.7 Conclusion

This chapter has reviewed literatures related to mass transfer effect on change of mechanical properties of PLA package. Currently used for relatively very short-term application, little attention was given to the load bearing capabilities. Considering a fluid-based application in relatively thick package, variation of mechanical properties over the service life of the package may occur due to non-uniform liquid content within the thickness. In addition, deterioration of PLA material properties with time could be more severe with increasing environment temperature. Effect of absorbed liquid by the package can be described into the viscoelastic constitutive equation representing the evolution of mechanical response with time. Using commercial FEA software, it is possible to simulate and provide a prediction of the package

performance under any realistic conditions without moulding and testing. A numerical modelling considering degradation of material properties due to sorption of aroma compound has been successfully developed for PP container (Abbès et al., 2010). However, influence of spatially inhomogenous material properties in evolution of mechanical behaviour with time is still not clear. Moreover, swelling-induced stress that may result in consequence of non-uniform liquid concentration requires further investigation.

For extended service in more durable and longer-term applications, knowledge on how the material responds to particular load at specified periods of time is essential in determining long term-stability and time-dependent performance of the package.

CHAPTER 3 EXPERIMENTAL METHOD

3.1 Introduction

This chapter outlines experimental method used in evaluating the changes of mechanical properties of the PLA-based material under the condition of fluid diffusion. The first section concerns a procedure in characterizing the diffusion of model fluid into the material, while the next section presents a series of mechanical testing to evaluate the shifting of material properties with different treatments of liquid exposure.

3.2 Characterisation of diffusion

3.2.1 Material

The biodegradable polymer used in this study was starch based PLA resin produced by BIOTEC, a subsidiary company of Biome Technologies. It was supplied by BioPak Pty Ltd Australia in granule form shown in Figure 3-1, known as Bioplast GS2189 (Biotec). This compound polymer is composed of 90% corn-derived PLA and reinforced with 10% potato starch (Almeida, 2011)

Figure 3-1: Granules of Bioplast GS2189

3.2.2 Melt flow analysis

In determining processing parameters to convert the pellet into test samples, it is necessary to identify the viscosity (melt flow index) of the material before being processed (Bryce, 1996). The melt flow index test was performed according to ASTM Standards, ASTM D1238-79 with the pellets of the samples using a CEAST MFI tester as shown in Figure 3-2.

Figure 3-2: Melt flow rate measurement in CEAST instrument

Measurement of melt flow index (MFI) is carried out with the load 2.16 kg at 190°C and the MFI value is determined as the weight of the extrudate (in grams) that passes through the die in 10 minutes.

3.2.3 Sample preparation

The material in pellet form was converted into test samples according to the manufacturer's product manual, using a Battenfeld BA 350/75 injection moulding machine shown in Figure 3-3. The pellets were injection moulded into standard rectangular izod impact specimens according to ASTMD256 (63.5 x 13 x 3 mm) and tensile specimens according to ASTM D638, as shown in Figure 3-4. Injection temperature profile was controlled at 230/220/190/30°C from the feeding zone to the nozzle with an injection pressure of 1740 bar.

Figure 3-3: Battenfeld BA 350/75 injection moulding machine

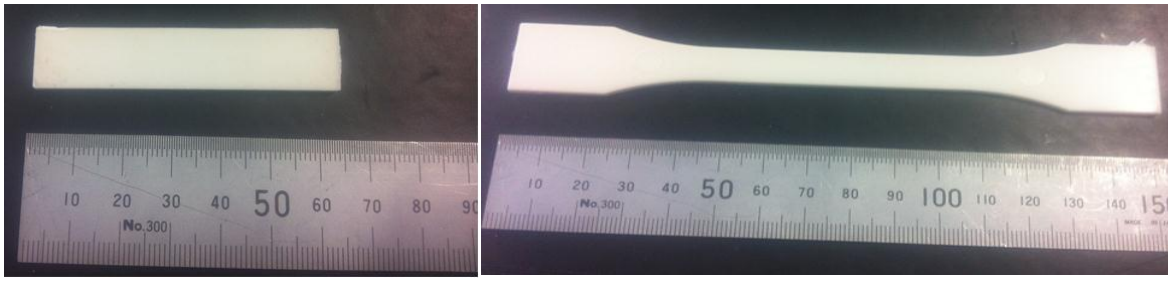

Figure 3-4: The injection moulded rectangular and tensile specimens

Figure 3-5: Drying of specimens before fluid immersion

Before immersion, the samples were dried in a vacuum oven at 50°C as shown in Figure 3-5. The samples were periodically weighted, and the saturated weight is recorded as the weight of dry material. It is found that dry saturated weight gain is achieved after 3 hours drying at 50°C vacuum oven.

3.2.4 Immersion of samples

Immersion fluid for conducting this experiment is gasoline, provided by a local fuel station. In varying levels of fluid concentration, different immersion temperatures were used to accelerate the level of liquid absorption. Unleaded gasoline was chosen as aggressive enough to accelerate the degradation that would occur in an application exposed to liquid and chemical solvent. Distilled water or moisture would be the most common media in evaluating the hygroscopic effects of polymer, but it is less aggressive and would require longer test duration. The unleaded fuel used as an immersion liquid constitutes 50/50 toluene-iso octane mixture.

Standard test method of SAE J1748 was used in the immersion test. This method provides standard for determining physical property of polymer material exposed to gasoline/oxygenated fuel mixture. The rectangular injection-moulded samples were completely immersed in hydrocarbon liquid in a ratio of 3 samples to 50 ml of liquid (Figure 3-6). Specimens were hanged with a stainless steel wire and separated with glass beads. The tubes were covered and the samples were immersed to the point of saturation under 4 different conditions: (1) room temperature where the temperature was monitored with a digital thermometer at 20 ± 3°C, (2) a fridge with temperature monitored at 5 ± 1°C and a chamber set at (3) 30°C and (4) 50°C.

Figure 3-6: Immersion of PLA samples in a covered tube

Gravimetric measurement was used to determine the fluid uptake during the diffusion process. The specimens were removed periodically for weight measurement until the saturation occur, taking average from 5 samples. The samples to be weighted were removed from the tube and place them in a container of the same fluid at room temperature. Then, each sample from the cool container were removed and gently wiped with a tissue before weighted. To prevent any further weight loss due to evaporation, the specimens are weighted using a PRECISA 125A analytical balance in a tightly closed bottle as shown in Figure 3-7.

Figure 3-7: Weight measurement of an immersed sample in closed weighting bottle using analytical balance

The apparent weight gain, ΔM is calculated using the following relationship

$$M_t(\%) = \frac{\{(weight\ of\ bottle + sample\ ) - weight\ of\ bottle\} - original\ weight\ of\ sample}{original\ weight\ of\ sample} x100 \tag{3.1}$$

or simply written as

$$M_t(\%) = \left(\frac{m_t - m_0}{m_0} \right) x\,100 \tag{3.2}$$

where m_0 and m_t are the weight of dry specimen before and during ageing, respectively. Length swelling (LS) was assessed by measuring the average length of each specimen during the immersion test (l_t) and the dry one (l_0) and then calculated using the following equation

$$LS = \left(\frac{l_t - l_0}{l_0} \right) x\, 100\% \tag{3.3}$$

Determination of equilibrium is based on standard recommended by SAEJ1748, which compares data from two or more period to see no significant difference among the periods (SAE, 2005). Once it has been determined that equilibrium has been reached, the equilibrium weight gain can be determined as an average from the last two consecutive weighting.

3.3 Evaluation of mechanical performance

This section will outline the methodology in evaluating the properties of material which consists of the test machinery, sample size and test procedure according to available standard test method. The mechanical tests performed measured the following properties: tensile, flexural, impact and dynamic modulus. Those properties which characterize strength, stiffness and toughness of material were measured before and after fluid immersion

In evaluating changes of mechanical properties with the amount of liquid absorption, mechanical tests are performed in saturated specimens to represent the properties in a particular liquid content. It is to ensure that mechanical properties are measured in specimens containing uniform liquid content (Jia et al., 2004) thereby allowing more accurate relationship between the two parameters. Mechanical tests in non-immersed (dry) samples are carried out to obtain results with zero liquid content in the same manner as with the immersed samples. Before measurement, the specimens are placed in another container filled with the same liquid at the standard laboratory temperature for a period of 0.5 to 1 hour. Testing is completed within 5 minutes of removal from the cooled fluid to minimize effect of dry out.

3.3.1 Tensile properties

Tensile testing was performed under an international recognized standard, the ASTM methods D638: Standard test method for tensile properties of plastics. The “dog bone” shaped samples produced by injection moulding machine shown in Figure 3-4 were used in this test. Width and thickness of each sample required to calculate the area were measured using a Kincrome digital vernier caliper with resolution of 0.01 mm.

Figure 3-8: Break of tested sample held by a twin-self clamping jaw after load applied in tensile test

The samples were tested to failure under tension at a cross head speed of 50 mm/min by using Zwick Z010 Universal Testing machine with a pre-load of 0 N (Figure 3-8). The tests data for maximum tensile strength, strain at maximum load and tensile modulus were collected from the TestXpert version 8.1 software. This software is also used to control the operation of test machinery. An axial force is applied to a specimen of original length (L_0) that would elongate until fracture occurs. Elastic modulus was measured between 2% and 4% strain by linear regression. The load and change in length between two fixed points (gauge length) is recorded and used to determine the stress-strain relationship.

3.3.2 Flexural properties

Flexural tests were done using the same Zwick universal testing machine (Figure 3-9) used for tensile testing outlined in section 3.3.1 with the 3-point bending rig setup. Testing procedure was performed following ASTM D790: Standard test method for flexural properties of unreinforced and reinforced plastics. The rectangular samples produced using injection moulding machine as shown in Figure 3-4 were used in this test.

Testing was performed with 5 mm radius loading nose and 5 mm radius support with a pre-load of 0.2N. The load was placed midway between the supports with a span of 40 mm. The crosshead speed applied was 1 mm/min. The TestXpert software version 8.1 was used to generate flexural strength of each sample tested.

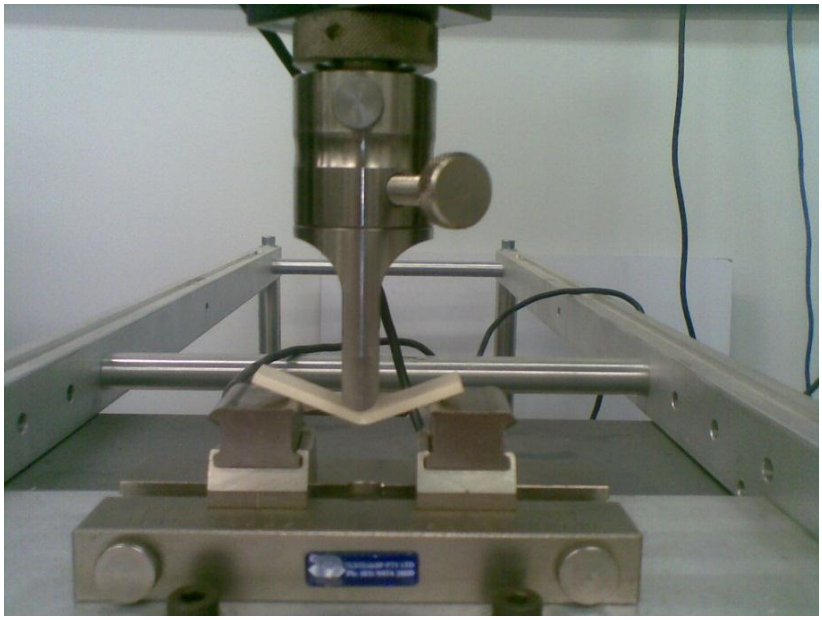

Figure 3-9: Flexural testing on Zwick Z010 Universal testing machine

3.3.3 Impact properties

The notched Izod impact strength test was conducted on a CEAST resil impact tester (Figure 3-10) according to ASTM D256 at room temperature.

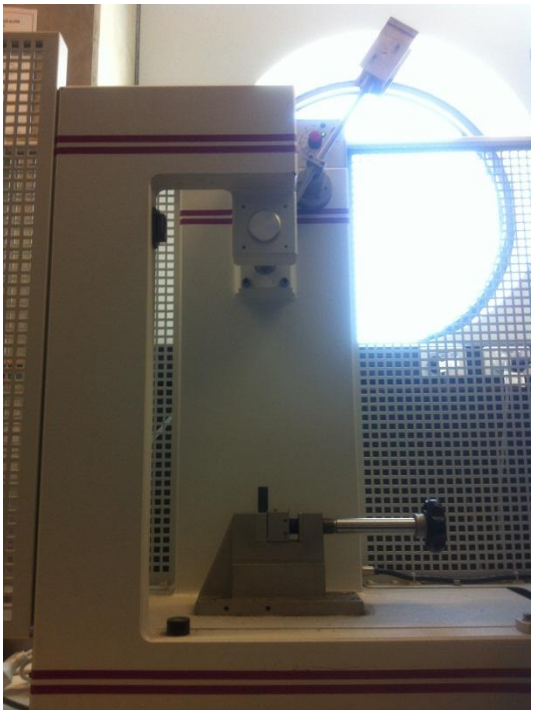

Figure 3-10: The CEAST resil impact tester

Impact strength was measured as impact energy required per width of specimen. At least five specimens of each sample were tested to obtain the average value of the mechanical parameters and their standard deviation. The samples tested were rectangular samples made using the injection moulding machine and notched as shown in Figure 3-11. The specimen is placed in the vise which is then submitted to the strike of the pendulum. The measured output from the instrument is the estimated breaking energy while simultaneously subtraction the compensation energy, which consist of the friction and wind age energy. The test may result in one of three types of failures in the specimen i.e.: a complete break, a partial break (hinge), or a non-break.

Figure 3-11: The notched samples for impact testing

3.3.4 Dynamic properties

Changes in viscoelastic properties, i.e. the glass transition (T_g) and storage modulus (E') of the material, along liquid content in the specimens, were measured using a TA Instruments Dynamic Mechanical Analyser (DMA) 2980 as shown in Figure 3-12.

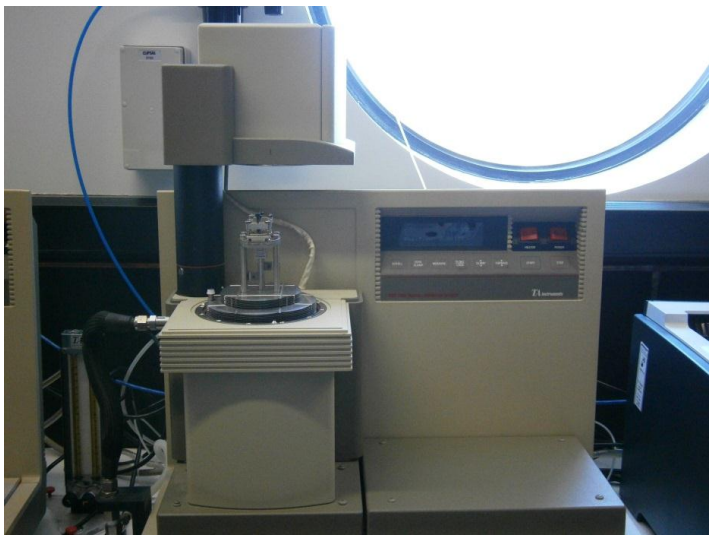

Figure 3-12: Measurement of viscoelastic properties using Dynamic Mechanical Amalyzer

Thermal Advantage software was used to control the testing apparatus, while TA Instruments Universal Analysis used to analyse the result. Specimens of dimension 60 x 10 x 3 mm were cut from injection moulded tensile shape shown in Figure 3-4. Width and thickness of each sample were measured using a Kincrome digital vernier caliper with resolution of 0.01 mm.

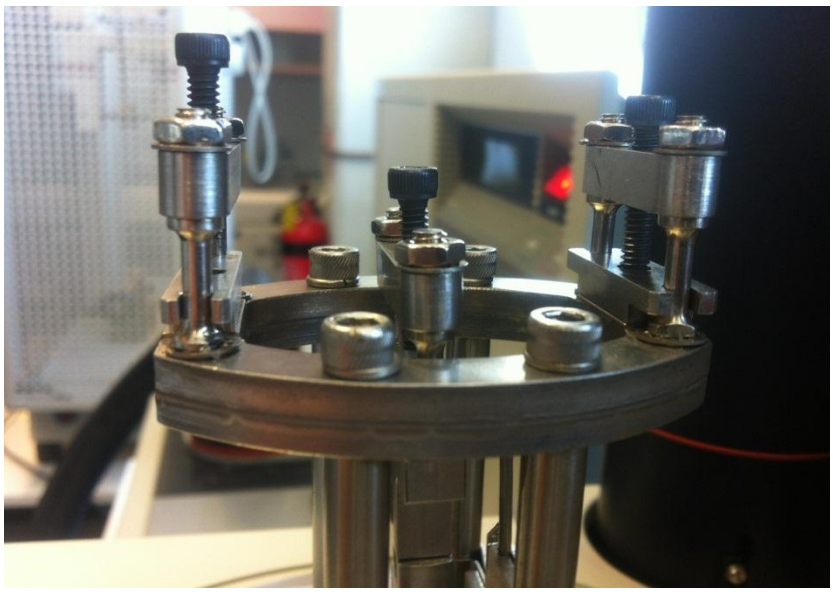

Figure 3-13: Cantilever stage for dynamic mechanical analysis using TA Instruments

Each sample containing different levels of liquid content is tested in a single cantilever mode shown in Figure 3-13 within the DMA thermal chamber. The dynamic properties were measured over a temperature range of 20° to 80°C, using a frequency of 1 Hz. The DMA will record material response to deformation and determines the following viscoelastic properties: storage modulus (E'), loss modulus (E") and tan δ. The value of T_g is determined from the peak in loss modulus and tan δ curves.

3.3.5 Creep test

Creep experiments are conducted in the same instrument used for DMA analysis in the film tensile creep mode for specimens with various levels of liquid content. Samples with different levels of liquid content were clamped within the DMA chamber as shown in Figure 3-14. Considering the DMA result, experiment is undertaken at 3 (three) different isotherms, 30, 40 and 50^0C, to evaluate the influence of temperature on creep performances. For each isotherm, a constant stress of 0.45 MPa was applied for 60 min, followed by a 10 min recovery period. The soak time, that is the equilibrium time to have the same temperature for all parts of the specimen, was set to 5 min. The sample dimensions were approximately 50 x 12 x 2 mm. The testing device is controlled using the Thermal Advantage software and analysed using the TA Instruments Universal Analysis software.

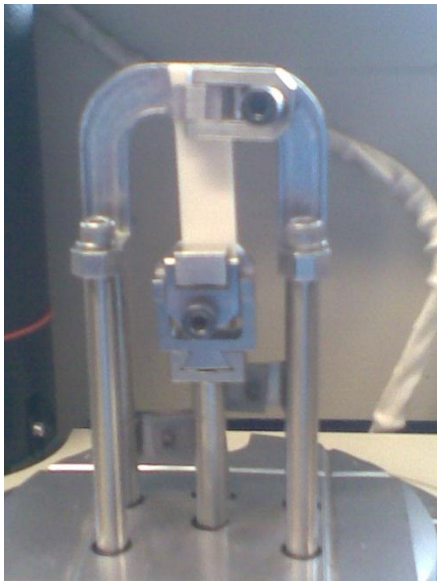

Figure 3-14: The tension film clamp of the TA Instruments DMA 2980

3.3.6 Thermal analysis

Thermal properties were determined using Differential Scanning Calorimeter (DSC 2010, TA Instrument) under nitrogen atmosphere as shown in Figure 3-15. Heating runs were conducted from room temperature to 200°C at a heating rate of 3°C/min. The weights of the PLA specimens for DSC were 7-10 mg, taken from cross sections of the creep test rectangular bars.

Figure 3-15: Thermal analysis using the Differential Scanning Calorimeter

The glass transition temperature (T_g), cold crystallization temperature (T_c), melting temperature (T_m), and melting enthalpy (ΔH_m) were obtained using the heating scans. The percentage crystallinity of the specimen was determined using a value of 87.92 KJ/kg for the heat of fusion for the full crystallinity of the Bioplast GS2189 material (Almeida, 2011) and calculated using the following equation:

$$\%\ Crystallinity = X_C = \frac{\Delta H_m - \Delta H_C}{\Delta H_m} \tag{3.4}$$

where ΔH_m is the measured endothermic enthalpy of melting and ΔH_c is the exothermic enthalpy that is absorbed by the crystals formed during the DSC heating scan. The heat of fusion was obtained by integrating the area under the endothermic peak.

In order to investigate effect of heat conditioned and applied stress on the structural changes of dry and immersed material, the samples are conditioned in DMA and TGA (Thermogravimetric) chamber prior to the DSC test. The samples are clamped in the DMA tensile creep method at 50°C isotherms with 0.45 MPa applied stress for 60 minutes to simulate the conditions at elevated temperature with stress applied. The TGA shown in Figure 3-16 is used to simulate the elevated temperature condition but with no stress applied by equilibrating the samples for 60 minutes at 50°C.

Figure 3-16: Conditioned of samples in thermogravimetric (TGA) chamber

3.3.7 Time-temperature superposition

The effect of liquid content on viscoelastic behaviour is described using a similar mathematical function of time-temperature superposition. Therefore, the analogy of time-temperature superposition is applied as time-liquid content superposition. This concept applies Equation (2.20) where the creep data to be plotted is obtained from different levels of liquid content instead from different temperature levels.

Creep experiment data and parameters are entered using the Creep TTS template available in the TA Instruments Thermal Advantage software. To obtain the master curve of time-liquid content superposition, all the log time-creep strain curves of diverse liquid content levels from each test temperature are overlaid. The selected reference liquid content is taken at 0% and the shifting automatically performed by software.

CHAPTER 4 CHARACTERIZATION OF THE MASS TRANSPORT

4.1 Introduction

Interaction of the package with its packaged product and the environment leads to mass transfer between them which in turn directly and indirectly affect the quality of product. Diffusion of external molecules from the environment and internal substances from the packaged product into the package can change the properties of material which alter the capability of the package in protecting the quality of the packaged product. Dependence of material properties on absorbed substances is of concern especially in the relatively thick package design since time taken to reach saturated concentration is proportional to the thickness. In many applications, the mass transport in the package is likely to be a transient rather than steady state. The diffusion of a liquid substance, for the example, may take quite long period of time for reaching a saturated condition. Because of time and spatial variation of absorbed substance, in-homogeneous properties may occur within the package. Therefore, an understanding of mass transport characteristics is essential to specify accurate material properties data used in analysing mechanical behaviour of the package.

Many different researches have examined mass transport in PLA materials in forms of gas, especially water vapour (Oliveira et al., 2006, Cairncross et al., 2006) and aroma compound (Auras et al., 2006a, Salazar et al., 2012, Colomines et al., 2010). Generally, there are two main reasons of their studies: (1) to describe effect of hydrolytic degradation in terms of changes of moisture sorption properties, (2) to specify the permeability of the substance in relation with the barrier properties. Some disagreements in sorption mechanism of moisture have been found in the literature. One study observed a typical Fickian diffusion which is a rapid uptake in the first period followed by a slower approach toward constant moisture content indicating equilibrium (Harris and Lee, 2010). Other study shows similar behaviour in the initial phase however equilibrium conditions cannot be attained after quite long period of exposure time (Holm et al.,

2006). In the case of aroma compound sorption, Auras et al. (2006a) showed a typical Fickian characteristic in PLA specimens with 23.2±1.78 μm thickness which took more than 30 days to have a saturated weight gain at 30°C. For packaging application, the permeability coefficient of gas sorption is considered as being most important parameter since it better describes the quality of the barrier of a material and more useful in calculating the shelf-life of packaged product. Permeability coefficient, P, in kg m m^{-2} s^{-1} Pa^{-1} is calculated as

$$P = D.S \tag{4.1}$$

where D is diffusion coefficient and S is the solubility coefficient of the permeant vapour (kg m^{-3} Pa^{-1}). The solubility is defined as fraction of the total mass of absorbed vapour, M_∞, with the product of the permeant driving pressure (Pa), p, and the volume of the specimen, V.

$$S = \frac{M_\infty}{V.p} \tag{4.2}$$

Particularly relevant in applications for plastic water bottles and coated drug eluting stents, some investigations were focused on sorption and diffusion of liquid water in PLA (Sharp et al., 2001, Davis et al., 2011). Gravimetric sorption methods which measure change of mass are commonly used in investigating liquid sorption in polymeric materials (Zaki et al., 2009). The diffusion coefficient of absorbed liquid can be measured by immersion of specimens in liquid and then removed regularly to be weighted. The mass uptake is fitted to a simple Fickian model to specify the value of diffusion coefficient.

This chapter presents the study of an organic liquid sorption in PLA material using simple gravimetric method following experimental work on immersion described in section 3.2.4. Actually, gasoline, a type of an organic liquid, is one of the most aggressive fluids to many commercial polymers. A study found that unleaded gasoline has greater effect on the performance of a polypropylene compared to water, chemical solutions (base and acid solvent) and diesel engine oil (Salvador, 2003). This model fluid was chosen in this study to test the performance of PLA in a rather unfavourable case. It is expected that the model fluid will be aggressive enough to accelerate the degradation in PLA material in a short time.

The objective of this work is to describe liquid content profile in a package by firstly defining the diffusion parameters. Varying conditions of temperature are used to have different levels of liquid content for further investigation. A FEA numerical model is proposed to analyse the sorption behaviour of liquid, which is capable to simulate different scenarios in evaluation of new applications for PLA package.

4.2 Analytical solution

Among several models describing the sorption phenomena in polymer, the Fick's diffusion model is the simplest and the most widespread model satisfactorily applied in many polymeric materials with certain temperature ranges. The Fick's second law is defined as follows (Neogi, 1996)

$$\frac{\partial C}{\partial t} = \nabla.(D\nabla C) \tag{4.3}$$

For isotropic material where $D = D_x = D_y = D_z$, equation (4.3) can be simplified as

$$\frac{\partial C}{\partial t} = D\left(\frac{\partial^2 C}{\partial x^2} + \frac{\partial^2 C}{\partial y^2} + \frac{\partial^2 C}{\partial z^2}\right) \tag{4.4}$$

Consider an infinite plate with thickness δ exposed to a diffusant concentration, C, and assume that the concentration varies only in the z direction (one-dimensional). The initial temperature and diffusant concentration are assumed to be uniform. In transient state condition, where the diffusant content varies within time, the governing equation to be solved is

$$\frac{\partial C}{\partial t} = D\frac{\partial^2 C}{\partial z^2} \qquad ,0 < z < \delta \tag{4.5}$$

The solution of Equation (4.5) can be expressed using separation variables, z and t as:

$$C(z,t) = f(z)g(t) \tag{a}$$

The general solutions of above equations are (Noda et al., 2003)

$$for\ s = 0,\ g(t) = E\ and\ f(z) = Fz + G \tag{b}$$

$$for\ s \neq 0,\ g(t) = He^{-Ds^2 t}\ and\ f(z) = I\sin sz + J\cos sz \tag{c}$$

where E, F, G, H, I and J are constants. Since the solutions must exist for arbitrary value of s, the general solution may be written in the following form

$$C(z,t) = (K\cos sz + L\sin sz)e^{-Ds^2 t} + Mz + N \tag{4.6}$$

where K = JH, L = IH, M = EF and N = EG

Distribution of fluid content C as function of time t and position z will be determined using Equation (4.6) based on the specified boundary conditions.

Consider a case where a slab is exposed to diffusant at one end, while another end is perfectly insulated. Figure 4-1 shows a slab with thickness, $l = \delta$ exposed to saturated diffusant uptake $C = C_m$ at $z = l$ and no diffusion allowed at $z = 0$.

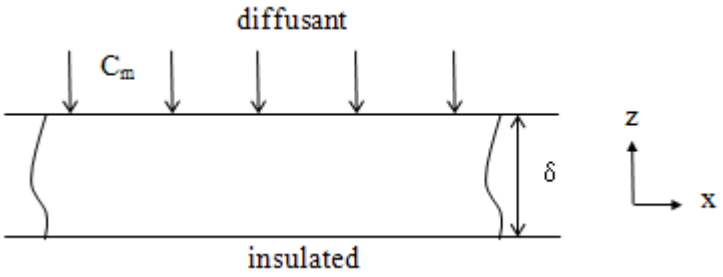

Figure 4-1: Illustration of one dimensional one-side plate diffusion

The initial and boundary conditions are

for $t = 0$, $C = 0$ at $0 < z < l$

for $t > 0$, $C = Cm$ at $z = l$ (4.7)

$\frac{\partial C}{\partial z} = 0$ at $z = 0$

Substitution of Equation (4.6) into the boundary conditions (4.7) gives the solution of equation (4.5), which describes the diffusant concentration C as a function of position z and time t is

$$C(z,t) = C_m\left(1 - \frac{4}{\pi}\sum_{0}^{\infty}\frac{(-1)^n}{(2n+1)}exp\left[-\frac{(2n+1)^2\pi^2 Dt}{4l^2}\right]cos\frac{(2n+1)\pi z}{2l}\right) \quad (4.8)$$

where C_m is the maximum diffusant concentration that is reached in the material for a given ambient condition (constant concentration at the surfaces).

Equation (4.8) can be written in terms of the dimensionless parameters

$$F_0 = \frac{Dt}{l^2} \qquad ,Z = \frac{z}{l} \quad (4.9)$$

Thus, the function of liquid concentration can be expressed as

$$C(z,t) = C_m\left(1 - \frac{4}{\pi}\sum_{0}^{\infty}\frac{(-1)^n}{(2n+1)}exp\left[-\frac{(2n+1)^2\pi^2 F_0}{4}\right]cos\frac{(2n+1)\pi Z}{2}\right) \quad (4.10)$$

Since $l = \delta$, the dimensionless parameters for one-side liquid diffusion is given by

$$F_0 = \frac{Dt}{\delta^2} \qquad ,Z = \frac{z}{\delta} \quad (4.11)$$

Equation (4.10) describes the relative diffusant concentration, which cannot be directly obtained through experiment. Thus, the integration of Equation (4.10) is performed to obtain the weight gain of immersed sample (Crank, 1967) as follows:

$$\frac{\int C(z,t)}{C_m} = \frac{M_t}{M_m} = 1 - \frac{8}{\pi^2}\sum_{n=0}^{\infty}\frac{1}{(2n+1)^2}exp\left[-\frac{(2n+1)^2\pi^2 F_0}{4}\right] \quad (4.12)$$

where M_t is the mass of diffusant after absorption time of t and M_m is mass of saturated absorption.

For another case in which the slab is exposed to liquid at both of its surfaces, as shown in Figure 4-2, the symmetric point at the central plane of the sheet is considered to be insulated (Crank, 1967). Therefore, this point is taken as z = 0 and the surfaces $= \pm l = \pm \delta/2$.

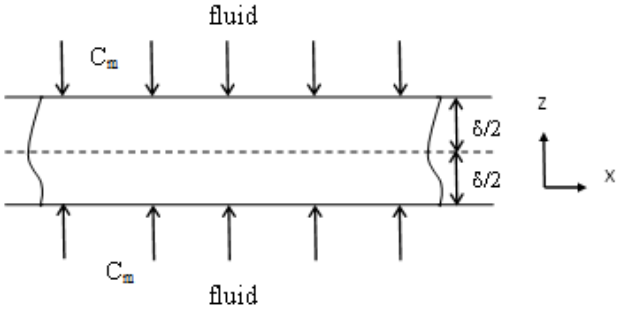

Figure 4-2: Illustration of one dimensional two-side plate diffusion

Therefore, the solution for equal surface concentrations in a plane sheet can be described using Equation (4.10) where the dimensionless quantities F_0 and Z are

$$F_0 = \frac{Dt}{\left(\delta/2\right)^2} \qquad ,Z = \frac{z}{\left(\delta/2\right)} \quad (4.13)$$

Value of diffusion coefficient is determined by considering the slope of the first part of weight gain curve versus square root of immersion time. It was assumed that diffusion coefficient in the model was independent of time.

At initial absorption stage $\left(\frac{M_t}{M_m} \leq 0.5\right)$, the following equation is used to calculate diffusion coefficient (Chen et al., 2005):

$$\frac{M_t}{M_m} = \int_0^t \frac{2}{\delta}\sqrt{\frac{D}{\pi t}}dt = \frac{4}{\delta}\sqrt{\frac{Dt}{\pi}} \tag{4.14}$$

where δ is the thickness of the material, M_t is the weight gain at time t and M_m is the saturated weight gain.

Considering the significant role of environment temperature on the diffusion process, it is necessary to develop a model predictive for a range of temperature conditions. The dependence of two important parameters: diffusion coefficient, D and saturated weight gain, M_m on temperature T was identified using the experimental data. The relation between the diffusion coefficient and temperature can be represented by an Arrhenius-type relation (Callister and Rethwisch, 2010)

$$D = D_0 . \exp\left[\frac{-E_a}{RT}\right] \tag{4.15}$$

where D_0 is a constant that depends on the material and the solvent, E_a is the activation energy, R is the universal gas constant, and T is the absolute temperature.

4.3 Experimental result

A series of PLA specimens were immersed in an organic liquid at various temperatures until saturated. For comparison, two kind of commercial polymer namely Polypropylene (PP) and High Density Polyethylene (HDPE) were also given the same treatment. Determination of equilibrium is based on standard recommended by SAEJ1748 which compares data from two or more period to see no significant difference among the periods (SAE, 2005).

The weight gain calculated using Equation (3.1) provided in section 3.2.4 is plotted to the immersion time for each material. Figure 4-3 shows the liquid uptake of three different types of polymer after exposure at room temperature as a function of immersion time. The theoretical curves deduced from Fick's second law expressed in Equation (4.12) are also plotted in the figure.

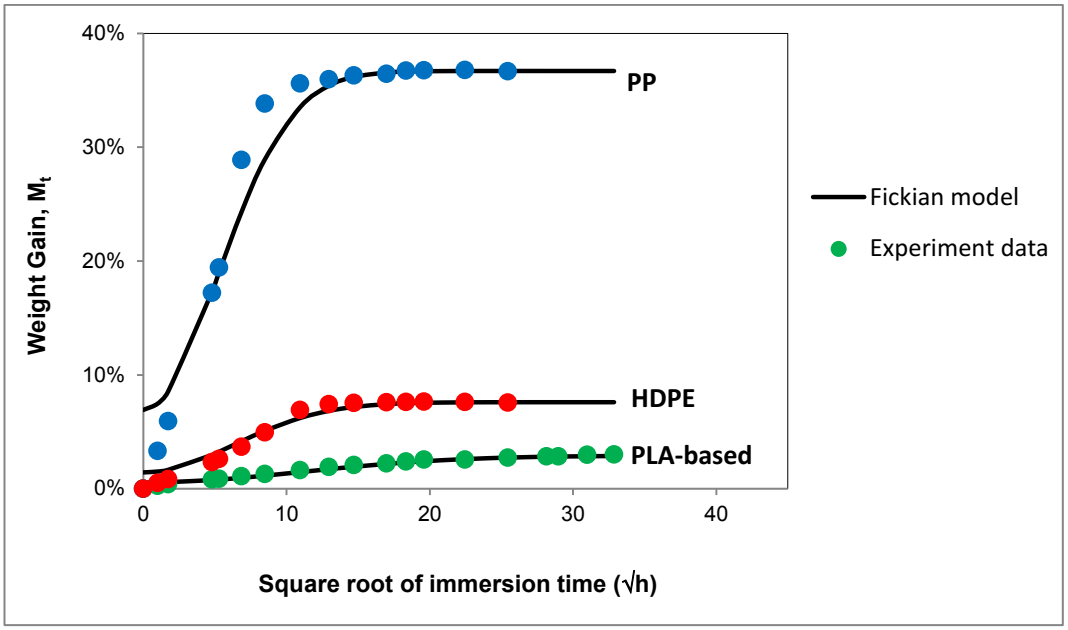

Figure 4-3: Percentage of fluid uptakes versus square root of immersion time for all materials at room temperature (the solid line represents the theoretical Fickian weight gain)

The diffusion of the model fluid into all types of polymer approximately follows Fick's law, which shows initial linear increase of weight gain followed by a transition region reaching saturation level at large values of times. Equilibrium plateau is obtained after 120, 168 and 432 h, for Polypropylene, HDPE and PLA-based material, respectively. The saturated weight gains at room temperature immersion for the three polymers can be determined from the equilibrium plateau. It is evident that polypropylene is most sensitive to sorption of this type of organic liquid, with more than 35% weight gain. Highest resistance at room temperature is observed for PLA based biopolymer, which was found to have 2.8% fluid uptake. Weight gain amount of HDPE -the most common material used for application in contact with oxygenated fuel- was 7.5%, a fact also stated by other research (Mouzakis and Karger-Kocsis, 1998).

4.3.1 Coefficient of diffusion

Figure 4-4 shows the fitting of linear regression for the plot of M_t/M_m versus $\sqrt{t}$ at the initial stage of liquid absorption. This figure indicates a large value of correlation coefficient ($R^2 > 0.9$) of the regression lines which shows that the linear regression lines could be easily fitted. It confirms that Fick's law can be applied to this diffusion process (Mouzakis and Karger-Kocsis, 1998).

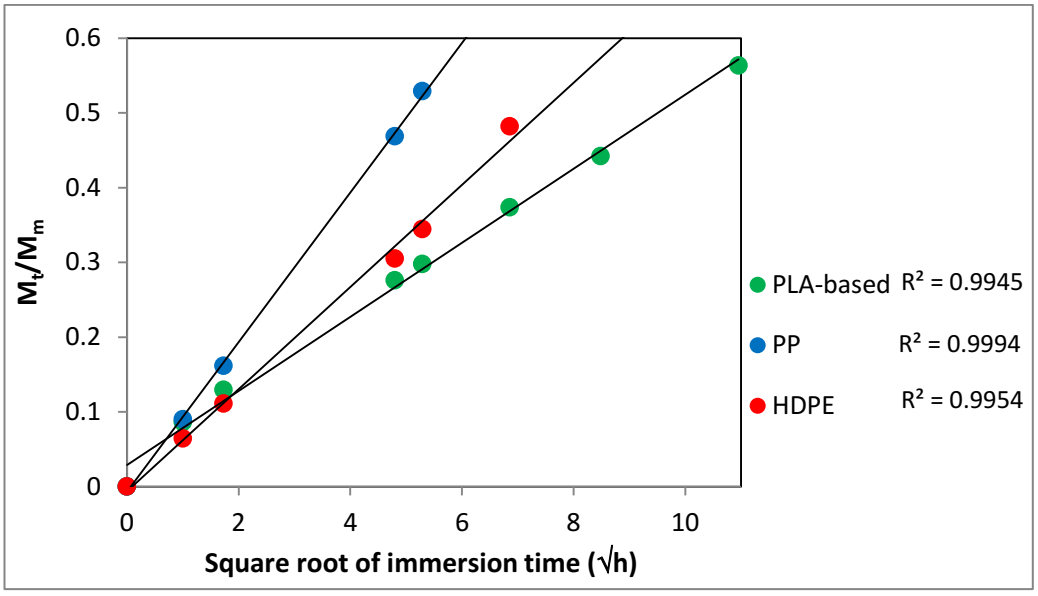

Figure 4-4: Plot of Mt/Mm from the initial value of fluid sorption for different materials at room temperature

The values of diffusion coefficient for all materials immersed at room temperature (20°C) calculated from the slope of the initial M_t/M_m plot are listed in Table 4-1. That table also presents a comparison of the findings of the present work with the literature values on PLA material exposed to different environment. The order of magnitude of D found here compares well with the values found in the literature; even if they have different characteristics in material and the diffusant.

Table 4-1: Diffusion Coefficient of Selected Polymers Immersed in Various Environment at Room Temperature

Material	Environment	D x 10^{-12}(m^2/s)
HDPE	Hydrocarbon liquid	3.35
Polypropylene	Hydrocarbon liquid	5.02
PLA: Bioplast GS2189	Hydrocarbon liquid	1.10
PLA: Biomer L9000 (Balakrishnan et al., 2011)	Water	2.07
PLA: Cargill Dow 4031D (Auras et al., 2004a)	Water vapour, Aw = 0.9	0.16
50%PLA/50% Chitosan (Correlo et al., 2007)	Water	2.28

4.3.2 Effect of immersion temperature

When considering service application, it is helpful to study the effect of temperature on the diffusion process. Accordingly, specimens were also immersed in model fluid at 5º and 30ºC. The effect of temperature on transport properties of PLA material is shown in Figure 4-5. Experiment data and its corresponding theoretical Fick's curve fitting are displayed in this figure represented by points and solid line, respectively. The results show progressive increase of weight gain in temperature, with significant increase at 30ºC immersion temperature (5.95%). Smaller increase was observed at lower temperature, achieving equilibrium at 1.90% and 2.91% after 1152 and 1008 hours. Figure 4-5 also indicates that at 5° and 20°C temperatures the experiment data agree well with the Fick's Law but there is deviation in the data for higher temperature (30°C). It means that at high temperature the diffusion behaviour of hydrocarbon liquid into PLA material is anomalous and it cannot be adequately described by Fickian diffusion.

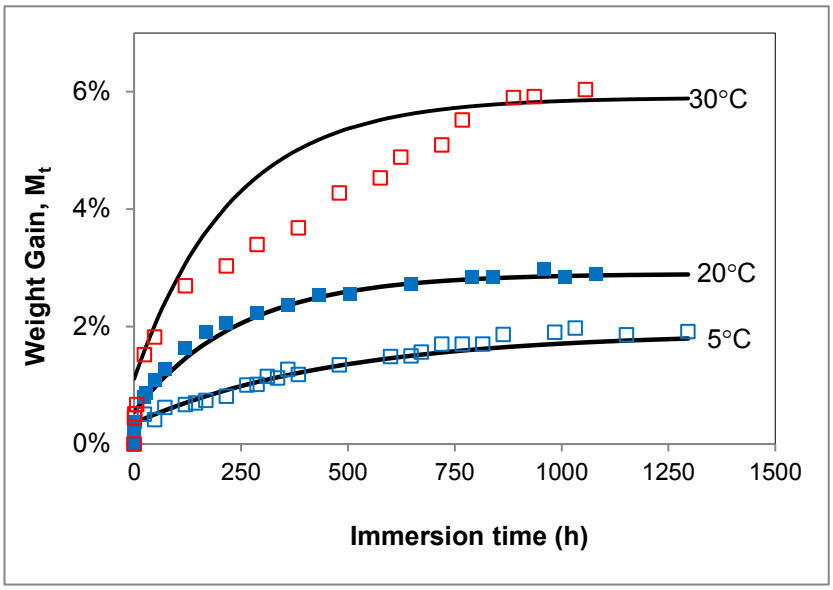

Figure 4-5: Percentage of weight gain of PLA material versus immersion time at various temperatures

The values of diffusion coefficient for samples in different temperature were also calculated using Equation (4.14) and presented in Table 4-2. This table also exhibits the values of sorption coefficient S, which is taken from the equilibrium plateau of the weight gain curves (Mouzakis and Karger-Kocsis, 1998) shown in Figure 4-5. The related permeability coefficient P can be calculated using Equation (4.1) as an alternative method to measure approximated permeation coefficient which can easily be converted to the substance transmission rate (Sangerlaub et al., 2013).

Table 4-2: The values of Diffusion (D) and Permeability Coefficient of the Material at Various Environment Temperatures

Immersion temperature	D x 10^{-12}(m^2/s)	S (g/g)	P x 10^{-14}(m^2/s)
5°C	0.57	0.019	1.083
20°C	1.10	0.03	3.201
30°C	1.13	0.0595	6.724

The estimated values of diffusion coefficient using Fick's law are plotted with temperature to have Arrhenius relation between those two variables. Figure 4-6 shows the influence of temperature on the diffusion coefficient of PLA-based biopolymer through a plot of D versus inverse temperature, 1/T. Least square regression shows that the D variation with (1/T) was sufficiently linear to be modelled using equation (4.15). The diffusion of an organic liquid into PLA-based material is observed to have a strong dependence on temperature. The above parameters are determined from the intercept and slope of the best-fit straight line on a log-log plot of equation (4.15) as D_0 = 1.56 x 10^{-12} m^2/s and E_a/R = 5.189 J/mol.

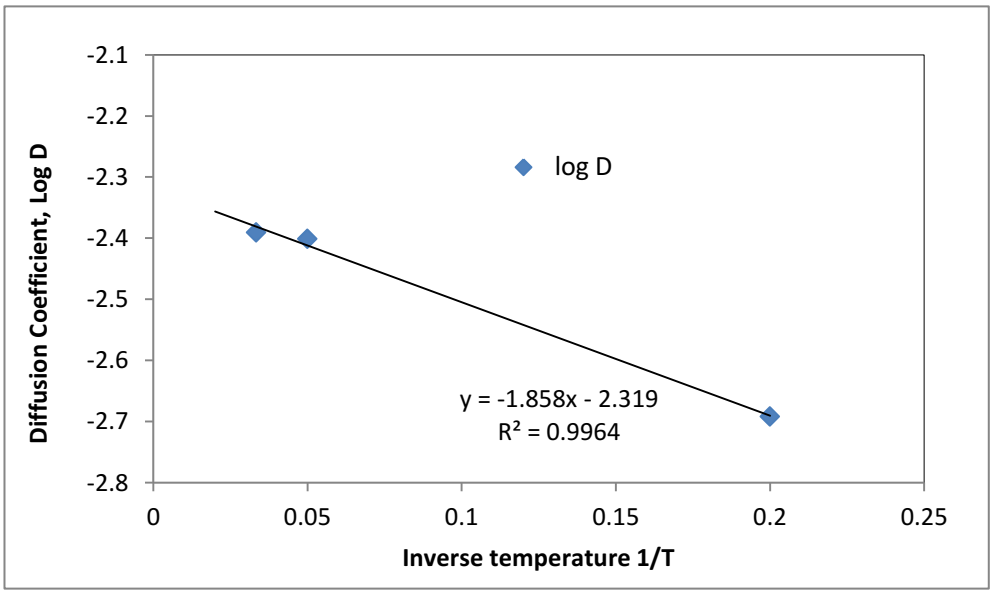

Figure 4-6: Plot of the logarithm of the diffusion coefficient versus reciprocal of absolute temperature for PLA material

4.3.3 Non-Fickian diffusion in PLA material

The experiment data of the model fluid sorption into PLA specimens at diverse temperature levels has been plotted in Figure 4-5 along with the corresponding theoretical Fick's solution presented in Equation (4.14) which shows a deviation at 30°C temperature. Figure 4-7 clearly shows the anomalous behaviour of the liquid sorption at 30°C compared to that at lower temperature. Results generated from numerical analysis are also shown for both cases. Numerical analysis was carried on using a commercial finite element package, ANSYS Mechanical APDL v. 14. The weight gain is obtained as the average concentration of liquid content within the thickness of the specimen. The liquid diffuses into the specimen through both of the surfaces as illustrated in Figure 4-2.

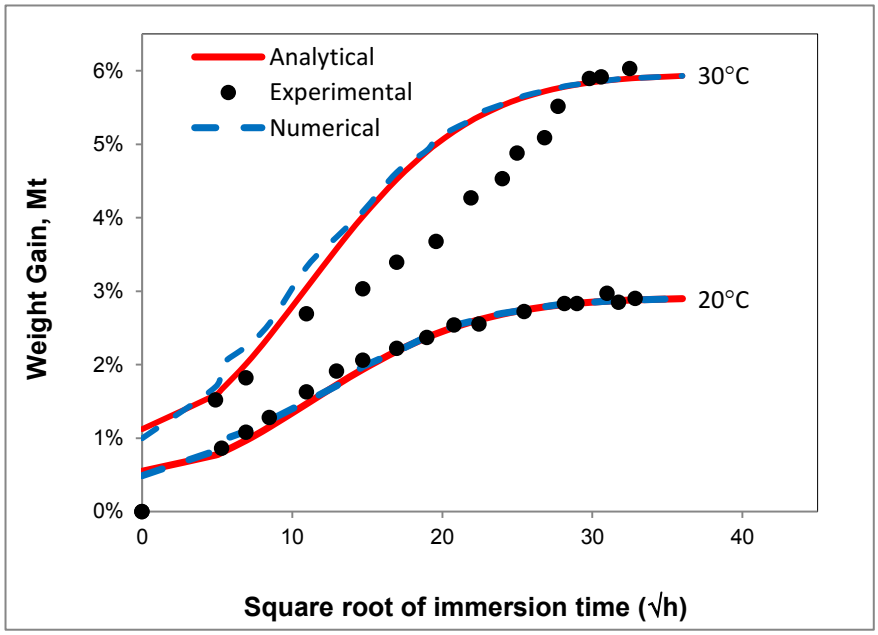

Figure 4-7: Analytical, experimental data and numerical solution at 20 °and 30 ℃ immersion temperatures

There have been several attempts to recognize and characterize the anomalous sorption in a polymer. It can be characterized by linearly decreasing diffusivity as a function of average liquid content (Chen et al., 2005), two-stage Fickian process (Frémont et al., 2001), time-dependent function similar to viscoelastic material response and modified Fick's Law with time-dependent diffusion coefficient (Roy, 1999).

The diffusion coefficient, D, in Equation (4.4) is assumed to be independent of liquid concentration, C, but this assumption may not hold to be true to the case of non-Fickian diffusion (Shirangi and Michel, 2010) and will cause inaccuracy when applied in that anomalous characteristic. An estimation of diffusion coefficient can be carried out by

developing the relation of diffusion coefficient to liquid concentration (Chen et al., 2005, Shirangi and Michel, 2010) as given by

$$D = D(C) \tag{4.16}$$

For the case of liquid diffusion at 30°C environment temperature as presented in Figure 4-7, no specific saturation point can be observed thereof, so an estimation of the diffusion coefficient by using Fick's low is not appropriate. The liquid content-dependent diffusion coefficient as shown in Equation (4.16) is determined by estimating a first value of diffusion coefficient from a virtual saturation level (Shirangi and Michel, 2010). This is repeated for longer immersion time until a relation between diffusion coefficient, D and saturated liquid content C_m can be obtained. Figure 4-8 shows the relation between D and C_m in the sample, which constructs the liquid content-dependent diffusion coefficient.

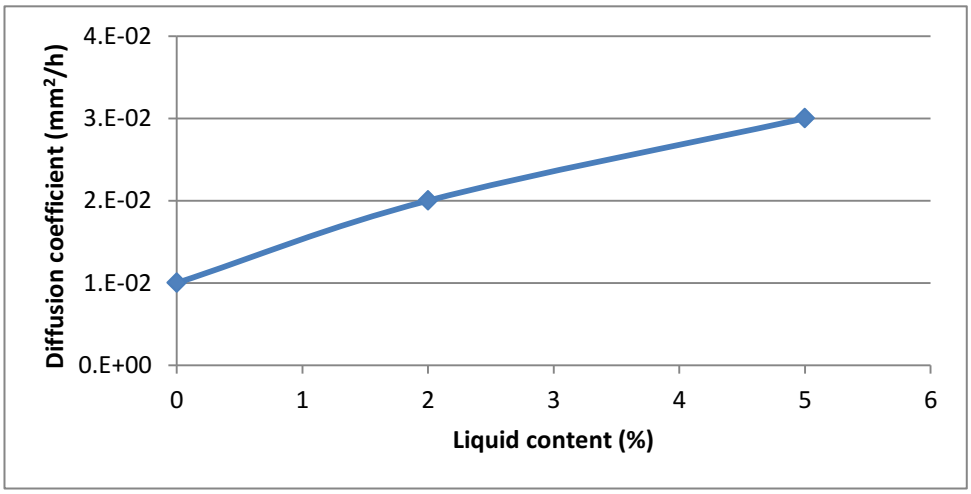

Figure 4-8: Function of diffusion coefficient with liquid concentration for samples exposed at 30℃ environment temperature

In automatically solving the anomalous organic liquid diffusion at high temperature, a finite element code is developed using the FE software, ANSYS Mechanical APDL using the liquid content-dependent diffusion shown in Figure 4-8. The curves of liquid content to time of absorption with both constant and liquid content-dependent diffusion coefficient, D are plotted in Figure 4-9. It is shown from the figure that the non-Fickian model displayed in solid line fits better to the experiment data compared to that using Fick's diffusion equation with constant value of D.

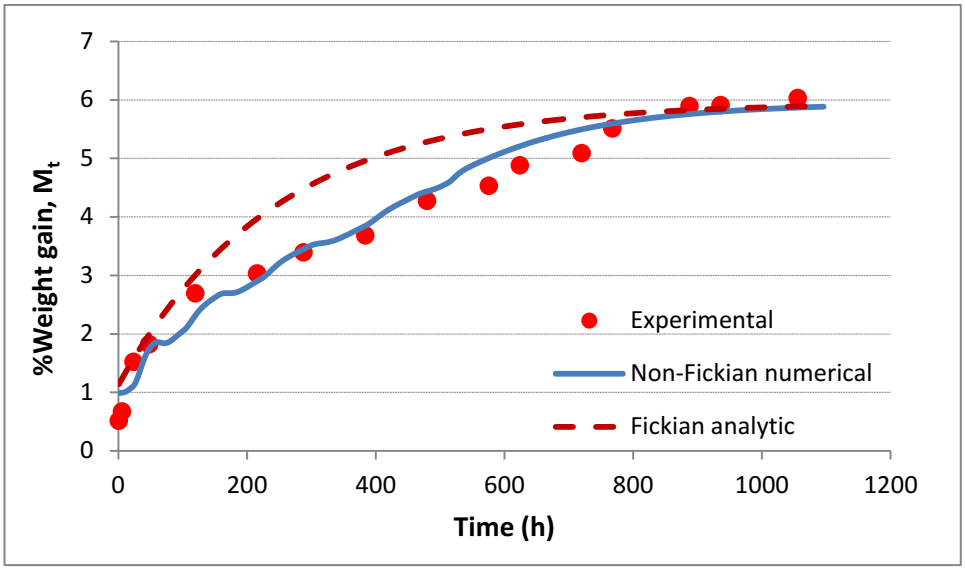

Figure 4-9: Fickian and non-Fickian curve of liquid sorption at 30℃ immersion temperature

Davis et al. (2011) and Davis et al. (2012) have also reported non-Fickian behaviour for the diffusion of liquid water as well as water vapour in PLA-based material at 25°C immersion temperature. The observed anomalous diffusion behaviour in PLA was attributed to water diffusion and water-induced polymer relaxation occurring on similar time scales, a fact also confirmed by Loh et al. (2005). Non-Fickian behaviour may also be consequences of chemical degradation and sorption-induced microcracks (Lekatou et al., 1997). Another mechanism leading to anomalous behaviour of liquid absorption could be the swelling of the polymeric material, which be discussed in the following section.

4.3.4 Swelling

Swelling is a specific response to fluid diffusion in polymer based materials. Hygroscopic swelling, a term describing expansion of material due to fluid absorption, is mechanically similar to the thermal expansion in that both are physical phenomena involving molecules equilibrating at a larger distance apart as a result of temperature increase and liquid absorption, respectively (Lin, 2006). Swelling of length was calculated using Equation (3.3) provided in Section 3.2.4 to identify the dimensional change resulting due to fluid sorption. Figure 4-10 shows the length swelling of observed materials. Generally, the measured length swelling had a positive correlation to the weight gain result. As was the case with the weight gain, the length swelling of PLA material increases with increasing of temperature. The material immersed at 30ºC had the largest degree of swelling, having gained a swelling of 1.2% after 1008 hours immersion period. It was observed that immersion of the model fluid has less significant effect

in length swelling at 20º and 5ºC temperature. This result was similar to swelling of poly(vinylidene fluoride) (PVDF) in toluene reported by McCourt et al. (2006). Swelling strains of the order of 1-3% have been reported for epoxy adhesives in exposure to water vapour (Duncan et al., 2005).

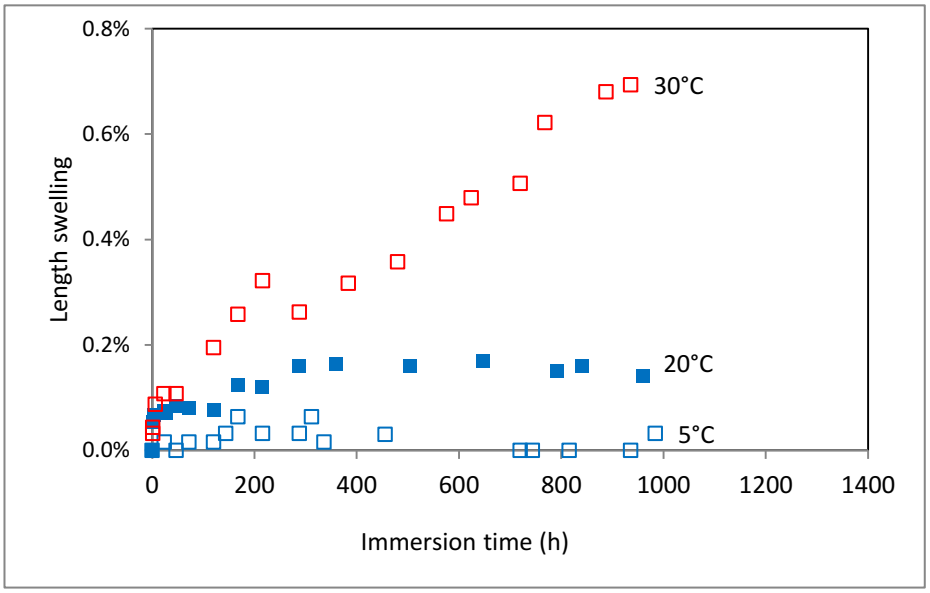

Figure 4-10: Length swelling of PLA material under model fluid exposure at various temperatures

The rapid increase in length observed for specimens immersed at 30°C represents significant increase in the volume of the bulk polymer. When the penetrant causes extensive swelling, the anomalous or non-Fickian behaviour may be exhibited especially in a glassy polymer (Crank, 1967, Neogi, 1996). Deviations from Fickian characteristics can be associated with the changes of the time-dependent properties of polymer in response to the sorption of penetrant molecules.

The relation between swelling and weight gain is developed using heat transfer analogy since both of them are mathematically equivalent. The sorption-induced expansion is equivalent to the thermal strain thereby it can be solely determined by a single physical property equivalent to coefficient of thermal expansion known as the coefficient of liquid absorption (β). The coefficient of swelling, β, was determined using an approach similar to the method presented by Lin (2006) by correlating the results from weight gain (ΔM) and dimensional change (ΔL) measurements. This approach is based on the basic equation where the expansion due to diffusion, ε_h, is linearly correlated with the concentration of diffusant, as

$$\varepsilon_h = \beta C \tag{4.17}$$

where C is the concentration of diffusant.

Linear relationship between percentage of liquid uptake, C and dimensional strain (percentage of length swelling),ε_h, is shown in Figure 4-11. A constant of linearity, the coefficient of expansion due to liquid absorption, $\beta = {}^{\varepsilon_h}/_{C}$, can be obtained by data-fit methods. This figure shows value of β (coefficient of swelling) for different immersion temperatures.

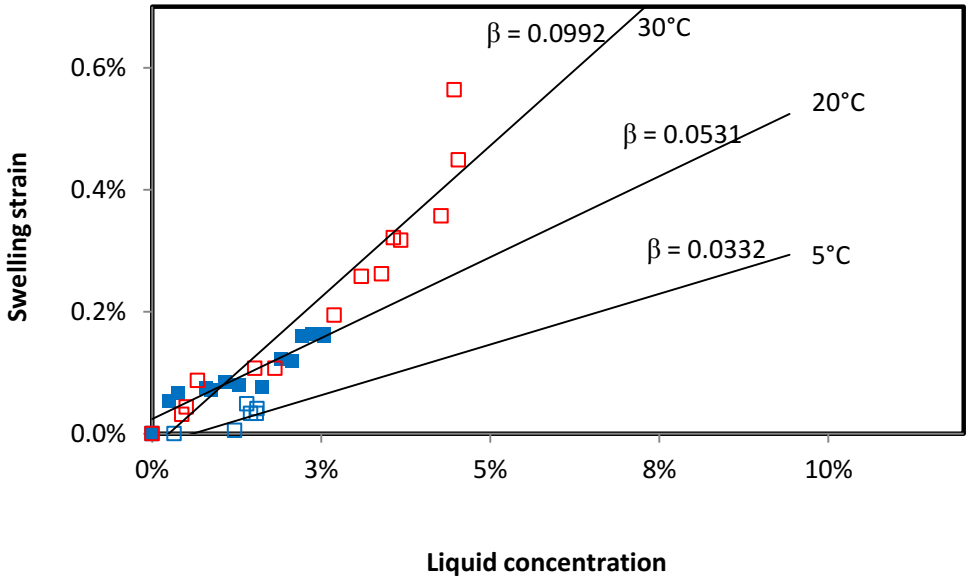

Figure 4-11: Swelling coefficient (β) obtained from the samples at various temperatures

4.4 Distribution of liquid content

The profile of diffused liquid into the material can be obtained by solving the analytical model presented in Equation (4.8). This section presents an analytical and numerical solution for distribution of fluid diffused into two simple geometries: a slab and a cylinder. In this case it is assumed that liquid diffusion is isotropic, that is the same in every direction. Finite element analysis (FEA) is used to numerically calculate the distribution of liquid diffusion with an assumption of constant temperature condition. The ANSYS APDL codes used to generate the solution are presented in Appendix E.

4.4.1 Diffusion in a plate

The geometry selected to illustrate the fluid diffusion is an infinitive thin plate with thickness (δ) of 1 mm. The material properties of the plate considered correspond to that of the PLA-based material experimentally studied in previous section. The plate is exposed to fluid environment from one side of the surfaces as shown in Figure 4-1. The temperature condition is at T = 20°C thereby has a diffusion coefficient D = 1.1e-12 m^2/s and saturated fluid uptake C_m =

2.91% according to Equation (4.15). Solution of this case is obtained both analytically and numerically using commercial FEA software. The boundary conditions for one-side are presented in Equation (4.7).

4.4.1.1 Effect of time increment

In ensuring that the FE model accurately predicts the profile of liquid content, it is imperative to examine effect of time increment on the accuracy of the results obtained. The convergence study is carried out by comparing the liquid content distribution resulted from FE analysis with the analytical solution of the plate.

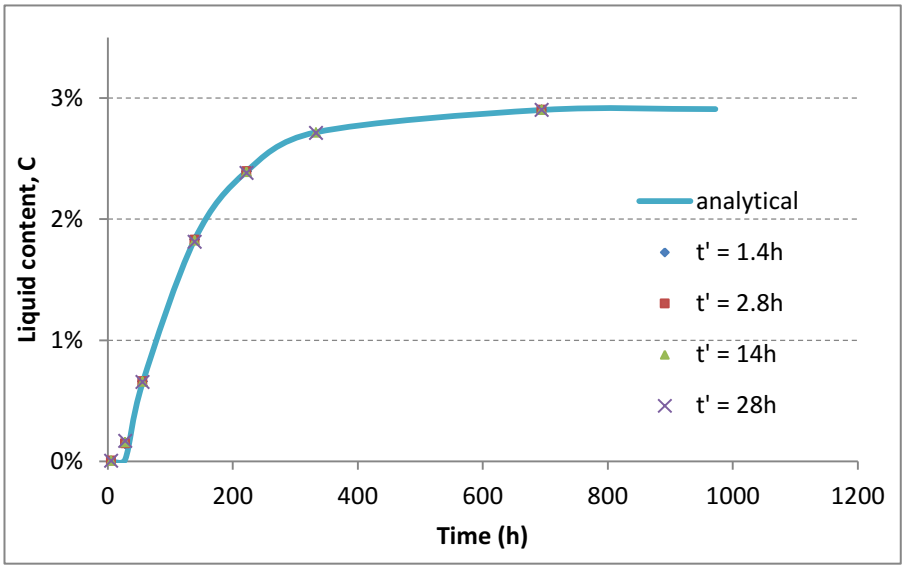

Figure 4-12: Effect of time-step size on the accuracy of liquid content distribution in finite element analysis

Figure 4-12 shows the plot of minimum liquid content within the thickness of plate which occurs in the inner part of plate (not directly exposed to liquid). The FE analysis with different time-step size of t' = 1.4, t' = 2.8, t' = 14 and t' = 28 h is performed until steady state is achieved. The figure displays that a time-step size less than 3h gives sufficiently accurate result as steady state is achieved at around t ≈ 430 h, which is similar to the analytical solution.

4.4.1.2 Fickian & non-Fickian diffusion

The evolution of the liquid content before reaching equilibrium concentration can be plotted by using Equation (4.10). The function parameters of Equation (4-10), the diffusion coefficient, D, and saturated liquid content, C_m, are temperature dependent as described in the Arrhenius

equation (Equation (4.15)). Figure 4-13 presents varying liquid concentrations with time and position along the thickness of the plate at an application temperature 20°C. In one-side diffusion of 1 mm plate thickness, the specimens will completely saturate in about 429 h. The figure shows the fluid content at 278 h to be at 2.8% weight gain from the initial dry weight throughout the thickness of plate. In one-side diffusion plate, it can be seen that fluid content at the inner side of the plate to be 0.8% at t = 55 h and after 139 h it increases to be 1.94%.

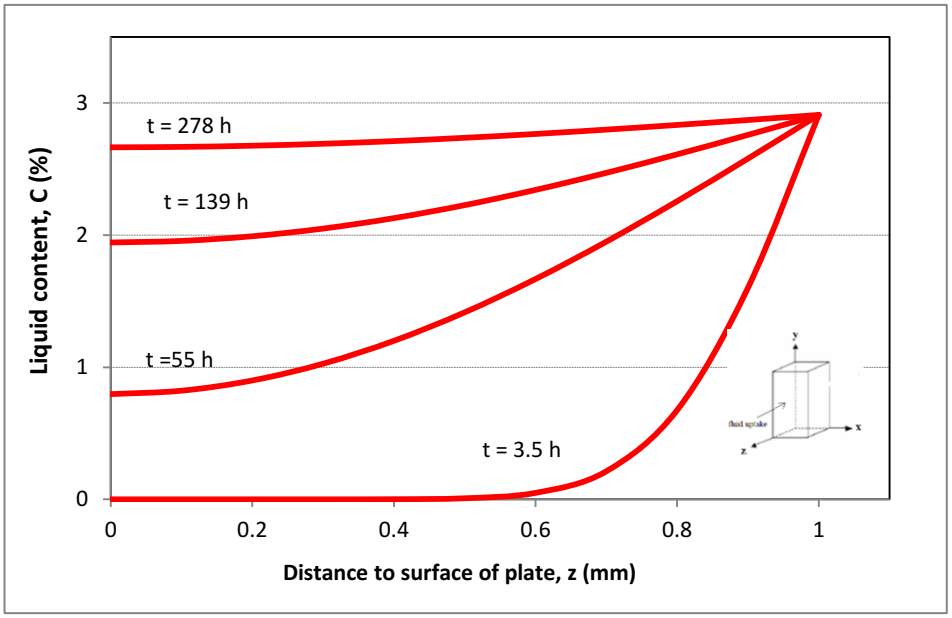

Figure 4-13: Concentration of liquid within the thickness of a plate from one-side diffusion

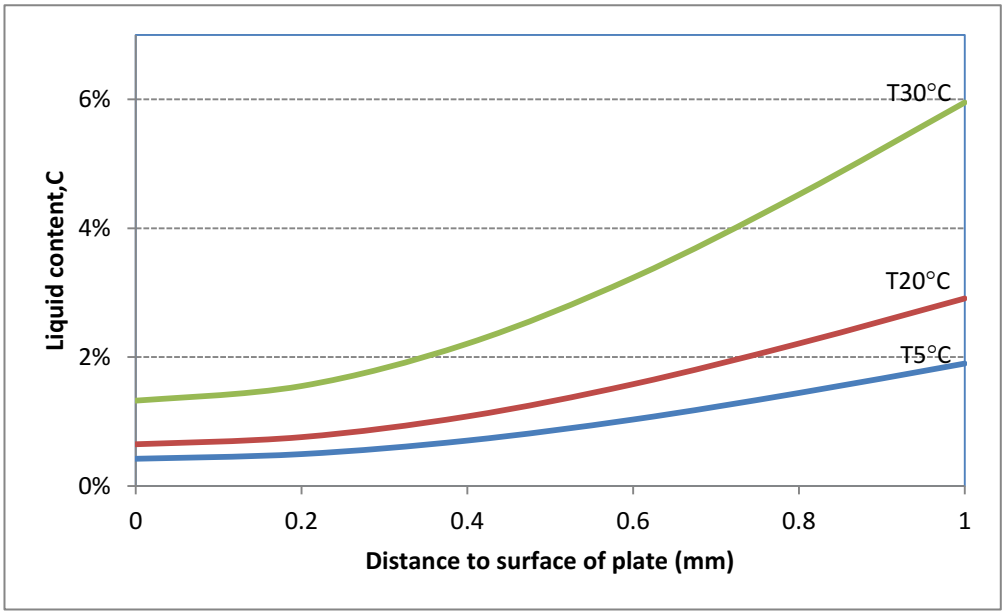

Figure 4-14: Concentration of liquid inside plate at F_0 = 0.2 at various exposure temperatures

In Figure 4-14, the liquid content at different temperatures in the same value of Fourier number, F_0 (Equation (4.11)) was plotted with position, z. The correspondence time for F_0 = 0.2 for environment temperature T = 5°, 20° and 30°C is t ≈ 98h, t ≈ 51h and t ≈ 47h, respectively. It is obvious from these figures that the spatial and time dependence of the liquid content during the diffusion process is affected by the environment temperature.

Using the converged time-step size, the distribution of liquid content of the specimen is numerically obtained and compared to the analytical solution. The plot of liquid content in different position within the thickness as function of time with surface distance at different time is shown in Figure 4-15. It can be seen that the analytical and numerical solution using FEA method agrees well in the case of diffusion within a rectangular plate.

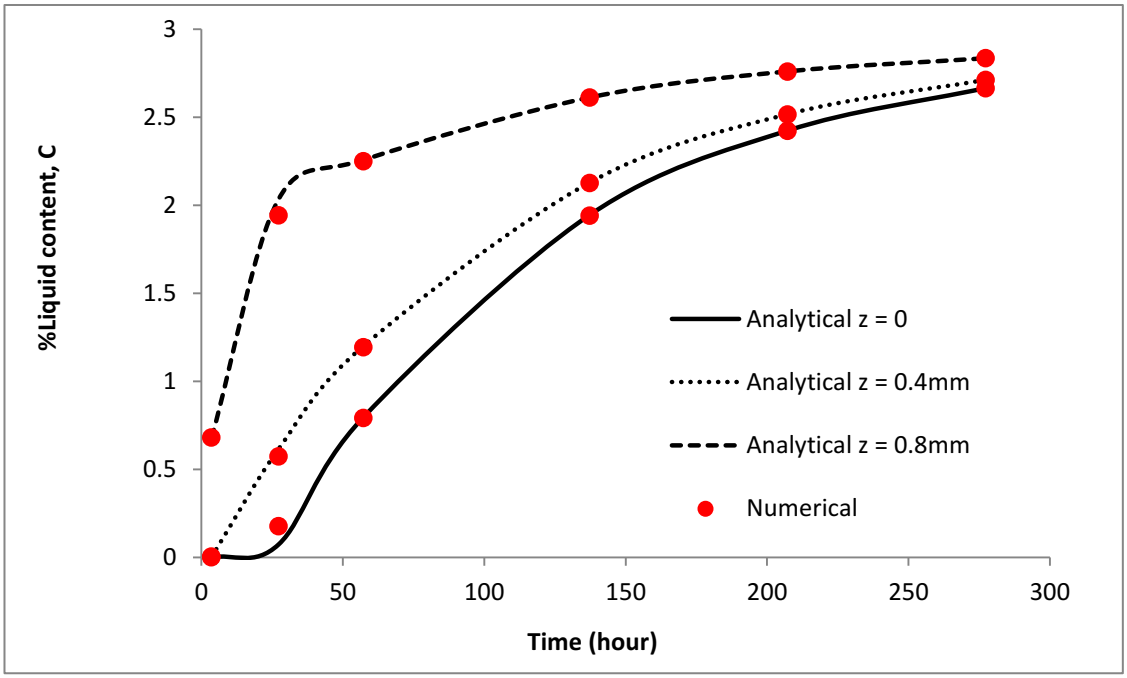

Figure 4-15: Comparison between analytical and numerical solution of fluid content at different position of z/δ within thickness of plate from one-side diffusion

The graphical representation of the fluid content profile for various times of observation during immersion period along the thickness is generated using the ANSYS Workbench 14.0 and is shown in Figure 4-16.

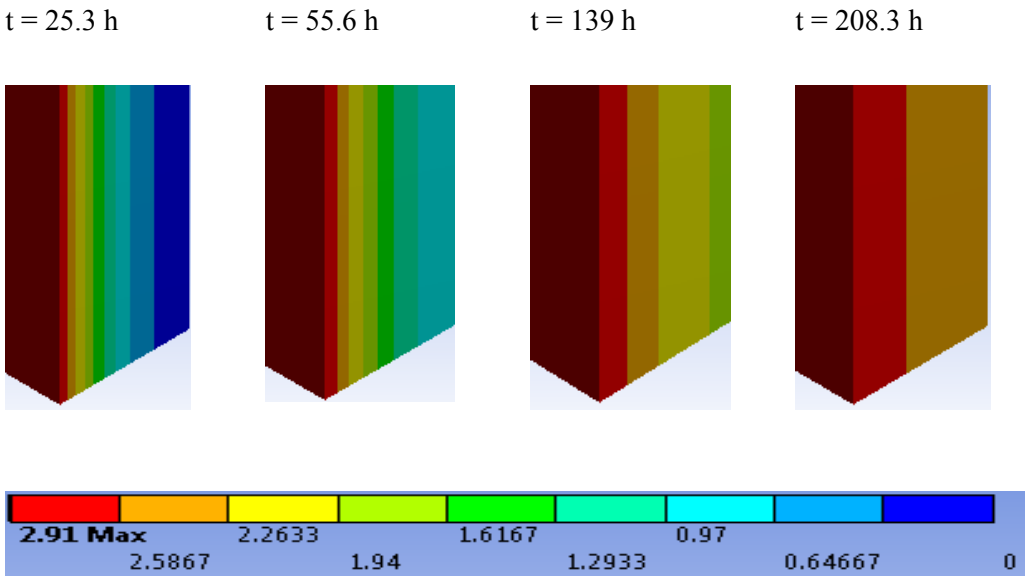

Figure 4-16: Profile of liquid content obtained from the FEA software at various exposure times

Using similar geometry of plate with thickness 1 mm, consider a plate conditioned at temperature T = 30°C, which has liquid content-dependent diffusion coefficient as shown in Figure 4-8. The numerical analysis is performed to obtain the distribution of liquid content for this case and displayed in Figure 4-17. A different profile with the case of Fickian diffusion shown in Figure 4-13 was observed.

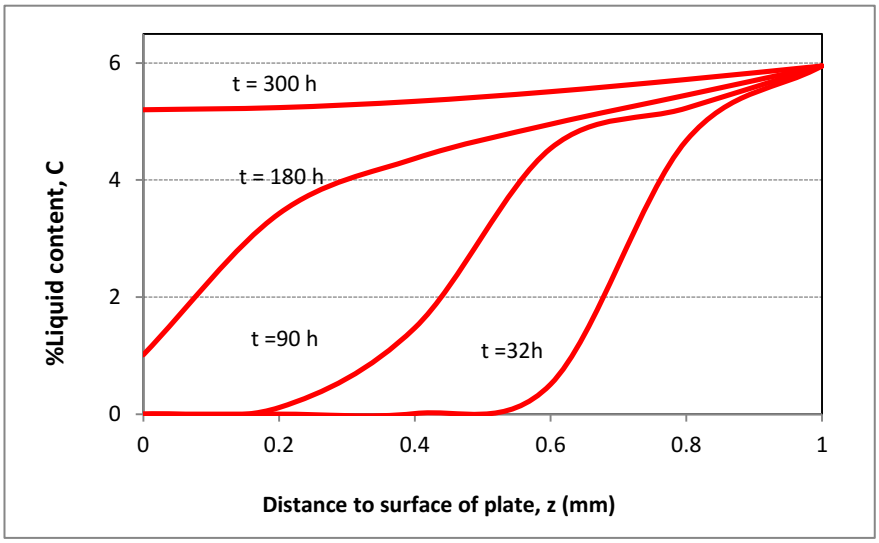

Figure 4-17: Concentration of liquid within the thickness of a plate from one-side non-Fickian diffusion

4.4.2 Diffusion in a pipe

Consider a long cylindrical pipe whose inner and outer radius are *a* and *b* respectively. If the diffusion coefficient is constant, the equation describing the concentration as a function of radius, r, and time, t is (Crank, 1967)

$$\frac{dC}{dt} = D\left(\frac{d^2C}{dr^2} + \frac{1}{r}\frac{dv}{dr}\right) \qquad a < r < b \tag{4.18}$$

In the hollow cylinder, if the initial concentration is zero and both concentrations at surface r = a and r = b is maintained at C_m, the boundary conditions are:

$$C = C_m, \qquad r = a, r = b \qquad t \geq 0$$

$$C = 0, \qquad a \leq r \leq b, \qquad t = 0 \tag{4.19}$$

Modified solution presented in Carslaw and Jaeger (1986) comes to the solution of Equation (4.18) as follow

$$C = C_m - \pi\sum_{n=1}^{\infty} F_n(t) f(\alpha_n, r) \tag{4.20}$$

where

$$f(\alpha_n, r) = J_0(r\alpha_n)Y_0(a\alpha_n) - J_0(a\alpha_n)Y_0(r\alpha_n) \tag{a}$$

$$F_n(t) = \frac{C_m J_0(b\alpha_n)}{J_0(a\alpha_n) + J_0(b\alpha_n)} \tag{b}$$

and α_n are the positive roots of the equation $f(\alpha_n,b) = 0$. $J_0(x)$ and $Y_0(x)$ are Bessel functions of order zero of the first and second kind.

$$\int_a^r f(\alpha_n, r) r\, dr = \frac{1}{\alpha_n}\left[rY_0(a\alpha_n)J_1\right] \tag{4.21}$$

This analytical solution was used along with the numerical solution to solve the distribution of liquid content in a hollow cylinder. The infinite length pipe with inner radius 1 mm and outer radius 3 mm was in contact with fluid in both its surfaces. The computed fluid concentration profile for the case study in an open infinite pipe is given in Figure 4-18 and 4-19 using analytical and numerical solution, respectively. In Figure 4-18, it can be seen that the sorption rate reach the equilibrium after around 800 h.

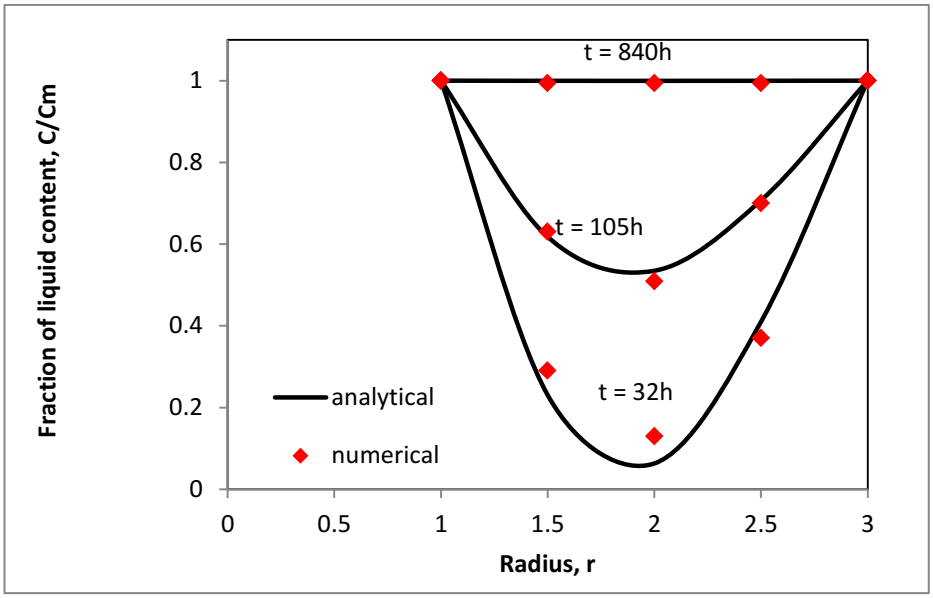

Figure 4-18: Profile of liquid concentration within the opened infinite pipe at room temperature

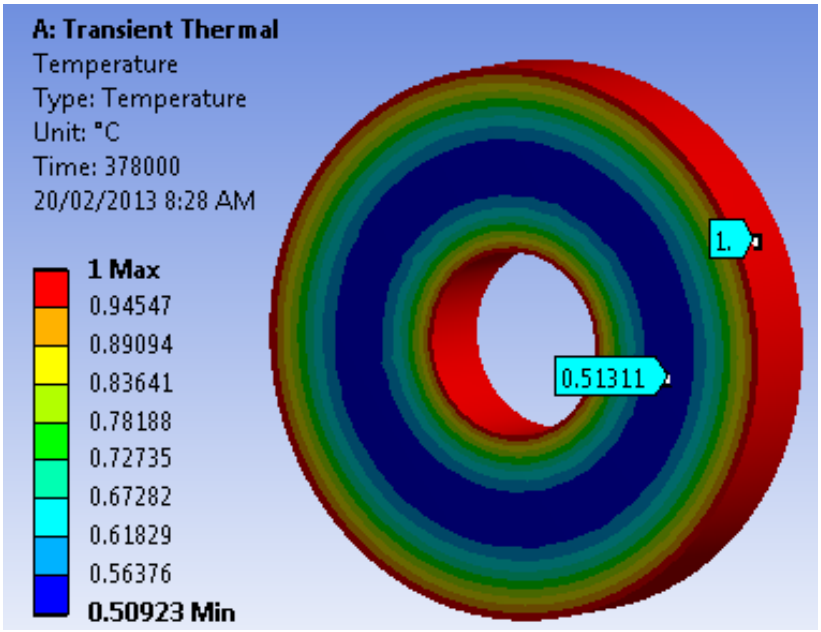

Figure 4-19: Numerical model of an opened infinite pipe at t = 105 h

4.5 Diffused substances in a package

From two different cases in simple geometries, it can be seen that the numerical solution using FEA method agrees well with the analytical solution. For this reason, this section develops a FE model to simulate the diffusion of a substance into a PLA package in evaluating the distribution of the diffusant within the thickness of the package overtime.

Consider a commercial extruded blown polymer bottle used for various fluid containers as shown in Figure 4-20. It is assumed that the package has uniform thickness of 1 mm.

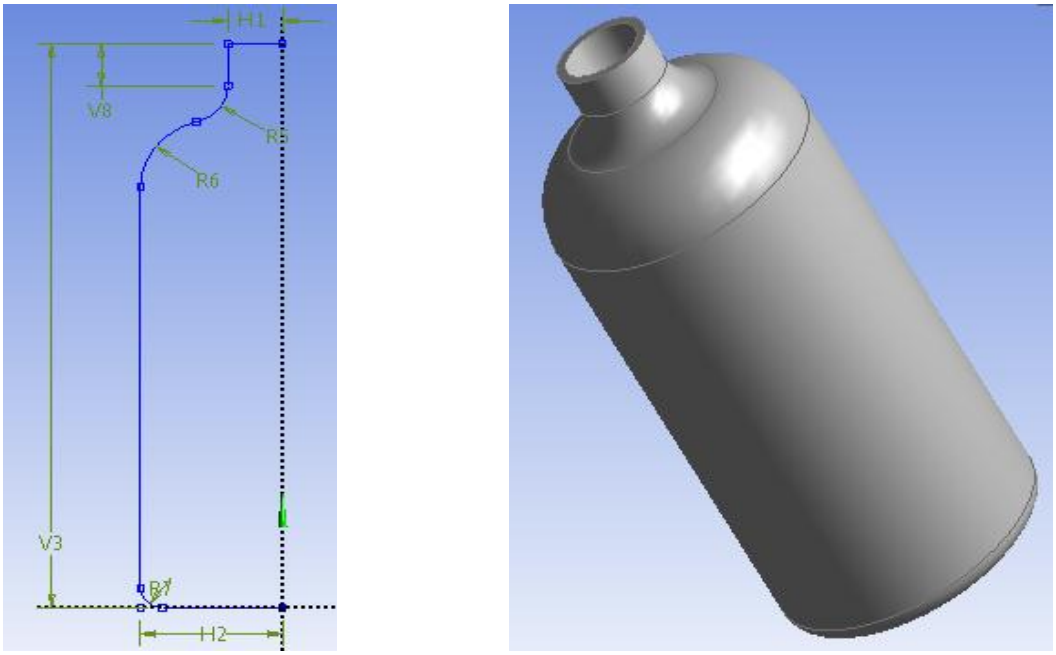

Figure 4-20: The dimensions of simulated PLA packaging

4.5.1 FE Modelling

ANSYS Workbench v.14 was utilized to perform simulation of the hydrocarbon substance diffusion into a PLA package. The analysis type of transient heat transfer was used as an analogy to non-steady state diffusion process. Basically, the FE analysis procedure is started with the development of model geometry and defining the material properties. The next step is generating the mesh which is made up of the nodes and elements to represent the geometry of the model. Defined saturated diffusant content is applied in particular area related to its boundary conditions. The model is then automatically solved and it provides a solution for the defined problem.

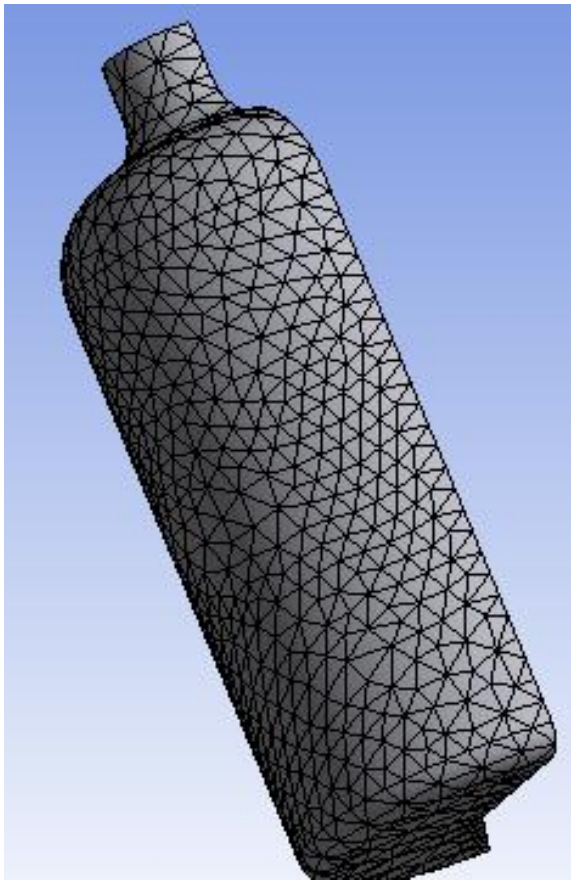

Figure 4-21: The mesh surface of the PLA container

One of the factors affecting the accuracy of the solution is the quality of meshing. A finer mesh produces more precise solution but it can increase the analysis time and the requirements of computer memory. Generating meshes on the package was performed on the mesh system component. Two different global size controls were employed: “coarse” and “fine”, to study the mesh relevance effect on the solution. In the simulations carried out in this research, the maximum element size used for the entire model and the meshing method control are automatically defined by the software. The complete mesh bottle is shown in Figure 4-21, while the difference between two global size controls is presented in Figure 4-22. It can be seen from the element quality plot in Figure 4-22(a) that many elements are of a relatively low quality, which then can be improved after mesh refinement.

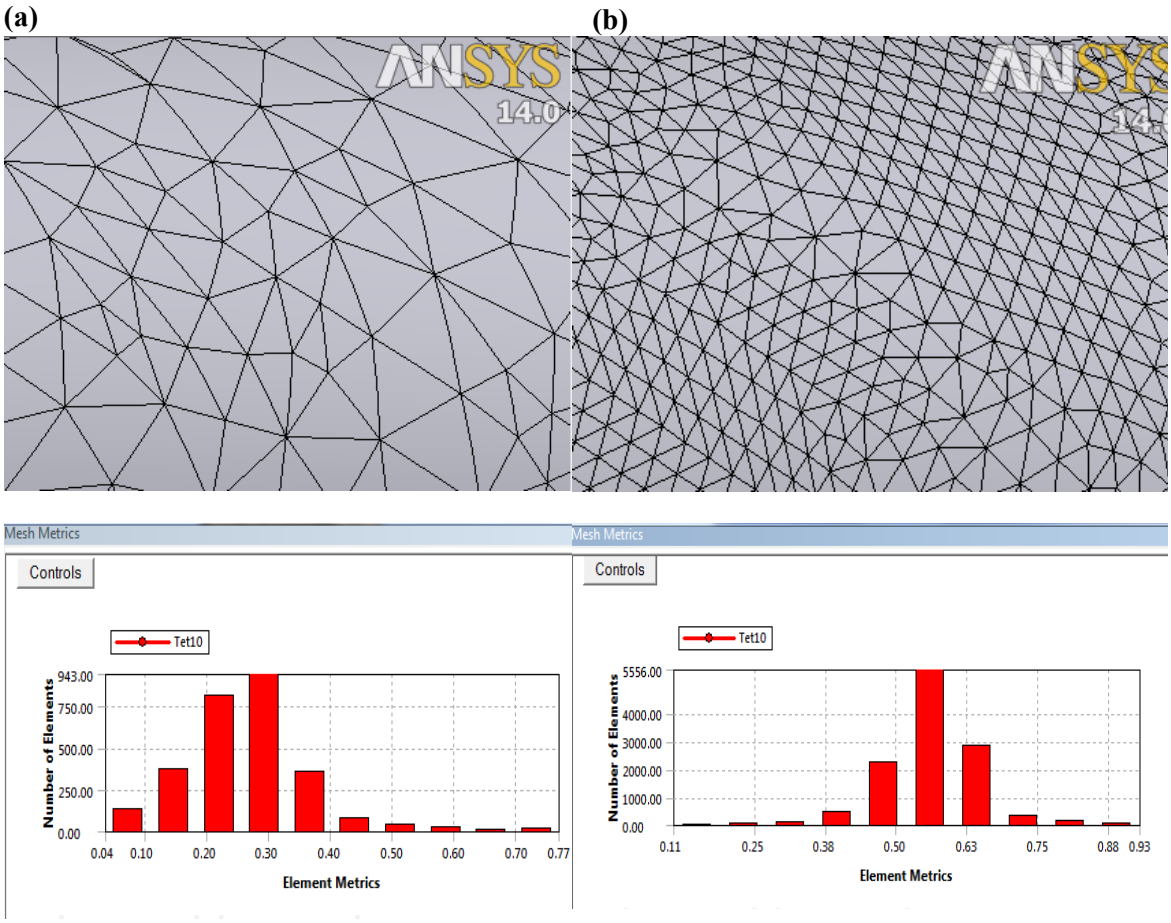

Figure 4-22: The mesh geometry and dimension of elements on the surface using: (a) initial (software default) and (b) refined mesh with the corresponding element quality plots

In FE analysis of diffusion process, the only required material property is the diffusion coefficient, which is represented by the thermal conductivity whereas the density and the specific heat are equal to one. Liquid content-dependent conductivity reflecting the non-Fickian diffusion can be input in the model as a table. In this study, two different diffusants are simulated to be absorbed into PLA package for which the properties are described in Tabel 4.2.

Table 4-3: Two simulant materials used in analysis of PLA package

	Diffusion coefficient, D (m^2s^{-1})	**M_m**	**Grade of PLA**
Hydrocarbon liquid, 20°C (current work)	1.10e-12	2.91%	Injection moulded grade, Bioplast G2189
Water, 20°C (Balakrishnan et al., 2011)	2.07e-12	0.44%	PLA Biomer L9000

Boundary conditions for the problem are shown in Figure 4-23. It shows the saturated diffusant concentration at the inner surface and for this case it is assumed that the outer surface of the package is perfectly insulated (no substance permeate from the package)

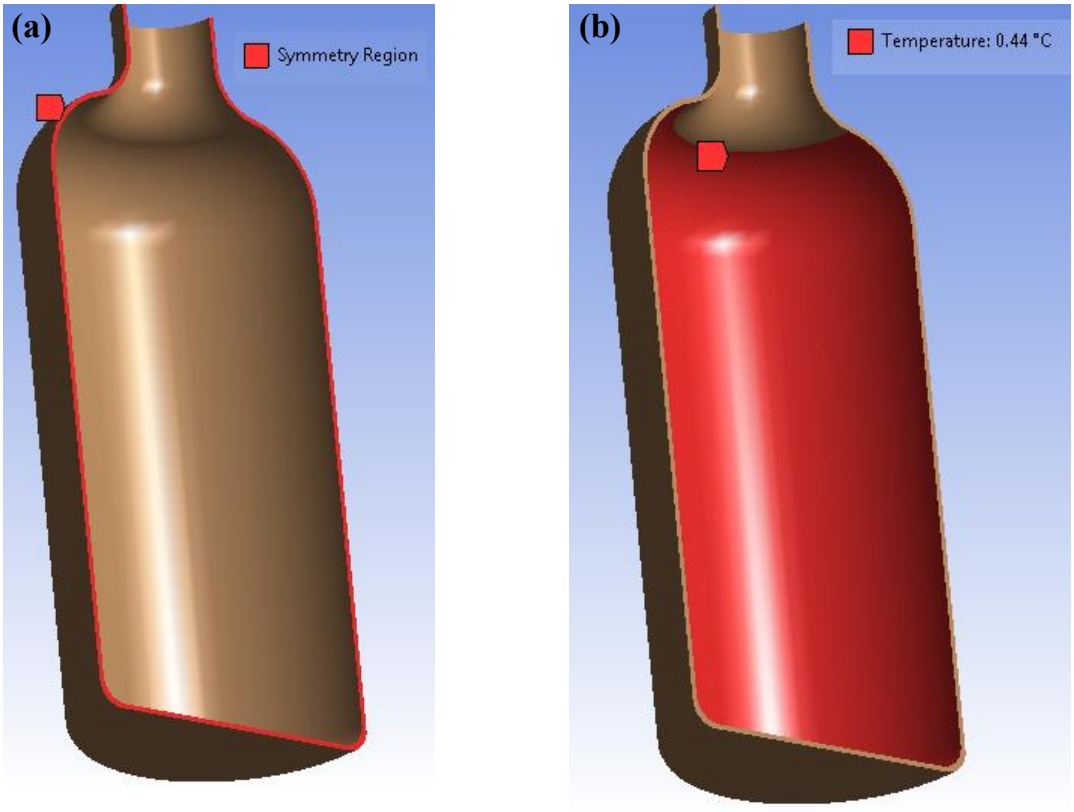

Figure 4-23: The boundary conditions applied for analysis of the diffusion process: (a) symmetrical condition and (b) saturated condition at the inner surface

4.5.2 Simulation result

4.5.2.1 Effect of mesh refinement

The diffusion of hydrocarbon liquid into PLA package was modelled using the two different meshes to explore how meshing changes can have significant effects on the quality of the result obtained. The end time of simulation step is set to be $1x10^6$ s or 278 h with initial time step 1000 s. The solutions obtained at the end of step time using two different mesh sizes are shown in Figure 4-24. This figure shows that the mesh refinement represent more detail profile of liquid content and it has slightly reduced the thermal error compared to the original mesh

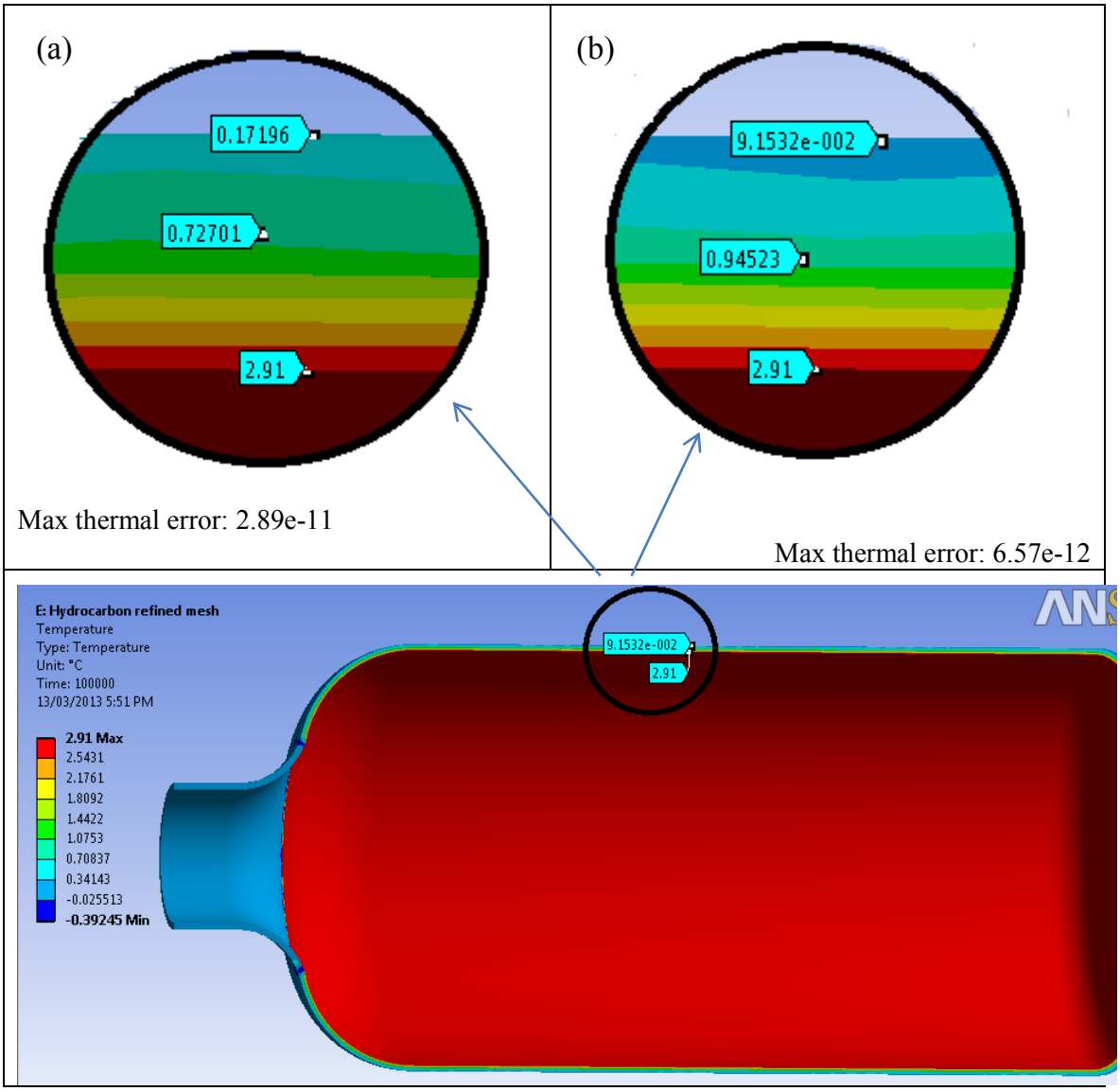

Figure 4-24: The distribution of liquid content within the bottle with: (a) initial (software default) mesh and (b) refined mesh

4.5.2.2 Profile of liquid content

The distribution of liquid water and hydrocarbon liquid in the PLA package at t = 24 h and t = 240 h is presented in Figure 4-25. It is clear that the package is being saturated with water after 240 h and it is predicted to have equilibrium hydrocarbon liquid after 320 h.

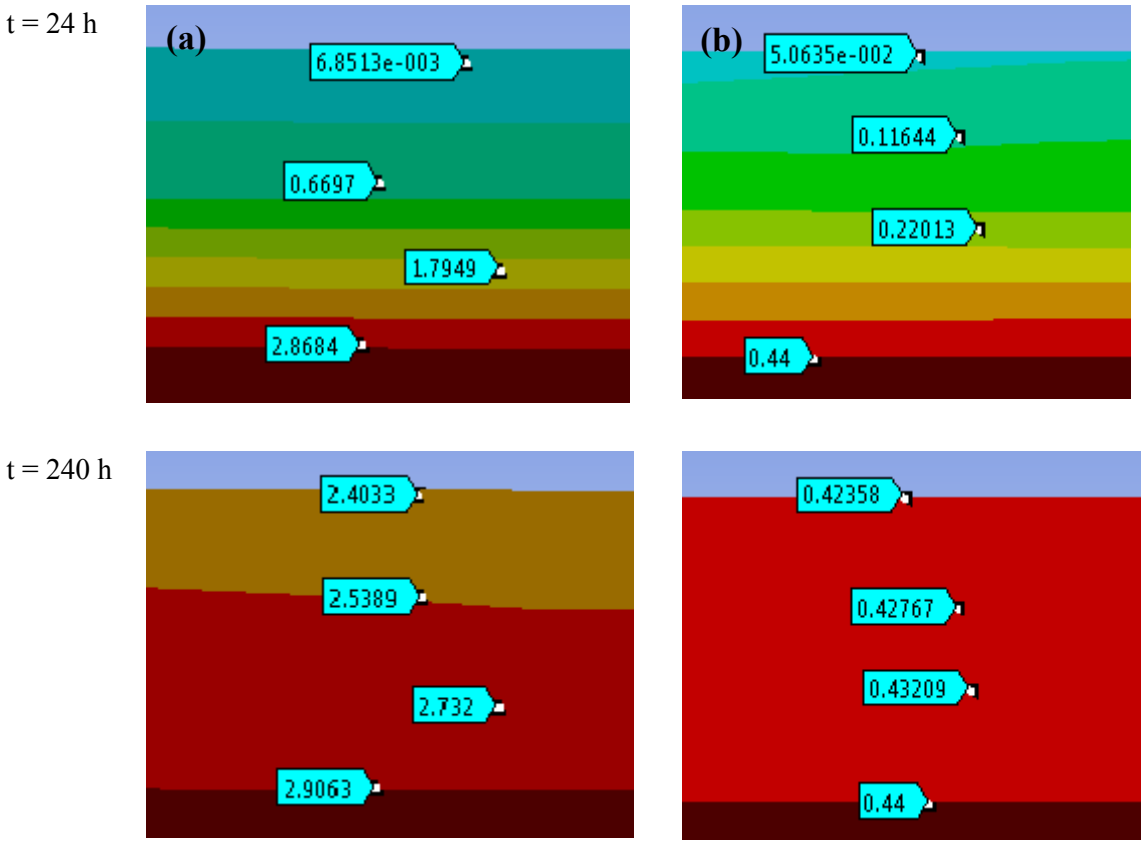

Figure 4-25: Profile of liquid diffusion: (a) hydrocarbon and (b) water within the thickness of PLA bottle at two different times

4.6 Permeant transport in PLA-package

In addition to sorption, permeation is another process included in mass transport during the interaction of the packaging material with both its packaged product and the environment (Auras et al., 2006a). Some PLA packages with relatively low barrier properties enable the permeant transfer through the package wall, which leads to loss of gas, water vapour and chemical compounds from the package.

Permeation of various substances in PLA-based material has been investigated for different packaging applications (Cairncross et al., 2006, Auras et al., 2004b, Welle, 2008). Most of those works carried out by experimentally measured the permeability parameters of the substances for PLA materials. The permeation coefficient of the PLA material toward hydrocarbon liquid is found to depend on environment temperature as presented in Table 4-2. In this section, a FE model is presented to illustrate the permeation process in determining the loss of product substances through a PLA-based package.

The permeation of product substances through the package is modelled using an analogue of transient heat convection in the FE software. The required inputs for this model are the exact package drawing with the measured thickness along the package sections and the value of the substance transmission rate, which is converted from the data of permeability coefficient obtained previously in Section 4.3.2. For comparison, the model will also illustrate the loss of water vapour using the data of water vapour transmission rate (WVTR) obtained from available literature (Shogren, 1997). The converted transmission rate for hydrocarbon liquid from the PLA-based material is found to be 227 g/m^2 per day while the WVTR data employed is the data of crystalline PLA in 25°C, which is 82 g/m^2 per day. The boundary condition of the FEA model is presented in Figure 4-26. The substance transmission rate is represented by the convection coefficient while the concentration difference between the surface and the environment is set to have a value of 1.

Figure 4-26: Boundary conditions of the gas permeation problem from a PLA-package

The simulation results generated from the FEA software is shown in Figure 4-27. The result for water permeation confirms that the native PLA material is considered to be sufficient for short term protection only (Almenar and Auras, 2010). As shown in the figure, the package made from native PLA material will lose 50% of the water and hydrocarbon content after about 40 and 17 days, respectively.

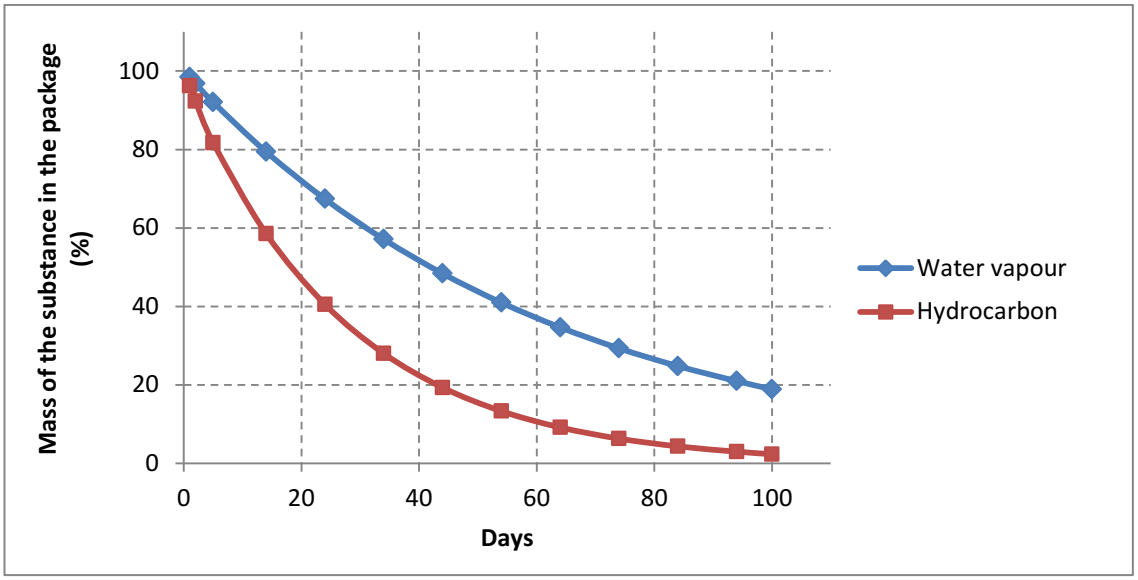

Figure 4-27: Simulation result of the loss of water and hydrocarbon substance in a PLA-package with 1 mm thickness at room temperature

To be qualifying for longer term packaging application as in PLA water bottles or other liquid container, there should be improvements in the barrier properties of the package. The reduction of water vapour permeability on neat PLA material has been reported by incorporating the PLA resin into inorganic silicate, which results a hybrid-coating materials by using surface modification and coating materials on neat PLA material (Bang and Kim, 2012, Kim et al., 2013, Park et al., 2012).

4.7 Conclusion

This chapter has reported a systematic investigation of sorption of an organic liquid into a PLA-based material. The experiment results confirm the time-dependent liquid sorption, which is highly influenced by the surrounding temperature. At low temperature, the kinetics of water sorption follows the Fick's law but at higher temperature, it showed a deviation from the Fickian curve. The anomalous diffusion can be associated with extensive swelling reported at high conditioned temperature.

Based on the diffusion parameters obtained experimentally, analytic and numerical solutions were obtained to determine the distribution of liquid content within the thickness of material. Conformity with the theoretical solution in the problem of simple geometries motivates to employ the FE analysis in modelling of diffusion process into a PLA package. The liquid uptake in the package distributed non-homogeneously as a function of time and position.

CHAPTER 5
EFFECT OF LIQUID DIFFUSION ON THE MECHANICAL PERFORMANCE OF PLA-BASED MATERIAL

5.1 Introduction

This chapter investigates changes of performance on the PLA-based material during diffusion of liquid, which is represented by its mechanical properties as critical service parameters. The mechanical properties of material are necessary in evaluating stability of material during the entire service life of a component. Since the liquid diffusion discussed previously in Chapter 4 is a time-dependent process, it is also important to evaluate its interaction with time-dependent nature of the material. Creep behaviour is a time dependent property that controls the dimensional stability especially when the material has to support load during a certain period of time. Creep measurement seems to be an excellent method in analysing compatibility of PLA material with a particular chemical or solvent for packaging applications subjected to external load during filling, transportation and storage process.

In Chapter 4, it has been presented that the liquid content within the material is distributed non-uniformly as function of time and position. The material is submitted to non-uniform distribution over an extended period before reaching a saturated condition, much more slowly than temperature because of the slow movement of liquid (Tounsi et al., 2003). Initially, a higher liquid concentration is present near the surface at which the absorption occurs more rapidly rather than in the inner layers and then the material moves toward equilibrium liquid concentration as time passes. It comes to a consequence, where property changes associated with the presence of liquid are not uniformly distributed within the material (Paterson and

White, 1992). This chapter reviews the dependence of mechanical properties with liquid content to develop material constitutive equations in accurately analysing the mechanical behaviour under different loading conditions.

5.2 Mechanical properties

This section presents the result of experimental testing on the mechanical properties of the PLA-based material before fluid immersion and after achieving saturated liquid content. The mechanical properties tested and discussed in this section are comprised of:

- Tensile
- Flexural
- Impact
- Dynamic

As discussed previously in Chapter 2, many studies have focused on the effect of water/moisture sorption on mechanical properties and evaluating the evolution of mechanical properties with time. In this thesis, however, measurement of mechanical properties was performed after it has reached or gets near to equilibrium. It is expected that the fluid uptake has uniformly distributed in the material and can be properly analysed (Jia et al., 2004). Therefore, the dependency of mechanical properties on liquid content was examined by measuring the properties of saturated specimens conditioned in different temperature levels as discussed previously in section 4.3.2. In other words, varying levels of liquid content was obtained by accelerating the level of liquid absorption through different immersion temperatures.

5.2.1 Tensile properties

This section reviews the experimental results of measured tensile properties and their relation to liquid content. The tensile properties evaluated are tensile strength, modulus, strain at break and strain at maximum stress, which were determined according to the testing methodology outlined in section 3.3.1. Figure 5-1 shows the stress-strain tensile curve for the PLA-based material at various levels of liquid concentration. It can be seen that the tensile strength decreases progressively as a function of liquid uptake, from 35 MPa in dry specimen to almost 12 MPa in specimen with 5.95% of liquid content. In contrast, the material deformation represented by tensile strain increases with increasing of the liquid content, which records significant increase at specimens immersed at 30°C.

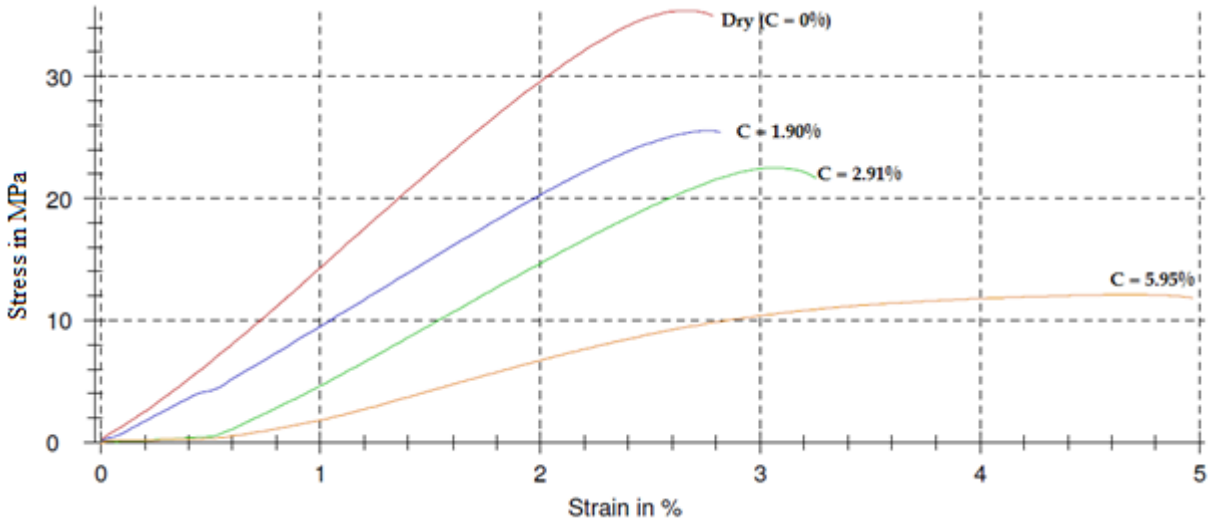

Figure 5-1: Tensile stress versus strain curve of the material with various levels of fluid content

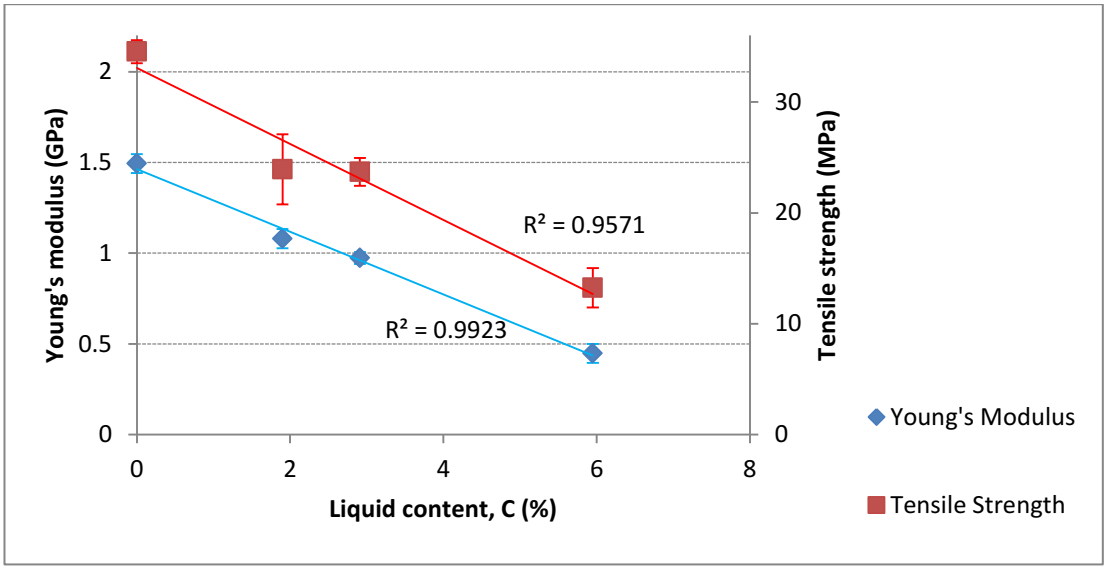

Figure 5-2: Linear relation of elastic modulus and tensile strength with fluid uptake

Tabulated results of tensile properties derived from the stress-strain curve are presented in Appendices C and plots of the average value with fluid content are shown in Figures 5-2 and 5-3. The elastic modulus and tensile strength are observed to be linearly dependent on the liquid content with a strong correlation coefficient. The linear regression fit to the experimental data for Young's Modulus and tensile strength is calculated using the form shown in Equation 5-1 resulting in the values shown Table 5-1.

$$y = aC(z,t) + b \tag{5.1}$$

Meanwhile, the elongations seem to have a better representation using an exponential regression form as follow

$$y = ae^{bC(z,t)} \tag{5.2}$$

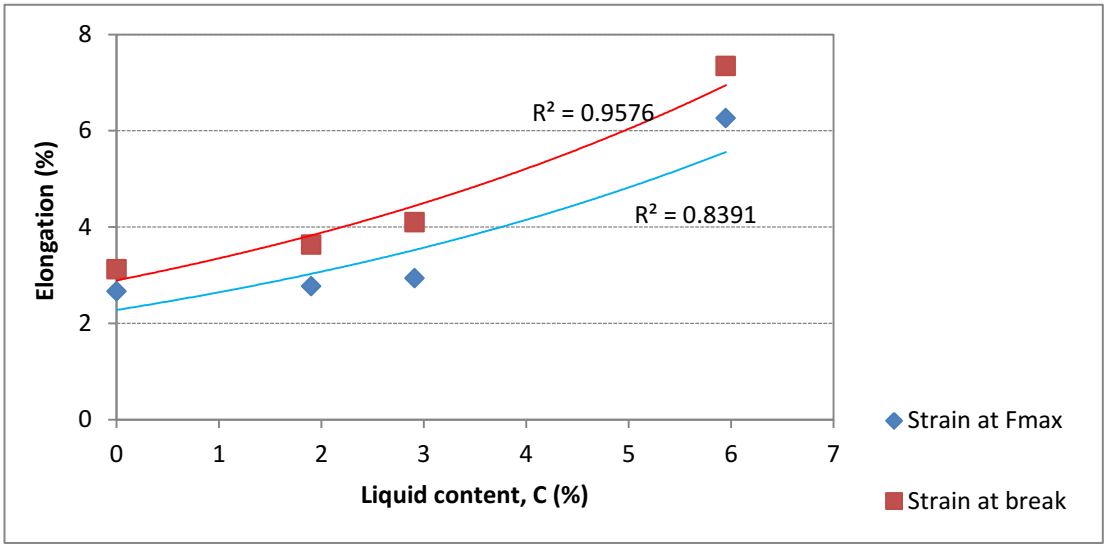

Figure 5-3: Exponential relation between elongation at maximum stress (F_{max}) and elongation at break from tensile test with fluid content

Table 5-1: Linear and exponential regression parameters of tensile properties with fluid content

Dependent Variable, y	Gradient (a)	Constant (b)
Modulus of elasticity	-0.173	1.46
Tensile strength	-3.423	33.06
Strain at max. stress	2.892	0.147
Strain at break	2.277	0.15

5.2.2 Flexural properties

The flexural tests performed according to outlined procedure in Section 3.3.2 measured properties such as flexural strength, modulus, elongation at break and elongation at maximum stress. Figure 5-4 shows the stress-strain flexural curve for the PLA-based material at various levels of fluid concentration. The figure shows that the flexural strength decreases with the liquid content, with a decrease of 30% from 30 MPa in increasing 5.95% of liquid uptake.

Figure 5-5 summarizes the test results which show the trends in flexural modulus and flexural strength. Linear relations exist but with lower correlation coefficient compared to that in tensile properties. The decreasing of flexural strength with increasing sorption amount is in agreement with other researches, which investigated the performance of PLA material in contact with liquid water (Dopico-García et al., 2012) and in high humidity conditions (Harris and Lee, 2010).

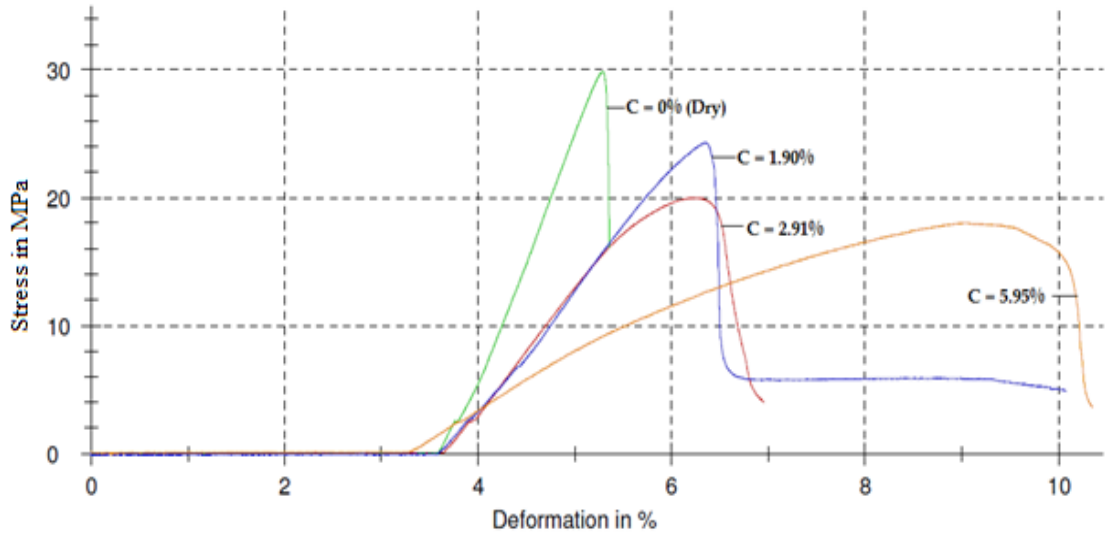

Figure 5-4: Flexural stress versus strain curve of the material with various levels of fluid content

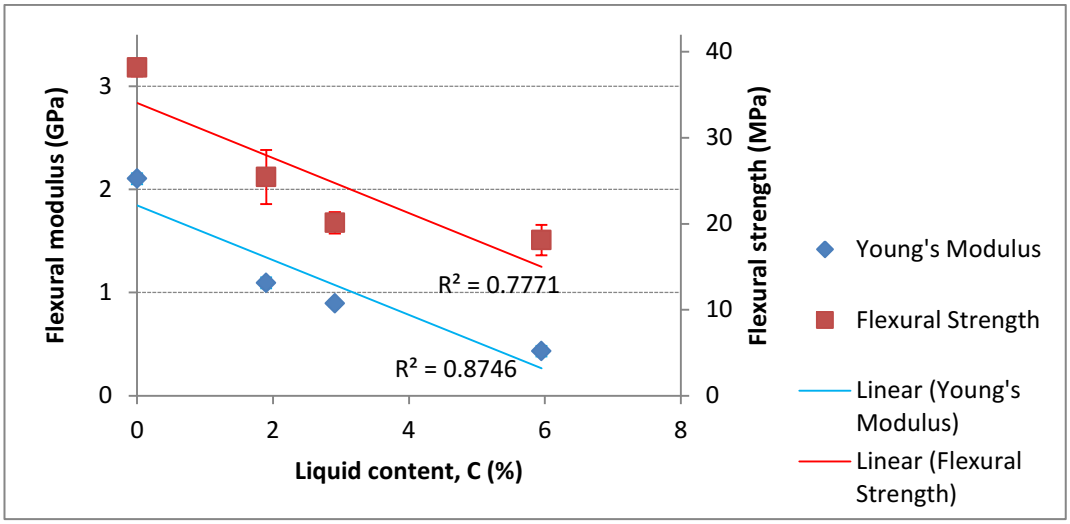

Figure 5-5: Exponential relation of flexural modulus and strength with fluid content

Similar to the result of tensile tests, an increasing trend of elongation at maximum stress and elongation at break was also observed from the flexural test. As shown in Figure 5-6, plot of

experimental data was fitted to the exponential form of Equation (5.2). It is revealed that the value of R^2, being an indicator of the goodness of a curve fit.

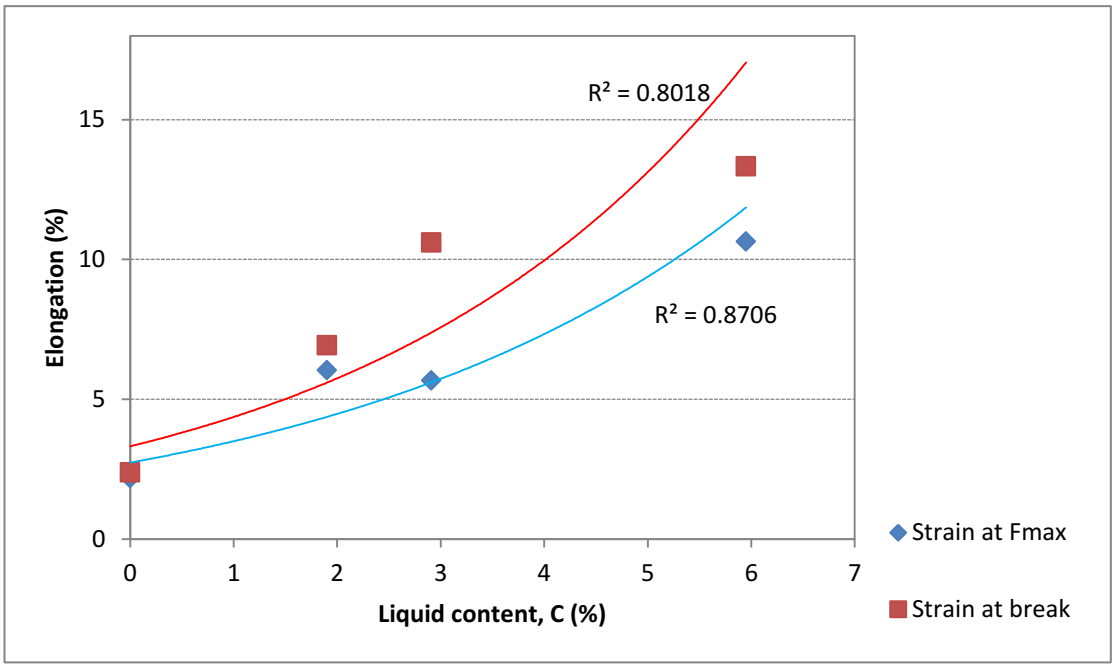

Figure 5-6: Exponential relation between elongation at maximum stress and elongation at break from flexural test with fluid content

5.2.3 Impact properties

The impact test is performed to determine the resistance of the material and the amount of energy it is capable of absorbing. The impact property which determines the toughness of the material was measured following the ASTM standard as explained in Section 3.3.3. The measured notched impact strength of dry PLA material, with a value of 1.67 kJ/m^2, has comparable result with the result reported by Jaratrotkamjorn et al. (2012). The impact strength measured from the recorded energy absorbed of specimens with different levels of liquid content are given in Figure 5-7.

The impact test result presented in Figure 5-7 shows different trend when compared to results of the tensile and flexural strength. As the liquid content increased, higher value of absorbed energy was observed after fracturing the specimens. However, after reaching maximum value of 2.7 kJ/m^2 in specimen with 2.91% liquid content, the impact strength of specimen with 5.95% liquid content declined to 2.1 kJ/m^2. This behaviour probably relates to significance degradation experienced by the high liquid concentration-material, as was also observed for PLA samples exposed to liquid water by Dopico-García et al. (2012).

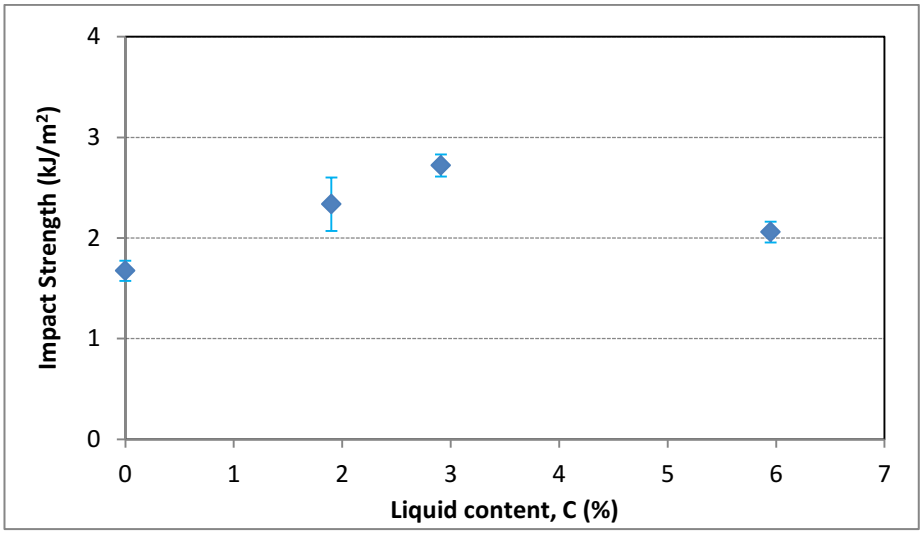

Figure 5-7: Impact strength of PLA-based specimen as a function of liquid concentration

5.2.4 Dynamic mechanical properties

Using dynamic mechanical analysis, the viscoelastic properties observed were storage modulus (E'), loss modulus (E''), and mechanical damping (tan δ). The storage modulus indicates the inherent stiffness of the material under dynamic loading conditions. Dividing the loss modulus by the storage modulus gives tan δ. The loss modulus and tan δ curves help to identify one or more regions where the onset of specific types of molecular motion causes relatively large changes in properties over relatively narrow bands of temperature. These events are transitions and the most important of these is the glass transition (Sepe, 1997).

Figure 5-8 presents the results of the dynamic mechanical analysis of an unexposed PLA based specimen. The storage modulus curve consists of three zones: a glassy region, a sudden-fall region that corresponds to the respective relaxation in the PLA-based polymer, and a high-temperature region. In the range of temperature below 55°C, the material presents high mechanical stiffness (E' > 1500 MPa). In this region, the polymer is glassy and frequently brittle (Chanda and Roy, 2009). Following this is a sharp drop of modulus, a phenomenon of mechanical relaxation of the amorphous phase during the glass transition of the polymer. Above T = 65°C, the softening of the crystalline phase (Habas-Ulloa et al., 2010) can be observed, which means that the polymer is in the molten state. The glass-transition temperature, T_g, is identified as a peak in tan δ or loss modulus trace and it is around 57-63°C, which is comparable to the material property data released by NatureWorks LLC for their injection mould-grade PLA (Jamshidian et al., 2010).

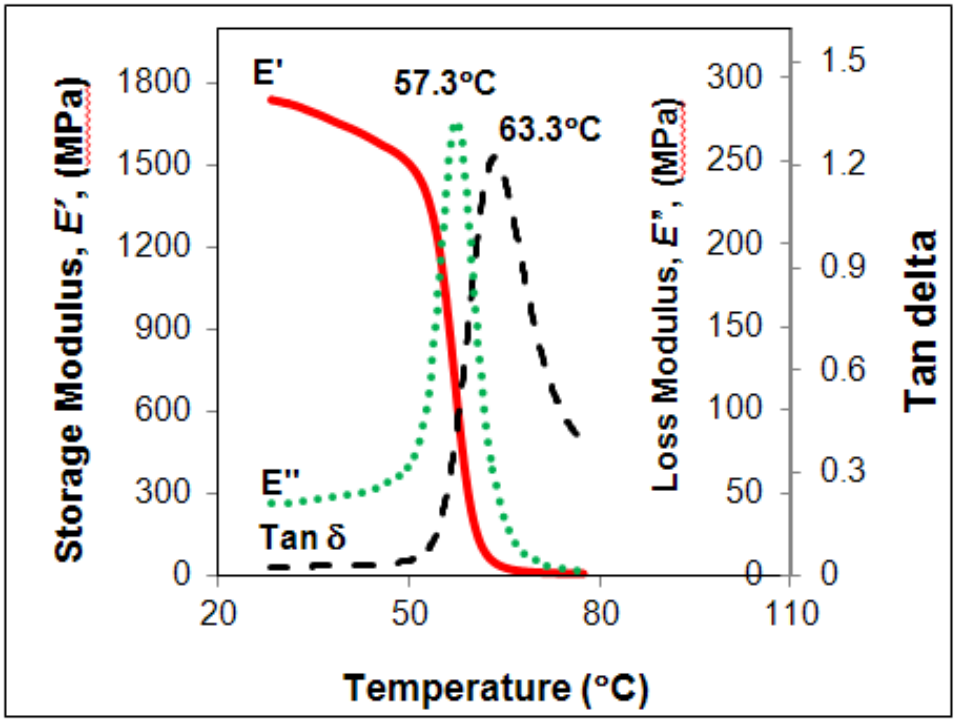

Figure 5-8: Thermomechanical analysis of dry specimen (0% fluid content) using frequency of 1 Hz

Figure 5-9 shows the dynamic mechanical properties as a function of temperature for the PLA based plastic specimens subjected to liquid absorption. The variation of the storage modulus (E') shows that it is affected by temperature and liquid uptake. At low temperatures (below 55°C), a reduction of E' with an increase in fluid concentration can be observed (Figure 5-9a). This figure also shows the reduction in the tan δ peak heights associated with the storage modulus plot. However, it is worth noting that a split on tan δ was observed in the 6% fluid containing sample, which suggests that an apparent phase separation had taken place in the material. Karad and Jones (2005) suggested that the second peak was indicative of degradation of the resin molecular structure, which was believed to be assisted by the higher rate of fluid absorption. Above 55°C, the decreasing rate of E' was higher compared to those in the low temperature region. It should also be noted that in this high temperature region, a higher E' was observed for specimens with a higher fluid concentration (Figure 5-9b).

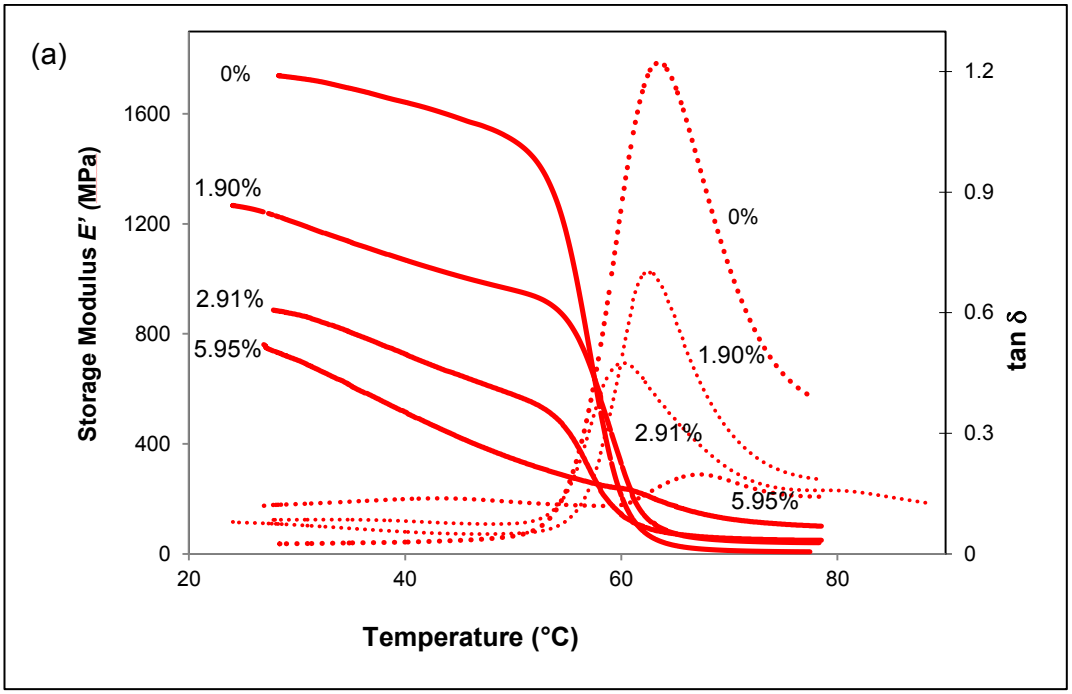

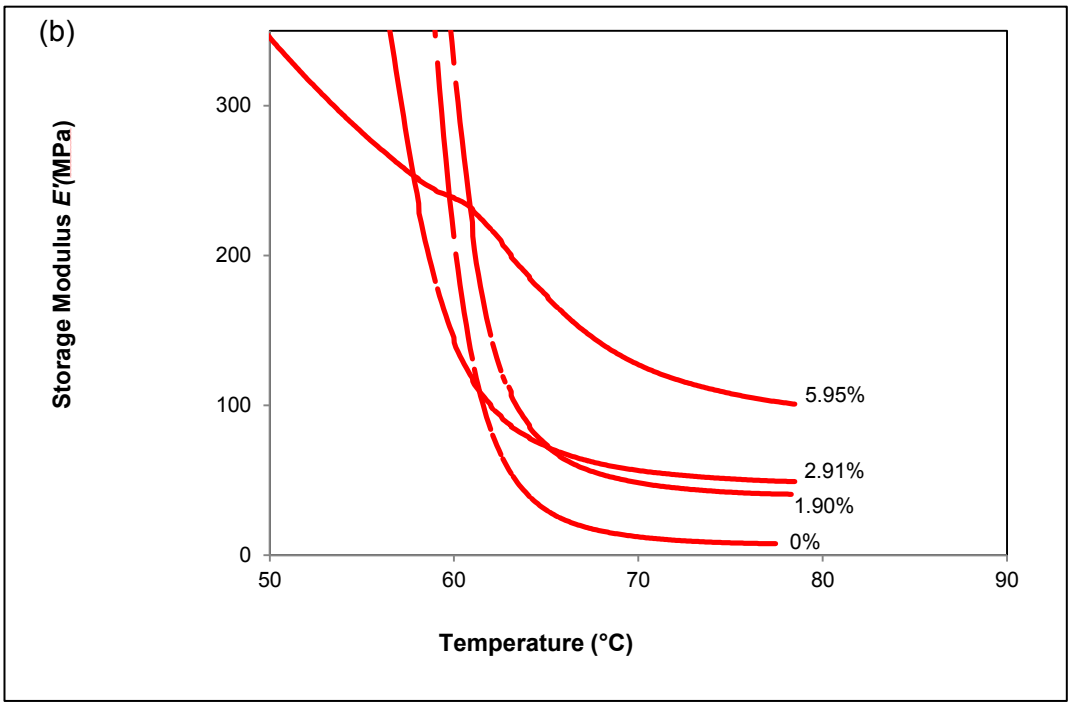

Figure 5-9: Effect of fluid content on viscoelastic properties (solid line is storage modulus whereas dot line is tan δ) at : (a) Low test temperature and (b) high test temperature

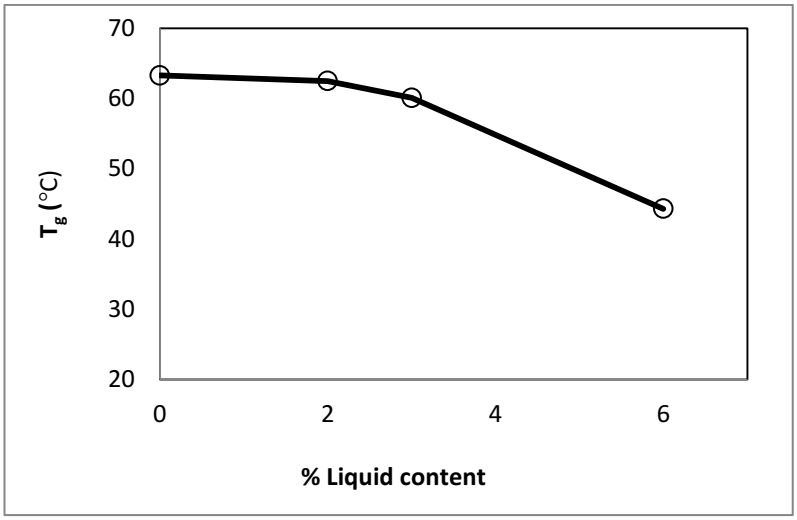

Figure 5-10: Effect of fluid content on glass transition temperature determined from peak of tan δ

The effect of absorbed fluid on changes of glass transition temperature (T_g) is displayed in Figure 5-10. As T_g is determined from the peak of tan δ curve, only a small shift of the glass transition region was observed. However, dramatic decrease of T_g was observed in specimens with 6% fluid content which has apparent split of tan δ curve. Decreasing of glass transition temperature is a common consequence observed with the presence of water and other small molecules (CO_2 and various organic solvents) in polymeric material (Zheng et al., 2004, Wu et al., 2000).

5.3 Creep behaviour

Plastics possess very temperature-sensitive creep behaviour, and exhibit significant creep even at room temperature (Chanda and Roy, 2009). Creep phenomenon occurs as a result of molecular relaxation under constant load at longer times. To further characterize the rheological properties of the polymer, creep tests were undertaken. In a creep test, a constant load or stress is applied to the material, and the variation of deformation or strain with time is recorded. This section presents the effect of fluid absorption on creep behaviour of PLA-based material which was explored in a series of creep tests. The test was performed at a constant stress 0.45 MPa on specimens subjected to different levels of fluid concentration at different test temperatures.

5.3.1 Effect of test temperature

The results of the creep tests are presented in Figures 5-11a, b and c for specimens tested at 30, 40 and 50°C, respectively.

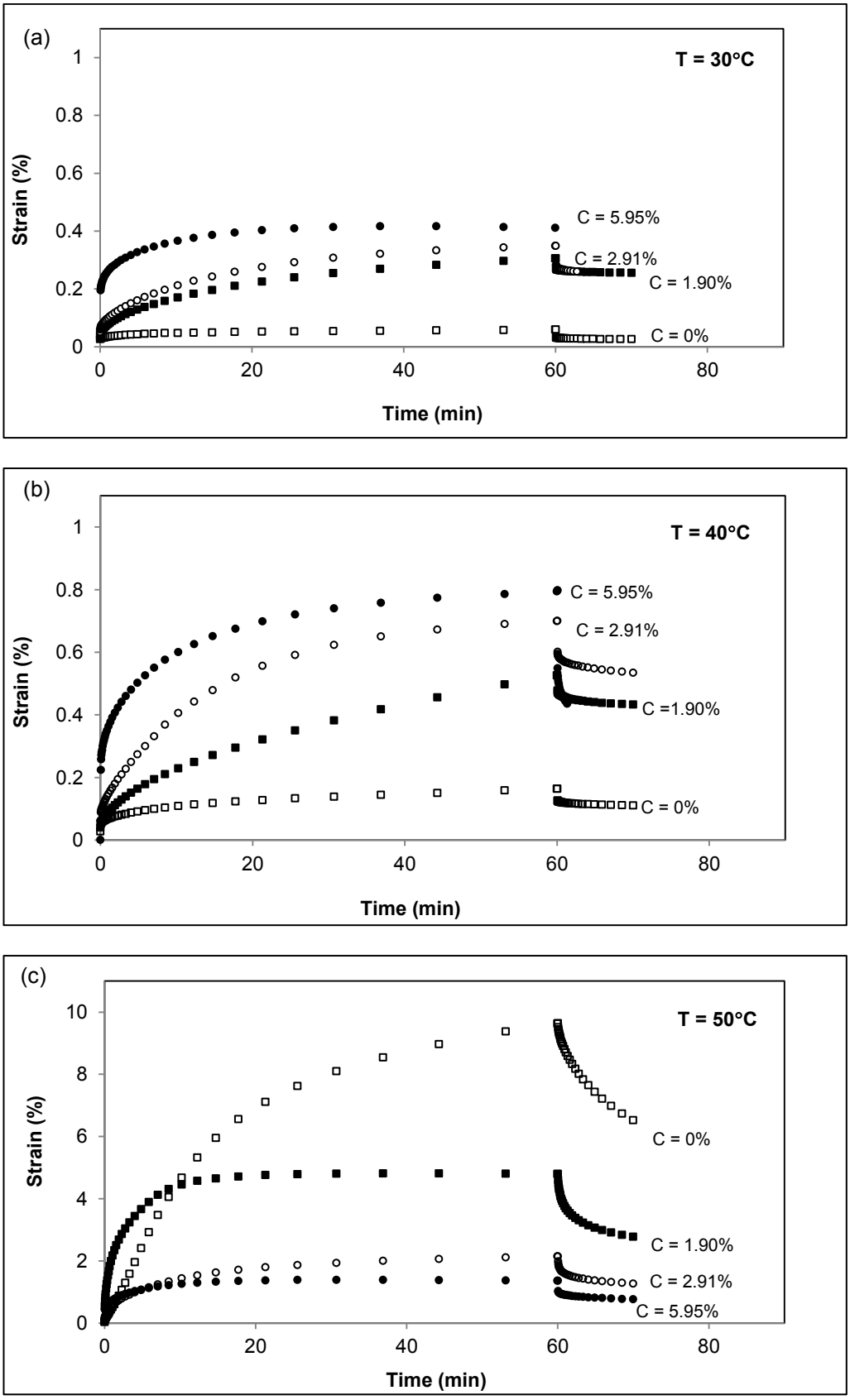

Figure 5-11: Creep strain versus time at 0.45 MPa in test temperature: (a) 30℃, (b) 40℃, and (c) 50℃ for specimens with various levels of fluid concentration

The creep curves produced at all the test temperatures exhibited typical creep behaviour for semi-crystalline materials subjected to constant stress, which falls into three regimes: (1) instantaneous elastic response, (2) retarded viscoelastic response and (3) permanent flow response (Sun et al., 2005). As the test temperature increased, the variation in the creep strain also increased. Similar results on bio-based polymer were observed by Sen et al. (2002) and Ditudompo et al. (2013a). As expected, at low temperatures (up to 40°C), the creep strain increased with an increase in fluid uptake (Figures 5-11a and 5-11b). This behaviour can be explained considering that fluid uptake plays a role of a plasticizer, allowing more chain movement in the amorphous phase of the biopolymer during liquid transport (Zheng et al., 2004). Therefore, lower modulus due to increasing liquid uptake leads to a higher strain, and the creep deformation of absorbed specimens will proceed more rapidly than that in the dry material. Najafi et al. (2008) revealed another mechanism that leads to higher creep deflections at higher liquid uptake. It is believed that liquid sorption causes the polymer molecules to relax more easily in the presence of liquid.

Nevertheless, the creep behaviour of specimens at 50°C follows a different trend. Figure 5-11c presents a significant decrease of creep strain as the fluid content increase. With respect to samples tested at 30 and 40°C, the drier samples at 50°C showed a lower creep strain rate in the initial part of the test but later in the test, the rate sharply increased and the final values were higher still. In other words, specimens with a higher fluid concentration have greater stiffening than those containing a lower fluid content. A similar finding with a different material was reported by Habas-Ulloa et al. (2010) , who researched gas-oil exposure effects on HDPE (high density polyethylene). They found that with only a short ageing time, the creep strain of the HDPE specimen containing a greater gas-oil uptake was higher than that containing a lower fluid uptake. However, with a longer gas-oil immersion time, a stiffening of the material containing a higher fluid concentration was observed. Papanicolaou et al. (2009) also reported the anomalous creep behaviour of glass epoxy composites in humid conditions. The creep strain of the material increased until the water uptake reaching a maximum value, but then rapidly decreased and after a long ageing time, the material became stiffer than the dry material.

In order to better understand this phenomenon, additional diagrams are presented. Figure 5-12 shows the creep strain accumulation of the samples at t = 60 minutes at different liquid concentrations. It displays different trends of creep strain with a liquid content at low and high temperatures, which confirms the findings explained by Figure 5-11. The magnified circle in Figure 5-12 shows the increasing creep strain with liquid uptake at a low temperature.

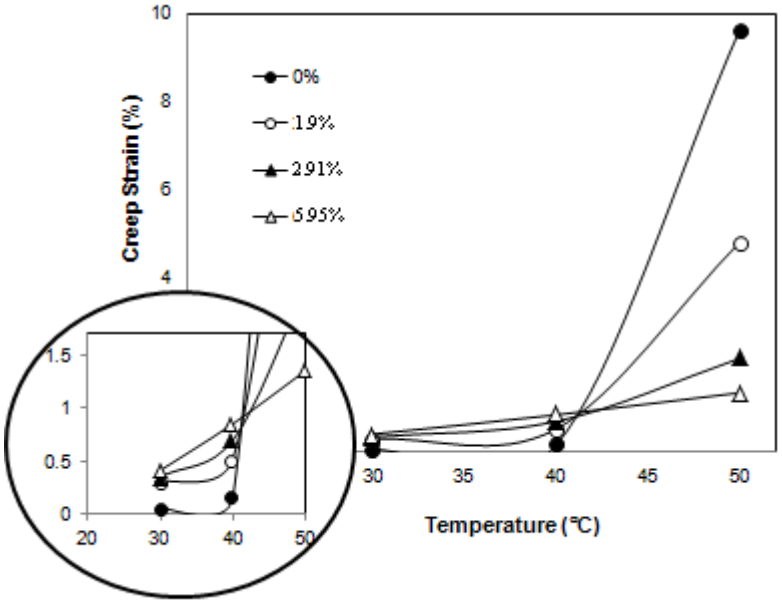

Figure 5-12: Creep strain accumulated at 60 min as a function of creep test temperature for different levels of fluid concentration

To evaluate the reciprocation law of visco-elasticity, creep compliance, J(t), was calculated. Figure 5-13 shows the creep compliance curves of the test specimens. Creep compliance is defined as the ratio of creep strain ε(t) to the applied stress σ as given below (Sheng et al., 2010).

$$J(t) = \frac{\varepsilon(t)}{\sigma} \tag{5.3}$$

Figure 5-13 shows that at the same value of imposed stress, the strain and creep compliance increase as the test temperature is raised. It can be seen that a higher mechanical flexibility is provoked by the enhanced chain mobility that results in increased creep deformation (Nunez et al., 2004, Cyras et al., 2002). The figure for dry specimens (Figure 5-13a) indicates a more significant increase of creep strain rate with increasing temperature compared to the specimens that absorbed liquid. However, as the liquid uptake inside the material increases, a decrease of creep strain rate with temperature can be observed (Figure 5-13b). In the case of dry material, creep compliance rapidly increases with temperature. In contrast, for material with a liquid content, the creep compliance is almost invariant with temperature, though an increased tendency can be observed. From these figures, it was assumed that the presence of liquid, particularly at elevated temperatures, induced physical structural changes of the polymeric material.

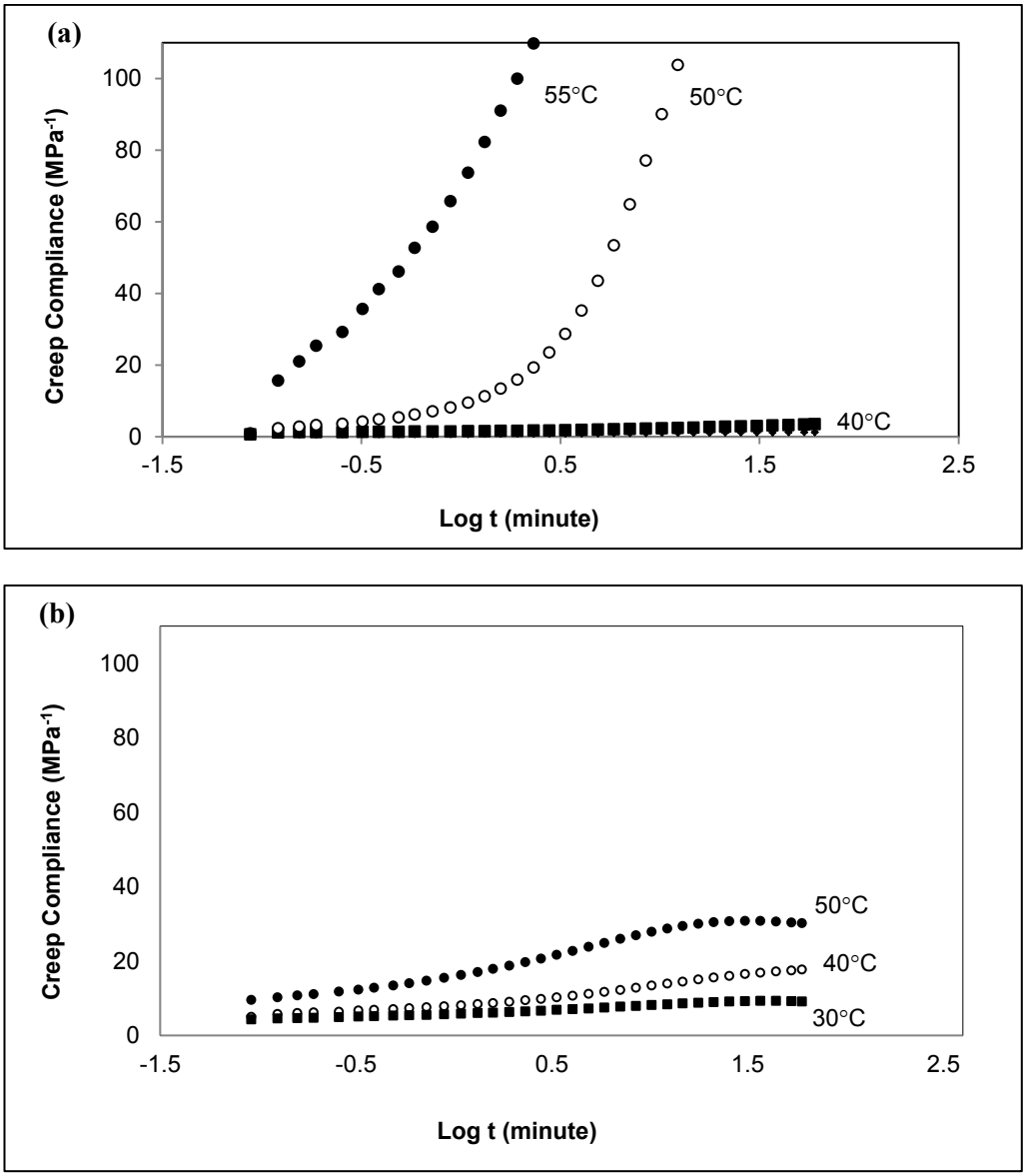

Figure 5-13: Creep compliance curves in time function at different test temperatures for (a) dry specimens and (b) specimens contain 5.95% fluid uptake

5.3.2 Thermal properties

Differential Scanning Calorimeter (DSC) measurement was employed to further investigate the structural changes of dry and immersed material after ageing at an elevated temperature typical for the creep test described earlier. The relative crystallinity, X_c, of the specimens was measured using Differential Scanning Calorimetry (DSC, TA Instrument). Heating runs were conducted from room temperature to 200°C at a heating rate of 3°C/min. The weights of the PLA specimens for DSC were 7-10 mg, taken from cross sections of the creep test rectangular bars.

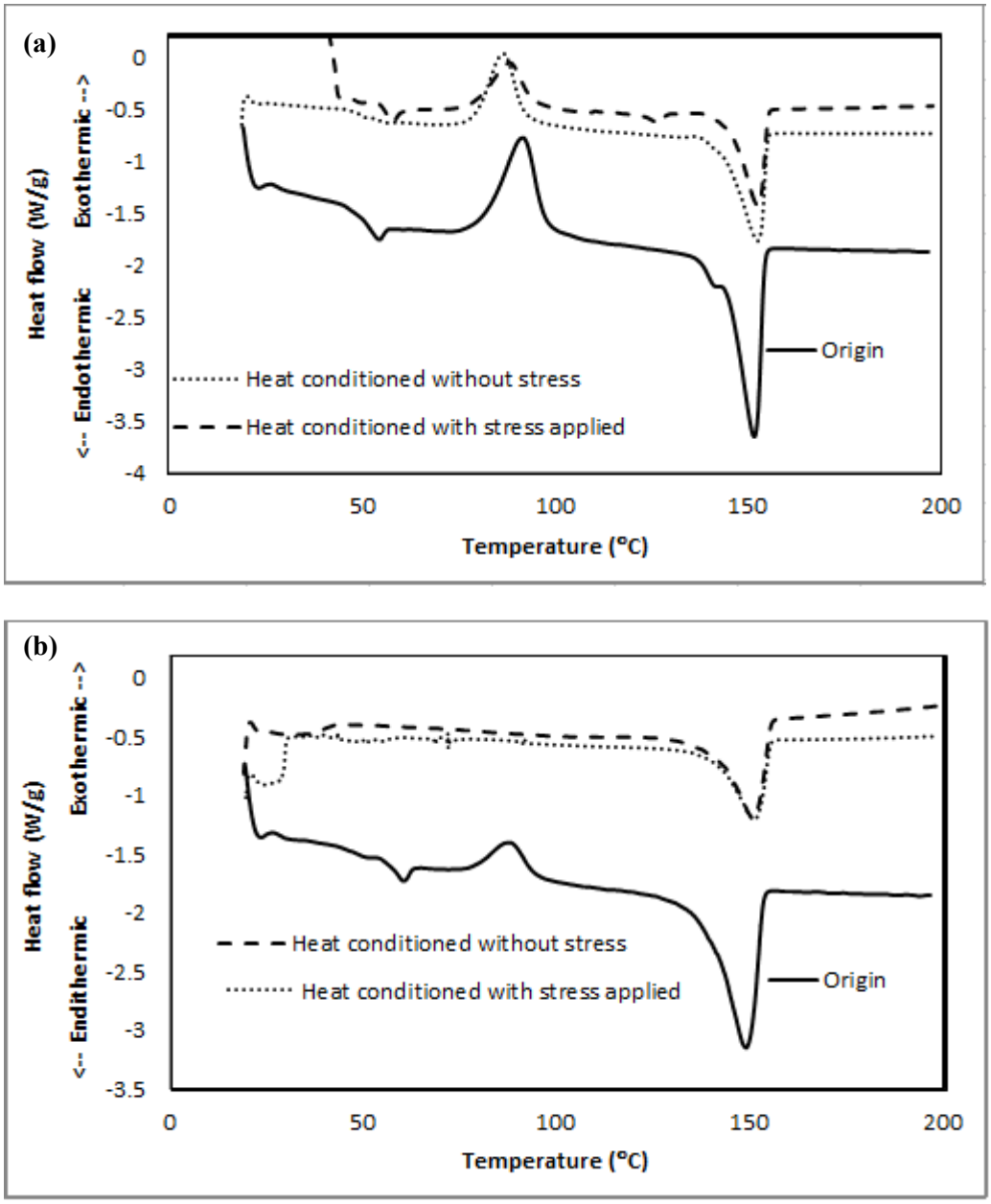

Figure 5-14: DSC curves of materials after 50℃ heat conditioned with and without applied stress compared to the origin samples for: (a) dry specimens and (b) specimens with 6% liquid content

Figure 5-14 shows the overlay DSC curves of specimens before and after the DMA creep test as a function of temperature. In the DSC profile of the original dry material before the creep test (Figure 5-14a), endothermic and exothermic peaks derived from glass transition, crystallization of the amorphous phase, and the melting of the crystalline phase were detected at 56.5°C, 91.55°C and 151.65°C, respectively. On the dry specimen, an exothermic peak of crystallization was detected both before and after the 50°C tests. Nevertheless, the peak disappeared in the 6% fluid content samples after the creep test (Figure 5-14b). This DSC profile indicates that the

crystallization process that occurs at 50°C had been completed. In addition, another DSC test was run for specimens that had been previously conditioned at 50°C in a thermogravimetric (TGA) device to simulate the same heat conditions but without applied stress. Figure 5-14 indicates that the effect of low applied stress (0.45 MPa) to crystallinity behavior was negligible.

Table 5-2: Heat of fusion and degree of crystallinity before and after 50℃ heat conditioned

Conditions	T_m (°C)	ΔH_c (J/g)	ΔH_m (J/g)	X_c (%)
Dry	151.65	13.96	19.11	5.74
Dry after 50°C heat conditioned	152.68	8.69	17.34	9.64
5.95% fluid content	149.42	3.01	17.44	16.09
5.95% fluid content after 50°C heat conditioned	149.59	-	20.00	22.30

The results indicate that the organic liquid absorption and heat condition have a significant effect on the degree of crystallinity. These results have also been reported by Naga et al. (2011), where a potential improvement in the PLA specimen crystallinity has been recorded due to organic solvent diffusion. Absorbed fluid plays the role of a plasticizer, which provokes movement in the amorphous phase that promotes a rearrangement of the structure and an increase in the crystallinity (Scaffaro et al., 2008), particularly at an elevated temperature. It is well known that the degree of crystallinity significantly affects the mechanical properties of polymeric materials. Earlier research has confirmed that the strength of semicrystalline polymers, including creep resistance, increases with an increase in the crystallinity ratio (Dusunceli and Colak, 2008, Sun et al., 2005). Therefore, the improvement in creep resistance of high fluid content samples (Figure 5-11c), as well as in the stiffness of the material at high temperatures (Figure 5-9b) can be attributed to a significant increase in the degree of crystallinity of PLA based specimens, as indicated in Table 5-2.

5.4 Dependence of viscoelastic properties on fluid content and temperature

As discussed previously in section 4.2.3, an application exposed to a fluid environment at temperature T will absorb a particular amount of liquid with a diffusion coefficient D(T) and then gain a saturated concentration $C_m(T)$. A higher liquid content initially presents at the surface exposed to liquid and it is then followed by the inner layers. Therefore, it is expected

that the viscoelastic property changes associated with the presence of liquid are not uniformly distributed within the material. This section presents the characteristics of material for which the viscoelastic properties changes due to the diffusion of fluid through its thickness. A viscoelastic model that accounts for changes in elastic moduli and relaxation time will be developed in characterizing the material response. The coefficients on the functions of material property are liquid-content dependent, which have a time and spatial function.

The first sub section concerns the effect of liquid content on changes of viscoelastic properties, including the concept of time-liquid content superposition. The viscoelastic constitutive law is expressed using a creep-based formulation and the coefficients of the models are determined by fitting the general equation to the data obtained from creep experiment presented previously in section 5.2.1. Since the viscoelastic property is not only time dependent but also temperature dependent, effect of environment temperature T will be taken into account in the model which is discussed in the next section.

5.4.1 The creep models

Two different types of viscoelastic model, the empirical mathematical model using Findley power model and mechanical analogy model using four-element Burger model were applied to represent the creep behaviour of the PLA-based material subjected to fluid diffusion.

The modulus of relaxation defined by the time-dependent constitutive equation for constants stress is given by Equations (5.5) and (5.6) using the power and Burgers model, respectively.

$$J(t) = \frac{1}{E_p}\left[1+\left(\frac{t}{\tau_p}\right)\right]^b \tag{5.4}$$

$$J(t) = \frac{1}{E_M} + \frac{1}{E_K}\left[1 - exp\left(-\frac{t}{\tau}\right)\right] + \frac{t}{\eta_M} \tag{5.5}$$

where J(t) is the creep compliance, the reciprocal of the modulus of relaxation, while E_M and E_K are the elastic moduli of the Maxwell and the Kelvin springs, and η_M and η_K are viscosities of the Maxwell and Kelvin dashpots with retardation time, $\tau = E_K/\eta_K$.

The creep compliance curves of the experiment data were drawn and were then fitted to the creep models using a nonlinear least-square method with MATLAB® software. The algorithm used for the fitting procedure was Trust-Region, and if it did not produce a reasonable fit, the Levenberg-Marquardt algorithm was used. The agreement of the fit with the experimental data is represented by the square of correlation (R^2) and sum of squared error (SSE). The R^2

measures how successful the fit in explaining the variation of data, while the SSE measures total deviation of the experimental data from the fitted data (MathWorks, 2013).

Table 5-3: Goodness of fit values for the fitting of partial creep data using the power and Burgers models

Liquid content	Test temperature	R^2		SSE	
		Power	Burgers	Power	Burgers
C = 0%	30°C	0.99	0.99	2.04E-5	1.77E-5
	40°C	0.99	0.97	4.29E-4	9.10E-4
	50°C	0.98	0.99	6.28	0.557
C = 6%	30°C	0.99	0.98	7.14E-4	3.17E-3
	40°C	0.99	0.98	4.02E-3	2.03E-2
	50°C	0.98	0.99	8.63E-2	3.32E-2

Both creep models presented in Equations (5.5) and (5.6) can be satisfactorily fitted to the experiment data within the time frame corresponding to the test as represented from the values of R^2 and SSE shown in Table 5-3. The table shows high value of R^2 and low value of SSE which indicates a good fit. However, those two models will make different prediction for longer term behaviour. Therefore, in evaluating the most suitable model for describing longer term creep behaviour, ¾ part of the experiment data (t = 0 to t = 45 minutes) were fitted to the model and the remaining (t = 45 to t = 60 minutes) were considered as prediction points. Figure 5-15 shows the curves of creep compliance in the same amount of absorbed fluid but at different test temperatures, where the points in the figure indicate experimental data and the lines are for the curve fit. Creep compliance of dry specimen at 50°C test temperature is not displayed in Figure 5-15 since the values are extremely higher compared to those at lower temperature.

As indicated in Figures 5-15 and 5-16, the Findley power law and the Burgers four-parameter model were suitable to predict longer term creep behaviour of dry PLA-based specimens conditioned at low temperatures (<50°C). The figures show that for specimens containing higher level of liquid content (6% liquid uptake) and the ones tested under high creep test temperatures, the creep compliance approaches as asymptotic value after a long time. Therefore, the Burger's model of Equation (5.6) will better predict the longer term creep behaviour.

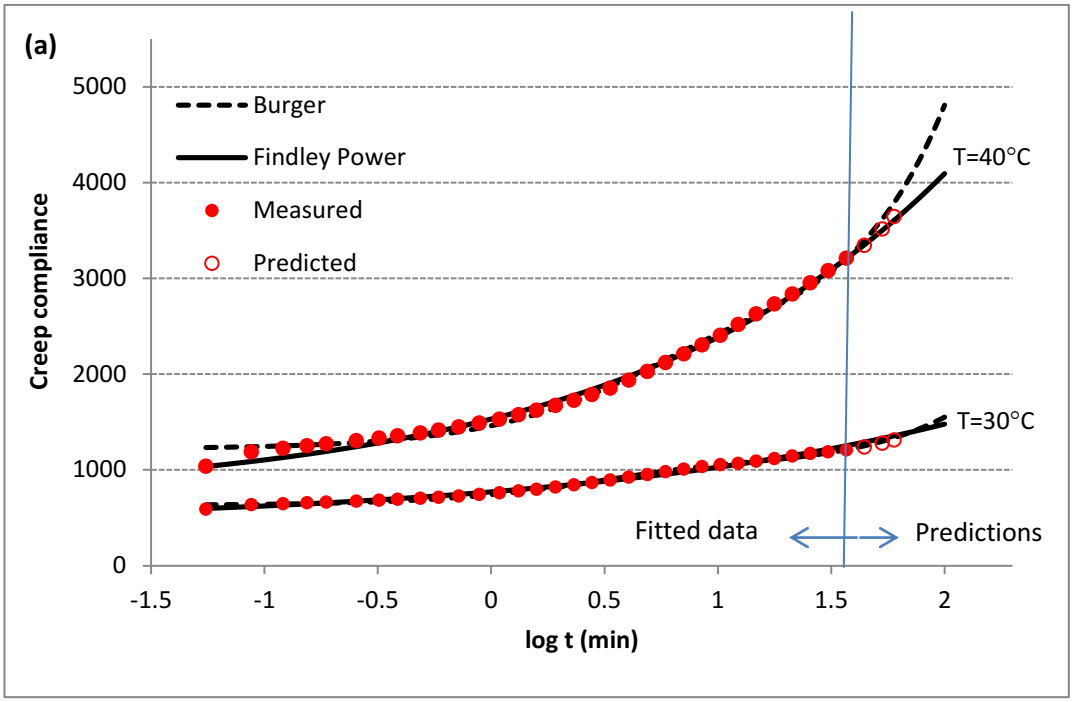

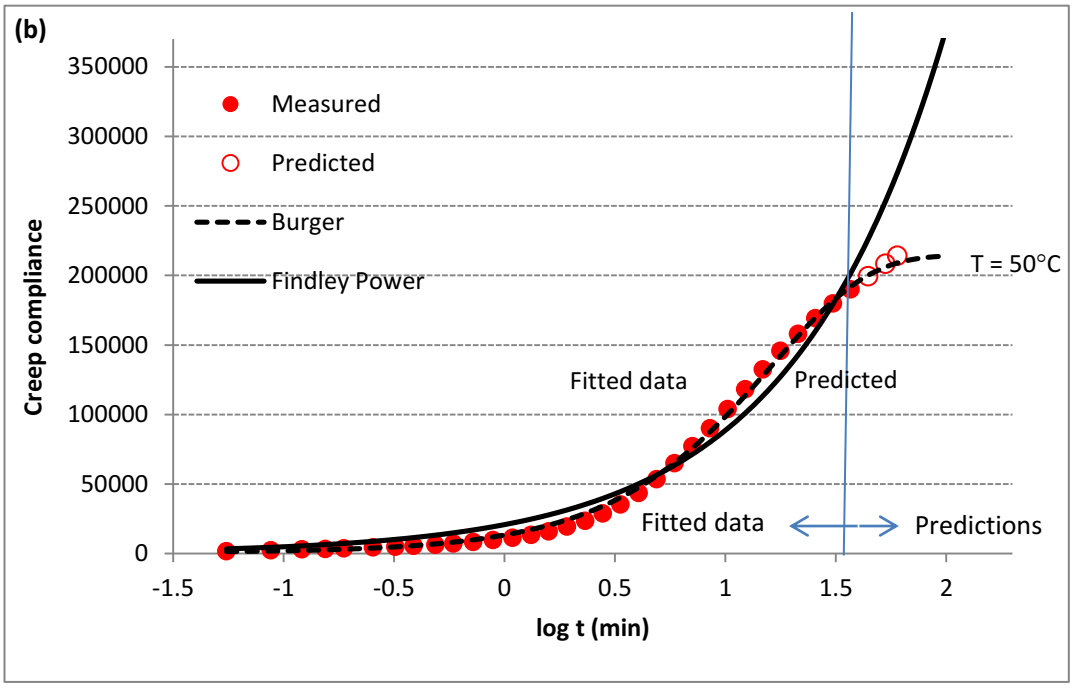

Figure 5-15: Creep compliance curves of dry material (C = 0%) in time function at (a) 30 °and 40 ℃ test temperature and (b) 50 ℃ test temperature

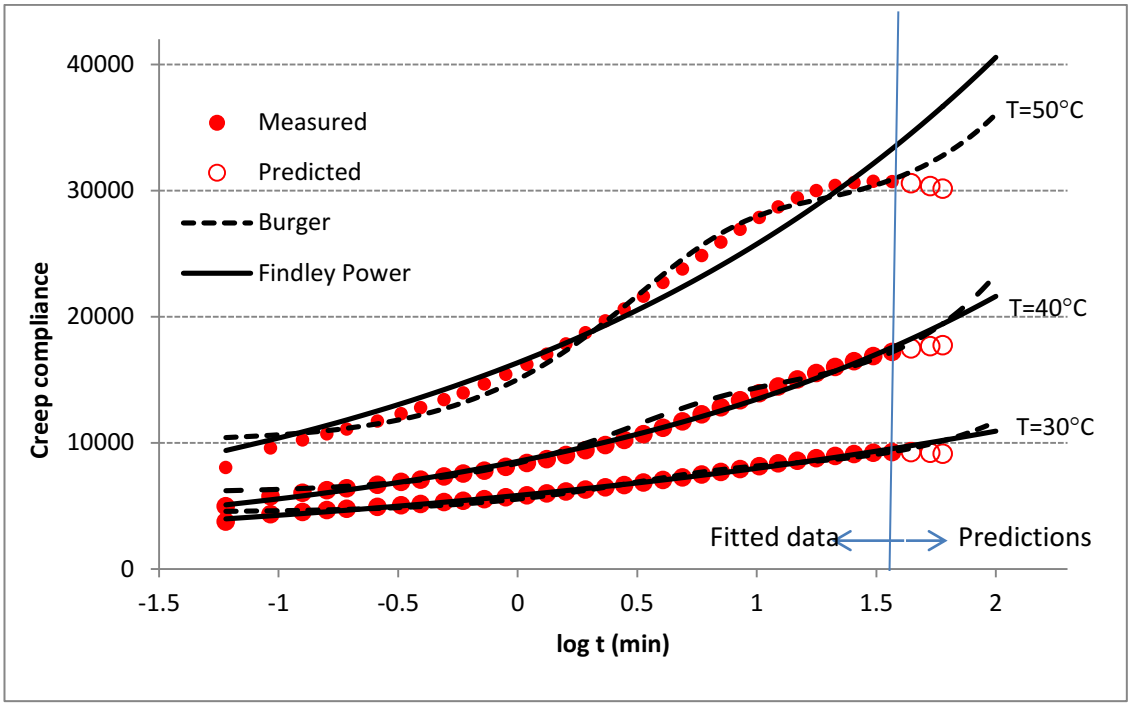

Figure 5-16: Creep compliance curves of material with C = 6% in time function at 30°, 40° and 50°C test temperature

5.4.2 Effect of liquid content on viscoelastic properties

Experimental curves from a set of creep tests under different levels of liquid content at constant isothermal temperatures described in Section 5.2.1 were fitted by means of Burger's creep model. The parameters of the viscoelastic models were determined by least squares curve fitting of the data using the Curve Fit toolbox in the MATLAB® software. Fit of experiments data to Burger's model at 30° to 50°C test temperature is shown in Figure 5-17. It could be seen from Figure 5-17 that the model prediction shows a satisfactory agreement with the experimental data under each condition. As discussed previously in Section 5.2.1, increasing creep strain with liquid content was observed, especially at low temperatures, corresponding to the plasticizing effect resulted from fluid sorption.

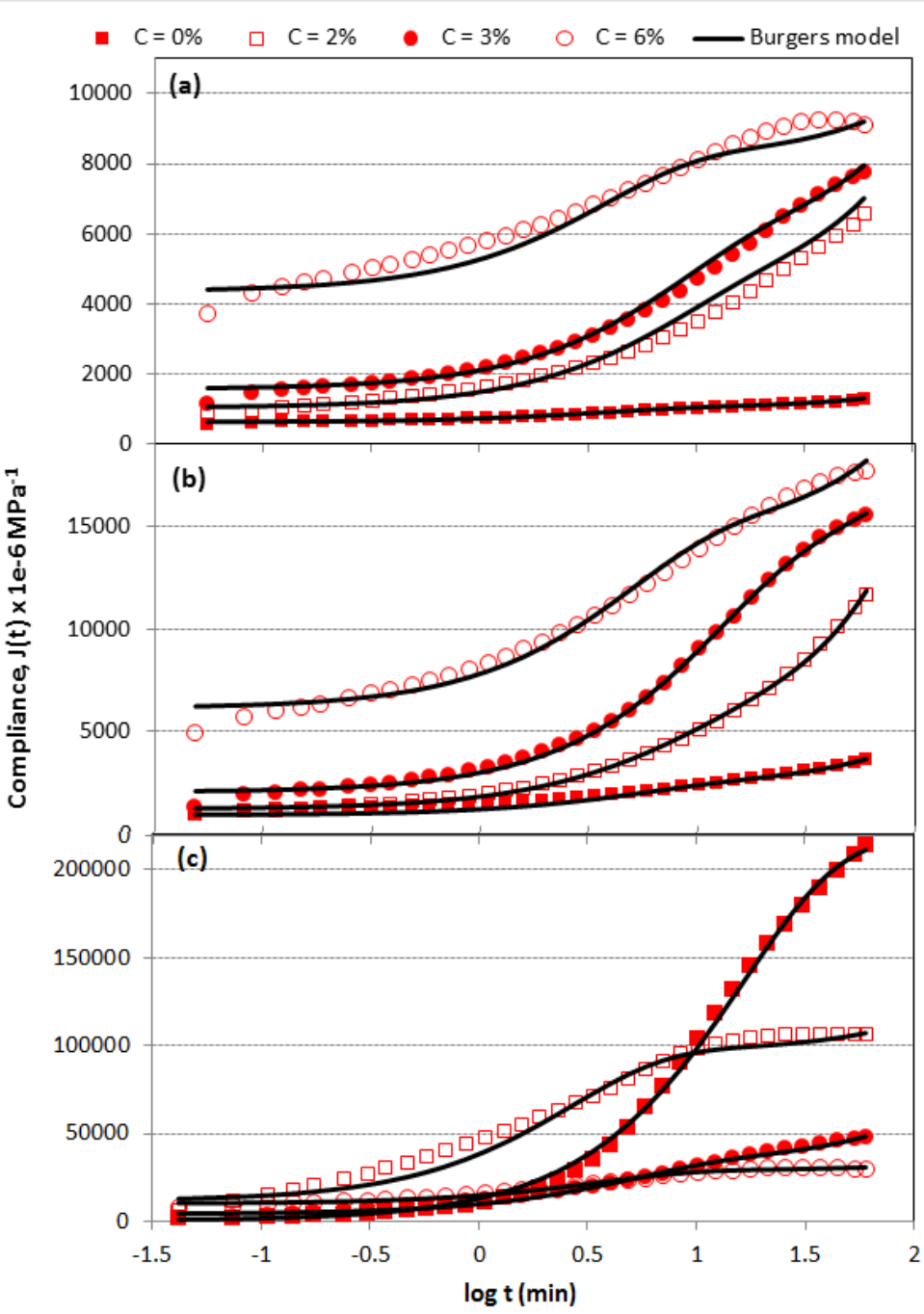

Figure 5-17: Creep compliance curves in time function at different levels of fluid concentration at: (a) 30℃, (b) 40℃ and (c) 50℃ test temperature

The Burgers model parameters obtained from the fitting of experimental data reflect the effects of liquid content and temperature on creep behaviour of material. The creep paramaters in each test temperature were plotted as a function of liquid content. Figure 5-18 summarizes the values of E_M parameter as a function of liquid content. The instantaneous modulus of the Maxwell spring (E_M) is time independent that establishes the instantaneous elastic creep strain. This

parameter would be immediately recovered on the removal of the stress and might be associated with the elasticity of the crystallized polymer or regular chain (Tang et al., 2012, Pérez et al., 2008), which took the immediate load due to high stiffness compared to amorphous polymers. The figure shows that E_M decreases with the increase in liquid content within the whole temperature range. This is a direct indication that liquid content increased the deformation of samples and reduced the elastic properties of materials (Ranade et al., 2005) which mirrors the tensile results previously discussed in Section 5.1.1. Additionally, at the same level of liquid content, decreasing of instantaneous modulus with temperature was observed. It is related to the softening of the bulk materials at elevated temperature, which leads to a decrease on the stiffness due to diminished instantaneous modulus (Tang et al., 2012). Similar result was reported by Ditudompo et al. (2013b) in the creep behaviour of a starch-based biopolymer.

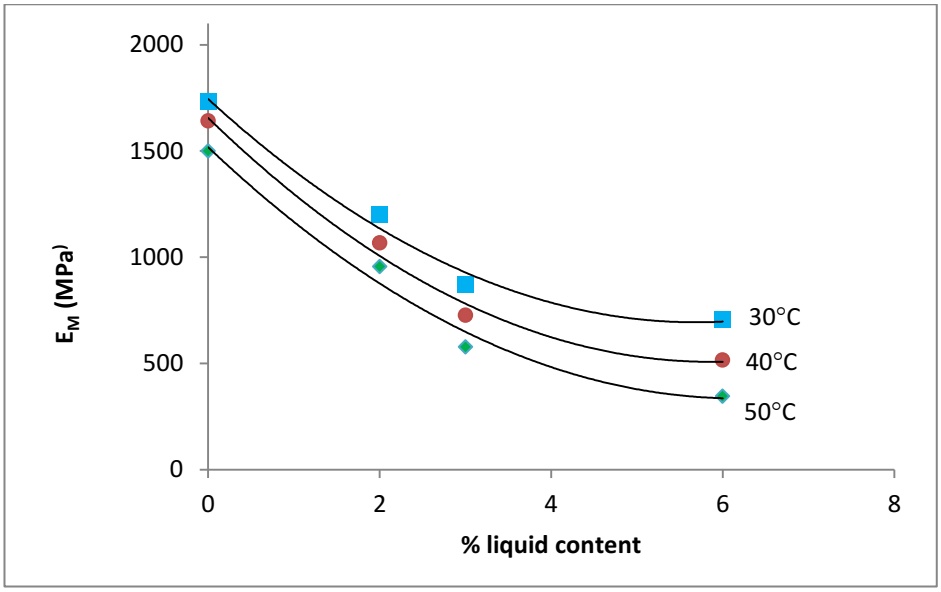

Figure 5-18: Relation between creep model parameters E_M and liquid concentration at different test temperatures

The retardant elasticity, E_K and viscosity η_K in the Kelvin unit can be related with the stiffness and the viscosity or flow of amorphous polymer chains in the short term (Tang et al., 2012), respectively. Figure 5-19(a) shows that E_K decreases significantly with an increase in liquid content at 30° and 40°C creep test temperature due to increase in the viscoelastic deformation. However, the samples tested at high test temperature (50°C) showed almost no enhancement of E_K with liquid content. At the same level of liquid content, the values of E_K decreased with temperature. The behaviour in high temperature corresponds to significant structural changes as previously discussed in Section 5.2.2. Similar trend was also observed for parameter η_K as shown in Figure 5-19(b). Lowering of η_K with increasing temperature was due to the

enhancement of the mobility of polymer chains (Xu et al., 2010), which would make the matrix softer and the orientation movement of amorphous chains easier.

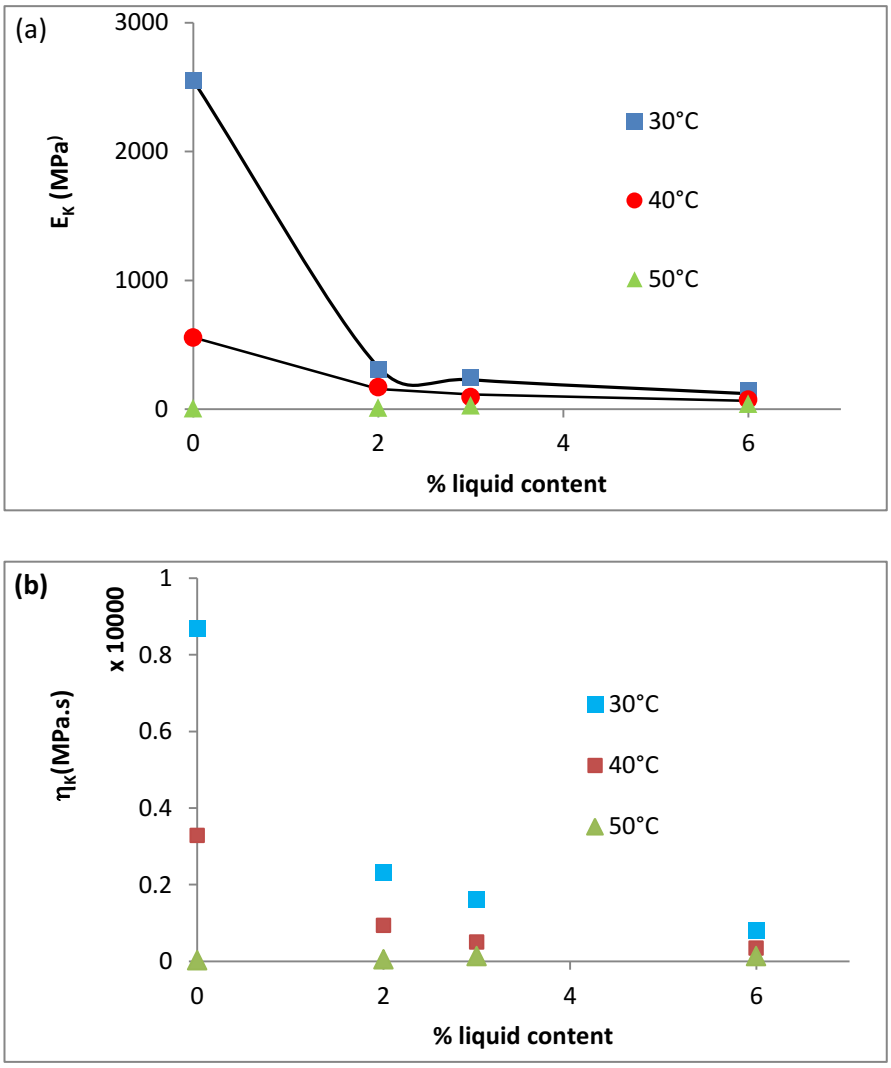

Figure 5-19: The fitting Burger's model parameters of Kelvin unit: (a) Retardant elasticity and (b) Viscosity as a function of liquid content at different test temperatures

The permanent viscous flow, η_M which represents the irrecoverable creep strain indicates the creep behaviour of the second creep stage. At the same test temperature condition, the fitting parameter of η_M shown in Figure 5-20 decreases with the increase of liquid content, except for specimens containing 6% liquid uptake. It could be related to the damage of crystalline polymer or oriented non-crystalline regions (Tang et al., 2012, Pérez et al., 2008), such as the pulling out of chain folds by a crystal slip process and the breaking of inter-crystalline tie molecules, and the irreversible deformation of amorphous regions. Increasing of η_M in 6% liquid containing samples may be attributed to the finding previously discussed in Section 5.1.4 whereas severe degradation of resin molecules structures occurs as indicated from a split in tan δ curve, which

leads to separation of bridging segment or crystalline. Meanwhile, the decrease of the viscosity, η_M ,for specimens containing lower level of liquid content is an indication of high flow in the dashpot and an increase in permanent deformation.

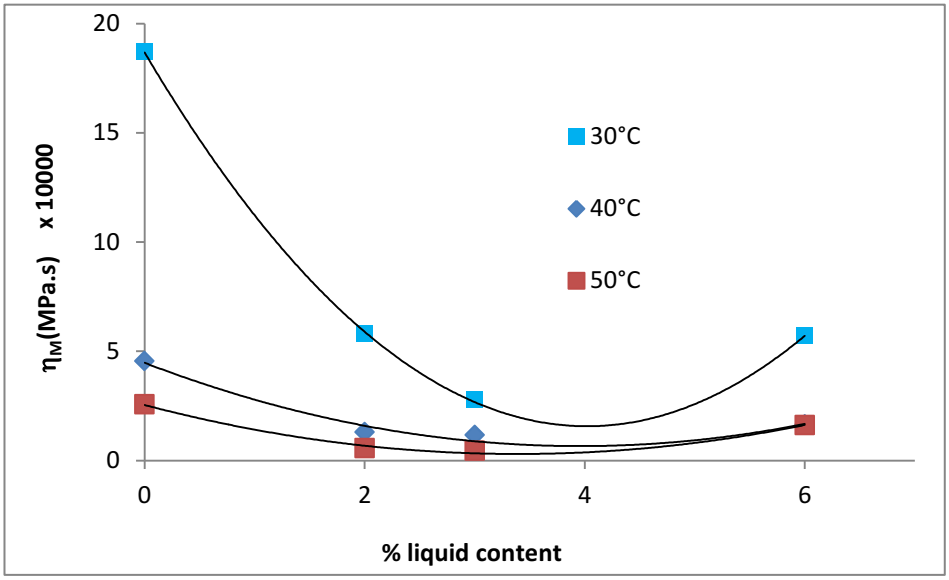

Figure 5-20: Relation between creep model parameters η_M and liquid concentration at different test temperatures

The relationship between all creep parameters and liquid content can be described mathematically in each level of temperature as

$$\varepsilon(t) = \frac{\sigma}{f_{E_M}(C)} + \frac{\sigma}{f_{E_K}(C)}\left[1 - exp\left(-\frac{t}{f_\tau(C)}\right)\right] + \frac{\sigma}{f_{\eta_M}(C)}t \qquad (5.6)$$

In this model, the functions f_{E_M} , f_{E_K} , f_τ and f_{η_M} represent changes of creep parameter as a function of liquid content at a given temperature. To accommodate change in retardation time with liquid content, the time shift factor is utilized to relate the compliance function in terms of the reference compliance function liquid (Gupta et al., 2012). The shift factor is represented by the function f_τ which exhibits the horizontal time scale distance between the compliance curve of dry specimen and another curve at liquid content, C. In this case, the creep curves from specimens with different levels of liquid uptake have different values of different time, which can be shifted to form a master curve in reduced time (Zheng et al., 2004).

Thus, from Equation (5.7), the liquid concentration dependence of creep strain can be presented in the form

$$\varepsilon(t) = \frac{\sigma}{f_{E_M}(C)} + \frac{\sigma}{f_{E_K}(C)}\left[1 - exp\left(-\frac{t}{a_C \tau_0}\right)\right] + \frac{\sigma}{f_{\eta_M}(C)}t \tag{5.7}$$

where

$$f_{E_M} = E_{M_0}\left(1 + A_{M_1}C + A_{M_2}C^2\right) \tag{5.8}$$

$$f_{E_K} = \frac{E_{K_0}.E_{K_1}}{C + E_{K_1}} \tag{5.9}$$

$$f_{\eta_M} = \eta_{M_0}\left(1 + A_1 C + A_2 C^2\right) \tag{5.10}$$

$$a_C = \frac{t}{t'} \tag{5.11}$$

The fitted mathematical functions, which describe the relationship between creep parameters and liquid content using Equations (5.9) to (5.11) are presented in Figures 5-18, 5-19a and 5-20 and drawn in solid lines. Those equations are applicable only for 30° and 40°C data, especially the function corresponding to Kelvin unit in Burger model including the time shift factor. This may be related to substantial structural change that occurs at 50°C as previously discussed in Section 5.2.2.

In identifying the timescale shifting of retardation time, creep compliance master curves were drawn by shifting the creep compliance curves of the specimen with certain liquid concentrations using 0% liquid concentration as the reference as shown in Figure 5-21.

Figure 5-21 shows the shifting creep strain on different levels of liquid concentration tested at the same temperature condition. It shows the creep compliance master curve of the PLA-based material where the horizontal axis indicates physical time. The shift factor of the curves from each level of liquid content can then be obtained and plotted in a William-Landel-Ferry (WLF)-type graph. The modified WLF equation (Sheng et al., 2010) in relating liquid concentration with the shift factor can be defined as:

$$log\, a(C,C_0) = \frac{-A(C - C_0)}{B + (C - C_0)} \tag{5.12}$$

where A and B are the coefficients of WLF function which were determined using the Curve Fitting tool available at MatLab.

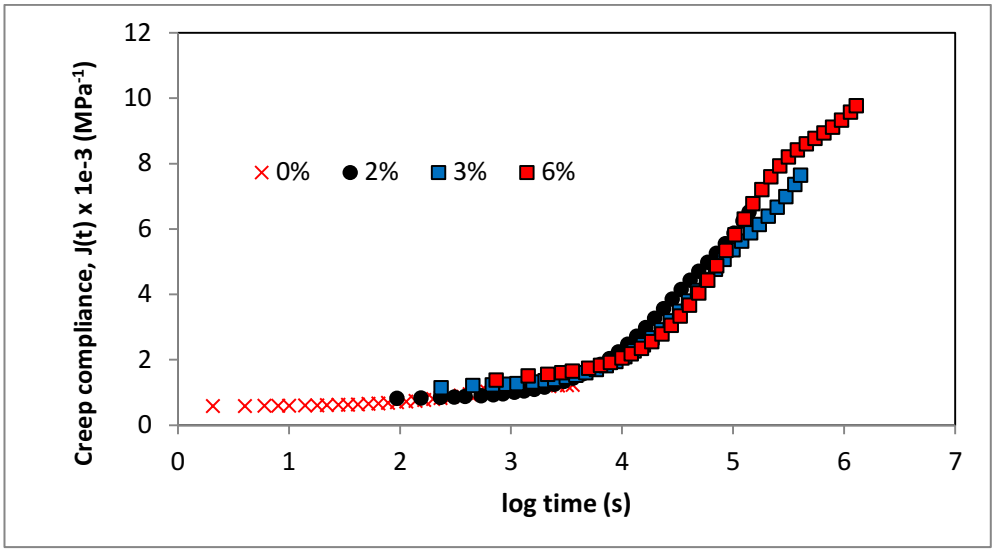

Figure 5-21: Master curve constructed from the creep data of specimens with different levels of liquid content using reference liquid content, C_{reff} = 0% at 30℃ test temperature

5.4.3 Effect of temperature on viscoelastic properties

Effect of temperature on the creep behaviour of the material has been presented in Figure 5-17 to 5-20. In addition, it has been discussed in Chapter 4 that different temperature conditions will lead to different level of absorbed liquid. In packaging application, the material is exposed to wet environment at a particular temperature condition during its service life. Therefore, it is necessary that the constitutive equation is capable to involve combined effect of temperature and liquid uptake.

Assuming that temperature condition of an application is not significantly changed during service life, it is possible to construct a temperature-dependent parameter constant based on the identified parameter functions of Equations (5-9) to (5-11) of different temperatures. Considering that substantial structural change occurs in 50°C, constitutive equation for time-dependent modulus will only be developed for material conditioned under 50°C. To have sufficient data for modelling purpose, additional creep test for specimens with various levels of liquid content were performed at 35°C as shown in Figure 5-22. The figure exhibits similar trend with the results at 30° and 40°C test temperatures, which shows an increase of creep compliance with increasing of liquid content.

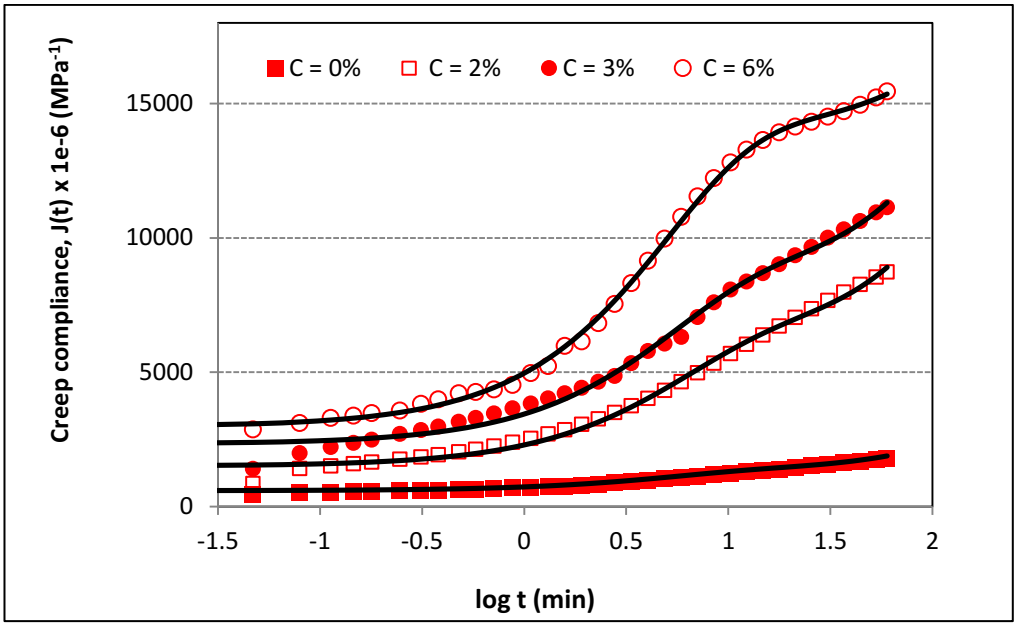

Figure 5-22: Creep compliance curves in time function at different levels of fluid concentration at 35 ℃, test temperature

The parameter constants for the creep parameter functions f_{E_M}, f_{E_K} and f_{η_M} from 30°, 35° and 40°C test temperatures are tabulated in Table 5-4. The values of E_{M0}, E_{K0}, E_{K1} and η_{M0} significantly decrease with increasing temperature while the trend for other parameters (A_{M1}, A_{M2}, A_1, and A_2) seems to have a constant pattern.

Table 5-4: Summary of parameter constants for the creep parameter functions in Equations (5-9), (5-10) and (5-11)

Function	Parameter	Test temperature (°C)		
		30	35	40
f_{E_M}	E_{M0}	1745	1705	1656
	A_{M1}	-0.212	-0.224	-0.237
	A_{M2}	0.0186	0.0194	0.0202
f_{E_K}	E_{K0}	2554	1430	556
	E_{K1}	0.295	0.359	0.781
f_{η_M}	η_{M0}	186800	100500	44730
	A_1	-0.456	-0.448	-0.431
	A_2	0.0585	0.0579	0.0545

The relations between creep parameter constants and temperature difference can be empirically obtained from Table 5-4 as shown in Figure 5-23.

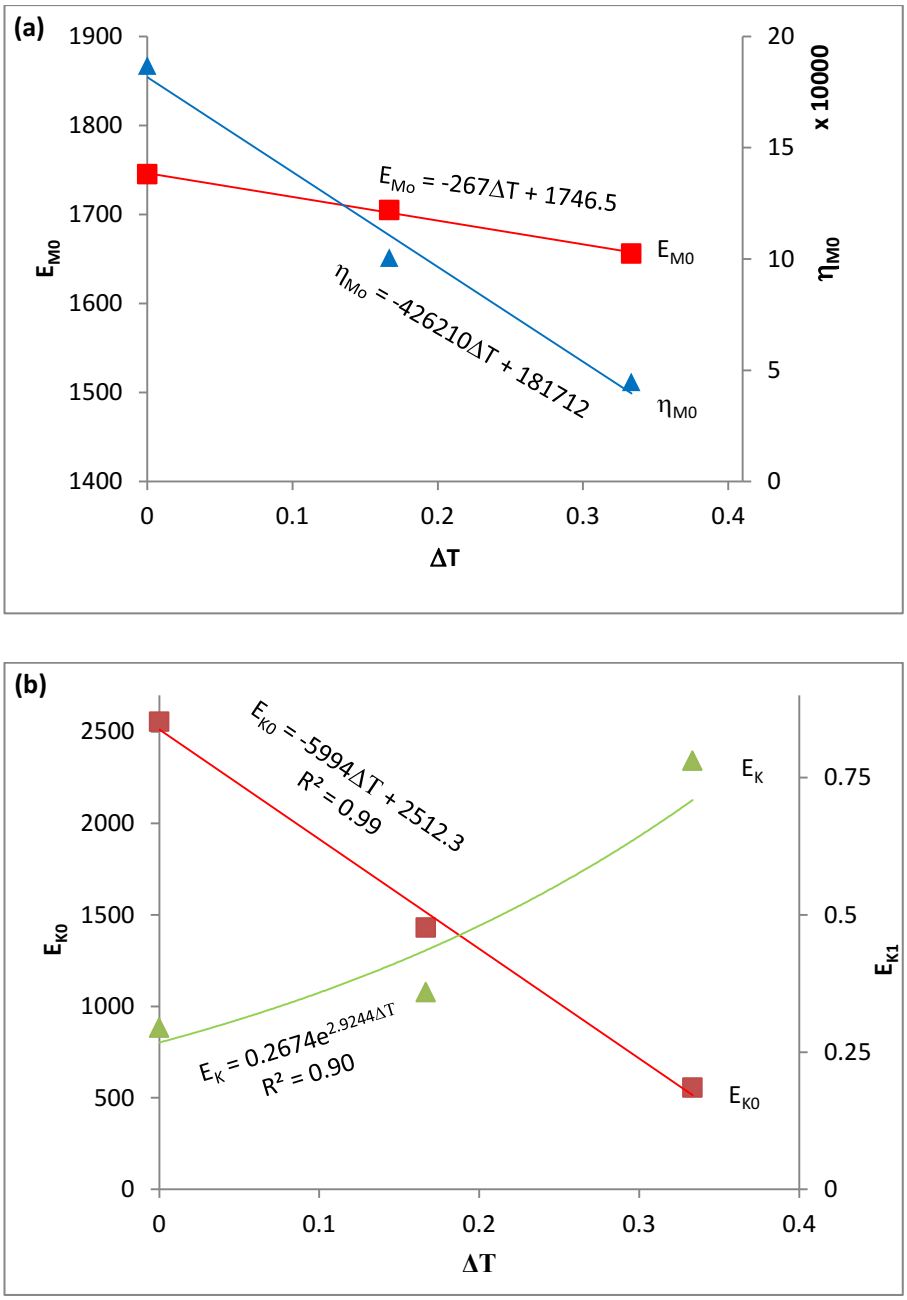

Figure 5-23: The creep parameter constants for: (a) Maxwell and (b) Kelvin unit as a function of temperature difference

Effect of temperature condition is represented in the function of creep compliance by modifying Equations (5-9) to (5-11) with temperature-dependent parameter constant as illustrated in Figure 5-23. The creep strain of an application under liquid exposure condition at environment temperature T at time t, ε(t) is obtained using Equation (5.8) with the following creep parameter functions.

$$f_{E_M} = f_{E_{M_0}}(T)\left(1 + A_{M_1}C + A_{M_2}C^2\right) \tag{5.13}$$

$$f_{\mathrm{E}_K} = \frac{f_{E_{K_0}}(T) * f_{E_{K_1}}(T)}{C + f_{E_{K_1}}(T)} \tag{5.14}$$

$$f_{\eta_M} = f_{\eta_{M_0}}(T)\left(1 + A_1C + A_2C^2\right) \tag{5.15}$$

The empirical model with temperature-dependent creep constant for PLA-based material exposed to hydrocarbon liquid can be defined from Figure 5-24 as

$$f_{E_{M_0}} = -267\Delta T + 1745 \tag{a}$$

$$f_{E_{K_0}} = -6e3\Delta T + 2512 \tag{b}$$

$$f_{\mathrm{E}_{K_1}} = 0.27\exp(2.9\Delta T) \tag{c}$$

$$f_{\eta_M} = -4.3e5\Delta T + 1.8e5 \tag{d}$$

where $\Delta T = \frac{T - T_0}{T_0}$ and T_0 is the reference temperature.

In modelling the retardation time, combined effect of liquid concentration and temperature is commonly performed using the basis of time superposition (Somiya et al., 2008, Patankar et al., 2012). It utilises a single factor that accounts for the combined effect of moisture and temperature which defined in the following equation (Miranda Guedes et al., 2000)

$$a_{TH} = a_T.a_{RH} \tag{5.16}$$

The concept of the so called time-moisture-temperature superposition was introduced by assuming that the effects of moisture and temperature factors can be expressed in separated shift factors. However, it has been reported that the influence of humidity and temperature on retardation time might not be equal (Miranda Guedes et al., 2000, Zheng et al., 2004). Those reports revealed that the experiment can only measure the combined factor of temperature and moisture but how it becomes uncoupled into two individual components is still not clear. In consequence, the superposition principle based on uncoupled effects of those two factors may not be valid. Accordingly, the effect of temperature on retardation time is represented using empirical model since the shifting of the retardation time is difficult to be described by a single expression given in Equation (5.17). An empirical model for temperature-dependent shift factor is developed in accordance the relation of WLF coefficients with the temperature as shown in Figure 5-24.

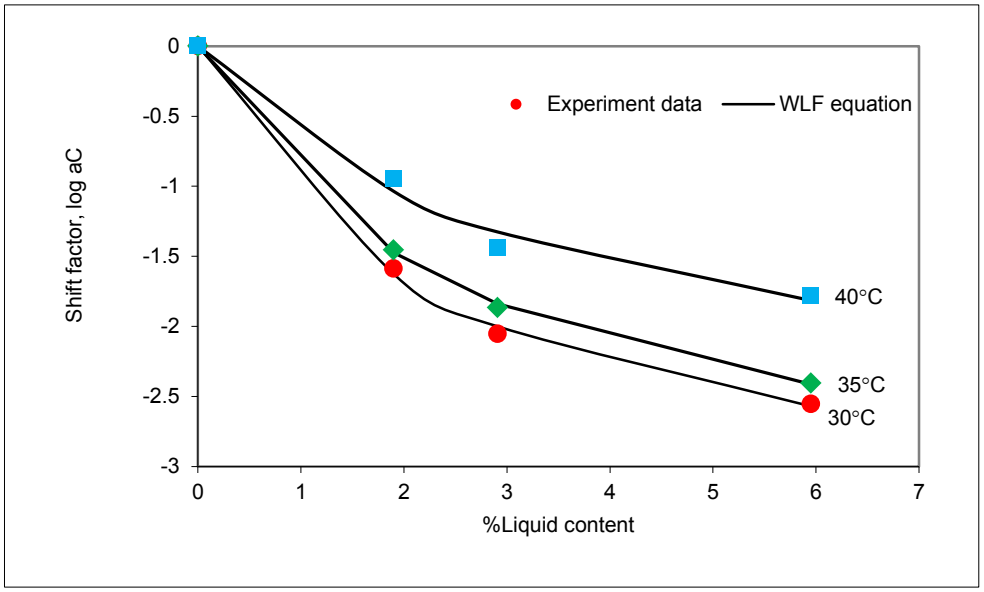

Figure 5-24: Application of time-liquid content superposition at different test temperatures

From Figure 5-24, the WLF coefficients, A & B presented in Equation (5-13) were obtained and then plotted as a function of temperature difference (ΔT) as depicted in Figure 5-25. The reference temperature, T_0 used is 30°C.

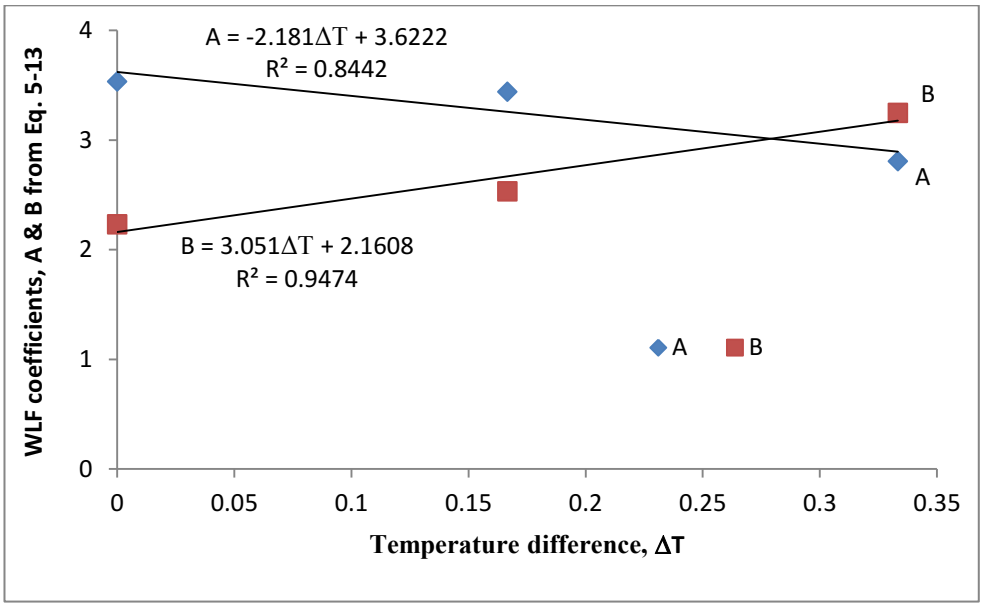

Figure 5-25: The empirical function of the WLF coefficients with temperature difference

The empirical function of WLF coefficients shown in Figure 5-25 indicates a decrease of coefficient A and an increase of coefficient B with increasing of temperature.

5.5 Conclusion

This chapter confirms a significant impact of liquid absorption on mechanical properties of PLA-based material through the measurement of static and dynamic properties. The response of this material to liquid absorption was consistent with other reports (Zheng and McKenna, 2003, Knauss and Kenner, 1980, Mouzakis and Karger-Kocsis, 1998, Somiya et al., 2008, Harris and Lee, 2010) on various types of polymeric material in contact with various liquid environments. Those reports suggested that the mechanical response due to liquid sorption was similar to the effect of temperature.

The results show progressive decrease of the modulus and strength by increasing of fluid content inside the material. The increase of elongation was observed indicating plasticizing effect of fluid exposure on the PLA-material. The dependency of property changes with liquid content leads to inhomogeneous properties inside the material. Since liquid content distribution is a function of time and position, the material is generally submitted to non-uniform distributions of liquid content over an extended period before reaching a saturated condition. Coupling of two-time dependent variables may result in viscoelastic material which possesses time-dependent variables in its material constitutive equation.

CHAPTER 6 MECHANICAL RESPONSE OF PLA-BASED PACKAGING UNDER LIQUID EXPOSURE

6.1 Introduction

The objective of this chapter is to examine the mechanical behaviour of PLA-based package, which subjected to external load while undergoing dimensional and material property changes due to the diffusion of liquid through its thickness. The characteristics of material response have been defined previously in chapter 5 by taking into account for changes in the properties due to liquid sorption. The coefficients on the functions of material property are liquid-content dependence, which have a time and spatial function. Therefore, the material properties at any given location and time are dependent on the liquid content. This chapter will present the evolution of mechanical behaviour using a stress model that accounts for the effect of time, liquid content, temperature and swelling-induced strain. It is assumed that deformation depends on the liquid concentration, but liquid concentration can be obtained without the knowledge of stress/strain.

In order to understand the effect of diffusion of liquid or other substances on the mechanical response of PLA-based material, the stress and deformation of an application will be analysed simultaneously with the problem of diffusion. The question is how significantly the stresses induced due the diffusion affect in relation to the mechanical loading. Sequentially coupled analysis of liquid diffusion and stress are carried out to predict the mechanical response of an application made up of PLA-based plastic. Effect of liquid diffusion is incorporated on the stress profile through the swelling coefficient and liquid-dependent material parameters for both

the elastic and transient (time-dependent) properties. The constitutive model wherein the material moduli depend on liquid content, which has been previously developed in Chapter 5, is used to characterize the material. It should be noted that this analysis does not address a fully coupled problem. Whereas the stress profile depends on the liquid content, the profile of liquid content can be obtained without the knowledge of stress or strain.

As presented in Figures 4-11 and 4-14 in Chapter 4, a higher liquid content is initially present at the surface exposed to liquid and it is then followed by the inner layers. Non-uniform liquid concentration may result in inhomogeneous mechanical properties due to dependency of the material properties on the presence of liquid, as clearly shown in the experiment discussed previously in Chapter 5. The constitutive models of the elastic and viscoelastic material discussed previously are used to characterize material for simulated package in the rest of this chapter.

6.2 Convergence Study of the Finite Element Analysis in Elastic Material

The stress associated with a diffused liquid can be analysed using the general technique of thermal stress analogy since liquid diffusion is mathematically equivalent to the heat transfer process (Huang et al., 2008). However, for complicated problems for which it might be difficult to obtain an exact closed form analytical solution, the finite element (FE) method is often used to find an approximate solution (Shah et al., 2009). A numerical analysis based on the FE approach is proposed to study the coupled diffusion and stress in packaging application. In ensuring that the FE model accurately predicts the mechanical response of the application, it is imperative to examine some factors that may affect the accuracy of the results obtained. The convergence study is carried out by comparing the field responses from the FE analysis with the analytical solution of the simplified version of the problem.

6.2.1 Effect of mesh size on results of FE analysis

The convergence study was performed by examining the mesh size on the stress and deformation field of a closed-end cylinder as presented in Figure 6.1 using FE analysis compared to the analytical solution.

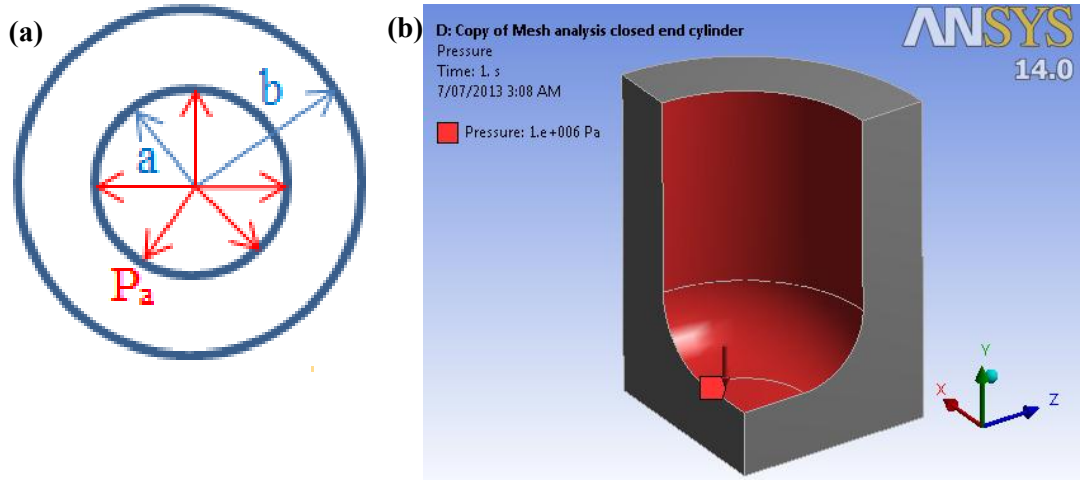

Figure 6-1: A Cylinder with capped end subjected to an internal pressure Pa: (a) cross section and (b) quarter solid body of closed end cylinder

The solution for thick-walled cylinder problem is available in many solid mechanics text books (Shigley et al., 2004, Ugural, 2009), in which the principle stresses are determined using the following equations

At inside surface, r = a,

$$\sigma_\theta = P_a\left[\frac{b^2+a^2}{b^2-a^2}\right] \quad ;\sigma_r = -P_i \quad ;\sigma_z = \frac{P_a a^2}{b^2-a^2} \tag{6.1}$$

At outside surface, r = b

$$\sigma_\theta = \left[\frac{2P_a^{\,2}a^2}{b^2-a^2}\right] \quad ;\sigma_r = 0 \quad ;\sigma_z = \frac{P_a a^2}{b^2-a^2} \tag{6.2}$$

where σ_θ = tangential stress, σ_r = radial stress and σ_z = axial stress.

The analytical solution was obtained to solve the problem of closed-end cylinder and was compared to numerical solution which simulated in three different mesh relevance sizes: (1) coarse, (2) medium and (3) fine as presented in Figure 6-2. The analytical and numerical results using different mesh sizes are summarized in Table 6-1.

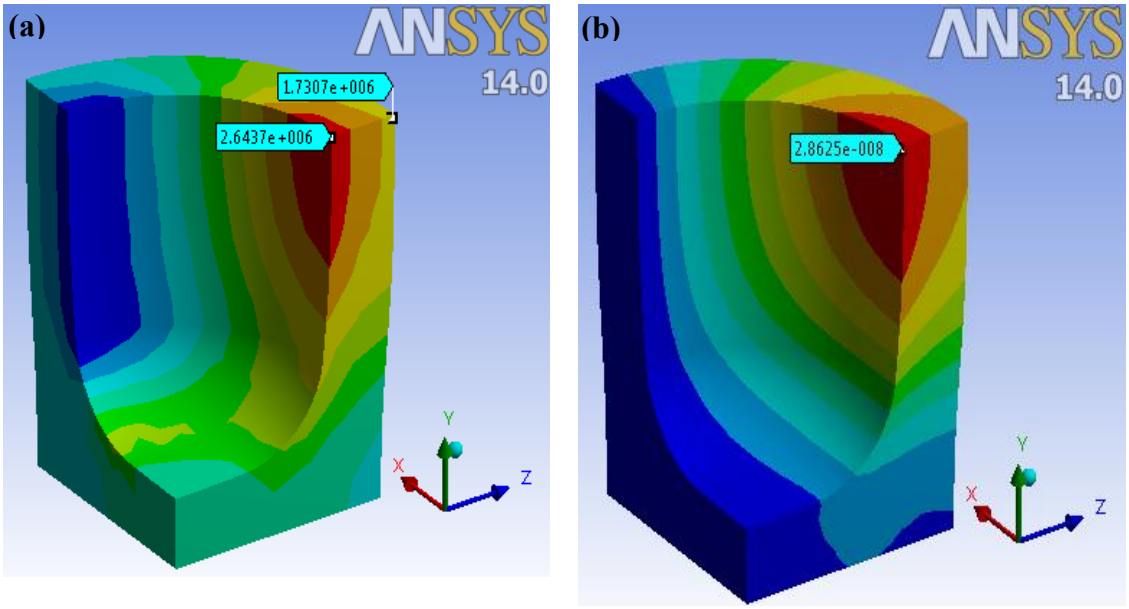

Figure 6-2: Numerical results of mesh size analysis in the closed-end cylinder: (a) tangential stress and (b) radial deflection

Table 6-1 shows that in the case of structural analysis in the cylindrical shape, the mesh size do not significantly affect the quality of results. However, smaller size gives slightly better picture of the actual stress and deformation states. It has also been presented in section 4.5.2 that smaller mesh size represents more detail profile of liquid content and results in lower thermal error compared to bigger mesh size.

Table 6-1: Comparison of field responses in the closed-end cylinder from analytical and numerical solutions

Fields	Analytical	Numerical		
		Coarse	Medium	Fine
Tangential stress at inner radius (σ_x), Pa	2.60E+06	2.65E+06	2.65E+06	2.65E+06
Tangential stress at outer radius (σ_x), Pa	1.60E+06	1.75E+06	1.73E+06	1.73E+06
Radial stress (σ_z) at inner radius, Pa	-1.00E+06	-9.62E+05	-9.82E+05	-9.84E+05
Radial stress (σ_z) at outer radius, Pa	0.00E+00	-9.41E+03	-1.07E+04	-6.20E+05
Radial deflection (mm)	2.90E-05	2.87E-05	2.87E-05	2.87E-05

6.2.2 Effect of time-step size on FE analysis

The next convergence study is carried out by analysing the effect of time increment size on the mechanical response for the geometries subjected to diffusant with no external load applied. The analytical and numerical solution for the stress and deformation fields were simultaneously presented on a rectangular plate and an opened-end cylinder made up of PLA-based material.

6.2.2.1 Governing equations diffusion-induced stress in simple geometries

The analytical solution of the liquid diffusion induced-stress is obtained using the constitutive relation of a plate and an opened-end cylinder derived from any book on the elementary strength of materials (Noda et al., 2003, Ugural, 2009, Barron and Barron, 2011) as discussed previously in Chapter 2, Section 2.3.1. The stress and deformation fields will be analysed by thermal stress analogy, where liquid content, C(z,t) and coefficient of swelling, β is analogous to temperature changes, ΔT and coefficient of thermal expansion, α, respectively.

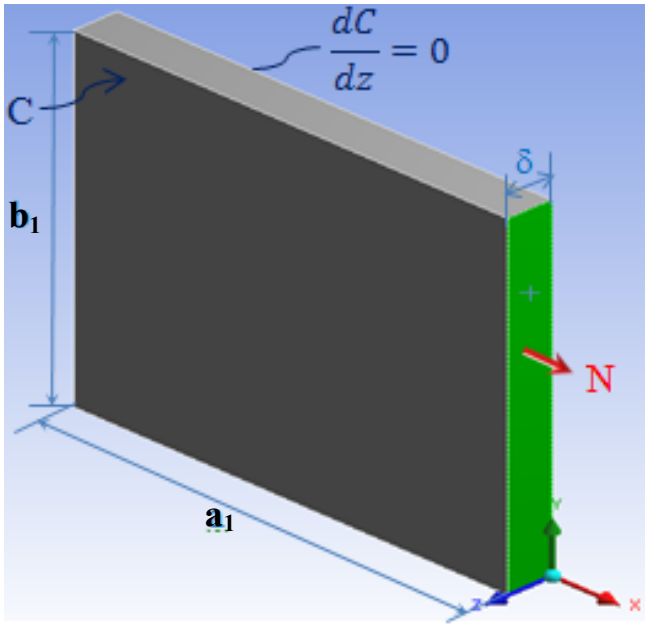

Figure 6-3: Boundary conditions of a rectangular plate illustrating the analytical solution

Consider a simple plate as presented in Figure 6-3, one of the faces of the plate with thickness δ is subjected to liquid at temperature T causing diffusion in the z direction (along the thickness) while the other faces are insulated. The diffused liquid reaches saturated concentration C_m after a certain time t_∞. The initial and boundary conditions used to solve the liquid diffusion problems in the plate are:

$$\begin{aligned} &for\ t=0,\quad C=0 \quad at \quad -\delta/2 < z < \delta/2 \\ &for\ t>0,\quad C=C_m \quad at \quad z=\delta/2 \\ &\frac{\partial C}{\partial z}=0 \quad at\ z=-\delta/2 \end{aligned} \tag{6.3}$$

The plate is also subjected to a uniform load N in the x direction at x = a with zero bending moments per unit length in the x and y direction. Therefore, the in-plane forces and the bending moments at the neutral plane z = 0 are

$$\begin{aligned} &\int_{-\delta/2}^{\delta/2} \sigma_x \, dz = N \\ &\int_{-\delta/2}^{\delta/2} \sigma_y \, dz = 0 \\ &\int_{-\delta/2}^{\delta/2} \sigma_x z \, dz = \int_{-\delta/2}^{\delta/2} \sigma_y z \, dz = 0 \end{aligned} \tag{6.4}$$

Restraint of movement exists in the x direction on edges x = 0 and in the y direction on edges y = 0 and y = b. Therefore, the boundary conditions at those points are

$$\begin{aligned} &u_{(x=0)} = 0 \\ &v_{(y=0)} = v_{(y=b)} = 0 \end{aligned} \tag{6.5}$$

The second case for illustration for the analytical solution is the case of opened-end cylinder as shown in Figure 6.4. A hollow circular cylinder with an inner radius a and outer radius b is exposed to liquid in the innermost part causing diffusion in the radial direction.

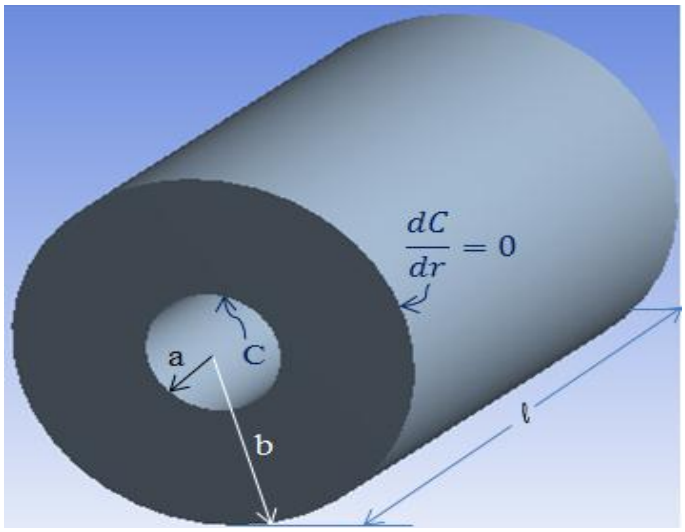

Figure 6-4: Boundary conditions of an opened-end cylinder illustrating the analytical solution

Thus, the initial and boundary conditions can be described as follow

for t = 0, C = 0 at $a < \mathrm{r} < b$

for t > 0, $C = C_m$ at r = a

$$\frac{\partial \mathrm{C}}{\partial \mathrm{r}} = 0 \quad \text{at r = b} \tag{6.6}$$

The boundary conditions for traction free surfaces are

$$\sigma_{rr} = 0 \quad \text{at r = a and r = b} \tag{6.7}$$

The convergence study will be performed within the framework of elastic analysis. From Equation (2-3) to (2-5), the stress and displacement of elastic components in rectangular plate can be written as

$$\begin{bmatrix} \sigma_x \\ \\ \sigma_y \end{bmatrix} = \frac{E}{1-v^2}\begin{bmatrix} 1 & v \\ \\ v & 1 \end{bmatrix}\left\{\begin{bmatrix} \frac{\partial u}{\partial x} \\ \\ \frac{\partial v}{\partial y} \end{bmatrix} - \begin{bmatrix} z\frac{\partial^2 w}{\partial x^2} \\ \\ z\frac{\partial^2 w}{\partial y^2} \end{bmatrix}\right\} - \frac{E}{1-v}C(z,t)\begin{bmatrix} \beta \\ \\ \beta \end{bmatrix}$$

$$\begin{bmatrix} \frac{\partial u}{\partial x} \\ \\ \frac{\partial v}{\partial y} \end{bmatrix} = \frac{1}{E\delta}\begin{bmatrix} 1 & -v \\ \\ -v & 1 \end{bmatrix}\begin{bmatrix} N_x \\ \\ N_y \end{bmatrix} + \frac{\beta}{\delta}\int_{-\delta/2}^{\delta/2} C(z,t)dz \tag{6.8}$$

$$\begin{bmatrix} \frac{\partial^2 w}{\partial x^2} \\ \\ \frac{\partial^2 w}{\partial y^2} \end{bmatrix} = -\frac{12}{E\delta^3}\begin{bmatrix} 1 & -v \\ \\ -v & 1 \end{bmatrix}\begin{bmatrix} M_x \\ \\ M_y \end{bmatrix} + \frac{12\beta}{\delta^3}\int_{-\delta/2}^{\delta/2} C(z,t)z\,dz$$

The opened-end hollow cylinder is assumed to be infinitely long and thus plane strain conditions are imposed. Using the prescribed boundary conditions, the solutions of plane strain problems for stress and displacement are

$$\sigma_r = \frac{\beta E}{1-\nu}\left[-\frac{1}{r^2}\int_a^r C(r,t)r\,dr + \frac{r^2-a^2}{r^2(b^2-a^2)}\int_a^b C(r,t)\,dr\right]$$

$$\sigma_\theta = \frac{\beta E}{1-\nu}\left[\frac{1}{r^2}\int_a^r C(r,t)r\,dr + \frac{r^2+a^2}{r^2(b^2-a^2)}\int_a^b C(r,t)\,dr - C(r,t)\right] \quad (6.9)$$

$$u_r = \frac{1+\nu}{1-\nu}\beta\left[\frac{1}{r}\int_a^r C(r,t)r\,dr + \left\{(1-2\nu)r + \frac{a^2}{r}\right\}\frac{1}{b^2-a^2}\int_a^b C(r,t)\,r\,dr\right]$$

The liquid content at any instant of time at a given material point is obtained by solving the Equation 4.5 for the diffusion through the thickness of a plate and Equation 4.18 for the opened-end pipe. Using the prescribed boundary conditions, the function of liquid content with time and position inside the plate can be described as

$$C(z,t) = C_m\left\{1 - \frac{4}{\pi}\sum_0^\infty \frac{(1)^n}{(2n+1)}exp\left[-\frac{(2n+1)^2\pi^2 F_0}{4}\right]cos\frac{(2n+1)\pi Z}{2}\right\} \quad (6.10)$$

where $F_0 = \frac{Dt}{\delta^2}$ and $Z = \frac{z}{\delta}$

and for the pipe

$$C = C_m\left[1 - \frac{ln\frac{r}{a}}{ln\frac{b}{a}} - \pi\sum_{n=1}^\infty F_n(t)f(\alpha_n,r)\right] \quad (6.11)$$

where

$$f(\alpha_n,r) = J_0(r\alpha_n)Y_0(a\alpha_n) - J_0(a\alpha_n)Y_0(r\alpha_n) \quad (a)$$

$$F_n(t) = \frac{J_0^{\,2}(b\alpha_n)}{J_0^{\,2}(b\alpha_n) - J_0^{\,2}(a\alpha_n)}e^{-D\alpha_n^2 t} \quad (b)$$

Using the dimensionless variable $\beta_n = b\alpha_n$ and $F_o' = \frac{Dt}{b^2}$, Equation (b) becomes

$$F_n(t) = \frac{J_0^{\,2}(\beta_n)}{J_0^{\,2}(\beta_n) - J_0^{\,2}\left(\beta_n\frac{a}{b}\right)}e^{-\beta_n^2 F_0'} \quad (c)$$

α_n are the positive roots of the equation $f(\alpha_n,b) = 0$, while $J_0(x)$ and $Y_0(x)$ are Bessel functions of order zero of the first and second kind.

6.2.2.2 Analytical and numerical result for stress and deformation in elastic material

Using elastic approach, the values of material property is as described in Table 6-2, while the dimensions of the geometries and the characteristics of liquid diffusion are described in Table 6-3 and Table 6-4.

Table 6-2: Elastic properties of the geometries for convergence analysis

Parameter	Value
Young's modulus, E_0 (MPa)	1.76×10^3
Poisson ratio, ν	0.3

Table 6-3: Dimension of the geometries for convergence analysis

Rectangular plate		Opened end cylinder	
Parameter	Value	Parameter	Value
a_1 (mm)	30	a (mm)	1
b_1 (mm)	30	b (mm)	3
δ (mm)	2	l (mm)	30

Table 6-4: Characteristics of liquid diffusion at environment temperature T = 20℃

Parameter	Value
Diffusion coefficient, D (m^2/s)	1.1×10^{-12}
Saturated liquid concentration, C_m	2.91%
Swelling coefficient, β	5.31×10^{-2}

The evolution of liquid content within the thickness of a plate and a cylinder has been presented in section 4.4. It is clearly shown that the liquid concentration varies with time and position, which has similar results from both of analytical and numerical solution. Using the prescribed material properties exhibited in Table 6-2 and 6-4, it is found that that steady state is achieved when $t \approx 7200$h for the plate and $t \approx 9400$h for the hollow cylinder. Figure 6-5 displays the profile of liquid content for the geometries used for convergence analysis.

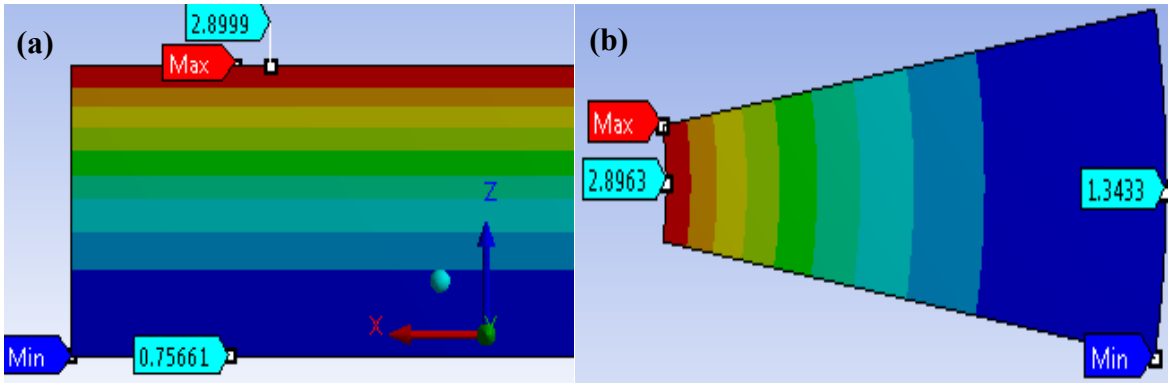

Figure 6-5: Liquid content profile of the geometries for convergence analysis at t = 550 h within the thickness of: (a) rectangular plate and (b) wedge of an opened-end pipe

For comparison purpose, the stress fields were numerically and analytically obtained with constant material properties, which do not depend on the liquid content. The non-uniform liquid concentration distribution during the diffusion process leads to a variation in the stresses as shown in Figure 6-6. The stresses are in maximum at the surfaces, which are not directly in contact with liquid exposure ($z = -\delta/2$ for the plate and r = b for the hollow cylinder).

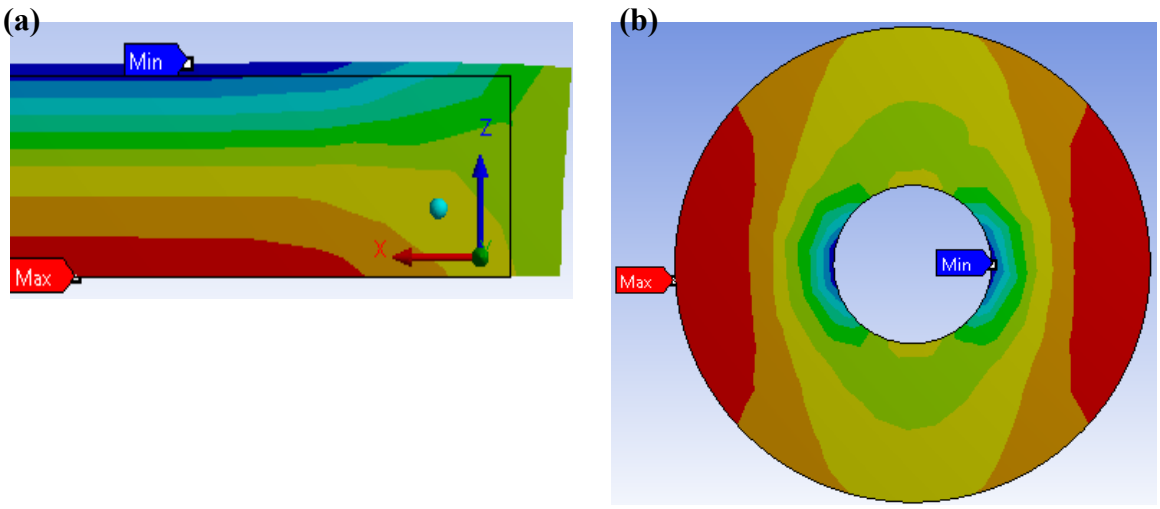

Figure 6-6: Profile of axial stress and tangential stress of the geometries for convergence analysis at t = 550 h for: (a) rectangular plate and (b) cross section of an opened-end pipe

The axial stress in x direction for the points on the surface $z = -\delta/2$ of the plate and the tangential stress for the points on r = b for the cylinder are calculated using Equations (6.8) and (6.9) which are then compared to the numerical solution for different time-step sizes as exhibited in Figure 6-7. As seen from the figure, smaller time-step sizes leads closer to a convergence solution. According to the figure, a time-step size of less than 10 h (less than 2% of analysis time) is recommended to represent the stress field of the PLA-based material.

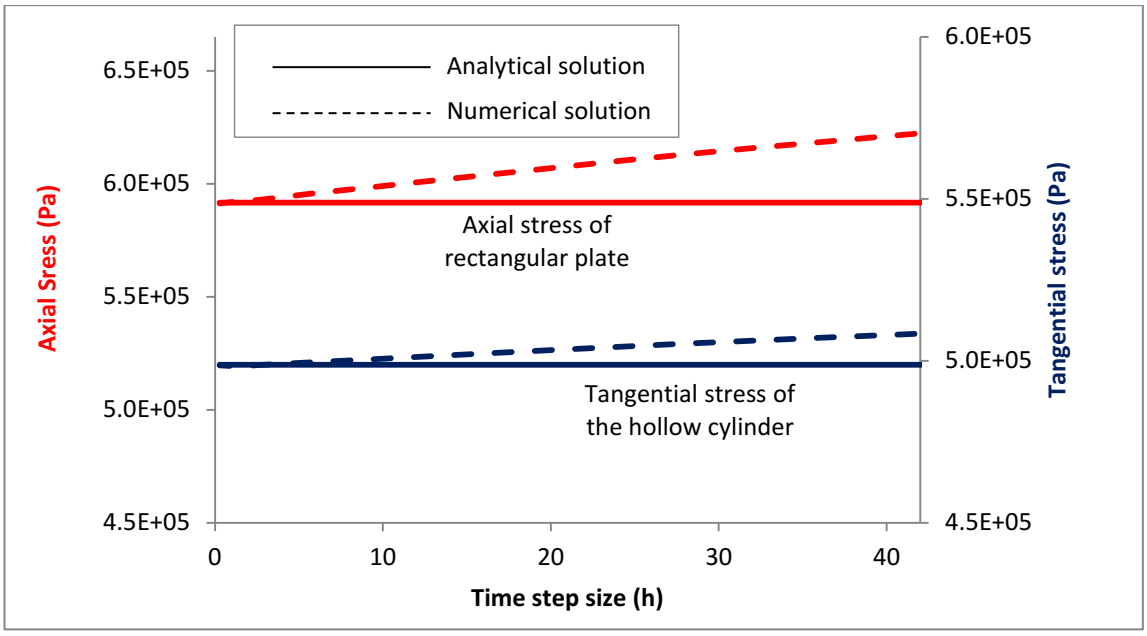

Figure 6-7: Effect of time-step size on the axial and tangential stress of the geometries at t = 550 h

Using the converged time-step size, the numerical analysis of stress and deformation fields in the plate with applied load and liquid-content dependent properties was performed and the results are compared to the analytical solution. In simplifying the problem, it is assumed that Poisson's ratio remains constant while the effective Young's modulus is liquid-content dependent. The plate with initial and boundary conditions shown in Figure 6-3 was subjected to a constant load of 0.1 MPa in x-direction. Material properties used for the analysis are as exhibited in Table 6-2 where E_0 is the elastic modulus of the dry material. The function of modulus with liquid contain is obtained from the result of storage modulus presented in Figure 5-9, which is plotted in Figure 6-8.

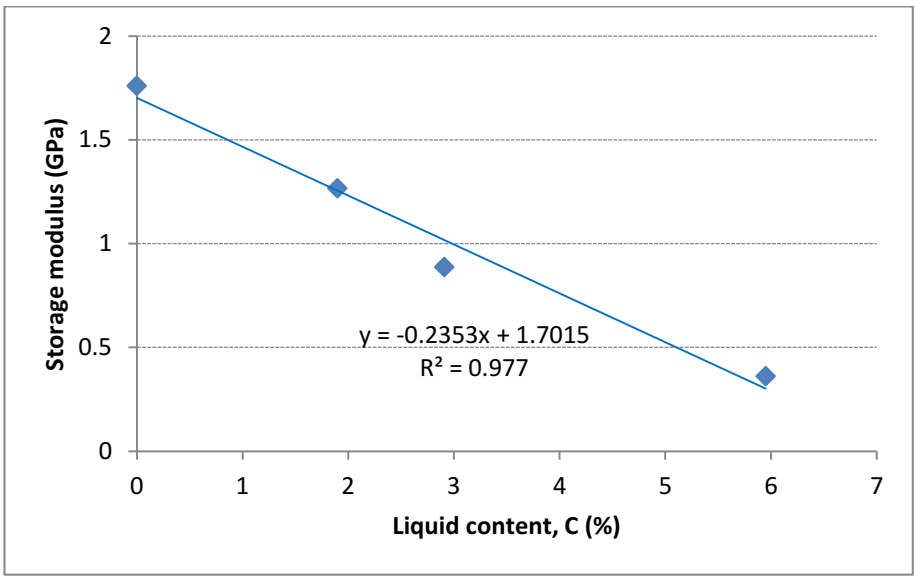

Figure 6-8: Linear relation of storage modulus with liquid content

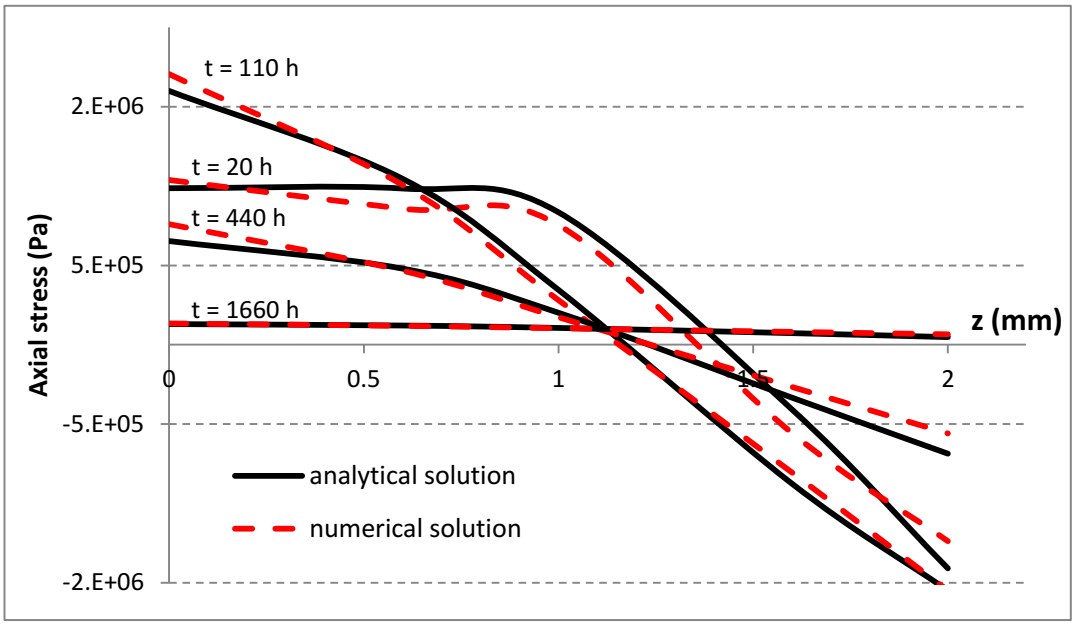

Figure 6-9: Distribution of axial stress within a plate exposed to liquid at T = 20 ℃ along the thickness at different times

Variation of the axial stress with time and position was observed until it reached an equilibrium value, as seen in Figure 6-9. The equilibrium stress is the nominal applied stress directly related to external load which is obtained at the condition of saturated liquid content or when absorbed

liquid effect is neglected. This indicates that a higher stress occurs with the presence of non-uniform liquid content inside the material. The maximum stress occurs at the points furthest from the liquid exposure area, especially during early phase of liquid diffusion. In regards to this study, the maximum stress occurs at t ≈ 110 h (F_0 ≈ 0.1). Further, the stress decreases to the nominal applied stress with increasing exposure time and decreasing distance towards the surface directly exposed to liquid. It can be seen from Figure 6-9 that the analytical and numerical solution using FEA method agrees well.

The numerical analysis for the hollow cylinder with load applied was also performed using the converged time-step size to examine the applicability of FE solution in stress and deformation analysis. The numerical results from FEA software using ANSYS Workbench were compared with the results generated in Mechanical APDL using the codes from VM33 ANSYS Verification Manual (ANSYS, 2009). The codes have been verified with the readily-obtainable theoretical solution from a text book of Roark and Young (Roark et al., 2002).

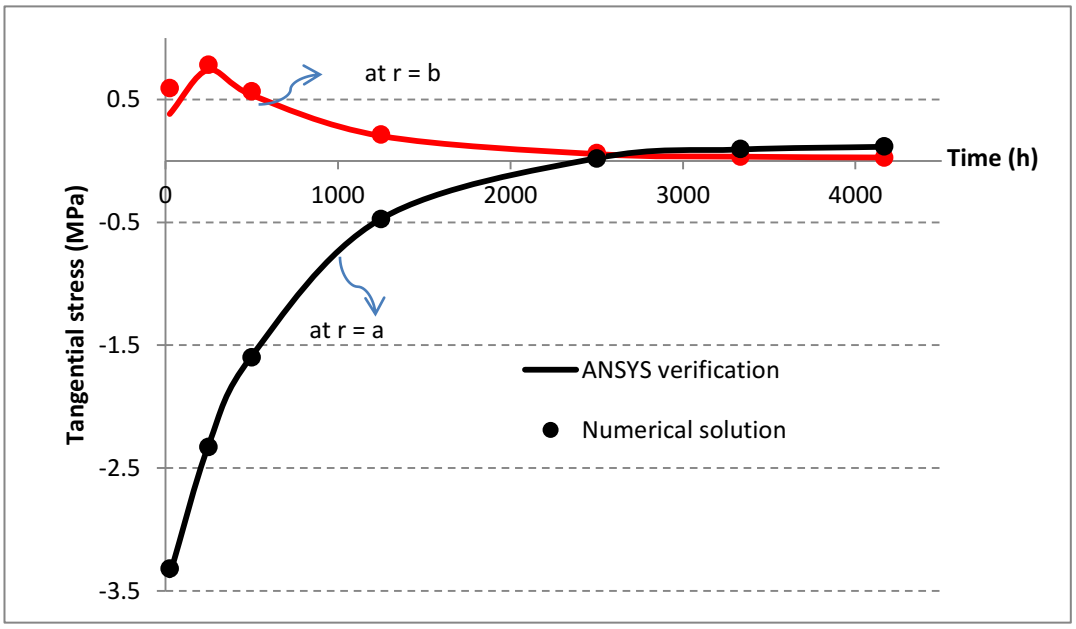

Figure 6-10: Evolution of tangential stress in hollow cylinder exposed to liquid at T = 20℃ subjected to 0.1 MPa internal pressure at the inner and outer radius

Consider the opened-end pipe as shown in Figure 6-1 with material properties and dimensions are as presented in Tables 6-2 to 6-4. The pipe, however, is subjected to an internal pressure of 0.1MPa. The evolution of tangential stress in the inner (r = a) and outer radius (r = b) is

exhibited in Figure 6-10. The figure shows similar result with that of rectangular plate, in which the stress is maximum at the areas not directly contact with diffusant. It is also shown that the tangential stress at the outer radius is in maximum at $F_0' \approx 0.1$, whereas in this case, the time is equal to 250 h.

6.3 Viscoelastic analysis

The main feature which differentiates the elastic and viscoelastic analysis lies essentially in the relation between stress and strain. The normal elastic analyses are based upon a (spring) constant proportionality between stress and strain with Young's modulus as the proportionality constant, in which the strain will return to its original state when the stress is removed. Meanwhile, the general viscoelastic relation must allow for time or strain-effects therefore the occurrence of strain in response of a constant stress is time-dependent and the elastic parameters in the constitutive equation of viscoelastic material are replaced by time-dependent values (Findley et al., 1976). The solution of viscoelastic approach is obtained by using the elastic-viscoelastic analogy through the application of the corresponding principle.

The responses of material in contact with liquid environment have been characterized in Section 5.3 through a constitutive model, which accounts for changes in elastic moduli and relaxation time. The coefficients on the functions of material property are liquid-content dependent, which have a time and spatial function. Therefore, the material properties at any given location and time are dependent on the liquid content. Using a stress model that accounts for the effect of time, liquid content, temperature and hygroscopic swelling based on linear viscoelastic theory, this section will discuss the evolution of mechanical behaviour during liquid diffusion.

6.3.1 Analytical solution

Variation of material properties during diffusion is represented by dependency of the modulus on liquid content, and is a function of position and time. The effect of liquid concentration is represented on the constitutive equation by assuming that the coefficient of each term in the viscoelastic model of Equation (5.6) be the function of time, temperature and liquid concentration. The unknown function of the equation was determined from a set of several creep tests and the result has been presented in Section 5.3.3. The relationship between all creep parameters and liquid content can be described mathematically in each level of temperature as

$$J(t)=\frac{1}{f_{E_M}(C,T)}+\frac{1}{f_{E_K}(C,T)}\left[1-exp\left(-\frac{t}{a_C(T)\tau_0}\right)\right]+\frac{1}{f_{\eta_M}(C,T)}t \tag{6.12}$$

The functions f_{E_M}, f_{E_K} and f_{η_M} are liquid content and temperature dependent which are given in Equations (5.14) to (5.16) in Chapter 5, while the temperature-dependent shift factor, a_C is empirically obtained in Figure 5-23 from the same chapter.

According to the constitutive relation for the stress and displacement of elastic components shown in Equation (6.8), the corresponding solution for strain components in a viscoelastic plate can be written as

$$\begin{bmatrix}\varepsilon_x(t)\\ \varepsilon_y(t)\end{bmatrix}=\frac{1}{E\delta}\begin{bmatrix}1 & -v\\ -v & 1\end{bmatrix}\begin{bmatrix}N_x(t)\\ N_y(t)\end{bmatrix}+\frac{12z}{E\delta^3}\begin{bmatrix}1 & -v\\ -v & 1\end{bmatrix}\begin{bmatrix}M_x(t)\\ M_y(t)\end{bmatrix}+\begin{bmatrix}N^*\\ N^*\end{bmatrix}+z\begin{bmatrix}M^*\\ M^*\end{bmatrix} \tag{6.13}$$

where $N^*=\frac{\beta}{\delta}\int_{-\delta/2}^{\delta/2}C(z,t)dz$ and $M^*=\frac{12\beta}{\delta^3}\int_{-\delta/2}^{\delta/2}C(z,t)z\,dz$

Applying the Laplace transform to the elastic solution first and then replacing E by $s\hat{E}(s)$ yields the following relation

$$\begin{bmatrix}\varepsilon_x(s)\\ \varepsilon_y(s)\end{bmatrix}=\frac{1}{s\hat{E}(s)\delta}\begin{bmatrix}1 & -v\\ -v & 1\end{bmatrix}\begin{bmatrix}\hat{N}_x(s)\\ \hat{N}_y(s)\end{bmatrix}+\frac{12z}{s\hat{E}(s)\delta^3}\begin{bmatrix}1 & -v\\ -v & 1\end{bmatrix}\begin{bmatrix}M_x(s)\\ M_y(s)\end{bmatrix}+\begin{bmatrix}N^*\\ N^*\end{bmatrix}+z\begin{bmatrix}M^*\\ M^*\end{bmatrix} \tag{6.14}$$

The relaxation modulus $\hat{E}(s)$ is related to creep compliance $\hat{J}(s)$ as given by (Findley et al., 1976)

$$\frac{1}{s\hat{E}(s)}=s\hat{J}(s) \tag{6.15}$$

The strain components can be obtained by applying the inverse Laplace transform of Equation (6.14) substituted with Equation (6.15). The convolution theorem yields the inverse Laplace transform, which are

$$s\hat{J}(s)\,\hat{N}_i(s) \equiv \int_0^t J(t-s)\frac{\partial N_i(s)}{\partial s}ds \qquad \text{(a)}$$

and

$$s\hat{J}(s)\,\hat{M}_i(s) \equiv \int_0^t J(t-s)\frac{\partial M_i(s)}{\partial s}ds \qquad \text{(b)}$$

Thus, the strain components can be calculated for a given set of boundary conditions and given values of J(t) as a function of the external force $N_i(t)$ and external moment $M_i(t)$. If the external force and moment are constants, N_{i_0} and M_{i_0} respectively, then

$$N_i(t) = N_{i_0}\,H(t) \text{ and } M_i(t) = M_{i_0}\,H(t) \qquad (6.16)$$

By applying the inverse Laplace transform, inserting (6.15) and (6.16) into (6.14) yields the following strain components in a plate:

$$\begin{bmatrix}\varepsilon_x(t)\\ \varepsilon_y(t)\end{bmatrix} = \frac{J(t)}{\delta}\begin{bmatrix}1 & -\nu\\ -\nu & 1\end{bmatrix}\begin{bmatrix}N_{x_0}\\ N_{y_0}\end{bmatrix} + \frac{12zJ(t)}{\delta^3}\begin{bmatrix}1 & -\nu\\ -\nu & 1\end{bmatrix}\begin{bmatrix}M_{x_0}\\ M_{y_0}\end{bmatrix} + \begin{bmatrix}N^*\\ N^*\end{bmatrix} + z\begin{bmatrix}M^*\\ M^*\end{bmatrix} \qquad (6.17)$$

The stress components, therefore, are

$$\begin{bmatrix}\sigma_x(t)\\ \sigma_y(t)\end{bmatrix} = \frac{1}{\delta}\begin{bmatrix}N_{x_0}\\ N_{y_0}\end{bmatrix} + \frac{12z}{\delta^3}\begin{bmatrix}M_{x_0}\\ M_{y_0}\end{bmatrix} + \frac{1}{(1-\nu)J(t)}\begin{bmatrix}N^*+zM^*\\ N^*+zM^*\end{bmatrix} \qquad (6.18)$$

The opened-end hollow cylinder is assumed to be infinitely long and thus plane strain conditions are imposed. The solution for linear elastic hollow cylinder shown in Equation 6.9 in the Laplace domain gives the stress components as:

$$\sigma_r = \frac{s\hat{E}(s)\beta}{1-v}\left[-\frac{1}{r^2}\int_a^r C(r,s)r\,dr + \frac{r^2-a^2}{r^2(b^2-a^2)}\int_a^b C(r,s)\,dr\right]$$

$$\sigma_\theta = \frac{s\hat{E}(s)\beta}{1-v}\left[\frac{1}{r^2}\int_a^r C(r,s)r\,dr + \frac{r^2+a^2}{r^2(b^2-a^2)}\int_a^b C(r,s)\,dr - C(r,s)\right] \quad (6.19)$$

The stress and radial displacement for the viscoelastic material are obtained by finding the inverse transform of Equations (6.19) which are given by

$$\sigma_r(t) = \frac{\beta}{J(t)(1-v)}\left[-\frac{1}{r^2}\int_a^r C(r,t)r\,dr + \frac{r^2-a^2}{r^2(b^2-a^2)}\int_a^b C(r,t)r\,dr\right]$$

$$\sigma_\theta(t) = \frac{\beta}{J(t)(1-v)}\left[\frac{1}{r^2}\int_a^r C(r,t)r\,dr + \frac{r^2+a^2}{r^2(b^2-a^2)}\int_a^b C(r,t)r\,dr - C(r,t)\right] \quad (6.20)$$

$$u_r(t) = \frac{1+v}{1-v}\beta\left[\frac{1}{r}\int_a^r C(r,t)r\,dr + \left\{(1-2v)r + \frac{a^2}{r}\right\}\frac{1}{b^2-a^2}\int_a^b C(r,t)\,r\,dr\right]$$

The relaxation response that corresponds to the time-dependent modulus in the plate is shown in Figure 6-11a, which shows the pronounced effect of temperature and liquid content on the relaxation of modulus. This shows the essential change in mechanical properties caused by the absorbed liquid, which is reflected by the decrease of the modulus. Deformation in the plate calculated using Equation 6.18 is presented in Figure 6-11b. It shows that higher deformation resulted with the presence of liquid, especially at the higher temperature. Degradation of viscoelastic material with liquid content significantly increases the deformation. This indicates an acceleration of the relaxation process due to the faster movement of molecules with an increase in temperature and liquid content (Muliana and Rajagopal, 2011).

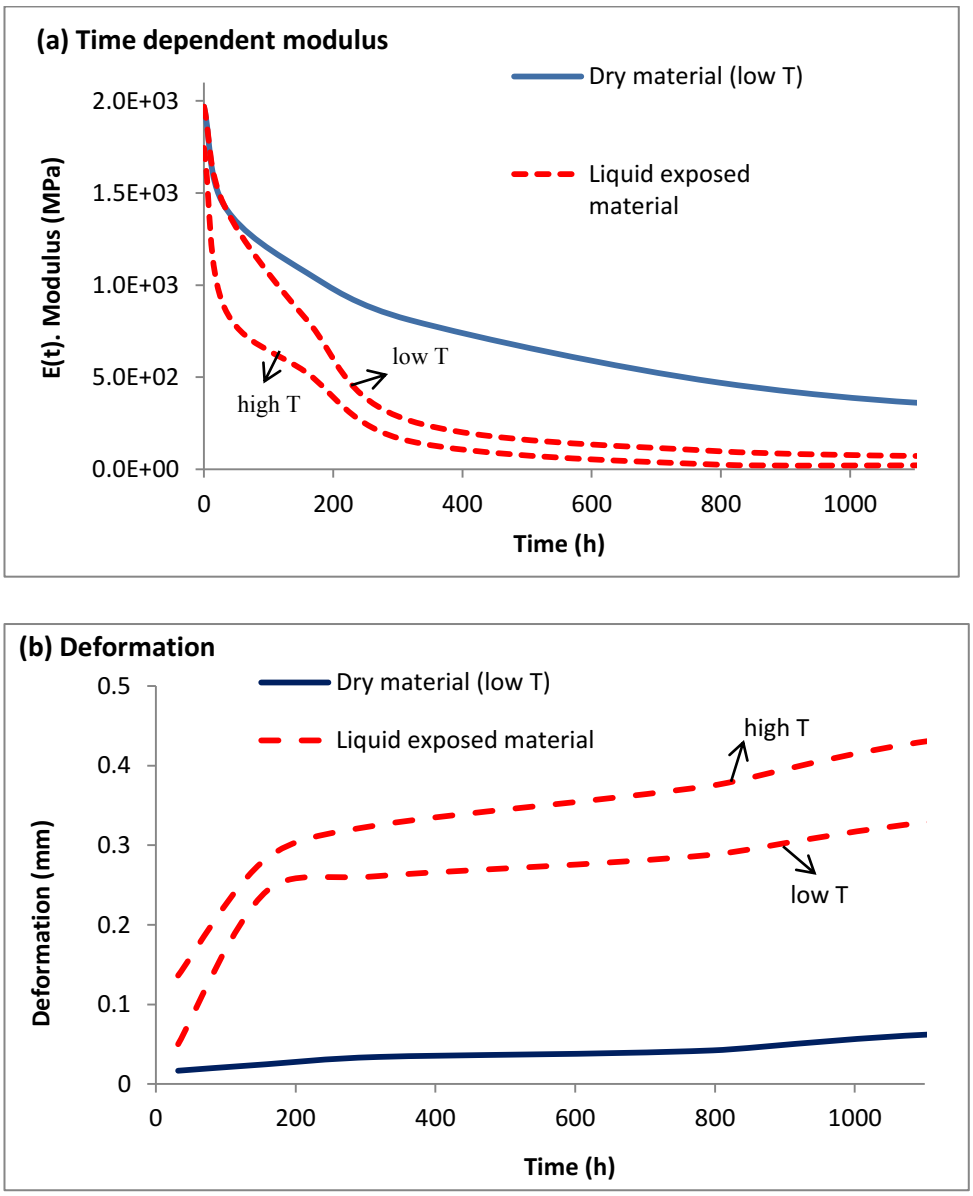

Figure 6-11: Effect of liquid on: (a) time-dependent modulus of material and (b) corresponding deformation in a plate at environment temperature T = 5 °and 30 ℃

The stress distribution within a plate exposed to liquid at various temperatures was calculated using Equation 6.20 with temperature and liquid content dependence as exhibited in Equation 6-12. Variation of axial stress also occurs in viscoelastic plate as in the case of elastic material. The distribution of axial stress which shown in Figure 6-12 indicates that the peak of stress at all environment temperatures occurs at the same value of Fourier number ($F_0 \approx 0.1$). The values of Fourier number is a function of diffusion coefficient, time and the thickness as presented in

Equation (4.11) for one-side liquid diffusion. Figure 6-12 also signifies an increase of stress with an increase of temperature.

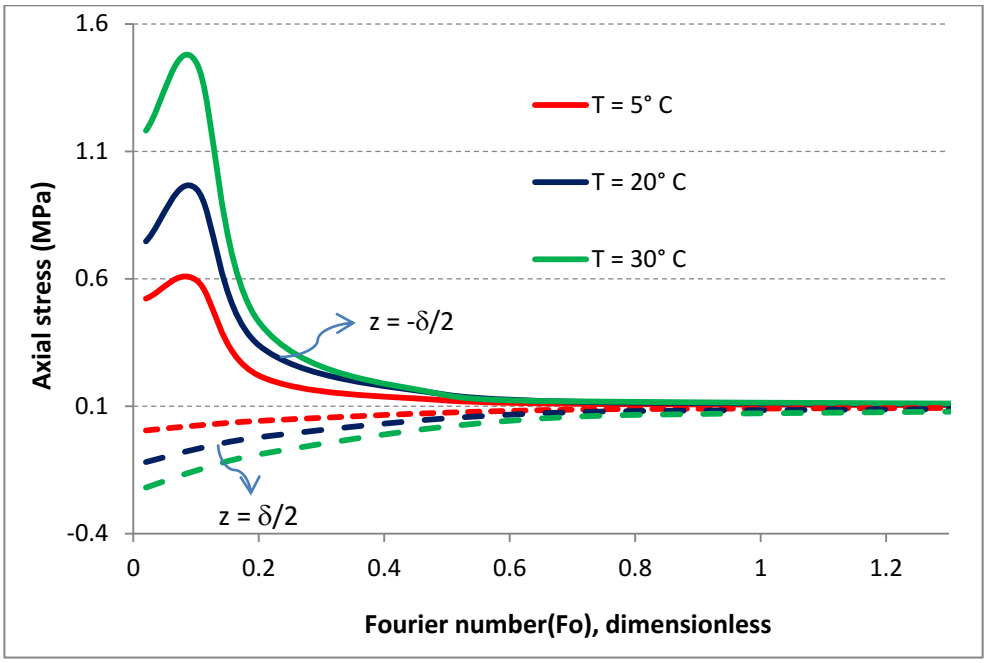

Figure 6-12: Evolution of axial stress in both faces of a plate exposed to liquid at different temperature conditions

6.3.2 Diffusion-induced stress and safety coefficient

The stress is concentrated around the inner part at the early phase of liquid diffusion process developing the concept of stress concentration. In preventing the risk of failure, it is necessary to provide a margin of safety in the design by taking into account the effects of liquid diffusion-induced stress. The safety coefficient gives the safety allowance to compensate for uncertainties in the operating conditions. In general, plastic component design should ensure that the maximum working stress during its entire service life of operation does not exceed the admissible stress. The admissible stress to a specific plastic material is defined as the ratio between the material strength and the safety coefficient (Rao and Schumacher, 2004) given by:

$$\sigma_{adm} = \frac{K}{(Sf.A_n)} \tag{6.21}$$

where K is material strength, S_f is the safety factor, and A_n is the material reduction factor which represents the effect of several factors such as dynamic loading and degradation of material properties due to environmental conditions.

Considering the effect of temperature condition on stress distribution as revealed in Figure 6-12, a stress factor, K_c,is introduced to represent the actual stress of a material during liquid diffusion. The value K_C may be determined from the maximum stress at time t related to F_0 = 0.1 as

$$K_C(T) = \frac{\sigma_{F_0=0.1}(T)}{\sigma_0} \tag{6.22}$$

where σ_0 is the nominal stress directly related to the applied load.

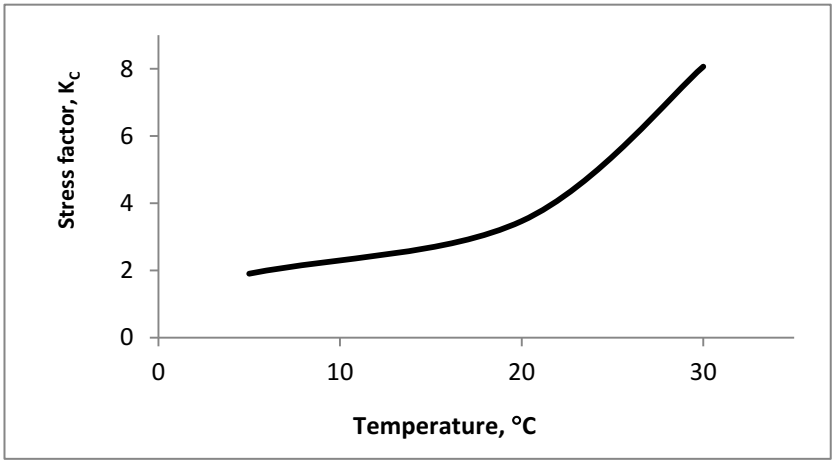

Figure 6-13: Relation between application temperature and the stress factor using an approach based on maximum stress

Figure 6-13 exhibits the function of the stress factor in terms of liquid diffusion obtained from Equation (6.22) with environment temperature. From this figure, the allowable applied load on an application at a particular temperature condition can be determined by modifying Equation (6.21) using the stress factor defined in Equation (6.22).

$$\sigma_{adm} = \frac{K}{(Sf.A_n.K_c)} \tag{6.23}$$

6.3.3 Modelling viscoelastic material in FE software

The definition of the material in the FE model is specified from the experiment data compiled in Section 5.3. In the computational program, the material is described as having an initial linear isotropic response to the load and thereafter, as having an ability to creep with time hardening over a primary and secondary phase. The FE software, ANSYS, analyses creep using implicit and explicit time integration schemes. The implicit model is recommended for general use and is suggested as the most accurate means to represent creep in ANSYS (Dropik et al., 2002, Gimbert, 2008). It is also said to be numerically unconditionally stable which means that it does not require as small a time-step as the explicit creep model (ANSYS, 2012). There are some implicit creep models available in ANSYS, which simulates the creep stages, not only either primary or secondary stages but also both stages. The software also provides a tool to generate and fit the experimental data in the Curve Fitting module of Mechanical APDL. In this case, the combine time hardening creep model, which is used to directly model the primary and secondary creep effects, is chosen to simulate the material response. The creep strain over time can be described as:

$$\varepsilon_{cr} = \left[\frac{C_1 \sigma^{C_2} t^{C_3+1} e^{\frac{-C_4}{C(t)}}}{(C_3+1)} \right] + \left[C_5 \sigma^{C_6} t e^{\frac{-C_7}{C(t)}} \right] \tag{6.24}$$

Tabulated creep experiment data were prepared and read into the software as a formatted text file to derive the coefficients of chosen mathematical model. The creep strain rate data required for the curve fitting was obtained by differentiating the creep strain equation presented in Equation 5.9, which defined in the following form

$$\dot{\varepsilon}(t) = \frac{\sigma}{E_K \tau} \left[exp\left(-\frac{t}{\tau} \right) \right] + \frac{\sigma}{\eta_M} \tag{6.25}$$

To perform curve fitting procedure in ANSYS, the initial elastic strain is eliminated from the set of data so that only primary and secondary creep strain data remain to be fitted in the selected creep model. The results of ANSYS nonlinear curve regression are verified by inserting the generated coefficients into Equation (6.24) as exhibited in Figure 6-14.

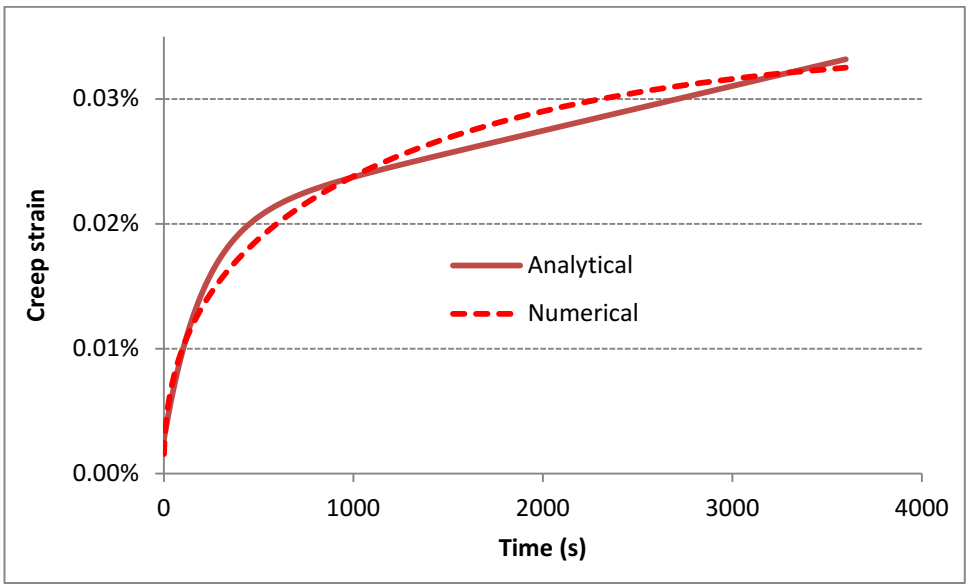

Figure 6-14: Curve fitting result to define the creep model for the dry material (C = 0%) at T = 30℃

As can be seen in Figure 6-14, the creep strain curve generated by the numerical model for the dry PLA-based material provides a good correlation with that of the analytical model shown in Equation (5.8) in Chapter 5. Curve fitting procedure is then applied for the material containing different levels of liquid concentration, which result in those creep model coefficients as given in Table 6.5.

Table 6-5: Creep model coefficients for the PLA-based material contains various levels of liquid content at T = 30℃

%Liquid content	Coefficients for implicit creep equation (Equation 6.24)						
	C1	C2	C3	C4	C5	C6	C7
0	6.20E-06	1.35E-09	-0.566	0	7.84E-08	6.02E-10	0
1.90	2.24E-05	1.04E-08	-0.542	0	3.46E-07	3.81E-07	0
2.91	3.64E-05	8.16E-08	-0.583	0	2.58E-07	-2.38E-08	0
5.95	1.57E-04	9.28E-08	-0.882	0	1.50E-07	-6.14E-09	0

The coefficients given in Table 6-5 are implemented by incorporating the instantaneous elastic response in the analysis. The numerical ANSYS results of the elastic and creep strains are

plotted against the analytical model presented in Section 5.3 and the observed experimental results presented in Section 5.2 as shown in Figure 6-15.

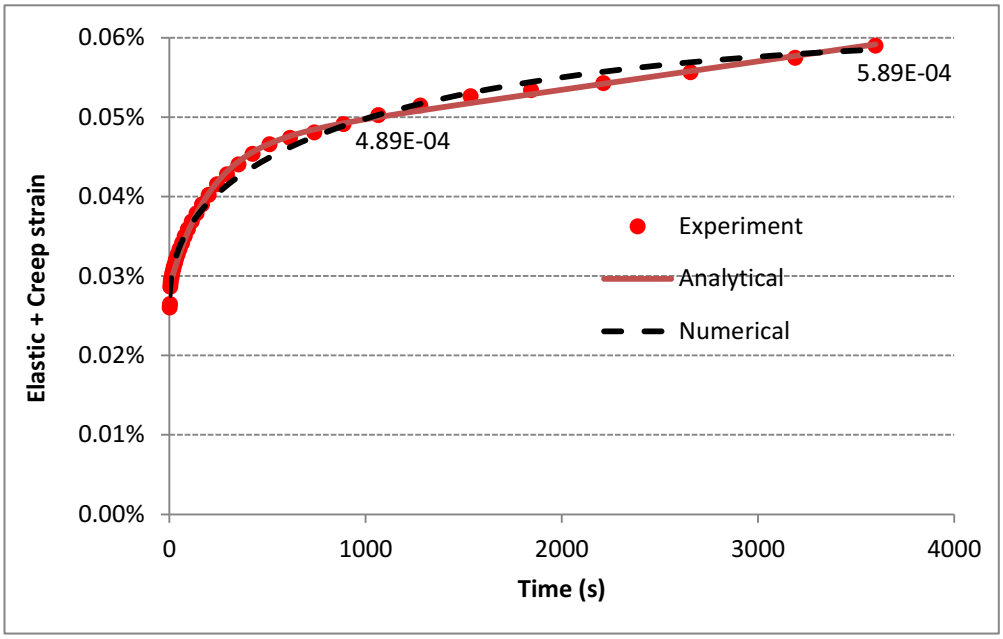

Figure 6-15: Numerical vs experimental results for elastic and creep strain in the dry material conditioned at T = 30 ℃

A numerical model was developed to calculate the total strain in the material subjected to a tensile stress with the same value as the constant applied stress used for the creep experiment test. A bar of 1 m length is set to have 1GPa of elastic modulus. While one side is constrained from axial displacement, the other side is subjected to 0.45 MPa tensile stress. It can be observed in Figure 6-16 that the total strain resulted from ANSYS is in good correlation to that observed in the experiment at t = 1000 s and t = 3600s, 4.89-4 mm/mm and 5.89E-4 mm/mm respectively. The value is also in good correlation to the predicted creep strain value ε = 0.049% achieved by the analytical model at t = 1000s.

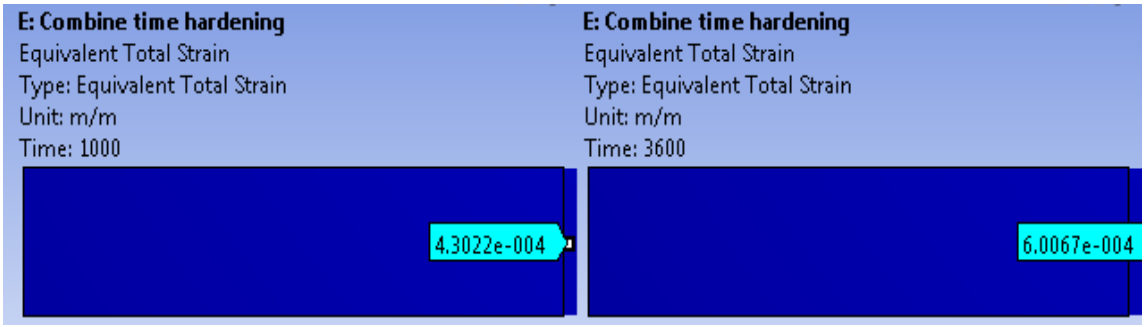

Figure 6-16: The total strain of a viscoelastic bar subjected to 0.45 MPa of tensile stress

6.4 Simulation

In development phase of a new package design, performance tests are usually performed before being qualified for packaging application, which includes the analysis of permeability to liquid and gas, environment stress cracking resistance (ESCR), crystallinity and structural tests (Demirel, 2008). Structural analysis in packaging application is executed to verify the mechanical strength of the package and identify key areas of structural weakness in relation to the design and thickness distribution of the package (Erbulut et al., 2009, Haddad et al., 2009). Mechanical performance tests commonly conducted are the burst pressure test, top load analysis and drop test. To evaluate the durability of the package during its life service, the strength of application is assessed by measuring the stress and deformation in response to the varying load (Demirel and Daver, 2012). Usually, it is then followed by analysing the critical load at the point of buckling as the buckling load (Van Dijk et al., 1998). Finite element (FE) method has been implemented in numerous studies to assess the structural performance of various package designs when subjected to different loading conditions (Demirel, 2008, Vaidya, 2012, Van Dijk et al., 1998, Abbès et al., 2010, Masood et al., 2006). Those studies confirmed the advantages of FE analysis in evaluating mechanical performance of a package in its early phase of design. Simulation driven product development is supplementing the expensive experimental cost and complex testing in packaging application (Robertson and Metwally, 2013).

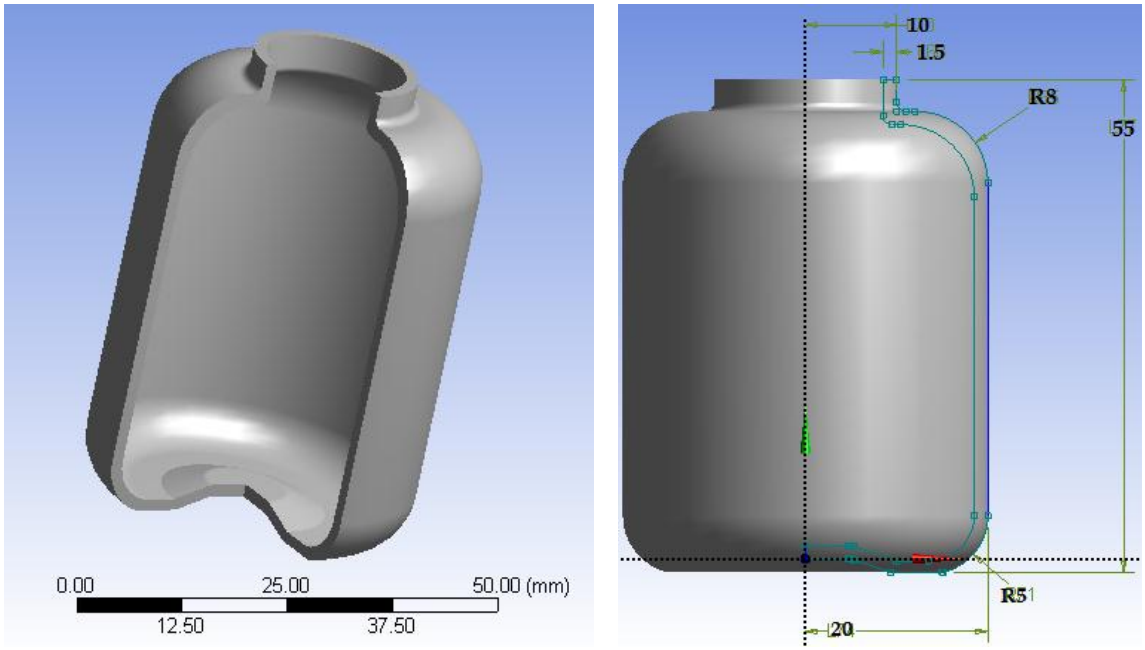

Figure 6-17: Design of the simulated liquid package with the corresponding dimensions (in mm)

For investigating effect of liquid transport in mechanical performance of a packaging application, this section presents a mechanical behaviour study for a general small-size package of 1 mm thickness by means of a finite element (FE) model, which can be focused on top load and internal pressure analysis. The FE analysis was performed using the converged mesh and time-step sizes evaluated previously in section 6.1 for a small container as presented in Figure 6-17.

As the purpose of this study is to evaluate the significance of diffusion in relation to the mechanical response, the simulation is concentrated on the region of the package base, which is constantly in contact with the diffusant. In the simulation stage, the boundary conditions are defined in the FE software according to the conditions of the package experience while in service during storage recently after filling. For the structural analysis of the package, instead of using a constant value to define the material properties, liquid content-dependant mechanical properties were used, especially for the modulus. The material properties required for stress and deformation analysis were defined based on mechanical testing as presented in Table 6-2 for the elastic properties and Table 6-5 for viscoelastic properties.

6.4.1 Profile of liquid content

The distribution of liquid content within the thickness of the package is firstly solved utilizing the transient heat transfer module in the FE software, which has been clearly explained in Chapter 4, section 4.5. Using the value of diffusion coefficient provided in Table 6-4 and saturated concentration data of 2.9% weight gain, the profile of liquid content at time t can be obtained as shown in Figure 6-18 for t = 550 h.

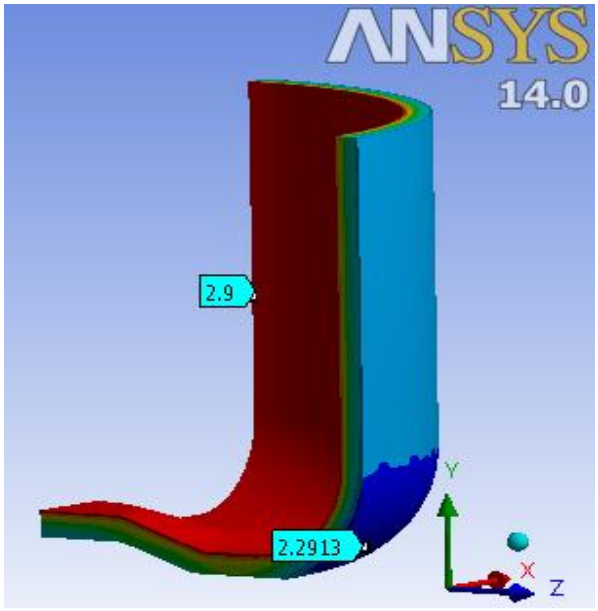

Figure 6-18: Profile of liquid content within thickness of the package base at t = 550 h

The simulation result in Figure 6-18 presents a non-uniform distribution of liquid concentration before saturation condition with minimum concentration occurring on the fillet section of the package base. The evolution of liquid content is then transferred into the static structural section of the FE software to investigate the mechanical response of various loading condition applied.

6.4.2 Top load analysis

In this section the performance of a liquid container made of PLA-based plastic containing a hydrocarbon liquid is evaluated by simulating the mechanical behaviour under a top-load by means of finite element model. The top-load analysis aims to assess the durability of the packages to withstand axial load necessary for filling and stacking the packages during manufacturing, storage and distribution (Demirel and Daver, 2012, Robertson and Metwally, 2013). The top load test is usually performed to identify the peak buckling load, which is the critical load resulting in buckling. The response to the applied load is initially linear, but at

certain point the compression force no longer increases linearly with applied deformation (Van Dijk et al., 1998). This is the critical point where buckling starts.

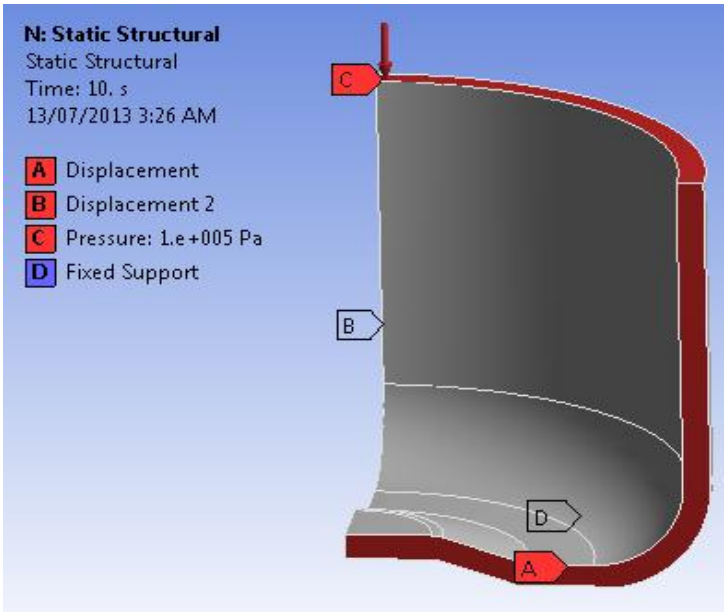

Figure 6-19: Boundary conditions for top load analysis of the package base

The equivalent (von Mises) stress and deformation profiles of the package resulting from FE software are shown in Figure 6-20. The von Mises stress was at maximum in the bottom part of the package base, which is related to constrained location, where the bottle rests (Erbulut et al., 2009).

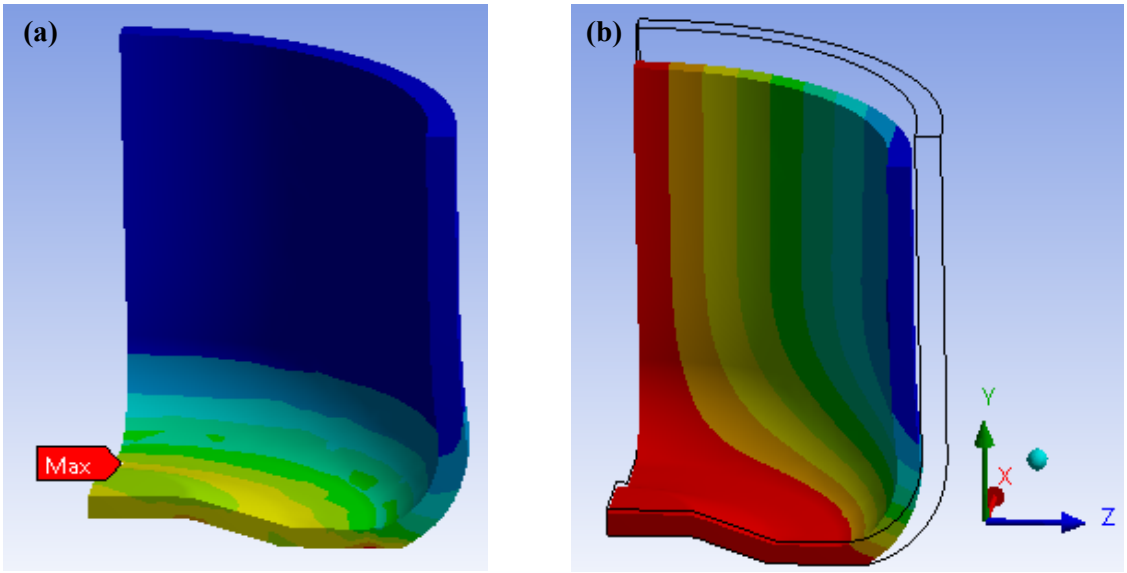

Figure 6-20: Distribution of: (a) the von Mises stress and (b) radial deflection of the package based under top loading

In the package wall, the tangential stress concentration is at the outer surface of the wall as exhibited in Figure 6-21 due to inhomogeneous liquid content, which results in swelling-induced stress. This critical stress point may become an indication for the possibility of failure of the package. When the resulting stress exceeds the yield stress of the package material, stress cracking may occur, especially with the presence of high deformation (Miranda et al., 2011).

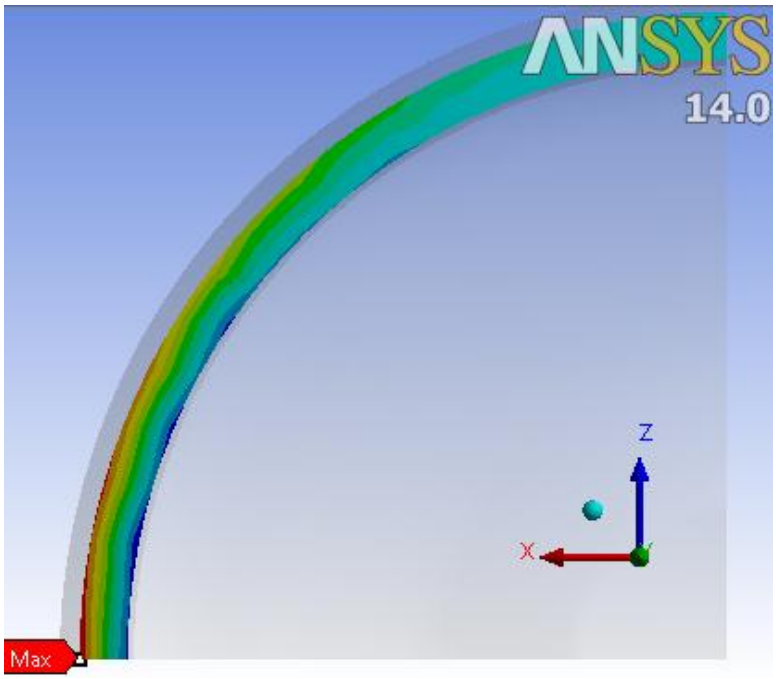

Figure 6-21: The critical tangential stress areas at the outer surface of package wall under top loading

Mechanical responses of the package with different wall thickness exposed to different levels of environment temperature can be obtained by applying a dimensionless variable of Fourier number (F_0) as illustrated previously in Figure 6-12. It is for this reason that the stress and deformation fields of the simulation results are presented as a function of the Fourier number. The corresponding time for particular value of F_0 in different values of wall thickness and environment temperature is exhibited in Figure 6-22.

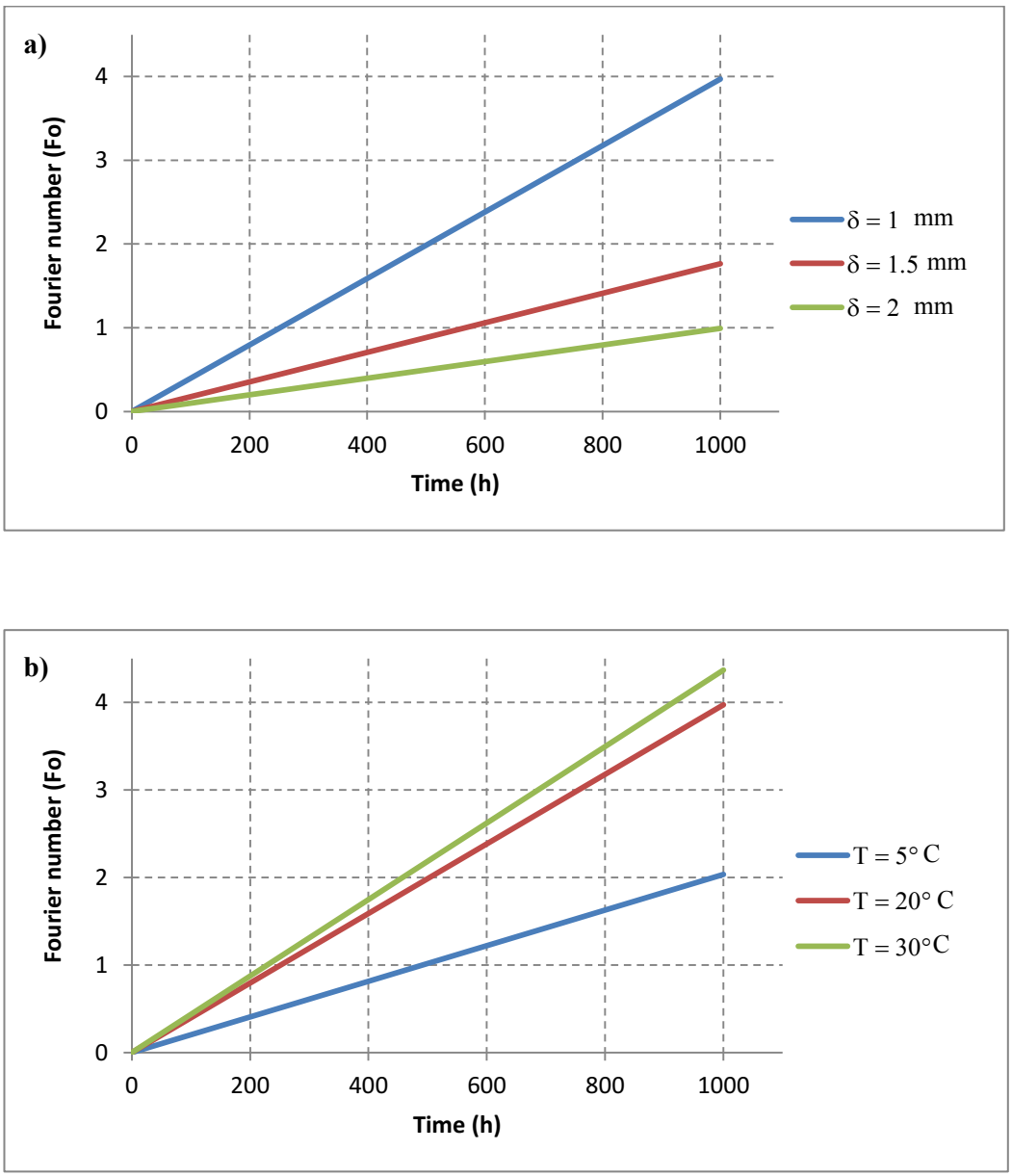

Figure 6-22: The corresponding time for a particular Fourier number for different values of: (a) wall thickness at 20℃ and (b) environment temperature for 1 mm wall thickness

Effect of degradation rate, swelling coefficient and environment temperature on the mechanical response will be investigated in the following sub sections. Since the peak load capacity of a package is influenced by the non-linear material properties (McNabb et al., 2002), the effect of those parameters on buckling load will also be evaluated.

6.4.2.1 Effect of degradation rate

The effect of the rate of liquid diffusion-induced degradation on the stress and deformation fields was studied. In elastic approach, the degradation rate is determined from the slope of the decreasing line of modulus with liquid concentration. According to experimental results as presented in Figure 6-8, the degradation rate of elastic modulus can be obtained from the gradient of the regression function which equals to 0.24. For comparison, another case with no degradation, as for dry material which has constant modulus, is considered.

Figure 6-23 portrays the evolution of total radial deflection and stresses at package wall for the two different cases of degradation rate. Figure 6-23(a) shows that the applied load to the material, which experienced degradation in its modulus, results in higher deflection compared to that which not consider deterioration of material properties. However, deformation may still be apparent for the case of constant modulus due to diffusion-induced swelling effect. Loss of the package integrity may occur with high undesirable deformations resulting from material properties deterioration induced by liquid diffusion. In terms of stress fields, evolution of equivalent (von-Mises) stress and tangential stress at package wall with time are obvious as a result of non-uniform expansion before reaching saturated condition. Figure 6-23(b) and (c) show that the peak of stress is observed at the value of Fourier number, $F_0 \approx 0.2$. As a result of lower modulus, less values of stresses for material,which experience degraded modulus, is revealed especially at the early period of diffusion process.

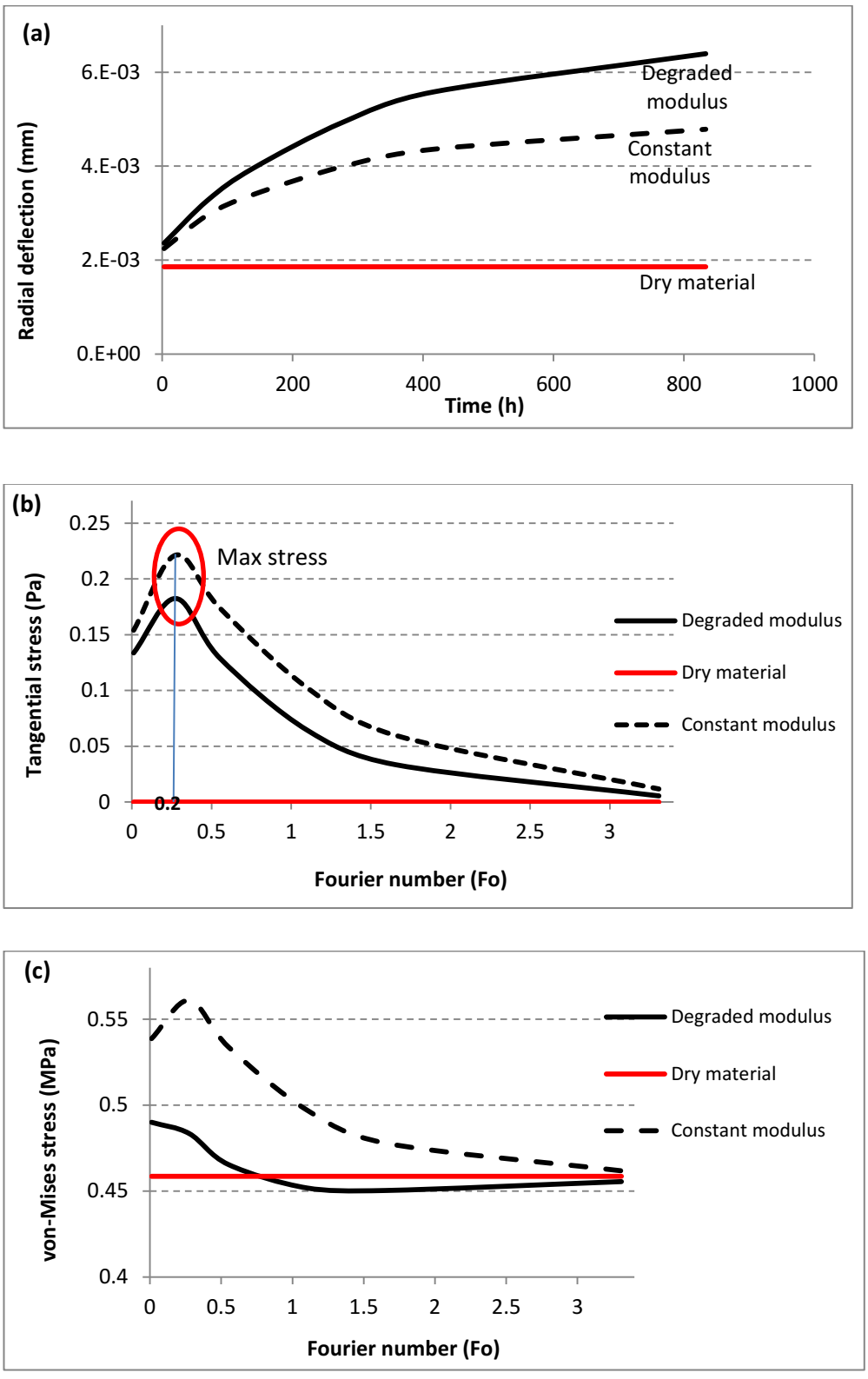

Figure 6-23: Evolution of mechanical responses of an elastic package for different rate of degradation on: (a) radial deflection, (b) tangential stress at package wall and (c) von-Mises stress

The buckling analysis was performed subsequent to the structural analysis to identify the changes of buckling strength with the rate of degradation. Result of linear buckling analysis generated from the FE software is presented in Figure 6-24.

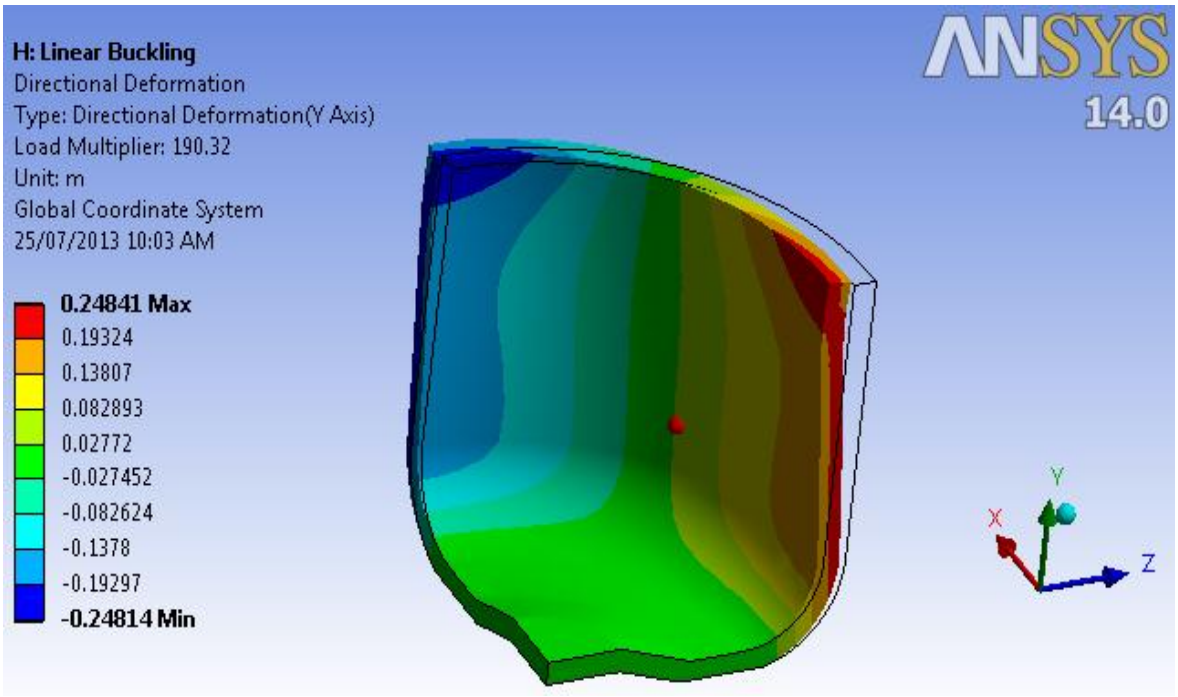

Figure 6-24: Simulated buckling in the PLA-based package under top load

The result indicates that the buckling strength falls from 190.3 MPa for material with no degradation to 103.5 MPa for material with 0.24 degradation rate. These results are coherent with the report presented in Section 5.1, which shows significant deterioration of mechanical strength in consequence of liquid diffusion. Decreasing of top-load strength was also observed by (Abbès et al., 2010) in the case of increasing ethyl acetate concentration of polypropylene bottles.

6.4.2.2 Effect of swelling coefficient

The effect of swelling coefficient on the mechanical response of the package is also analyzed. Two different cases with different values of swelling coefficient are considered and compared with one case without swelling coefficient. All of the cases are using constant modulus, which means degradation of properties is neglected, in order to investigate only the effect of swelling coefficient. The swelling coefficients of 0.00531 and 0.00231 are utilised to represent the high and low swelling, respectively.

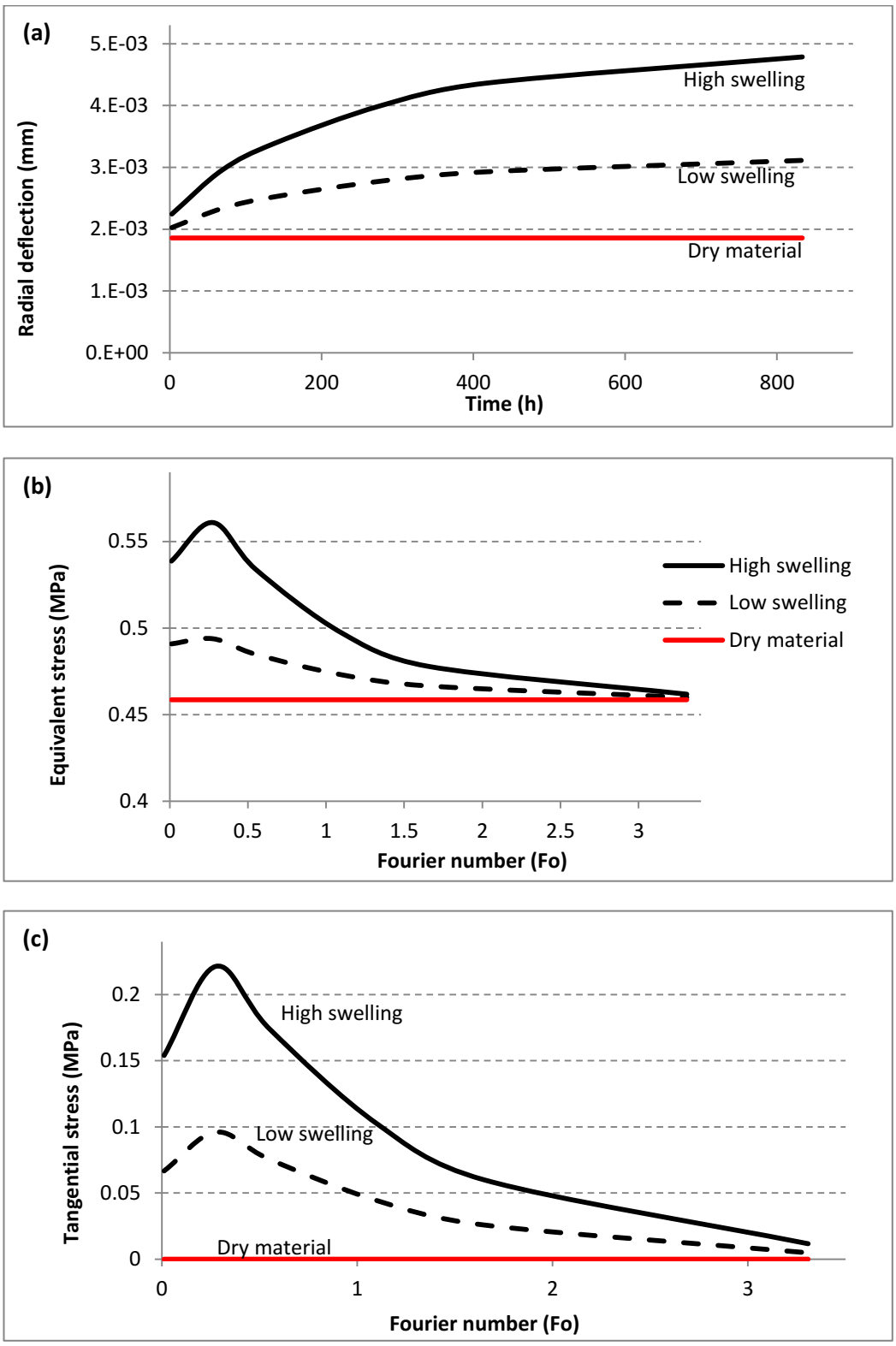

Figure 6-25: Evolution of mechanical responses of an elastic package for different values of swelling coefficient on: (a) radial deflection, (b) von-Mises stress and (c) tangential stress at package wall

Significant effect of swelling coefficient on the strain and stress states of the package is clearly shown in Figure 6-25. The more the swelling coefficient, the higher deflection and tangential stress are resulted. As seen in Figure 6-25c, high tangential stress at the package wall increases with increasing of swelling coefficient which potentially weakens the sidewall panel of the package (Duncan et al., 2005, NatureWorks, 2011). Diffusion-induced swelling is an essential parameter in the package, which may also indicate the high permeability to molecules transport.

6.4.2.3 Effect of time-dependent properties

Effect of time-dependent values in the material constitutive equation is investigated in this subsection by simulating two different cases with different creep parameters. These two cases are simulated using viscoelastic properties presented in Table 6-3. The material properties of Case 1 are modelled by employing the creep model in Equation (6.25) using the coefficients of the dry material (0% liquid concentration). While in Case 2, the material properties are modelled with liquid content dependent creep coefficients instead of constant coefficient by modifying Equation (6.24) as:

$$\varepsilon_{cr} = \left[\frac{C_1(C(t))\sigma^{C_2(C(t))} t^{C_3(C(t))+1}}{\{C_3(C(t))+1\}} \right] + \left[C_5(C(t))\sigma^{C_6(C(t))} t \right] \tag{6.26}$$

where C_i are obtained empirically from the data presented in Table 6-3.

The deformation and stress fields for those two cases are shown in Figure 6-26. For comparison, another case of time-independent properties is also presented.

The deflection of material calculated using both elastic and viscoelastic approach increases significantly with time as a result of time dependent diffusion-induced swelling. Higher deflection in viscoelastic material is pronounced especially when the viscoelastic material properties degrade with liquid content as represented in Case 2. The evolution of tangential stress with time was also observed which peaks at the same value of Fourier number, around 0.2. Figure 6-26(b) shows that elastic solution gives overestimation of the stress component, but the curves will coincide with the viscoelastic solution after saturated liquid concentration is achieved in the material.

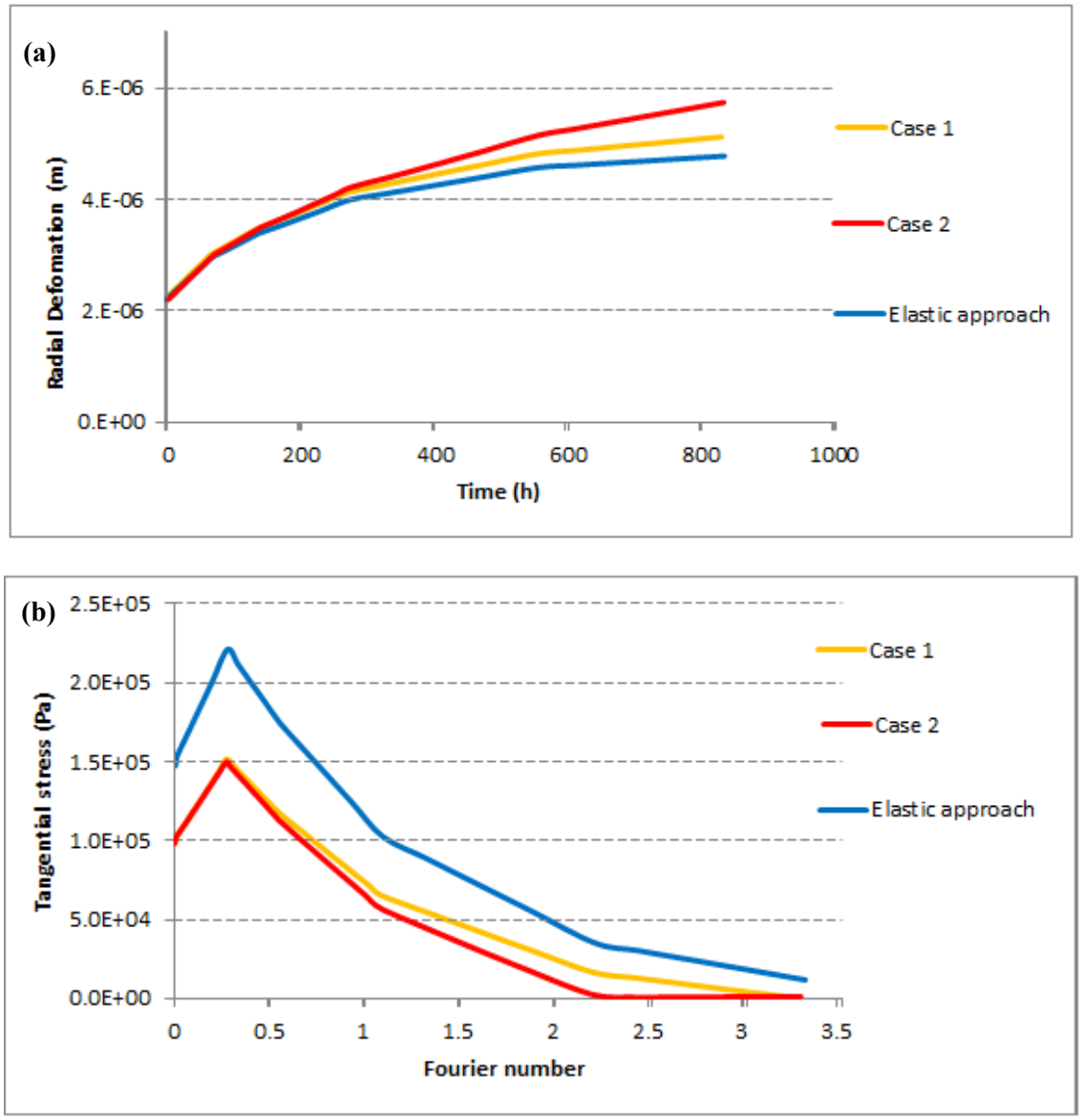

Figure 6-26: Evolution of mechanical responses of a viscoelastic package for different liquid dependence of creep parameters on: (a) radial deflection and (b) tangential stress at package wall

6.4.3 Internal pressure analysis

The mechanical performance of a package can also be assessed through a burst strength analysis which evaluates the stability of the package subjected to an internal pressure. This test is usually performed for bottles intended for carbonated beverages in order to ensure that the bottles do not blow up at the filling stage and filled bottles do not expand excessively during storage and/or during bottle warming for pasteurization purposes (Demirel and Daver, 2012). In

performing internal pressure analysis using FE model, the top section of the bottle was clamped and internal pressure was applied on the inner surface. The test result provides an assessment of the overall stability of the bottle under carbonation pressure of the content which establishes qualitative and quantitative statements on the widening of the package. In addition to the internal pressure analysis, a similar test but with a vacuum pressure can also be performed to assess the vacuum resistance of the package (Van Dijk et al., 1998). A phenomenon called panelling can be observed when the internal stress under pressure exceeds the vacuum resistance.

In application of PLA material for liquid packaging, it has been found that inward deformation or panelling occurs in the container after storage for a particular period (Singh, 2008, Cairncross et al., 2006). The inward buckling takes place in the package because of a pressure difference with the ambient air pressure outside (O.Berk, 2012). The permeation of gas/water vapour creates a negative pressure and causes the walls of the package to be sucked in compensating for the loss of volume.

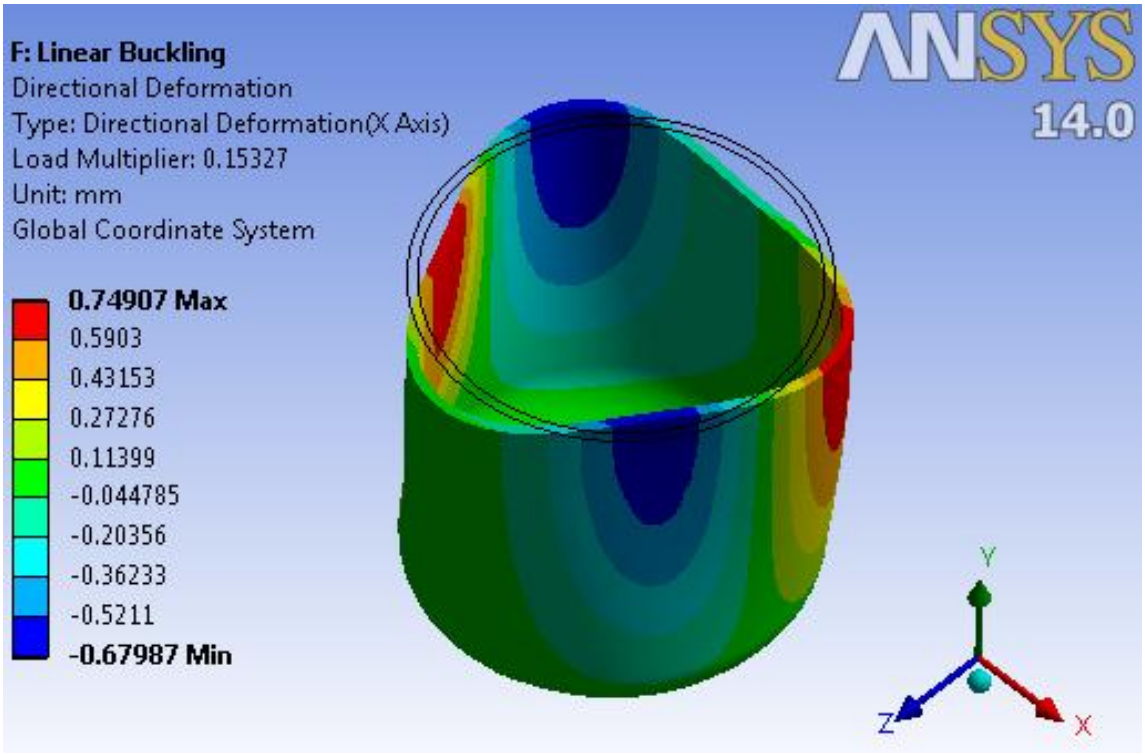

Figure 6-27: Buckling of the package in response for internal vacuum pressure

In order to illustrate the phenomenon of panelling due to gas/water vapour permeation, this section proposes a FEA model in predicting the critical period which corresponds to the inward buckling point. The critical buckling load is obtained first in static structural model of the FE software based on specified loading and boundary conditions. The estimated critical load is then correlated to the radial stress at the internal package wall in response to the package shrinkage due to permeation. The critical buckling load in part of a package subjected to internal vacuum pressure is presented in Figure 6-27, which shows a value of 0.153 MPa.

Another FEA model is developed to simulate the process of substance permeation through the package as previously illustrated in section 4.6. The static structure module is then added to the model to determine the stress induced in the package. The maximum axial stress at x direction in the package wall is reported in Figure 6-28.

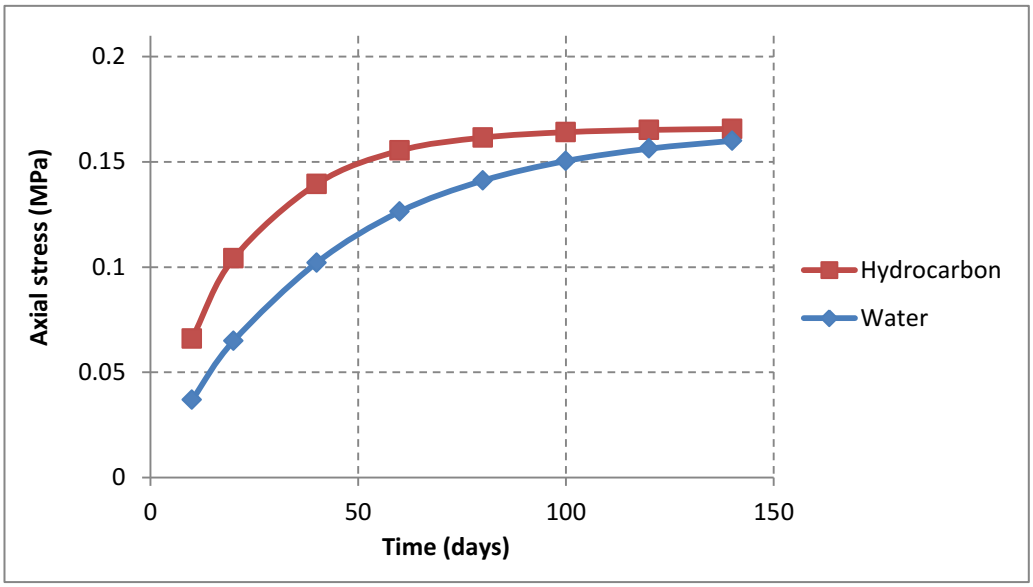

Figure 6-28: Evolution of axial stress resulting from water and hydrocarbon loss through the wall of a package

Figure 6-28 shows the increasing trend of axial stress during storage of period due to water and hydrocarbon loss through the package wall. Inward buckling occurs at a time when axial stress exceeds the specified buckling limit as shown in Figure 6-27. It shows that buckling of the package containing water and hydrocarbon occurs at t = 110 days and t = 60 days, respectively.

6.5 Conclusion

This chapter presents the response of a PLA-based package in contact with liquid and subjected to mechanical loading using a FE model. The effect of time-varying liquid content is examined in terms of stress and deformation fields. The model is developed according to a series of convergence analysis to ensure that the results obtained are adequately accurate. It is found that the size of time increment significantly affects accuracy of the results.

Viscoelastic model is developed in the FE software using the creep implicit schemes to represent the time-dependent properties of material. As it is to be expected, higher temperature accelerates more relaxation in the material, which increases the deformation. The resulted stress increases with increasing temperature since the time dependent modulus and swelling coefficient are temperature dependent.

The package is subject to uniform load at the top of the package and the effect of degradation rate and swelling coefficient is investigated. The stress concentration arises at the outer surface at the wall as a result of different expansion due to non-uniform liquid content. The variation of swelling acts as an internal constraint, as it induces stresses that are developed during liquid diffusion process. The combination of mechanical and swelling stress may become exceptionally large, reducing the load bearing capacity that results in crack initiation that leads to failure of the application. The result confirms the substantial influence of swelling coefficient, which shows higher stress with increasing swelling coefficient. Diffusion-induced swelling is also an indication of high permeability to molecules transport in the package. For packaging application, serious consideration must be given to degradation of material properties after sorption of a product substance into the package. Higher degradation rate with liquid content may result in loss of the package integrity due to high undesirable deformations occurring in the package.

CHAPTER 7
CONCLUSION AND SUGGESTION FOR FUTURE WORKS

This chapter reviews the research work conducted, the important findings from the work and the possible future works that could follow from this current study.

7.1 Overview of research

This research aimed to provide a methodology in evaluating mechanical performance of a package which was substantially influenced by the sorption of packaged product. The proposed methodology attempted to correlate the sorption effect in term of material properties degradation and chance of swelling on the mechanical response of a package. PLA-based plastics is one type of renewable materials which has been found to be an ideal candidate for packaging applications considering its good mechanical properties, ease of processing and biodegradable properties. The thesis evaluated new application for PLA-based material for short-term packaging of chemical solvent or other organic liquid by taking into account the effect of absorbed liquid into the package.

A review into studies in the field of PLA packaging has shown the significant effect of mass transport on both the packaged product quality and the integrity of the package material. The mass transport in PLA package involves the interaction with the packaged product, the package and the environment. The integrity of PLA material in relation with its surrounding environment such as humidity and temperature has been widely studied. Deterioration of mechanical performance was observed with increasing relative humidity and temperature. In term of product quality, many studies have been performed to evaluate loss of product substance through the package material and the permeation of undesirable compound from the environment. However, to date, interaction of PLA material with product containing higher

molecules has been the subject of only a few studies, which may be related to relatively short shelf-life and low requirements of current products packaged in PLA material.

In this work, the mechanical performance is evaluated according to the distribution of absorbed liquid content which is related to the changes of mechanical properties and deformation due to swelling. Liquid content profile as a function of time and position can be analytically and numerically described based on the diffusion parameters obtained from a series of gravimetric analysis. Mechanical tests were performed to identify changes of mechanical properties with increasing liquid content inside the material. The time dependent properties were also investigated through creep experiment to construct material constitutive equation which has time, temperature and liquid content dependence. The evolution of mechanical behaviour of the PLA-based package is then examined using the FEA model with previously defined material responses. The stress and deformation fields are analysed for a package, which is subjected to top load and internal pressure while undergoing dimensional and material property changes due to the diffusion of liquid through its thickness.

7.2 General conclusions

In this section the important findings obtained from this study are presented in relation to the specified research objectives.

In general, it is found that the diffusion rate and permeability coefficient are greatly influenced by the environment temperature. The diffusion of the model fluid into PLA-based materials at low temperature (less than 30°C) approximately follows Fick's law, which shows initial linear increase of weight gain followed by a transition region reaching saturation level at large values of times. However, at higher temperature, the diffusion behaviour of the liquid into PLA material is anomalous and it cannot be adequately described by Fickian diffusion (Research objective 1).

Extensive length swelling has been found as a consequence of liquid diffusion and the swelling coefficient is obtained by correlating the results from weight gain and dimension change measurement.

Profile of diffused liquid in the package is obtained numerically using the FEA software based on convergence of numerical solution in a slab and cylinder. The FEA model is developed using the heat transfer analogy with diffusion coefficient and rate of mass transport as the required material property for the diffusion and permeation process, respectively. Liquid concentration is

distributed as the function of time and position within the thickness of the package until reaching a saturated condition at a particular period. Higher liquid content initially presents at the surface directly exposed to liquid, which is then followed by the inner layer. The time-step size of less than 1% of time of saturated concentration is recommended to provide an accurate result. Smaller mesh size is found to represent more detail profile of liquid content in the package. The FEA model is developed to simulate the function of liquid in time and position within the package for either Fickian or non-Fickian characteristics (Research objective 2).

It has been shown that in term of product substance loss due to permeation, it is necessary to improve the barrier properties of neat PLA-based package to be qualifying for water, hydrocarbon or other chemical liquid packaging in longer term application.

The relationship between mechanical properties and liquid concentration can be developed by measuring the properties at different levels of saturated concentration. Non-uniform liquid content results in inhomogeneous material properties due to dependency of material properties on the presence of liquid. Progressive decrease of the modulus and strength of material was observed with increasing liquid content. The material loses its strength by more than 60% when exposed to the model fluid at 30°C for 40 days. Considering the anomalous diffusion characteristics at higher temperature level, it can be more severe at longer exposure time (Research objective 3).

Time and temperature dependent properties were also clearly determined from the measurement of dynamic mechanical properties. The modulus decreases with increasing temperature and liquid content with a sharp drop around its glass transition temperature (55°C). However, in the temperature region above the T_g, higher modulus was observed for specimens with higher liquid content indicating a significance structural changes at elevated temperature condition. The result was also confirmed by increase of relative crystallinity, which improves the creep resistance of liquid-absorbed samples at high temperature. The decreasing of time-dependent modulus in the viscoelastic material leads to higher deformation compared to that in an elastic material. This relaxation process was accelerated with an increase of the environment temperature (Research objective 4).

The material constitutive equation is constructed by taking into account for changes in the properties due to changes of temperature and liquid content dependence of the creep parameters which were empirically obtained from fitting of experimental data. The Burgers four-parameter creep model is selected to predict the creep behaviour of PLA-based material. The relationship between all creep parameters and liquid content can be described mathematically at each level

of temperature as presented in Equation (5.7) in Chapter 5. Therefore, the material properties at any given location and time are dependent on the liquid content and temperature. In viscoelastic material, these spatially inhomogeneous properties vary with time and result in the full coupling of two time-dependent variables (Research objectives 3 and 4).

The mechanical behaviour of a package application subjected to external load while undergoing dimensional and material properties change due to liquid diffusion is examined through a stress-strain analysis using the previously defined material constitutive equation. Effect of liquid diffusion is incorporated on the stress profile through the swelling coefficient and liquid-dependent material parameters for both the elastic and transient (time-dependent) properties. The stress associated with a diffused liquid is analysed using the general technique of thermal stress analogy. Results show that non-uniform liquid concentration distribution during diffusion process leads to a variation in the stress profile. Variation of the stress components with time and position was observed until it reaches an equilibrium value of the nominal stress (the stress which is directly related to the applied load). The stresses are at maximum at the points furthest from the liquid exposure area (Research objective 5).

A finite element model was implemented to analyse the mechanical performance of a liquid package in response of the top load by taking into account the dimensional and mechanical property changes due to liquid diffusion. In numerical stress analysis, a smaller time-step size leads closer to a convergence solution. Therefore, it is recommended to set a time-step size for less than 2% of analysis time to accurately gain the stress profile of the application. As expected, the equivalent stress was at maximum in the bottom part of the package, which was related to the constrained location where the bottle rests. The stress concentrated at the outer surface of the package wall as a result of diffusion-induced swelling should be taken into consideration as it may become an indication for the possibility of package failure. In preventing the risk of failure, it is necessary to provide adequate safety margin by taking into account the effect of liquid diffusion-induced stress. The stress concentration factor is introduced to represent the stress concentration of material during liquid diffusion (Research objective 6).

Loss of the package integrity may occur with high undesirable deformations resulting from degradation of material properties induced by liquid diffusion and also from viscoelastic nature of the material. The buckling strength, which indicates the capability of material to withstand buckling failure, significantly drops with increasing degradation rate of modulus. High swelling

coefficient results in high tangential stress at package wall, which potentially weakens the sidewall of the package (Research objective 7).

In evaluating new opportunities of PLA-based material for chemical product or other aggressive liquid packaging, it is important to understand not only the chemical resistance of the material but also the potential route for degradation. Some considerations in application of PLA-based material for hydrocarbon liquid packaging can be summarized as follow: (Research objective 8)

- Despite of possessing quite lower diffusion rate compared to polypropylene and high density polyethylene, the material absorbed higher amount of hydrocarbon liquid than water. It is for this reason that the permeability coefficient of the material toward hydrocarbon liquid is relatively high
- The presence of hydrocarbon liquid greatly influences the mechanical properties of material. The results show significant decrease of modulus and strength with an increase in liquid content. Degradation of mechanical properties will lead to a decrease in the capability of the material to withstand the applied load as shown by the decreasing of the buckling strength. It should be noted that the material possesses quite low impact properties, which need to be improved for packaging application
- The material is temperature sensitive, since the rate of diffusion is highly influence by surrounding temperature. The diffusion-induced swelling represented by the swelling coefficient progressively increases with increasing of environment temperature. As shown from the stress analysis, high swelling coefficient will result in stress concentration in the point furthest from the surface directly exposed to liquid at the beginning of the diffusion process. Therefore, higher temperature level will result in higher stress that may lead to failure of an application
- Environment temperature also substantially affects the mechanical properties of the material. The mechanical performance progressively decreases with temperature with a sharp drop around the glass transition temperature (T_g). The competing process of plasticization at low temperature and crystallisation at high temperature induced by liquid sorption effect leads to unstable material behaviour due to change of material stiffness at temperature above the T_g.
- Time-dependent properties of the material are clearly observed through the analysis of its creep behaviour. Neglecting the viscoelastic nature of the material may give overestimation of the stress resultant. The coupling of two time-dependent variable

using viscoelastic approach results in higher deformation compared to the elastic approach.

7.3 Suggestion for future works

This section gives recommendations which, in the view of author, present valuable extensions to the present work. This work aimed to provide a framework in evaluating the mechanical performance of a package by taking into account the mass transfer of product substance into the package, especially the one made from PLA-based material. Since the mechanical behaviour is greatly influenced by changes in dimensions and mechanical properties due to diffusion of a product substance, it would be interesting to investigate effect of interaction of neat or modified PLA package with other product substances including sorption of large volatile molecules such as aroma or flavour compounds. Chemical analysis such as IR (infra-red) spectroscopy, NMR (Nuclear Magnetic Resonance) and MS (mass spectrometry) can also be performed to investigate the changes of chemical structure due to liquid diffusion. Those studies would help to understand the degradation mechanism, which can, in turn, assist in improving the material performance for liquid packaging application.

The present work may complement the shelf life analysis of a packaged product according to its permeation characteristics. However, additional researches in development of a promising blow-moulded PLA package are essential for future works. According to the results revealed in this work, recommendations for improving the current material studied included some important variables such as: decreasing the swelling rate, delaying the degradation rate, reducing the solubility coefficient. which indicates the amount of the absorbed penetrant into the polymer and improving the thermal stability of the material. The next step is to assess manufacturing feasibility and then conduct a series of analysis based on the methodology proposed in this work.

In this study, a Finite Element Analysis (FEA) software is implemented to model the diffusion of liquid into a package design. Even though one-dimension time-dependent diffusion model used was capable to provide profile of liquid content within the thickness of a component, it is useful to be analysed in 2D or 3D diffusion model to obtain more precise results. The creep experiment performed in this present work has revealed the significance of the effects of liquid content at different temperature conditions. Adapting the conditioned immersion chamber would provide a more accurate output preventing evaporation of immersed liquid under heat

conditioned. But it should be noted that this test will take longer for at least until reaching saturated liquid concentration. The short time frame of creep analysis in this current study limited the understanding of the secondary phase. A longer creep experiment is desirable for the purpose of studying creep failure or the transition between the secondary and the tertiary phase. The study can also be extended to include the non-linear viscoelastic analysis.

A series of structural performance analysis in packaging application, which takes into account the effect of liquid diffusion through the thickness of the package has been presented by means of finite element method. Numerical analysis of a package design with non-uniform thickness distribution can also be performed to precisely simulate the real package application. The thickness distribution could be obtained from integrated virtual prototype of product design and manufacturing simulation.

REFERENCES

ABBÈS, B., ZAKI, O. & SAFA, L. 2010. Experimental and numerical study of the aging effects of sorption conditions on the mechanical behaviour of polypropylene bottles under columnar crush conditions. *Polymer Testing,* 29**,** 902-909.

AHMED, J. & VARSHNEY, S. K. 2011. Polylactides-chemistry, properties and green packaging technology: A review. *International Journal of Food Properties,* 14**,** 37-58.

AHMED, J., ZHANG, J. X., SONG, Z. & VARSHNEY, S. K. 2009. Thermal properties of polylactides: Effect of molecular mass and nature of lactide isomer. *Journal of Thermal Analysis and Calorimetry,* 95**,** 957-964.

ALLRED, R. E., AND BUSSELLE, L.D. 2000. Tertiary Recycling of Automotive Plastics and Composites. *Journal of Thermoplastic Composite Materials,* 13**,** 92.

ALMEIDA, D. N. F. D. 2011. *Life Cycle Engineering approach to analyse the performance of biodegradable injection moulding plastics.* Master, Instituto Superior Tecnico Universidade Tecnica de Lisboa.

ALMENAR, E. & AURAS, R. 2010. Permeation, Sorption and Diffusion of poly(lactic acid). *In:* AURAS, R., LIM, L.-T., SELKE, S. E. M. & TSUJI, H. (eds.) *Poly(lactic acid): Synthesis, Structures, Properties, Processing and Application.* Canada: John Wiley and Sons, Inc.

ANDERSON, K. S. & HILLMYER, M. A. 2004. The influence of block copolymer microstructure on the toughness of compatibilized polylactide/polyethylene blends. *Polymer,* 45**,** 8809-8823.

ANSYS. 2009. Verification Manual for the Mechanical APDL Application.

ANSYS 2012. Modelling creep behaviour in ANSYS Mechanical and Mechanical APD14.0.

ASHORI, A. 2008. Wood–plastic composites as promising green-composites for automotive industries! *Bioresource Technology,* 99**,** 4661–4667.

AURAS, R., HARTE, B. & SELKE, S. 2004a. Effect of water on the oxygen barrier properties of poly(ethylene terephthalate) and polylactide films. *Journal of Applied Polymer Science,* 92**,** 1790-1803.

AURAS, R., HARTE, B. & SELKE, S. 2004b. An overview of polylactides as packaging materials. *Macromolecular Bioscience,* 4**,** 835-864.

AURAS, R., HARTE, B. & SELKE, S. 2006a. Sorption of ethyl acetate and d-limonene in poly(lactide) polymers. *Journal of the Science of Food and Agriculture,* 86**,** 648-656.

AURAS, R., SINGH, S. P. & SINGH, J. 2006b. Performance evaluation of PLA against existing PET and PS containers. *Journal of Testing and Evaluation,* 34**,** 530-536.

AURAS, R. A., HARTE, B., SELKE, S. & HERNANDEZ, R. 2003. Mechanical, physical, and barrier properties of poly(lactide) films. *Journal of Plastic Film and Sheeting,* 19**,** 123-135.

AURAS, R. A., SINGH, S. P. & SINGH, J. J. 2005. Evaluation of oriented poly(lactide) polymers vs. existing PET and oriented PS for fresh food service containers. *Packaging Technology and Science,* 18**,** 207-216.

BALAKRISHNAN, H., HASSAN, A., IMRAN, M. & WAHIT, M. U. 2011. Aging of Toughened Polylactic Acid Nanocomposites: Water Absorption, Hygrothermal Degradation and Soil Burial Analysis. *Journal of Polymers and the Environment,* 19**,** 863-875.

BANDHYOPADHYA, A. & BOSE, S. 2013. *Characterization of Biomaterials,* Oxford, UK, Elsevier, Inc.

BANG, G. & KIM, S. W. 2012. Biodegradable poly(lactic acid)-based hybrid coating materials for food packaging films with gas barrier properties. *Journal of Industrial and Engineering Chemistry,* 18**,** 1063-1068.

BARRON, R. F. & BARRON, B. R. 2011. *Design for Thermal Stresses,* Canada, John Wiley & Sons, Inc.

BEIJER, J. G. J. & SPOORMAKER, J. L. 2002. Solution strategies for FEM analysis with nonlinear viscoelastic polymers. *Computers and Structures,* 80**,** 1213-1229.

BELLMANN, K., AND KHARE, A. 1999. European response to issues in recycling car plastics. *Technovation,* 19**,** 721–734.

BIOTEC. 2008. *Technical Information: Bioplast GS2189* [Online]. Biotec. Available: http://www.biotec.de/engl/products/bioplast%20gs2189_engl.pdf.

BRANNON-PEPPAS, L. 1995. Recent advances on the use of biodegradable microparticles and nanoparticles in controlled drug delivery. *International Journal of Pharmaceutics,* 116**,** 1-9.

BRAZEL, C. S. & ROSEN, S. L. 2012. *Fundamental Principles of Polymeric Materials,* Hoboke, New Jersey, USA, John Wiley & Sons.

BRYCE, D. M. 1996. *Plastic Injection Molding: Manufacturing Process Fundamentals,* Michigan, USA, Society of Manufacturing Engineers.

CABEDO, L., FEIJOO, J. L., VILLANUEVA, M. P., LAGARÓN, J. M. & GIMÉNEZ, E. 2006. Optimization of biodegradable nanocomposites based on aPLA/PCL blends for food packaging applications. *Macromolecular Symposia,* 233**,** 191-197.

CAI, X., HUANG, W., XU, B., KALTENPOTH, G. & CHENG, Z. 2002. A study of moisture diffusion in plastic packaging. *Journal of Electronic Materials,* 31**,** 449-455.

CAIRNCROSS, R. A., BECKER, J. G., RAMASWAMY, S. & O'CONNOR, R. 2006. Moisture sorption, transport, and hydrolytic degradation in polylactide. *Applied Biochemistry and Biotechnology,* 131**,** 774-785.

CALLISTER, W. D. & RETHWISCH, D. G. 2010. *Materials Science and Engineering: An Introduction,* Hoboken, NJ, John Wiley.

CARSLAW, H. S. & JAEGER, J. C. 1986. *Conduction of Heat in Solids* New York, Oxford University Press

CHALÉAT, C. M., MICHEL-AMADRY, G., HALLEY, P. J. & TRUSS, R. W. 2008. Properties of a plasticised starch blend - Part 2: Influence of strain rate, temperature and moisture on the tensile yield behaviour. *Carbohydrate Polymers,* 74**,** 366-371.

CHANDA, M. & ROY, S. K. 2009. *Plastic Fundamentals, Properties, and Testing,* Boca Raton, CRC Press.

CHEN, T. 2000. Determining a Prony series for a viscoelastic material from time varying strain data. Hampton, VA, USA: NASA Langley research center.

CHEN, X., ZHAO, S. & ZHAI, L. 2005. Moisture absorption and diffusion characterization of molding compound. *Journal of Electronic Packaging, Transactions of the ASME,* 127**,** 460-465.

CHIANG, M. Y. M. & MCKENNA, G. B. 1996. Hygrothermal Effects on the Performance of Polymers and Polymeric Composites. *Journal of Research of the National Institute of Standards and Technology,* 101.

COLOMINES, G., DUCRUET, V., COURGNEAU, Ć., GUINAULT, A. & DOMENEK, S. 2010. Barrier properties of poly(lactic acid) and its morphological changes induced by aroma compound sorption. *Polymer International,* 59**,** 818-826.

CONN, R. E. 1995. Safety assessment of polylactide (PLA) for use as a food-contact polymer. *Food and Chemical Toxicology,* 33**,** 273-283.

COPINET, A., BERTRAND, C., GOVINDIN, S., COMA, V. & COUTURIER, Y. 2004. Effects of ultraviolet light (315 nm), temperature and relative humidity on the degradation of polylactic acid plastic films. *Chemosphere,* 55**,** 763-773.

CORRELO, V. M., PINHO, E. D., PASHKULEVA, I., BHATTACHARYA, M., NEVES, N. M. & REIS, R. L. 2007. Water absorption and degradation characteristics of chitosan-based polyesters and hydroxyapatite composites. *Macromolecular Bioscience,* 7**,** 354-363.

COURGNEAU, C., DOMENEK, S., LEBOSSÉ, R., GUINAULT, A., AVÉROUS, L. & DUCRUET, V. 2012. Effect of crystallization on barrier properties of formulated polylactide. *Polymer International,* 61**,** 180-189.

CRANK, J. 1967. *The Mathematics of Diffusion,* Oxford, Oxford University Press.

CYRAS, V. P., MARTUCCI, J. F., IANNACE, S. & VAZQUEZ, A. 2002. Influence of the fiber content and the processing conditions on the flexural creep behavior of sisal-PCL-starch composites. *Journal of Thermoplastic Composite Materials,* 15**,** 253-265.

DAVIS, E. M., MINELLI, M., BASCHETTI, M. G., SARTI, G. C. & ELABD, Y. A. 2012. Nonequilibrium sorption of water in polylactide. *Macromolecules,* 45**,** 7486-7494.

DAVIS, E. M., THERYO, G., HILLMYER, M. A., CAIRNCROSS, R. A. & ELABD, Y. A. 2011. Liquid water transport in polylactide homo and graft copolymers. *ACS Applied Materials and Interfaces,* 3**,** 3997-4006.

DEMIREL, B. 2008. *Optimisation of Petaloid Base Dimensions and Process Operating Conditions to Minimise Environmental Stress Cracking In Injection Stretch Blow Moulded PET Bottles.* Doctor of Philosophy, RMIT University.

DEMIREL, B. & DAVER, F. 2009. Optimization of poly(ethylene terephthalate) bottles via numerical modeling: A statistical design of experiment approach. *Journal of Applied Polymer Science,* 114**,** 1126-1132.

DEMIREL, B. & DAVER, F. 2012. Effects of preform deformation behavior on the properties of the poly(ethylene terephthalate) bottles. *Journal of Applied Polymer Science,* 126**,** 1300-1306.

DITUDOMPO, S., TAKHAR, P. S., GANJYAL, G. M. & HANNA, M. A. 2013a. the effect of temperature and moisture on the mechanical properties of extruded cornstarch. *Journal of Texture Studies,* 44**,** 225-237.

DITUDOMPO, S., TAKHAR, P. S., GANJYAL, G. M. & HANNA, M. A. 2013b. The effect of temperature and moisture on the mechanical properties of extruded cornstarch. *Journal of Texture Studies*.

DMYTRÓW, I., SZCZEPANIK, G., KRYZA, K., MITUNIEWICZ-MAŁEK, A. & LISIECKI, S. 2011. Impact of polylactic acid packaging on the organoleptic and physicochemical properties of tvarog during storage. *International Journal of Dairy Technology,* 64**,** 569-577.

DOPICO-GARCÍA, M. S., ARES-PERNAS, A., GONZÁLEZ-RODRÍGUEZ, M. V., LÓPEZ-VILARIÑO, J. M. & ABAD-LÓPEZ, M. J. 2012. Commercial biodegradable material for food contact: Methodology for assessment of service life. *Polymer International,* 61**,** 1648-1654.

DROPIK, M. J., JOHNSON, D. H. & ROTH, D. E. 2002. Developing an ANSYS Creep Model for Polypropylene from Experimental Data *ANSYS Conference.*

DROZDOV, A. D. 1997. A model for the non-isothermal viscoelastic behavior of polymers. *Polymer Engineering and Science,* 37**,** 1983-1997.

DUNCAN, B., URQUHART, J. & ROBERTS, S. 2005. Review of Measurement and Modelling of Permeation and Diffusion in Polymers. Hampton Road, Teddington, Middlesex, UK: National Physical Laboratory.

DUSUNCELI, N. & COLAK, O. U. 2008. Modelling effects of degree of crystallinity on mechanical behavior of semicrystalline polymers. *International Journal of Plasticity,* 24**,** 1224-1242.

ENVIRONMENT_AUSTRALIA 2002. Biodegradable Plastics - Development and Environment Impacts. *In:* AUSTRALIA, E. (ed.). Melbourne.

ERBULUT, D. U., VASA, S., MASOOD, S. H. & DAVIES, K. Structural strength of blow moulded PET bottle using microwave pre-heated preforms. 2009 Annual Technical Conference 2009 Chicago, United States. Society of Plastic Engineers, 55-59.

FINDLEY, W. N., LAI, J. S. & ONARAN, K. 1976. *Creep and Relaxation of Nonlinear Viscoelastic Materials,* United States, Dover Publications.

FISH, J. & BELYTSCHKO, T. 2007. *A First Course in Finite Elements,* West Sussex, England, John Wiley and Sons.

FRÉMONT, H., DELÉTAGE, J. Y., PINTUS, A. & DANTO, Y. 2001. Evaluation of the moisture sensitivity of molding compounds of IC's packages. *Journal of Electronic Packaging, Transactions of the ASME,* 123**,** 16-18.

GALLOWAY, J. E. & MILES, B. M. 1997. Moisture absorption and desorption predictions for plastic ball grid array packages. *IEEE Transactions on Components Packaging and Manufacturing Technology Part A,* 20**,** 274-279.

GARLOTTA, D. 2001. A literature review of poly(lactic acid). *Journal of Polymers and the Environment,* 9**,** 63-84.

GEORGE, S. C. & THOMAS, S. 2001. Transport phenomena through polymeric systems. *Progress in Polymer Science (Oxford),* 26**,** 985-1017.

GIANNIS, S., ADAMS, R. D., CLARK, L. J. & TAYLOR, M. A. 2008. Investigation of the water and fuel exposure characteristics of aircraft fuel tank sealants and the effect on their glass transition temperature. *Journal of Applied Polymer Science,* 108**,** 3073-3091.

GIMBERT, S. 2008. *A Combined Empirical and Computational Approach to Creep in Replicas of Historic Mortar.* Master of Science, Pennsylvania State University.

GRIZZI, I., GARREAU, H., LI, S. & VERT, M. 1995. Hydrolytic degradation of devices based on poly(DL-lactic acid) size dependence. *Biomaterials,* 16**,** 305-311.

GUPTA, R., BALDEWA, B. & JOSHI, Y. M. 2012. Time temperature superposition in soft glassy materials. *Soft Matter,* 8**,** 4171-4176.

HABAS-ULLOA, A., D'ALMEIDA, J. R. M. & HABAS, J. P. 2010. Creep behavior of high density polyethylene after aging in contact with different oil derivates. *Polymer Engineering and Science,* 50**,** 2122-2130.

HADDAD, H., MASOOD, S. & ERBULUT, D. U. 2009. A study of blow moulding simulation and structural analysis for PET bottles. *Australian Journal of Mechanical Engineering,* 7**,** 69-76.

HARPER, C. A. 2002. Plastics in Packaging. *Handbook of Plastics, Elastomers, and Composites*

4th Ed ed. New York, USA: McGraw Hill Professional.

HARRIS, A. M. & LEE, E. C. 2008. Improving mechanical performance of injection molded PLA by controlling crystallinity. *Journal of Applied Polymer Science,* 107**,** 2246-2255.

HARRIS, A. M. & LEE, E. C. 2010. Heat and humidity performance of injection molded PLA for durable applications. *Journal of Applied Polymer Science,* 115**,** 1380-1389.

HARTE, B. R., GIACIN, J. R., IMAI, T., KONCZAL, J. B. & HOOJJAT, H. Effect of sorption of organic volatiles on the mechanical properties of sealant films. 1991. 18-30.

HATZIGRIGORIOU, N. B., VOUYIOUKA, S. N., JOLY, C., DOLE, P. & PAPASPYRIDES, C. D. 2012. Temperature-humidity superposition in diffusion phenomena through polyamidic materials. *Journal of Applied Polymer Science,* 125**,** 2814-2823.

HAUGAARD, V. K., WEBER, C. J., DANIELSEN, R. & BERTELSEN, G. 2002. Quality changes in orange juice packed in materials based on polylactate. *European Food Research and Technology,* 214**,** 423-428.

HENTON, D. E., GRUBER, P., LUNT, J. & RANDALL, J. 2005. Polylactic Acid Technology. *In:* MOHANTY, A. K., MISRA, M. & DRZAL, L. T. (eds.) *Natural Fibers, Biopolymers, and Their Biocomposites* London: CRC Press.

HERNANDEZ, R. J. 2002. Plastics in Packaging. *In:* HARPER, C. A. (ed.) *Handbook of plastics, elastomers, and composites.* United States of America: McGraw-Hill Professional.

HO, K. L. G., POMETTO III, A. L. & HINZ, P. N. 1999. Effects of temperature and relative humidity on polylactic acid plastic degradation. *Journal of Environmental Polymer Degradation,* 7**,** 83-92.

HOLM, V. K., NDONI, S. & RISBO, J. 2006. The stability of poly(lactic acid) packaging films as influenced by humidity and temperature. *Journal of Food Science,* 71**,** E40-E44.

HUANG, M., THOMPSON, V. P., REKOW, E. D. & SOBOYEJO, W. O. 2008. Modeling of water absorption induced cracks in resin-based composite supported ceramic layer structures. *Journal of Biomedical Materials Research - Part B Applied Biomaterials,* 84**,** 124-130.

IMAOKA, S. 2008. Analyzing viscoelastic materials. *ANSYS Advantage.* Canonsburg, P.A, USA: ANSYS Inc.

ISHISAKA, A. & KAWAGOE, M. 2004. Examination of the time-water content superposition on the dynamic viscoelasticity of moistened polyamide 6 and epoxy. *Journal of Applied Polymer Science,* 93**,** 560-567.

JAMSHIDIAN, M., TEHRANY, E. A., IMRAN, M., JACQUOT, M. & DESOBRY, S. 2010. Poly-Lactic Acid: Production, applications, nanocomposites, and release studies. *Comprehensive Reviews in Food Science and Food Safety,* 9**,** 552-571.

JARATROTKAMJORN, R., KHAOKONG, C. & TANRATTANAKUL, V. 2012. Toughness enhancement of poly(lactic acid) by melt blending with natural rubber. *Journal of Applied Polymer Science,* 124**,** 5027-5036.

JIA, M., XUE, P., ZHAO, Y. & WANG, K. 2009. Creep behaviour of wood flour/poly(vinyl chloride) composites. *Journal Wuhan University of Technology, Materials Science Edition,* 24**,** 440-447.

JIA, N., FRAENKEL, H. A. & KAGAN, V. A. 2004. Effects of moisture conditioning methods on mechanical properties of injection molded nylon 6. *Journal of Reinforced Plastics and Composites,* 23**,** 729-737.

JIANG, H., MA, X. S. & CHEN, N. Analysis and comparison of thermal stress and hygrothermal stress of SiP device by QFN packaging. International Conference on Electronic Packaging Technology and High Density Packaging, ICEPT-HDP, 2008.

KAJORNCHEAPPUNNGAM, S. 1999. *The Effects of Environmental Aging on the Durability of Glass/Epoxy Composites.* Doctor of Philosophy, West Virginia University.

KARAD, S. K. & JONES, F. R. 2005. Mechanisms of moisture absorption by cyanate ester modified epoxy resin matrices: The clustering of water molecules. *Polymer,* 46**,** 2732-2738.

KARALEKAS, D., RAPTI, D., PAPAKALIATAKIS, G. & TSARTOLIA, E. 2001. Numerical and experimental investigation of the deformational behaviour of plastic containers. *Packaging Technology and Science,* 14**,** 185-191.

KIM, H., LEE, B. & CHOI, S. 2011. Sustainable bio-composites for automotive interior parts. *18TH INTERNATIONAL CONFERENCE ON COMPOSITE MATERIALS.* Jeju island, Korea: Korean society for composite material.

KIM, H. K., KIM, S. J., LEE, H. S., CHOI, J. H., JEONG, C. M., SUNG, M. H., PARK, S. H. & PARK, H. J. 2013. Mechanical and barrier properties of poly(lactic acid) films coated by nanoclay-ink composition. *Journal of Applied Polymer Science,* 127**,** 3823-3829.

KIM, Y. F., CHOI, C. N., KIM, Y. D., LEE, K. Y. & LEE, M. S. 2004. Compatibilization of immiscible poly(l-lactide) and low density polyethylene blends. *Fibers and Polymers,* 5**,** 270-274.

KIMURA, K. & HORIKOSHI, Y. 2005. Bio-based polymers. *Fujitsu Scientific and Technical Journal,* 41**,** 173-180.

KNAUSS, W. G. & KENNER, V. H. 1980. On the hygrothermomechanical characterization of polyvinyl acetate. *Journal of Applied Physics,* 51**,** 5131-5136.

KOLYBABA, M., TABIL, L. G., PANIGRAHI, S., CRERAR, W. J., POWELL, T. & WANG, B. 2003. Biodegradable Polymers: Past, Present, and Future. *2003 CSAE/ASAE Annual Intersectional Meeting*. Fargo, North Dakota, USA: The Society for Engineering in Agricultural, Food and Biological Systems.

LEBLANC, N., SAIAH, R., BEUCHER, E., GATTIN, R., CASTANDET, M. & SAITER, J. M. 2008. Structural investigation and thermal stability of new extruded wheat flour based polymeric materials. *Carbohydrate Polymers,* 73**,** 548-557.

LEKATOU, A., FAIDI, S. E., GHIDAOUI, D., LYON, S. B. & NEWMAN, R. C. 1997. Effect of water and its activity on transport properties of glass/epoxy particulate composites. *Composites Part A: Applied Science and Manufacturing,* 28**,** 223-236.

LIN, Y. C. 2006. Investigation of the moisture-desorption characteristics of epoxy resin. *Journal of Polymer Research,* 13**,** 369-374.

LOH, W. K., CROCOMBE, A. D., WAHAB, M. M. A. & ASHCROFT, I. A. 2005. Modelling anomalous moisture uptake, swelling and thermal characteristics of a rubber toughened epoxy adhesive. *International Journal of Adhesion and Adhesives,* 25**,** 1-12.

LUDUEÑA, L., VÁZQUEZ, A. & ALVAREZ, V. 2012. Viscoelastic behavior of polycaprolactone/clay nanocomposites. *Journal of Composite Materials,* 46**,** 677-689.

MADHAVAN NAMPOOTHIRI, K., NAIR, N. R. & JOHN, R. P. 2010. An overview of the recent developments in polylactide (PLA) research. *Bioresource Technology,* 101**,** 8493-8501.

MARAIS, C. & VILLOUTREIX, G. 1998. Analysis and modeling of the creep behavior of the thermostable PMR-15 polyimide. *Journal of Applied Polymer Science,* 69**,** 1983-1991.

MARQUES, S. P. C. & CREUS, G. J. 2012. *Computational Viscoelasticity,* New York, Springer.

MARSH, G. 2003. Next step for automotive materials. *Materials Today,* 6**,** 36-43.

MARTIN, O. & AVÉROUS, L. 2001. Poly(lactic acid): Plasticization and properties of biodegradable multiphase systems. *Polymer,* 42**,** 6209-6219.

MASOOD, S. H., SATYANARAYANA, V. & ERBULUT, U. Design and development of large collapsible PET water cooler bottles. International Conference on Computer Graphics, Imaging and Visualisation, 26 - 28 July 2006 2006 Sydney; Australia. 528-533.

MATHWORKS 2013. Curve Fitting Toolbox. *User's Guide.* Natick, MA, USA: Mathworks.

MCCOURT, M. P., MC NALLY, G. M., ZHAN, B. & MURPHY, W. R. The performance of PVDF in fuel handling applications. Annual Technical Conference - ANTEC, 2006. SPE, 32-36.

MCCOURT, M. P., MC NALLY, G.M., MURPHY, W.R. A review of diffusion in automotive polymers. Annual Technical Conference - ANTEC, 2004. SPE, 3464-3468.

MCNABB, R., KEMP, M. & MCMAHON, S. 2002. *An Advanced Method for Optimizing Packaging Design* [Online]. Altair Engineering Ltd,. [Accessed June 2013.

MIRANDA, C. A. S. D., CÂMARA, J. J. D., MONKEN, O. P. & SANTOS, C. G. D. 2011. Design Optimization and Weight Reduction of 500 mL CSD PET Bottle through FEM Simulations. *Journal of Materials Science and Engineering B 1*, 947-959.

MIRANDA GUEDES, R., MORAIS, J. J. L., MARQUES, A. T. & CARDON, A. H. 2000. Prediction of long-term behaviour of composite materials. *Computers and Structures,* 76, 183-194.

MITSUBISHI, P. 2012. *Mitsubishi Plastics launches industry's first co-extruded multilayer film using plant-based plastics. Employed by Prima Meat Packers, Ltd. for packaging of its two new products* [Online]. Available: http://www.mpi.co.jp/english/news/201202150477.html.

MORLAND, L. W. & LEE, E. H. 1960. Stress analysis for linear viscoelastic materials with temperature variation. *Trans. Soc. Rheol.,* 4, 233-263.

MOUZAKIS, D. E. & KARGER-KOCSIS, J. 1998. Effects of gasoline absorption on the tensile impact response of HDPE/Selar™ laminar microlayer composites. *Journal of Applied Polymer Science,* 68, 561-569.

MULIANA, A. & RAJAGOPAL, K. R. 2012. On the response of viscoelastic biodegradable polymeric solids. *Mechanics Research Communications,* 39, 51-58.

MULIANA, A. H. & RAJAGOPAL, K. R. 2011. Changes in the response of viscoelastic solids to changes in their internal structure. *Acta Mechanica,* 217, 297-316.

MUTSUGA, M., KAWAMURA, Y. & TANAMOTO, K. 2008. Migration of lactic acid, lactide and oligomers from polylactide food-contact materials. *Food Additives and Contaminants - Part A Chemistry, Analysis, Control, Exposure and Risk Assessment,* 25, 1283-1290.

NAGA, N., YOSHIDA, Y., INUI, M., NOGUCHI, K. & MURASE, S. 2011. Crystallization of amorphous poly(lactic acid) induced by organic solvents. *Journal of Applied Polymer Science,* 119, 2058-2064.

NAJAFI, S. K., SHARIFNIA, H. & TAJVIDI, M. 2008. Effects of water absorption on creep behavior of wood-plastic composites. *Journal of Composite Materials,* 42, 993-1002.

NATUREWORKS. *Technical data sheet: Ingeo™ Biopolymer 7001D:* [Online]. NatureWorks LLC. 2012].

NATUREWORKS. 2011. *Evaluation of Jojoba Oil in Ingeo Bottles* [Online]. NatureWorks LLC. Available: http://www.natureworksllc.com/~/media/Technical_Resources/Fact_Sheets/Fact Sheet_Evaluation-of-Jojobo-Oil-in-Ingeo-Bottles_pdf.pdf.

NATUREWORKS. 2103. *Product and applications* [Online]. Available: http://www.natureworksllc.com/Product-and-Applications.

NEC. 2006. *NEC & UNITIKA Realize Bioplastic Reinforced with Kenaf Fiber for Mobile Phone Use* [Online]. Japan: NEC Corporation. [Accessed 19 July 2011].

NEOGI, P. 1996. Transport phenomena in Polymer Membranes. *In:* NEOGI, P. (ed.) *Diffusion in Polymer* New York USA: Marcel Dekker Inc. .

NIAOUNAKIS, M., KONTOU, E. & XANTHIS, M. 2011. Effects of aging on the thermomechanical properties of poly(lactic acid). *Journal of Applied Polymer Science,* 119**,** 472-481.

NODA, N., HETNARSKI, R. B. & TANIGAWA, Y. 2003. *Thermal Stresses,* New York, Taylor & Francis.

NUNEZ, A. J., MARCOVICH, N. E. & ARANGUREN, M. I. 2004. Analysis of the creep behavior of polypropylene-woodflour composites. *Polymer Engineering and Science,* 44**,** 1594-1603.

O.BERK. 2012. *Plastic Bottle Paneling: 5 Causes and The Cures* [Online]. New Jersey, USA: O.Berk.

OBUCHI, S. & OGAWA, S. 2011. Packaging and other commercial application. *In:* AURAS, R. A., LIM, L.-T., SELKE, S. E. M. & TSUJI, H. (eds.) *Poly(Lactic Acid) : Synthesis, Structures, Properties, Processing, and Applications.* Hoboken, New Jersey: John Wiley and Sons.

OLIVEIRA, N. S., GONÇALVES, C. M., COUTINHO, J. A. P., FERREIRA, A., DORGAN, J. & MARRUCHO, I. M. 2006. Carbon dioxide, ethylene and water vapor sorption in poly(lactic acid). *Fluid Phase Equilibria,* 250**,** 116-124.

ONOGI, S., SASAGURI, K., ADACHI, T. & OGIHARA, S. 1962. Time-Humidity Superposition in Some Crystalline Polymers *JOURNAL OF POLYMER SCIENCE,* 58**,** 1-17.

OZA, A., VANDERBY JR, R. & LAKES, R. S. 2003. Interrelation of creep and relaxation for nonlinearly viscoelastic materials: Application to ligament and metal. *Rheologica Acta,* 42**,** 557-568.

PAPANICOLAOU, G. C., XEPAPADAKI, A. G. & ZAROUCHAS, D. S. 2009. Effect of water uptake on creep behaviour of glass-epoxy composites. *Plastics, Rubber and Composites,* 38**,** 72-79.

PARK, B. D. & BALATINECZ, J. J. 1998. Short term flexural creep behavior of wood-fiber/polypropylene composites. *Polymer Composites,* 19**,** 377-382.

PARK, S. H., LEE, H. S., CHOI, J. H., JEONG, C. M., SUNG, M. H. & PARK, H. J. 2012. Improvements in barrier properties of poly(lactic acid) films coated with chitosan or chitosan/clay nanocomposite. *Journal of Applied Polymer Science,* 125**,** E675-E680.

PATANKAR, K. A., DILLARD, D. A., CASE, S. W., ELLIS, M. W., LAI, Y. H. & GITTLEMAN, C. S. 2012. Linear hygrothermal viscoelastic characterization of nafion NRE 211 proton exchange membrane. *Fuel Cells,* 12**,** 787-799.

PATERSON, M. W. A. & WHITE, J. R. 1992. Effect of water absorption on residual stresses in injection-moulded nylon 6,6. *Journal of Materials Science,* 27**,** 6229-6240.

PCIA. 2007. *Submission to the Development of a National Waste Policy* [Online]. Plastics and Chemicals Industries Association. Available: http://www.environment.gov.au/wastepolicy/consultation/submissions/pubs/131-pacia.pdf 2012].

PEREGO, G., CELLA, G. D. & BASTIOLI, C. 1996. Effect of molecular weight and crystallinity on poly(lactic acid) mechanical properties. *Journal of Applied Polymer Science,* 59**,** 37-43.

PÉREZ, C. J., ALVAREZ, V. A. & VÁZQUEZ, A. 2008. Creep behaviour of layered silicate/starch-polycaprolactone blends nanocomposites. *Materials Science and Engineering A,* 480**,** 259-265.

PETERSEN, K., NIELSEN, P. V. & OLSEN, M. B. 2001. Physical and mechanical properties of biobased materials - Starch, polylactate and polyhydroxybutyrate. *Starch/Staerke,* 53**,** 356-361.

PINTO, A. M., CABRAL, J., TANAKA, D. A. P., MENDES, A. M. & MAGALHÃES, F. D. 2013. Effect of incorporation of graphene oxide and graphene nanoplatelets on mechanical and gas permeability properties of poly(lactic acid) films. *Polymer International,* 62**,** 33-40.

PLUTA, M., GALESKI, A., ALEXANDRE, M., PAUL, M. A. & DUBOIS, P. 2002. Polylactide/montmorillonite nanocomposites and microcomposites prepared by melt blending: Structure and some physical properties. *Journal of Applied Polymer Science,* 86**,** 1497-1506.

PRAMANICK, A. & SAIN, M. 2006. Temperature-stress equivalency in nonlinear viscoelastic creep characterization of thermoplastic/agro-fiber composites. *Journal of Thermoplastic Composite Materials,* 19**,** 35-60.

RANADE, A., NAYAK, K., FAIRBROTHER, D. & D'SOUZA, N. A. 2005. Maleated and non-maleated polyethylene-montmorillonite layered silicate blown films: Creep, dispersion and crystallinity. *Polymer,* 46**,** 7323-7333.

RAO, N. S. & SCHUMACHER, G. 2004. *Design Formulas For Plastics Engineers,* Ohio, USA, Hanser Gardner Publications, Inc.

RAY, S. S., YAMADA, K., OGAMI, A., OKAMOTO, M. & UEDA, K. 2002. New polylactide/layered silicate nanocomposite: Nanoscale control over multiple properties. *Macromolecular Rapid Communications,* 23**,** 943-947.

ROARK, R. J., YOUNG, W. & BUDYNAS, R. 2002. *Roark's Formulas for Stress and Strain,* New York, USA, McGraw-Hill

ROBERTS-TOMPKINS, A. L. 2009. *Viscoelastic Analysis of Sandwich Beams Having Aluminum And Fiber-Reinforced Polymer Skins With A Polystyrene Foam Core.* MASTER OF SCIENCE, Texas A&M University.

ROBERTSON, N. & METWALLY, H. 2013. Virtual prototyping in the manufacture and design of plastic packaging. ANSYS, Inc.

ROY, S. 1999. Modeling of anomalous moisture diffusion in polymer composites: a finite element approach. *Journal of Composite Materials,* 33**,** 1318-1343.

SAE 2005. *SAE J1748: SAE Handbook,* Warrendale USA, Society of Automotive Engineers, Inc.

SAEIDLOU, S., HUNEAULT, M. A., LI, H. & PARK, C. B. 2012. Poly(lactic acid) crystallization. *Progress in Polymer Science,* 37**,** 1657-1677.

SAJILATA, M. G., SAVITHA, K., SINGHAL, R. S. & KANETKAR, V. R. 2007. Scalping of flavors in packaged foods. *Comprehensive Reviews in Food Science and Food Safety,* 6**,** 17-35.

SALAZAR, R., DOMENEK, S., COURGNEAU, C. & DUCRUET, V. 2012. Plasticization of poly(lactide) by sorption of volatile organic compounds at low concentration. *Polymer Degradation and Stability,* 97**,** 1871-1880.

SALVADOR, M. D. A., V. ; VIDAL, M.J. ; RIBES, A. AND CONTAT, L. 2003. Evaluation of chemical degradation of commercial polypropylene. *Journal of Materials Processing Technology,* 143–144**,** 693–697.

SANGERLAUB, S., PANT, A., HUBER, C. & MULLER, K. Alternative Testing Methods for Oxygen and Water Vapour Permeability. 14th TAPPI European PLACE Conference 2013, 2013 Dresden. TAPPI.

SANGWAN, P., WAY, C. & WU, D. Y. 2009. New insight into biodegradation of polylactide (PLA)/clay nanocomposites using molecular ecological techniques. *Macromolecular Bioscience,* 9**,** 677-686.

SCAFFARO, R., TZANKOVA DINTCHEVA, N. & LA MANTIA, F. P. 2008. A new equipment to measure the combined effects of humidity, temperature, mechanical stress and UV exposure on the creep behaviour of polymers. *Polymer Testing,* 27**,** 49-54.

SEN, A., BHATTACHARYA, M., STELSON, K. A. & VOLLER, V. R. 2002. Creep in injection molded starch/synthetic polymer blends. *Materials Science and Engineering A,* 338**,** 60-69.

SEPE, M. P. 1997. *Thermal analysis of polymers*, Rapra Technology Limited.

SHAH, S., MULIANA, A. & RAJAGOPAL, K. R. 2009. Coupled heat conduction and deformation in a viscoelastic composite cylinder. *Mechanics of Time-Dependent Materials,* 13**,** 121-147.

SHARP, J. S., FORREST, J. A. & JONES, R. A. L. 2001. Swelling of poly(DL-lactide) and polylactide-co-glycolide in humid environments. *Macromolecules,* 34**,** 8752-8760.

SHENG, X., AKINC, M. & KESSLER, M. R. 2010. Creep behavior of bisphenol E cyanate ester/alumina nanocomposites. *Materials Science and Engineering A,* 527**,** 5892-5899.

SHIGLEY, J. E., MISCHKE, C. R. & BUDYNAS, R. G. 2004. *Mechanical Engineering Design,* New York, USA, McGraw-Hill Professional.

SHIRANGI, M. H. & MICHEL, B. 2010. Mechanism of moisture diffusion, hygroscopic swelling and adhesion degradation in epoxy molding compounds. *In:* FAN, X. J. & SUHIR, E. (eds.) *Moisture sensitivity of plastic packages of IC devices.* Springer Science+Business Media.

SHOGREN, R. 1997. Water vapor permeability of biodegradable polymers. *Journal of Environmental Polymer Degradation,* 5**,** 91-95.

SIN, L. T., RAHMAT, A. R. & RAHMAN, W. A. W. A. 2012. *Mechanical properties of poly(lactic) acid,* Waltham, MA, USA, Elsevier Inc.

SINGH, B. & SHARMA, N. 2008. Mechanistic implications of plastic degradation. *Polymer Degradation and Stability,* 93**,** 561-584.

SINGH, V. M. 2008. *Synthesis of Polylactide with Varying Molecular Weight and Aliphatic Content: Effect on Moisture Sorption* Master of Science, Drexel University

SINHA RAY, S., YAMADA, K., OKAMOTO, M., OGAMI, A. & UEDA, K. 2003. New polylactide/layered silicate nanocomposites. 3. High-performance biodegradable materials. *Chemistry of Materials,* 15**,** 1456-1465.

SIRACUSA, V., BLANCO, I., ROMANI, S., TYLEWICZ, U., ROCCULI, P. & ROSA, M. D. 2012. Poly(lactic acid)-modified films for food packaging application: Physical, mechanical, and barrier behavior. *Journal of Applied Polymer Science,* 125**,** E390-E401.

SOMIYA, S., LEE, Y. & SAKAI, T. Time-temperature and humidity superposition principle on creep of PBS. Society for Experimental Mechanics -11th International Congress and Exhibition on Experimental and Applied Mechanics 2008 Orlando, Florida USA. Society for Experimental Mechanics Inc., 957-963.

SPRINGER, G. S. 1988. Environmental Effects. *In:* TSAI, S. W. (ed.) *Composites Design.* 4th ed. Dayton, Ohio: Think Composites.

STOUFFER, D. C. & WINEMAN, A. S. 1971. Linear viscoelastic materials with environmental dependent properties. *International Journal of Engineering Science,* 9**,** 193-212.

SUN, H., COOKE, R. S., BATES, W. D. & WYNNE, K. J. 2005. Supercritical CO2 processing and annealing of polytetrafluoroethylene (PTFE) and modified PTFE for enhancement of crystallinity and creep resistance. *Polymer,* 46**,** 8872-8882.

TAIB, R. M., GHALEB, Z. A. & MOHD ISHAK, Z. A. 2012. Thermal, mechanical, and morphological properties of polylactic acid toughened with an impact modifier. *Journal of Applied Polymer Science,* 123**,** 2715-2725.

TANG, X. G., HOU, M., ZOU, J., TRUSS, R. & ZHU, Z. 2012. The creep behaviour of poly(vinylidene fluoride)/"bud-branched" nanotubes nanocomposites. *Composites Science and Technology,* 72**,** 1656-1664.

TOMOPOLUOS, S. & GENIN, G. M. 2013. Tendon and Ligament Biomechanics. *In:* WINKELSTEIN, B. A. (ed.) *Orthopaedic Biomechanics.* Boca Raton, FL, USA: CRC Press Taylor and Francis Group.

TOUNSI, A., ADDA-BEDIA, E., SEREI, Z. & BENHASSAÏNI, H. 2003. Effect of fiber orientation and cyclic environmental conditions on the non-mechanical residual stresses in resin matrix composite panels. *Arabian Journal for Science and Engineering,* 28**,** 23-43.

TSCHOEGL, N. W. 1989. *The Phenomenological Theory of Linear Viscoelastic Behavior: An Introduction*, Springer-Verlag.

TSUJI, H. 2010. Hydrolytic degradation. *In:* RAFAEL A. AURAS, L.-T. L., SUSAN E. M. SELKE, HIDETO TSUJI (ed.) *Poly(lactic acid): Synthesis, Structures, Properties, Processing, and Applications.* Canada: John Wiley & Sons.

UGURAL, A. C. 2009. *Stresses in Beams, Plates and Shells,* Boca Raton, FL, USA, Taylor and Francis.

VAIDYA, A. N., PANDEY, R. A., MUDLIAR, S., KUMAR, M. S., CHAKRABARTI, T. & DEVOTTA, S. 2005. Production and recovery of lactic acid for polylactide - An overview. *Critical Reviews in Environmental Science and Technology,* 35**,** 429-467.

VAIDYA, R. 2012. *Structural Analysis of Poly Ethylene Terephthalate Bottles Using Finite Element Method.* MASTER OF SCIENCE, Oklahoma State University.

VAN AARDT, M., DUNCAN, S. E., MARCY, J. E., LONG, T. E., O'KEEFE, S. F. & SIMS, S. R. 2007. Release of antioxidants from poly(lactide-co-glycolide) films into dry milk products and food simulating liquids. *International Journal of Food Science and Technology,* 42**,** 1327-1337.

VAN DIJK, R., STERK, J. C., SGORBANI, D. & VAN KEULEN, F. 1998. Lateral Deformation of Plastic Bottles: Experiments, Simulations and Prevention. *Packaging Technology and Science,* 11**,** 91-117.

WANG, Y., CHIAO, S. M., HUNG, T. F. & YANG, S. Y. 2012. Improvement in toughness and heat resistance of poly(lactic acid)/polycarbonate blend through twin-screw blending: Influence of compatibilizer type. *Journal of Applied Polymer Science,* 125**,** E402-E412.

WEITSMAN, Y. J. 2012. *Fluid Effects in Polymers and Polymeric Composites,* New York, USA, Springer.

WELLE, F. Sorption and Migration Behavior of Polylactic Acid (PLA) Bottles in Comparison to PET Bottles. 4th International Symposium on Food Packaging, 2008 Prague. Fraunhofer Institute for Process Engineering and Packaging.

WILLIGE, R. W. G. V. 2002. *Effects of flavour absorption on foods and their packaging materials.* Doctor of Philosophy, Wageningen University

WINEMAN, A. S. & RAJAGOPAL, K. R. 2000. *Mechanical Response of Polymers: an Introduction,* New York, USA, Cambridge University Press.

WU, C. S. & LIAO, H. T. 2007. Study on the preparation and characterization of biodegradable polylactide/multi-walled carbon nanotubes nanocomposites. *Polymer,* 48**,** 4449-4458.

WU, L., YOU, B., LI, D. & QIAN, F. 2000. Effect of hydration on the mechanical properties, composition and molecular weight of polyurethaneureas. *Polymer International,* 49**,** 1609-1614.

XU, Y., WU, Q., LEI, Y. & YAO, F. 2010. Creep behavior of bagasse fiber reinforced polymer composites. *Bioresource Technology,* 101**,** 3280-3286.

YOUNG, R. J. & LOVELL, P. A. 2011. *Introduction to Polymers,* Boca Rotan, FL, USA, CRC Press. Taylor & Francis Group.

ZAKI, O., ABBÈS, B. & SAFA, L. 2009. Non-Fickian diffusion of amyl acetate in polypropylene packaging: Experiments and modelling. *Polymer Testing,* 28**,** 315-323.

ZHANG, C. & WANG, J. 2012. Interface stress redistribution in FRP-strengthened reinforced concrete beams using a three-parameter viscoelastic foundation model. *Composites Part B: Engineering,* 43**,** 3009-3019.

ZHANG, G., ZHANG, J., WANG, S. & SHEN, D. 2002. Miscibility and phase structure of binary blends of polylactide and poly(methyl methacrylate). *Journal of Polymer Science, Part B: Polymer Physics,* 41**,** 23-30.

ZHENG, Y. & MCKENNA, G. B. 2003. Structural recovery in a model epoxy: Comparison of responses after temperature and relative humidity jumps. *Macromolecules,* 36**,** 2387-2396.

ZHENG, Y., PRIESTLEY, R. D. & MCKENNA, G. B. 2004. Physical aging of an epoxy subsequent to relative humidity jumps through the glass concentration. *Journal of Polymer Science, Part B: Polymer Physics,* 42**,** 2107-2121.

ZHOU, J., LAHOTI, S. P., SITLANI, M. P., KALLOLIMATH, S. C. & PUTTA, R. Investigation of non-uniform moisture distribution on determination of hygroscopic swelling coefficient and finite element modeling for a flip chip package. The 6th International Conference on Thermal, Mechanical and Multi-Physics Simulation and Experiments in Micro-Electronics and Micro-Systems - EuroSimE, 2005. 112-119.

ZHOU, S. M. & TASHIRO, K. 2001. Confirmation of universality of time-humidity superposition principle for various water-absorbable polymers through dynamic viscoelastic measurements under controlled conditions of relative humidity and temperature. *Journal of Polymer Science, Part B: Polymer Physics,* 39**,** 1638-1650.

List of publications

1. I. Widiastuti, I. Sbarski, and S.H. Masood. 2014. **Mechanical Response of PLA-Based Packaging under Liquid Exposure**. Accepted for Publication in *The Journal of Applied Polymer Science*.

2. I. Widiastuti, I. Sbarski, and S.H. Masood. 2014. **Mechanical Behavior of a Fluid-sensitive Material during Liquid Diffusion**. *Mechanics of Time-Dependent Materials*. Online Ed. DOI 10.1007/s11043-014-9233-9

3. I. Widiastuti, I. Sbarski, and S.H. Masood. 2012. **Creep behaviour of PLA-based biodegradable plastic exposed to a hydrocarbon liquid**. *Journal of Applied Polymer Science* . Volume 127, Issue 4, pp. 2654-2660

4. I. Widiastuti, I. Sbarski, and S.H. Masood. 2012. **Modelling of hygroscopic stresses due to non-uniform liquid distribution in homogeneous bioplastics**. *Conference Proceedings* 1, pp. 192-197. Annual Technical Conference - ANTEC, New Orlando, F.L, Society of Plastic Engineers

5. I. Widiastuti, I. Sbarski, and S.H. Masood. 2011. **Gasoline absorption and mechanical characteristics of biodegradable polymer in automotive application**. *Conference Proceedings* 3, pp. 2120-2125. Annual Technical Conference - ANTEC, Boston, MA, Society of Plastic Engineers

Appendix A

Result of Melt Flow Index Measurement

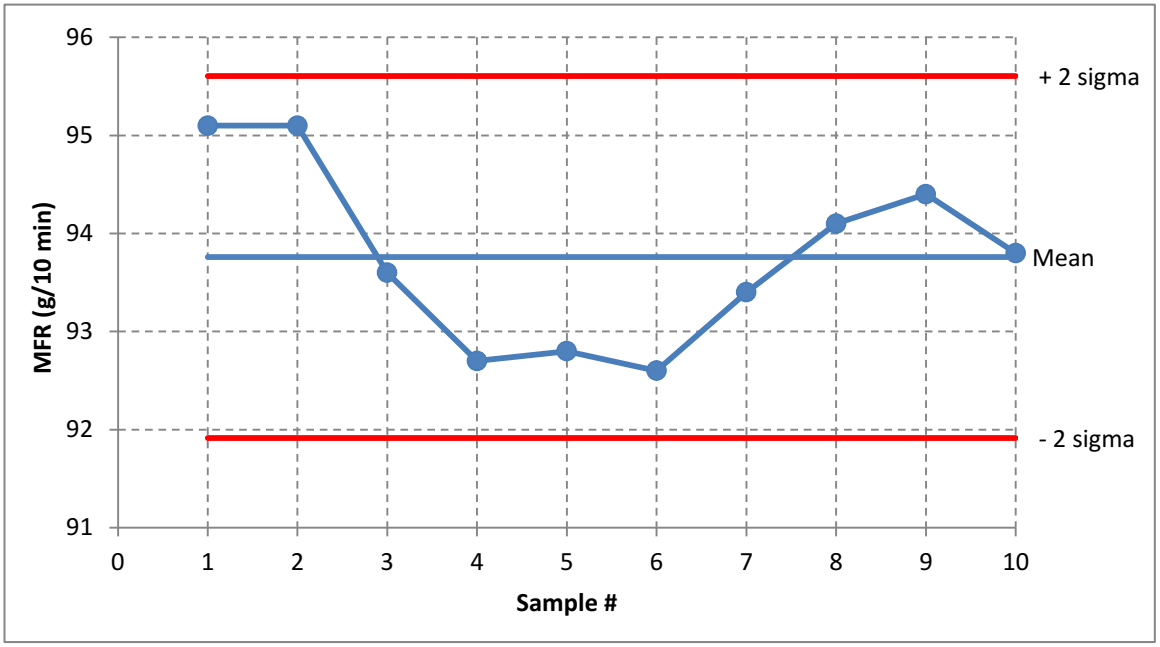

Figure A-1: Melt flow rates of the sample in gram per 10 minutes from ten measurements

Melt flow measurement

Measurement Device	: Melt Flow Modular – CEAST
Test condition	: ISO 1133 D
Temperature	: 190.0°C
Nominal load	: 2.160 kg
Die Length	: 8.00 mm
Die Diameter	: 2.095 mm
Preheating Without Load	: 240.00 s
Measure Start	: 46.00 mm
Measure Length	: 30.00 mm
Step Length	: 1.50 mm

Appendix B

Tabulated Results of Mechanical Performances

Table B-1: The tensile properties of the samples with various levels of liquid content

Dry (0%)				
Sample	Emod (GPa)	Max stress (MPa)	Strain at max (%)	Strain at break (%)
1	1.54	35.4	2.7	2.8
2	1.55	33.8	2.6	3.00
3	1.44	33.1	2.6	3.00
4	1.44	35.2	2.6	3.6
5	1.50	35.2	2.8	3.2
Average	**1.494**	**34.54**	**2.66**	**3.12**
SD	0.0527	1.0286	0.0894	0.3033
5°C immersion (1.9%)				
Sample	Emod (GPa)	Max stress (MPa)	Strain at max (%)	Strain at break (%)
1	1.14	20.5	2.2	2.2
2	1.06	26.7	3.3	5.9
3	1.04	24.6	2.8	2.80
Average	**1.08**	**23.93**	**2.77**	**3.63**
SD	0.0529	3.1533	0.5508	1.9858
20°C immersion (2.91%)				
Sample	Emod (GPa)	Max stress (MPa)	Strain at max (%)	Strain at break (%)
1	1.01	22.5	3.1	3.3
2	0.946	23.6	2.7	3.1
3	0.966	25	3	5.90
Average	**0.974**	**23.7**	**2.93**	**4.10**
SD	0.0327	1.2530	0.2082	1.5620
30°C immersion (5.95%)				
Sample	Emod (GPa)	Max stress (MPa)	Strain at max (%)	Strain at break (%)
1	0.449	12.1	4.7	5
2	0.492	12.5	4.3	4.90
3	0.479	11.7	3.5	3.90
4	0.456	16.1	9.6	11.60
5	0.36	13.8	9.2	11.30
Average	**0.4472**	**13.24**	**6.26**	**7.34**
SD	0.0517	1.7827	2.9022	3.7780

Table B-2: The flexural properties of the samples with various levels of liquid content

Dry BP				
Sample	Emod (GPa)	Max stress (MPa)	Strain at max (%)	Strain at break (%)
1	1.98	41.9	2.6	3.00
2	2.01	33.3	1.9	2.00
3	2.21	38.3	2.2	2.3
4	2.22	42.9	2.5	2.6
5	2.10	34.5	1.7	2
Average	**2.104**	**38.18**	**2.18**	**2.38**
SD	0.1106	4.2863	0.3834	0.4266
5°C immersion (1.9%)				
Sample	Emod (GPa)	Max stress (MPa)	Strain at max (%)	Strain at break (%)
1	1.08	27.6	7	8.8
2	1.18	24.3	4.9	5
3	1.02	24.4	6.2	7.00
Average	**1.09**	**25.43**	**6.03**	**6.93**
SD	0.0808	1.8974	1.0599	1.9009
20°C immersion (2.91%)				
Sample	Emod (GPa)	Max stress (MPa)	Strain at max (%)	Strain at break (%)
1	0.9	21.6	3.7	
2	0.938	18.7	6.3	10.1
3	0.849	20	7	11.10
Average	**0.895667**	**20.1**	**5.67**	**10.60**
SD	0.0447	1.4526	1.7388	0.7071
30°C immersion (5.95%)				
Sample	Emod (GPa)	Max stress (MPa)	Strain at max (%)	Strain at break (%)
1	0.411	18	9	12.30
2	0.446	19.1	13.3	14.30
3	0.438	18.2	9.6	13.40
Average	**0.431667**	**18.1**	**10.63**	**13.33**
SD	0.0183	0.1	2.3288	1.0017

Table B-3: The impact properties of the samples with various levels of liquid content

Dry						
Sample	Energy measured (J)	Width (mm)	Thickness (mm)	Izod Impact Strength (kJ/m^2)	Izod Impact Strength (J/m)	Mode
1	0.052	10.03	3.1	1.672	5.184	C
2	0.056	10.01	3.07	1.822	5.594	C
3	0.05	10.03	3.04	1.640	4.985	C
4	0.048	10.02	3.1	1.545	4.790	C
5	0.052	10.02	3.08	1.685	5.190	C
Average	0.0516			1.673	5.149	
SD	0.0030			0.100	0.299	
5°C immersion (1.9%)						
Sample	Energy measured (J)	Width (mm)	Thickness (mm)	Izod Impact Strength (kJ/m^2)	Izod Impact Strength (J/m)	Mode
1	0.082	10.08	3.09	2.633	8.135	C
2	0.071	10.05	3.14	2.250	7.065	C
3	0.065	10.05	3.05	2.121	6.468	C
Average	0.0860			2.334	7.222	
SD	0.0035			0.266	0.845	
20°C immersion (2.91%)						
Sample	Energy measured (J)	Width (mm)	Thickness (mm)	Izod Impact Strength (kJ/m^2)	Izod Impact Strength (J/m)	Mode
1	0.082	10.16	3.11	2.595	8.071	C
2	0.088	10.11	3.12	2.790	8.704	C
3	0.088	10.15	3.12	2.779	8.670	C
Average	0.0727			2.721	8.482	
SD	0.0086			0.109	0.356	
30°C immersion (5.95%)						
Sample	Energy measured (J)	Width (mm)	Thickness (mm)	Izod Impact Strength (kJ/m^2)	Izod Impact Strength (J/m)	Mode
1	0.068	10.48	3.28	1.978	6.489	C
2	0.07	10.17	3.24	2.124	6.883	C
3	0.068	10.09	3.25	2.074	6.739	C
Average	0.06867			2.059	6.704	
SD	0.0012			0.103	0.279	

C = Complete break, H = Hinge break

Appendix C

Curve Fitting of Creep Curves using MatLab

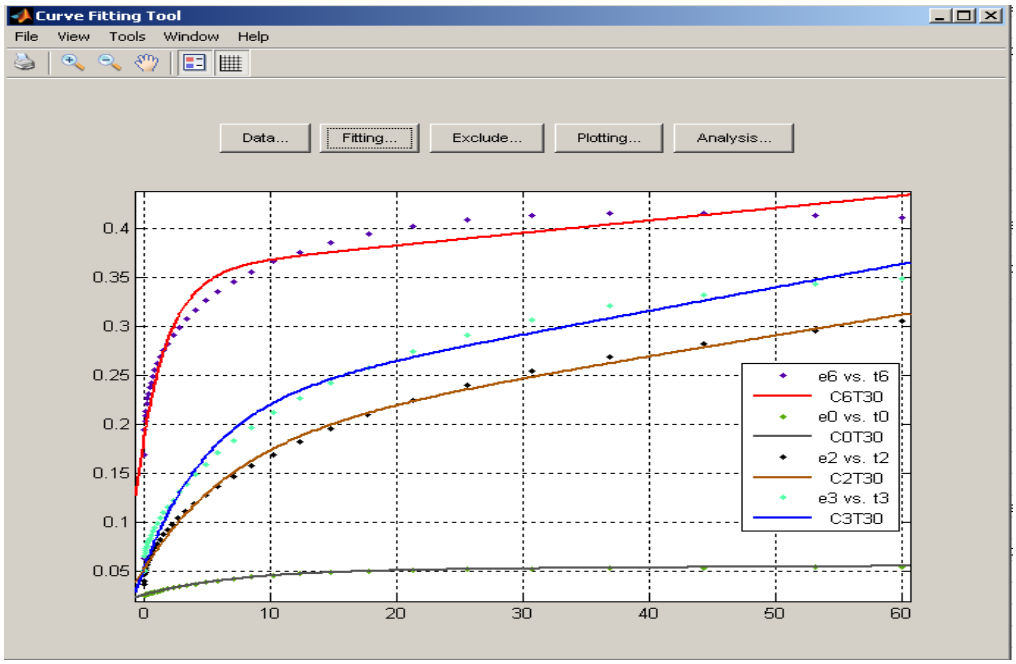

Figure C-1: Curve fitting of the creep curves for the specimens conditioned at T = 30 ℃

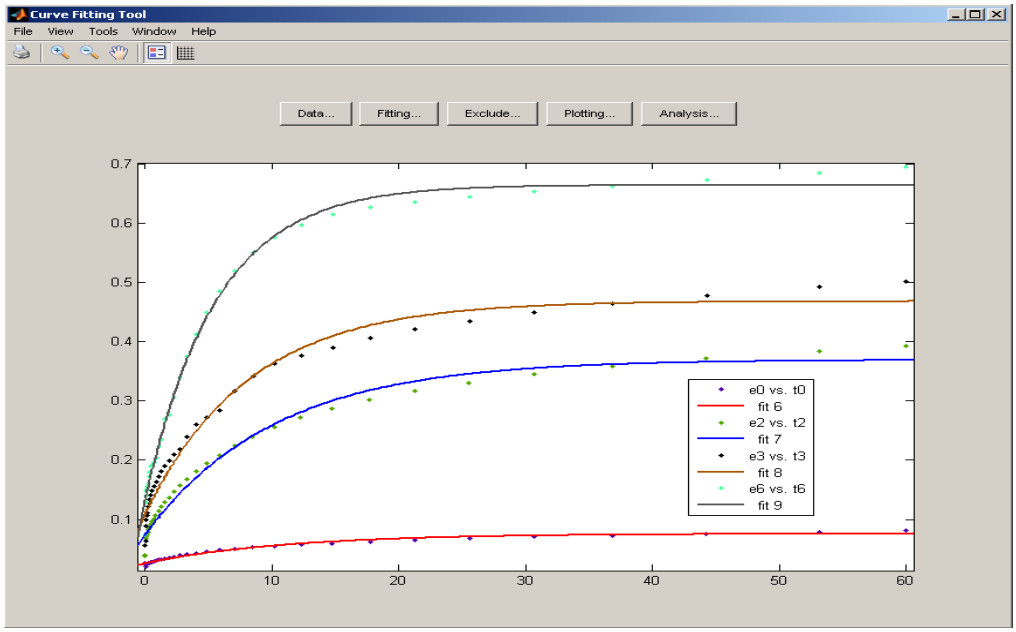

Figure C-2: Curve fitting of the creep curves for the specimens conditioned at T = 35 ℃

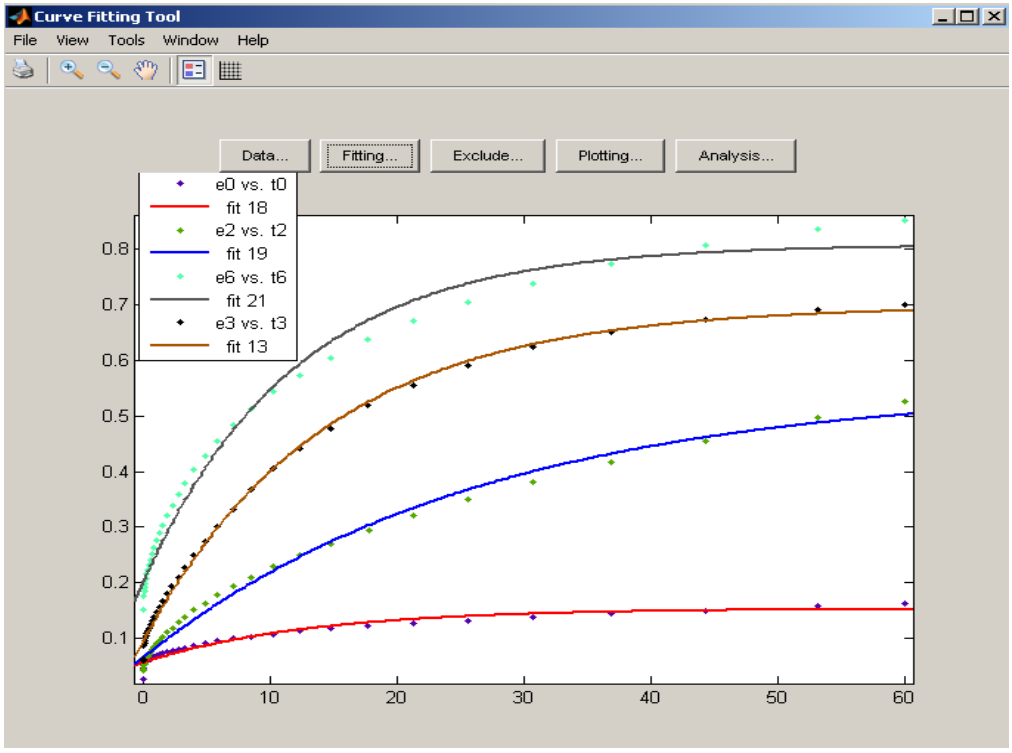

Figure C-3: Curve fitting of the creep curves for the specimens conditioned at T = 40 ℃

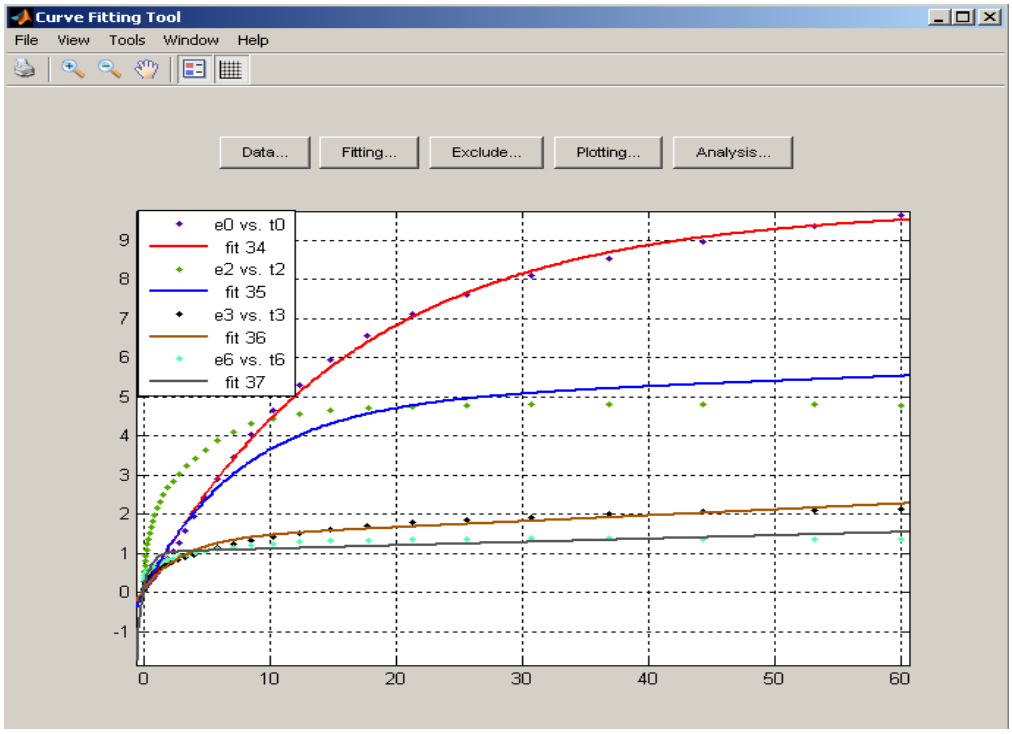

Figure C-4: Curve fitting of the creep curves for the specimens conditioned at T = 50 ℃

Appendix D

Curves of Time-Liquid Content Superposition

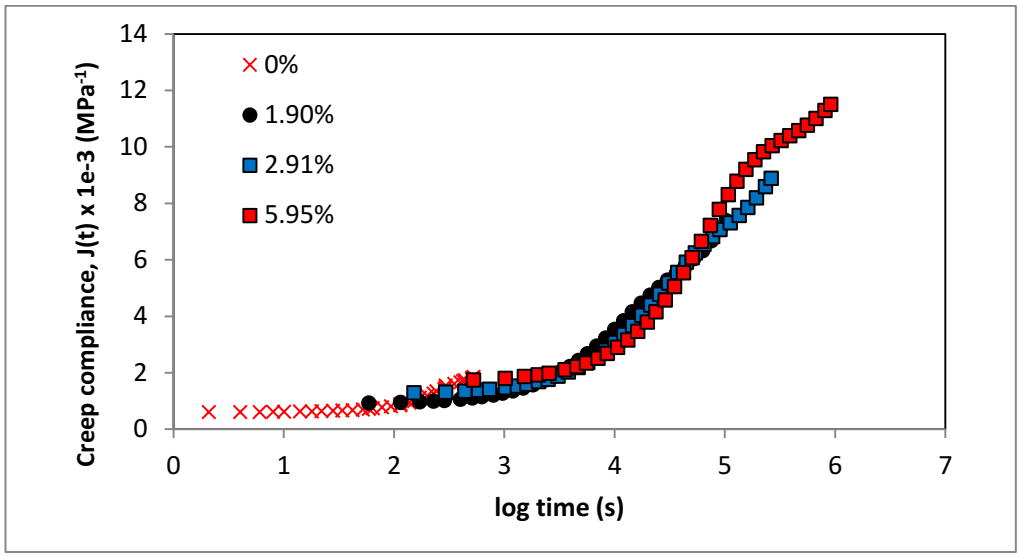

Figure D-1: Curve of time-liquid content superposition for the specimens conditioned at T = 35 ℃

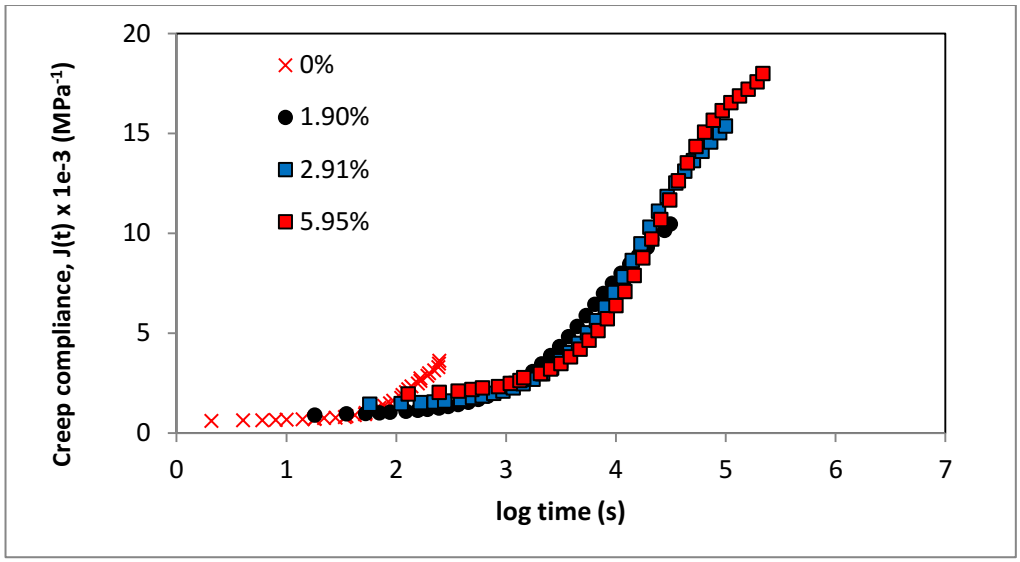

Figure D-2: Curve of time-liquid content superposition for the specimens conditioned at T = 40 ℃

Appendix E

Command Input for FEA software

1) Input listing for diffusion problem

```
/PREP7
ANTYPE,TRANS
ET,1,SOLID5
MP,KXX,1,0.00397
MP,DENS,1,1
MP,C,1,1
K,1,0,0,0
K,2,1,0,0
KGEN,2,1,2,1,,,0.25
KGEN,2,1,4,1,0,0.25,0
L,1,2
*REPEAT,4,2,2
LESIZE,ALL,,,10,1
ESIZE,,1
V,1,2,4,3,5,6,8,7
MSHK,1
MSHA,0,3D
VMESH,1
FINISH
/SOLU
OUTRES,,ALL
TIME,300
DELTIM,1,,10
TREF,0
TUNIF,0
NSEL,S,LOC,X,1
D,ALL,TEMP,2.91
NSEL,ALL
KBC,1
AUTOTS,ON
SOLVE
FINISH
/POST26
```

```
NSOL,2,1,TEMP,,C1
NSOL,3,4,TEMP,,C2
NSOL,4,6,TEMP,,C3
NSOL,5,8,TEMP,,C4
NSOL,6,10,TEMP,,C5
NSOL,7,2,TEMP,,C6
PRVAR,2,3,4,5,6,7
/POST1
PRNSOL,TEMP
/OUT
FINISH
```

2) Input command for creep curve fitting

/seqv,450000

/temp,0

/1, creq

/2,dcreq

0.026011561	0.049052144
0.0264248	0.049038785
0.0286223	0.049026323
0.0291164	0.049013667
0.0294855	0.049001134
0.0298025	0.048988719
0.0303192	0.04896426
0.0307543	0.048940271
0.0311386	0.048916748
0.0316483	0.048882318
0.0321171	0.048848885
0.0326855	0.048805811
0.0333695	0.048754286
0.0341528	0.048695699
0.0350008	0.048631563
0.0358731	0.048563451

0.0368442	0.048485489
0.0378604	0.048401477
0.0389558	0.048315167
0.0401795	0.048225097
0.0414996	0.048132677
0.0427635	0.048044787
0.0440282	0.047964141
0.0453507	0.047893993
0.0465679	0.047836971
0.0473729	0.047793526
0.0480512	0.047763757
0.0490748	0.047745389
0.0502247	0.047735352
0.051423	0.047730668
0.052618	0.047728862
0.0533627	0.0477283
0.0542506	0.047728167
0.0556264	0.047728143
0.0574173	0.047728141
0.0589486	0.047728141